Phylogeny and divergence ages in Crocodylia: implications for crown-clades and paleobiogeography

Dissertation

der Mathematisch-Naturwissenschaftlichen Fakultät

der Eberhard Karls Universität Tübingen

zur Erlangung des Grades eines

Doktors der Naturwissenschaften

(Dr. rer. nat.)

vorgelegt von

Gustavo Darlim de Oliveira

aus Extrema, MG, Brasilien

Tübingen

2023

Gedruckt mit Genehmigung der Mathematisch-Naturwissenschaftlichen Fakultät der Eberhard Karls Universität Tübingen.

Tag der mündlichen Qualifikation:	27.02.2024
Dekan:	Prof. Dr. Thilo Stehle
1. Berichterstatter:	Dr. Márton Rabi
2. Berichterstatter:	Prof. Dr. Hervé Bocherens
3. Berichterstatter, falls zutreffend:	PD Dr. Andreas Matzke

Acknowledgements

I would like to start my acknowledgements by thanking my supervisor Dr. Márton Rabi for the opportunity to be part of and develop unique and high-quality studies during the past three years, contribute to my academic education as a scientist, and for the valuables professional and personal advices. I have learned so many different skills during my PhD time that I will carry along my scientific career. I am happy to be able to learn and contribute with quality work in this amazing field of study that palaeontology represents. Not only restricted to methods, writing, and presentations, I also have grown as a person. I also thank my second supervisor Prof. Hervé Bocherens that I am very grateful for all the conversations, suggestions, feedback and guidance along my PhD, which were essential for the completion of my studies.

I would like to thank the agency Deutsche Forschungsgemeinschaft (DFG, grant no. 417629144, awarded to Dr. Márton Rabi) for providing the funding for my PhD research, including collection visits and conferences attendances. Furthermore, I would like to thank the collective support of the following colleagues for discussions, collaborations, and access to museum collections: Henri Thomassen (Univeristy of Tübingen, Germany), Michael Lee (Flinders University, Australia), Christopher Brochu (University of Iowa, USA), Massimo Delfino (University of Turin, Italy), Pedro Godoy (University of São Paulo, Brazil), Silvio Onary (University of São Paulo, Brazil), Rafael Delcourt (University of São Paulo), Gabriel Ferreira (University of Tübingen, Germany), Giovanne Cidade (Universidade Estadual Paulista, Brazil), Ana Laura (University of São Paulo, Brazil), Rodolfo Salas-Gismondi (Universidad Peruana Cayetano Heredia, Peru), Dieter Schreiber (Staalichen Naturkundenmuseums Karlsruhe, Germany), Kantapon Suraprasit (Chulalongkorn University, Thailand), Yaowalak

Chaimanee (University of Poitiers, France), and Doungrutai Saesaengseerung, Kasidit Ken Eiamlaor, Pannipa Tian, Chotima Yamee, Mana Rugbumrung, Adulwit Kaweera and all staff from the Department of Mineral Resources (DMR, Bangkok, Thailand), Sitg Phongkitkarun (Mahidol University, Bangkok, Thailand), Frank Glaw and Michael Franzen (Bavarian State Colletion of Zoology in Münich, Germany), Erick Weber (Zoologische Schausammlung Tübingen, Germany), H. D. Schreiber (Staatlichen Naturkundemuseums Karlsruhe, Germany); Arvid Aase (Fossil Butte National Monument, USA), Agnes Fatz (University of Tübingen, Germany). I want to furthermore thank Wolfgang Bott, Iris Dreher, Helen Donath, and all the staff of University of Tübingen for the assistance throughout my PhD and stay in Tübingen.

To all of my colleagues of the Biogeology Working group Prof. Dorothée Drucker, Valentina Garcia, Freya Riedel, Mártin Ebner, Tatiana Miranda, Chris Baumann, Peter Tung, Sophie Habinger, Anne Kremmer, Giuseppe Briatico, Felix Augustin, Magdalena Krajcarz, Maciaj Krajcarz, and Huei Ying Gan for all the discussions, meetings and great time together, as well as for the Crocktail Hour group (Márton, Tobias, Jules, and Jeremias) for all the meetings and project planning during the past years.

I want to thank my friends Panos, Sarah, Felix, Nina, Christina, Nikos, Maria, Andy, Vale, Tobi, Will, Franzi, Kim, for all the great time together, laughs, pizza evenings, and so many fun times together. Furthermore, a very special thanks to my dearest friends that have been in this journey with me, Luiza (and the new baby!), Bruna, Guilherme (Squirtle), Gabriel (Fumaça), Silvio, Fellipe, Gabriel Mestriner, that I am so happy to be able to share and live such an exciting part of my life with you. So many happy memories that I'm going to carry for life. To my friends that made my stay in Germany way more lovely and provided me home feeling even when I am so far

from home, Svenja, Belinda and Sarah. So many nice experiences together, and I cannot wait for those that are still to come. I love you, guys.

I extend my gratitude to my former supervisor Max Langer, with whom I have the opportunity to have great scientific discussions and ideas that inspires me to pursue the paleontological career.

I want to express my gratitude to the most important part of my life, my family: Renato, Maria Helena, Juliano, Helena, Damian and now our little Lucca. I miss them every single day of my life. They have supported me with my career, my choice to live abroad and they have helped me to grow personally and professionally. They are my reason to keep going and I want to be able to share a life closer to them in a near future. I love them unconditionally.

This work is dedicated to my family.

Statement of collaborative work

This thesis is the product of collaborative work conducted in the scope of the DFG Grant Project supervised by Dr. Márton Rabi.

The contributions of the candidate and of the co-authors are indicated at the start of a chapter. These contributions follow the basic categories of Conceptualization, Investigation, Visualization, Formal analysis, Writing (original draft), and Writing (review and editing), but are adapted to each chapter according to the type of research work. Authors are listed per category according to their relative contribution to the specified task.

Unless otherwise indicated in the figure caption, figures were prepared by the candidate. Additionally, this dissertation contains work that is intended to be published but which has not yet been edited by co-authors (thus, representing what is for now the sole work of the candidate).

Candidate Bibliography

The following bibliography represents the sum of work (original research, analyses, and reviews) performed by the candidate during his doctoral studies. Publications or manuscripts that appear either in part or in whole in the present dissertation are marked with *.

Publications

* Walter, J., **Darlim, G**., Massonne, T., Aase, A., Frey, E., & Rabi, M. (2021). On the origin of Caimaninae: insights from new fossils of *Tsoabichi greenriverensis* and a review of the evidence. *Historical Biology*, *34*(4), 580-595. https://doi.org/10.1080/08912963.2021.1938563

*** Darlim, G.,** Lee, M. S., Walter, J., & Rabi, M. (2022). The impact of molecular data on the phylogenetic position of the putative oldest crown crocodilian and the age of the clade. *Biology Letters*, *18*(2), 20210603. https://doi.org/10.1098/rsbl.2021.0603

*** Darlim G**., Suraprasit, K., Chaimanee, Y., Tian, P., Yamme, C., Rugbumrung, M., Kaweera, A., & Rabi, M. (2023). An extinct deep-snouted *Alligator* species from the Quaternary of Thailand and comments on the evolution of crushing dentition in alligatorids. *Scientific Reports*, 13, 10406. https://doi.org/10.1038/s41598-023-36559-6

In Preparation

*** Darlim G.,** Rabi, M. Revisiting the phylogeny of *Alligator* and implications on the origin of the Chinese alligator.

Silva Paiva A., **Darlim G.**, Rabi M. Alternative phylogenetic position of the blunt-snouted *Gnatusuchus pebasensis* (Alligatoridae, Caimaninae) as a crown caimanine,

Massonne T, **Darlim G**, Wings O, Rabi M. The status of *Hassiacosuchus haupti* Weitzel, 1935: revision of short snouted Alligatorinae from the Messel and Geiseltal locality of Germany and their implications for a monophyletic short snouted alligatorine group.

Abstract

Crocodylia is represented by semi-aquatic ambush predators that inhabit freshwater and estuarine environments in the tropical and subtropical regions of the globe. Composed by 25 extant recognized species in three main lineages (Crocodyloidea, Gavialoidea and Alligatoroidea), mitogenomic studies recognizes a higher diversity of crocodylians within cryptic species complexes that are otherwise unrecognizable based on morphological analyses. Extinct crocodylian species furthermore outnumber the living diversity as evidenced by a considerable fossil record extending to late Stages of the Cretaceous Period. The combination of well sampled fossil record and low extant diversity that allows comprehensive sampling for molecular data makes Crocodylia a good model clade for macroevolutionary studies. In spite of phylogenetic analysis using molecular data consistently recover a common topology, paleontological studies in Crocodylia often continue to use morphology-only datasets, which in turn impacts on on the inferred phylogenetic position of many fossil taxa. Examples of topological discrepancies in Crocodylia are represented by: (i) the phylogenetic position of the Indian gharial *Gavialis gangeticus* represents one of the long-standing conflicts in crocodylian systematics, as phylogenetic inferences based on morphology alone places *Gavialis* sister to all other living crocodilians (i.e. alligators and crocodiles), whereas molecular data unite *Gavialis* with the false gharial *Tomistoma schlegelii* as a sister clade to Crocodylidae alone. These topological discrepancies in turn affects particularly taxa close to the root of Crocodylia and/or with a *Gavialis*-like morphology. Hence, the ambiguous phylogenetic position of basal fossil taxa may eventually lead to unreasonable selection of fossil calibrations for divergence age estimates in molecular studies, which in turn majorly affects macroevolutionary inferences in Crocodylia; (ii) Similarly, topological conflicts are furthermore observed in the crown clades of Alligatoridae (Caimaninae, Alligatorinae), as incomplete fossil and unstable phylogenies of extinct caimanines hamper a reconstruction of early evolution in the clade, in addition to poorly justified selection of fossil as calibration in molecular studies overestimate the origin of total and crown-Caimaninae; and finally (iii) the origin of the Chinese alligator (*A. sinensis*) is considered a biogeographical puzzle, as the timing and climatic context of *Alligator* dispersal from North America to Asia is poorly constrained: paleontological evidence and molecular estimates for the split between *A. sinensis* and its only closest living relative *A. mississippiensis* (American

alligator) are in conflict; *Alligator* fossils have never been recovered in the stem-lineage of *A. sinensis*; and *Alligator* fossil species from Asia have never been included into a phylogenetic framework. In the present thesis, in order to investigate the three abovementioned conflicts in crocodylian systematics, I explore (I) the effects of the use of molecular data on the position of fossil taxa close to the root of Crocodylia; (II) the phylogeny of Caimaninae as an extensive reappraisal of the position of fossil taxa in addition to provide well-justified fossil calibrations for the total and crown-groups; (III) the evolution of *Alligator* focusing on expanding the dataset by describing a new *Alligator* species, *Alligator munensis*, and by including fossil species from Asia into a phylogenetic context, contributing to the understanding of *Alligator* intercontinental dispersal. A series of methodologies were explored in order to meet the objectives, including traditional alpha-taxonomy descriptions, use of computed tomography, extensive literature review, phylogenetic analysis under Maximum Parsimony, undated Bayesian inference and total evidence tip dating. The studies composing this thesis contribute significantly for the comprehension crocodylian systematics by providing time-scaled phylogenies, highlighting the importance of DNA-informed phylogenetic inference for basal crocodylian relationships and divergence age estimates together with the use of well-justified fossil calibrations, and contributes to the understanding of *Alligator* evolution and biogeography.

Abstrakt

Crocodylia sind semiaquatische Lauerjäger, die im Süßwasser und in Flussmündungen in den tropischen und subtropischen Regionen der Welt leben. Es gibt 25 anerkannte rezente Arten aus drei Hauptlinien (Crocodyloidea, Gavialoidea und Alligatoroidea). Mitogenomische Studien zeigen eine größere Vielfalt von Crocodylia innerhalb kryptischer Artenkomplexe, die ansonsten auf der Grundlage morphologischer Analysen nicht zu erkennen wären. Ausgestorbene Krokodilarten übertreffen zudem die Vielfalt ihrer lebenden Verwandten, wie ein beachtlicher Fossilienbestand belegt, der bis in die späten Stadien der Kreidezeit zurückreicht. Beispiele für seit langem bestehende Konflikte in der Systematik der Krokodile sind (i) die phylogenetische Position des Gangesgavials *Gavialis gangeticus*. Phylogenetische Analysen, die allein auf morphologischen Daten beruhen, sehen *Gavialis* als Schwesterart aller anderen lebenden Krokodile (Alligatoren und Krokodile), während Analysen mit molekularen Daten *Gavialis* zusammen mit dem Sunda-Gavials *Tomistoma schlegelii* als Schwestergruppe der Crocodylidae finden. Vor allem die Kombination aus zahlreichen Fossilien und einer geringen rezenten Vielfalt, die eine umfassende Probenahme für molekulare Daten ermöglicht, macht Crocodylia zu einer guten Modellgruppe für makroevolutionäre Studien. Obwohl phylogenetische Analysen auf der Grundlage molekularer Daten durchweg eine allgemein anerkannte Topologie ergeben, verwenden paläontologische Studien zu Crocodylia häufig weiterhin nur morphologische Datensätze. Diese topologischen Diskrepanzen wirken sich auf die phylogenetische Position vieler fossiler Taxa aus, insbesondere derjenigen, die sich nahe der Basis der Crocodylia befinden und/oder eine Gavialis-ähnliche Morphologie aufweisen. Daher kann die unklare phylogenetische Position basaler fossiler Taxa schließlich zu einer nicht sinnvollen Auswahl fossiler Kalibrierungen zur Alterseinschätzung von Aufspaltungsereignissen in molekularen Studien führen, was wiederum die makroevolutionären Schlussfolgerungen für Crocodylia erheblich beeinträchtigt. (ii) In ähnlicher Weise treten topologische Konflikte in den Kronengruppe der Alligatoridae (Caimaninae, Alligatorinae) auf, da unvollständig erhaltene Fossilien und instabile Phylogenien ausgestorbener Caimaninae eine Rekonstruktion der frühen Evolution der Gruppe erschweren. Darüber hinaus wird auf Grund einer schlecht begründeten Auswahl von Fossilien als Kalibrierungspunkte in molekularen Studien der Ursprung der Gesamt- und Kronen-Caimaninae überschätzt. Schlussendlich (iii) wird der

Ursprung des China-Alligators (*A. sinensis*) als biogeografisches Rätsel betrachtet, da der Zeitpunkt und der klimatische Umstand der Ausbreitung der Gattung *Alligator* von Nordamerika nach Asien nur unzureichend geklärt sind. Grund dafür ist, dass paläontologische Belege und molekulare Schätzungen für die Aufspaltung zwischen *A. sinensis* und seinem einzigen lebenden Verwandten *A. mississippiensis* (Mississippi-Alligator) im Widerspruch zueinander stehen; fossile Alligatorenarten wurden nie in der Stammlinie von *A. sinensis* gefunden und fossile Alligatorenarten aus Asien wurden nie für eine phylogenetischen Analyse berücksichtigt. Um die drei oben genannten Konflikte in der Systematik der Crocodylia zu untersuchen, untersuche ich in der vorliegenden Thesis (I) die Auswirkungen der Verwendung molekularer Daten auf die Position fossiler Taxa nahe der Basis der Crocodylia und Auswirkungen auf das Alter der Gruppe; (II) die Phylogenie der Caimaninae als umfassende Neubewertung der Position fossiler Taxa, um gut begründete fossile Kalibrierungen für die Gesamt- und Kronengruppe zu liefern und damit die Paläobiogeographie der Caimaninae zu überarbeiten; (III) die Evolution der Gattung *Alligator* mit Schwerpunkt auf der Erweiterung des Datensatzes zum einen durch die Beschreibung einer neuen Alligatorenart, *Alligator munensis*, und zum anderen durch die Einbeziehung fossiler Arten aus Asien in eine phylogenetische Analyse, was zum Verständnis der interkontinentalen Ausbreitung der Gattung *Alligator* beiträgt. Um diese Ziele zu erreichen, wurden eine Reihe von Methoden angewendet, darunter traditionelle Alpha-Taxonomie-Beschreibungen, die Verwendung von Computertomographie, eine umfassende Literaturanalyse, sowie phylogenetische Analysen unter Parsimony, undatierter Bayesian Inference und Total Evidence Tip Dating. Die Studien, aus denen sich diese Arbeit zusammensetzt, leisten einen wichtigen Beitrag zum Verständnis der Krokodilsystematik, indem sie zeitlich skalierte Phylogenien liefern, die Bedeutung der DNA-gestützten phylogenetische Schlussfolgerungen für basale Krokodilbeziehungen und Alterseinschätzungen von Aufspaltungsereignissen zusammen mit der Verwendung gut begründeter Fossilkalibrierungen hervorheben und zum Verständnis der *Alligator*-Evolution und -Biogeographie beitragen.

Summary

Institutional abbreviations

AMNH–American Museum of Natural History, New York, New York, USA;

DMR–Department of Mineral Resources, Bangkok, Thailand;

FMNH–Field Museum of Natural History, Chicago, USA;

IRScNB–Institut Royal des Sciences Naturelles de Belgique, Brussels, Belgium;

LPM – Linqu Paleontology Museum, Shandong, China;

MCZ–Museum of Comparative Zoology, Harvard University, Cambridge, Massachusetts, USA;

NMNS – National Museum of Natural Science, Taiwan;

SNSB–Staatliche Naturwissenschaftliche Sammlungen Bayerns, Munich, Germany;

SZ–Museum der Universität Tübingen, Zoologisches Schausammlung, Tübingen, Germany;

YPM–PU–Princeton University collection housed at Peabody Museum, New Haven, Connecticut, USA;

1. INTRODUCTION

1.1 Crocodylia Gmelin, 1789: an overview

Crocodylia (crown-group of Crocodyliformes) is represented by semi-aquatic ambush predators that inhabit freshwater and estuarine environments in the tropical and/or subtropical regions (Grigg & Kirshner, 2015). Phylogenetically defined as the clade including the last common ancestor of *Gavialis gangeticus, Alligator mississippiensis*, *Crocodylus niloticus* and all of its descendants (amended definition of Brochu, 2003), Crocodylia is currently represented by 25 living species, although studies based on molecular data suggest a higher diversity based on the presence of cryptic species complexes and it is expected that the current number of living species to almost double in the next few years (Grigg & Kirshner, 2015; Bittencourt et al., 2019; Roberto et al., 2020; Brochu & Sumrall, 2020). The extinct diversity of Crocodylia on the other hand is extremely high as evidenced by the fossil record (Figure 1) comprising approximately 140 species nearly worldwide distributed mostly during the Cenozoic Era, although earliest unambiguous fossil crocodylians are dated to late stages of the Cretaceous Period, around 80 million years (Brochu, 1999; Brochu, 2003; Rio & Mannion, 2021).

The main crocodylian lineages are represented by Gavialoidea, Alligatoroidea, and Crocodyloidea. The gavialoids (clade including *G. gangeticus* and all crocodylians closer to it than to *A. mississippiensis* or *C. niloticus*, Brochu, 2003), are longirostrine crocodylians (i.e., presence of extremely long and slender snout) with a homodont conical dentition specialized for the capture of fish, represented by *G. gangeticus* (gharial) and *Tomistoma schlegelii* (false gharial) (details on Chapter 1), restricted to Ganges River drainage waters in the Northern India and Nepal, and Malaysia, Borneo, and Sumatra, respectively (Grigg & Kirshner, 2015).

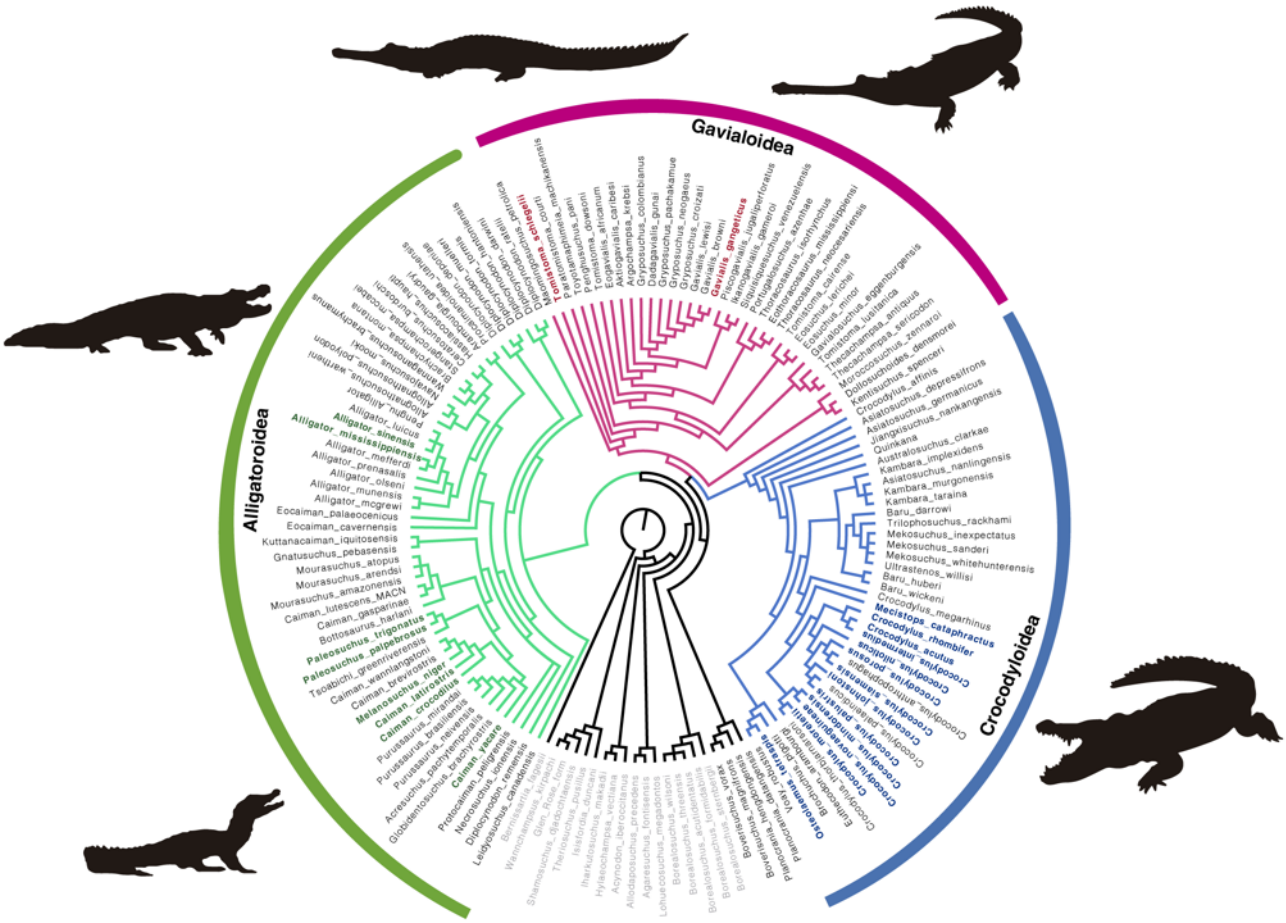

Figure 1. Topology of Crocodylia modified after Darlim et al. (2022) (chapter 1) showing the past and current diversity of the group. Main clades indicated by the colours green (Alligatoroidea), blue (Crocodyloidea), and red (Gavialoidea). Coloured names indicate extant species. Non-crocodylian taxa are displayed in faded grey colour.

Crocodyloids are represented by the crocodiles (*Crocodylus* spp., *Mecistops* spp., and *Osteolaemus* spp.) and widespread along the tropical and subtropical regions of the Americas, extensively present in Africa, south and southeast Asia, and in Australasia (Oaks, 2011). Defined as a clade including *Crocodylus niloticus* and all crocodylians closer to it than to *A. mississippiensis* or *G. gangeticus* (Brochu, 2003), crocodyloids are generally characterised by a 'V-shaped' snout in dorsal view and

interlocking of the teeth from upper and lower jaws, thus the teeth are visible laterally when jaws are occluded (Brochu, 1999; Figure 2a) as evidenced by the presence of a notch at the articulation of the premaxilla and maxilla for the reception of the fourth dentary tooth. Both gharials and crocodiles present salt glands in the keratinised tongue as an osmoregulatory adaptation to salt water, although the osmoregulatory biology of gharials is still poorly known and needs further investigation (Leslie & Taplin, 2001; Grigg & Kirshner, 2015). Furthermore, although living gavialoids (*Gavialis* and *Tomistoma*) are restricted to fresh water, the ancestral condition based on the fossil record is predominantly marine, specifically is coastal flooded areas (e.g. shallow coastal habitats, Salas-Gismondi et al., 2022).

Finally, representatives of Alligatoroidea (clade including *Alligator mississippiensis* and all crocodylians closer to it than to *C. niloticus* and *G. gangeticus,* Brochu, 2003) (i.e. alligators and caimans) are predominantly present in the Americas, with exception of *A. sinensis* in China (Brochu, 1999; Thorbjarnarson and Wang, 2010). Alligatoroids are generally characterized by a 'U-shaped' snout, and the occlusion of lower and upper jaw dentition is charactered by an overbite, in which the ventral surface of the upper jaw is marked by occlusal pits for the reception of lower jaw dentition (Brochu, 1999, 2004; Figure 2e). Living alligatoroids furthermore lack lingual salt-excreting glands and are restricted to fresh water environments, although specimens of the American alligator (*A. mississippiensis*) have been reported in salt waters, they cannot survive indefinitely in hyperosmotic conditions (Lauren, 1985; Grigg & Kirshner, 2015).

Figure 2. Skull morphology of selected extant crocodilians in lateral and dorsal views, respectively. (**a.b**) *Crocodylus palustris* (SNSB 380/1907); (**c,d**) *Gavialis gangeticus* (SZ 7458); (**e,f**) *Alligator mississippiensis* (SZ 1057); and (**g,h**) *Tomistoma schlegelii* (SNSB 523/1909). Scale bars: 5cm.

Crocodylians are equivocally referred as ‘living fossils’ mainly based on the argument of species sharing to some extant a morphologically similar body plan, which fails to illustrate how in fact species are considerably different from each other and how

much they have changed over time (Brochu, 2003). The evolutionary history of Crocodylia is marked by independent ecological transitions from freshwater to marine and terrestrial habitats, illustrating the morphological disparity of the group and a widespread niche occupation (Wilberg et al., 2019). For instance, during the Miocene Epoch, complex aquatic environments that composed the Pebas Mega-Wetland System in Western Amazonia (Hoorn et al., 2010) were once inhabited by a hyperdiverse assemblage of caimanines (alligatoroids) and longirostrine crocodylians (gavialoids) representing a wide range of snout morphotypes (Salas-Gismondi et al., 2015). Particularly, examples of the Miocene Amazonia caimanines includes: giant predators exceeding 10m long in body size (*Purussaurus* spp., Aureliano et al., 2015); "gulp-feeder" forms (*Mourasuchus* spp.) suggested of being able to capture of large amount of small preys due the presence of platyrostral-broad rostrum (i.e., long, wide, and dorsoventrally flatted rostrum, *sensu* Busbey, 1994) (Cidade et al., 2019); and blunt-snouted smaller forms (*Gnatusuchus pebasensis*) characterised by a morphology that reflects strong adaptations for a durophagous feeding strategy (i.e. short and wide skull shape, mandibular reduced dentition, mandibular rami firmly sutured, and posterior maxillary and dentary bulbous teeth) (Salas-Gismondi et al., 2015).

Crocodylians furthermore have been suggested to occupy terrestrial environments as evidenced by the combination of altirostral/oreinirostral snout (i.e. deep rostrum with a convex upper margin and rostral length less than 55 percent of basal skull length, *sensu* Busbey, 1995), anterodorsal orientation of the nares, ziphodont dentition (i.e. labiolingually compressed and serrated teeth, Langston, 1975), less curved femoral shaft, heavily osteoderm coverage (Rauhe, 1995) and even presence of hoof-like unguals (Brochu, 2012).

As outlined above, the morphological diversity in Crocodylia is remarkable, and the combination of well sampled fossil record and low extant diversity (which allows comprehensive sampling for molecular data) makes Crocodylia a good model clade for macroevolutionary studies (Brochu, 2003). Particularly, fossils represent an essential source of temporal information for time-scaling topologies and for divergence age estimates, which in turn are the base of macroevolutionary studies (Parham et al., 2012; Ksepka et al., 2015; Benton et al., 2015). However, major topological conflicts regarding fossil placement remain across studies, compromising the accuracy of divergence age estimates and phylogenies. In this thesis, specific topological conflicts in Crocodylia are addressed and explored in detail along the chapters, with implications for divergence ages and paleobiogeography in the clade.

1.2 Identification of contentious crocodylian divergencies

Datasets of phylogenetic analyses frequently differ in character and taxon sampling among paleontological studies in Crocodylia, which in turn leads to topological conflicts along the crocodylian evolutionary tree. Many are the conflicts in the crocodylian evolutionary tree, including for example the phylogenetic relationships of orientalosuchines as basal alligatoroids, basal crocodyloids or even recovered as closely related to the Australasian mekosuchines (Massonne et a., 2019; Ristevski et al., 2023); the *Tomistoma*-*Gavialis* clade (and fossil taxa closely related to it) that is affected by the topological conflict regarding the use of molecular or morphological-based datasets (Brochu, 1997; Lee & Yates, 2018; Iijima & Kobayashi, 2019; Rio & Mannion, 2021); the unresolved phylogenetic relationships of early caimanines and the complex palaeobiogeographic history of the crown-clade (Brochu, 2004; Bona et al., 2018; Stocker et al., 2021); and the unknown phylogenetic relationships of the Chinese

alligator (*A. sinensis*) with respect to *Alligator* fossil species from Asia and how it affects the understanding of *Alligator* dispersal from North America to Asia (Brochu, 1999, 2004; Massonne et al., 2019), besides many other conflicts along the crocodylian evolutionary tree (Rio & Mannion, 2021). As a consequence, ambiguous topologies critically compromise divergence and divergence age inferences, as the utility of fossil taxa as age calibrations for molecular divergence age estimations is affected (Parham et al., 2015). Moreover, macroevolutionary interpretations of clades in which those fossil taxa are associated with are furthermore biased.

In the present thesis, three topological conflicts of different parts of the crocodylian evolutionary tree are addressed: (i) the placement of fossil taxa hinging on the '*Gavialis* problem' in which morphological and molecular datasets recover highly contradicting topologies for Crocodylia, mainly regarding the position of the Indian gharial *G. gangeticus*, resulting in conflicting ages of the crocodilian crown (Brochu, 1997; Brochu, 2003; Oaks, 2011; Lee & Yates, 2018; Pan et al., 2021; Rio & Mannion, 2021); (ii) the conflicting position of fossil caimanines which often results in overestimated divergence ages of Caimaninae (total and crown-groups) in molecular studies, besides implying complex biogeographic history for the clade, and hampering the reconstruction of the early evolution of Caimaninae (Bittencourt et al., 2019; Walter et al., 2021); and finally, (iii) the enigmatic origin of the Chinese alligator (*Alligator sinensis*) is addressed as the lack of phylogenetic analyses including *Alligator* fossil species from Asia results in an uncertainty regarding timing of the dispersal of *Alligator* from North America to Asia (Brochu 1999, 2004; Massonne et al., 2019).

These phylogenetic conflicts are investigated in the present thesis based on a dataset expansion approach, including reappraisal of phylogenetic position of fossil taxa, review of characters codifications and inclusion of taxa/specimens into the dataset.

Additionally, different methodologies such as CT scanning of fossil taxa for more detailed descriptions, phylogenetic approaches (Maximum Parsimony, Bayesian inference) for a more comprehensive understanding of the phylogenetic position of fossil crocodylians compose the thesis. In the following sections, a detailed framework, objectives and contributions of the chapters are presented.

2. Summary of Chapter 1

2.1 Framework

Topological conflict and the age of Crocodylia: morphology *vs* DNA

One of the long-standing conflicts in crocodylian systematics is the phylogenetic position of the Indian gharial *Gavialis gangeticus*. The extreme feeding specialization morphology for a fish-based diet including long and narrow snout, slender, sharp and regularly-spaced teeth (Brochu, 1997; Lee & Yates, 2018; Figure 2 c,d) are shared between the Indian gharial and the Malayan or 'false' gharial *Tomistoma schlegelii* (Figure 2 g,h). Whereas phylogenetic analysis based on morphological datasets mostly recover the Indian gharial separated from *Tomistoma* as a first divergent lineage at the base of Crocodylia (i.e. sister-group to all other living crocodilians, including alligators and crocodiles) (Norell, 1989; Brochu, 1997; Piras et al., 2010; Iijima & Kobayashi, 2019), molecular studies using nuclear and mitochondrial DNA sequences on the other hand find that both gharial species are sister taxa and phylogenetically placed in a more derived position composing a clade with crocodyloids (i.e. Longirostres *sensu* Harshman et al., 2003; Figure 3). The closer relationship of both living gharials furthermore suggests specialized piscivorous snout morphology as homologous rather than convergent (Gatesy & Amato, 1992; Gatesy et al., 2003; Janke et al., 2005;

Harshman et al., 2003; Roos et al., 2007; Willis et al., 2007; Willis, 2009; Oaks, 2011; Green et al., 2014; Lee & Yates, 2018; Pan et al., 2020; Salas-Gismondi et al., 2022).

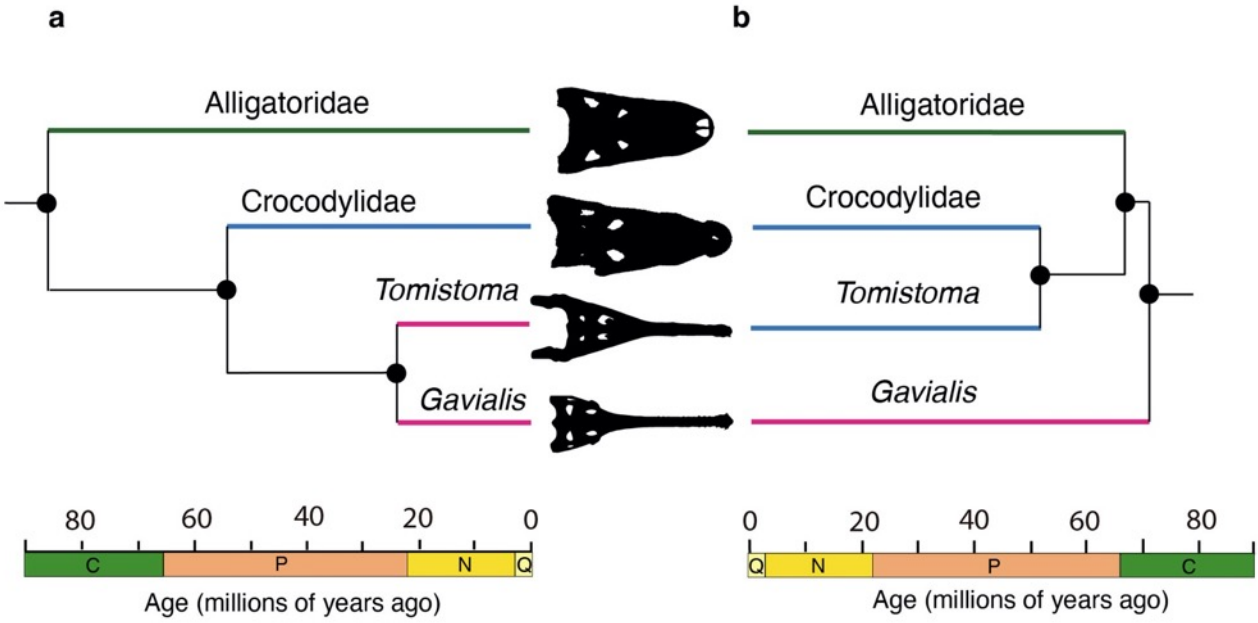

Figure 3. Conflict between topologies based on (**a**) molecular, and (**b**) morphological datasets. Note the change on the position of *Tomistoma*. Abbreviations: C, Cretaceous; P, Paleogene; N, Neogene; Q, Quaternary.

By mapping morphological characters into molecular trees, early studies investigating the *Gavialis* problem suggest the presence of secondary signals or 'hidden support' in morphological datasets for the *Gavialis*-*Tomistoma* clade (i.e. molecular topology, Gatesy et al., 2003). In addition to that, phylogenetic signals supporting *Gavialis* as an early divergent lineage in Crocodylia in the morphological topology are reinterpreted as reversals in Gavialine to plesiomorphic states present in outgroup taxa or basal fossil crocodylians (Gatesy et al., 2003). Morphological support for the molecular topology in Crocodylia is furthermore provided by gavialine atavistic characters present in extinct 'tomistomines' (i.e. *Penghusuchus pani* from the Miocene of Taiwan, Shan et al., 2009; *Toyotamaphimeia machikanensis* from the Pleistocene of

Japan, Aoki, 1983; Kobayashi et al., 2006), as these species display a mosaic of tomistomine and gavialine traits, contributing to fill the 'morphological gap' that was once present between both crown gharial lineages (Iijima & Kobayashi, 2019). However, considerable stratigraphic gap remains at the base of Gavialidae due the presence of Mesozoic taxa (i.e. thoracosaurs) occupying stem phylogenetic position in the clade. Recently, a phylogenetic analysis by Rio & Mannion (2021) using an extensively revised dataset was able to reproduce the molecular topology (i.e. *Gavialis* and *Tomistoma* closely related) for the first time based on morphology alone, however still not resolving the temporal incongruence on the divergence age in crown gharials caused by the presence of thoracosaurs in the stem lineage (Rio & Mannion, 2021).

Thoracosaurs is the name used to refer to a non-monophyletic group of long-snouted taxa mainly represented by fossils from marine deposits from the Late Cretaceous and Early Paleogene of Europe and North America, originally inferred as stem-taxa to the *Gavialis* lineage (Brochu, 1997; Brochu, 2004; Mateus et al., 2019). Although molecular data favour a closer relationship between *Tomistoma* and *Gavialis*, it does not prevent thoracosaurs to be recovered within crown gharials using morphology (Brochu, 1997; Iijima & Kobayashi, 2019; Rio & Mannion, 2021; Puértolas-Pascual et al., 2023; Figure 4). The oldest unambiguous gavialid is dated ca. 16 Ma (Iijima & Kobayashi, 2019), whereas thoracosaurs are reported for up to ca. 72Ma (Brochu, 2004; Müller & Reisz, 2005; Oaks, 2011; Green et al., 2014). The age of the thoracosaurs is highly inconsistent with the young age of crown gharials and it considerably contradicts molecular divergence estimates (Oaks, 2011; Pan et al., 2020; Lee & Yates, 2018), besides suggesting the origin of crown-gharials further back into the Mesozoic. Most analyses combining morphological and molecular data fail to find a phylogenetic position of thoracosaurs that are stratigraphically and phylogenetically

congruent with the age of crown gharials (Brochu, 2004; Mateus et al., 2019; Lee & Yates, 2018; Rio & Mannion, 2021; Puértolas-Pascual et al., 2023). On the other hand, analyses under total evidence tip dating approach (under Bayesian inference) are capable of recovering thoracosaurs in a phylogenetic position consistent with the age of those taxa and not associated with crown gharials, in addition to divergence date estimates furthermore consistent to those of molecular clock studies (ca. 40 Ma for crown gharials, Lee & Yates, 2018).

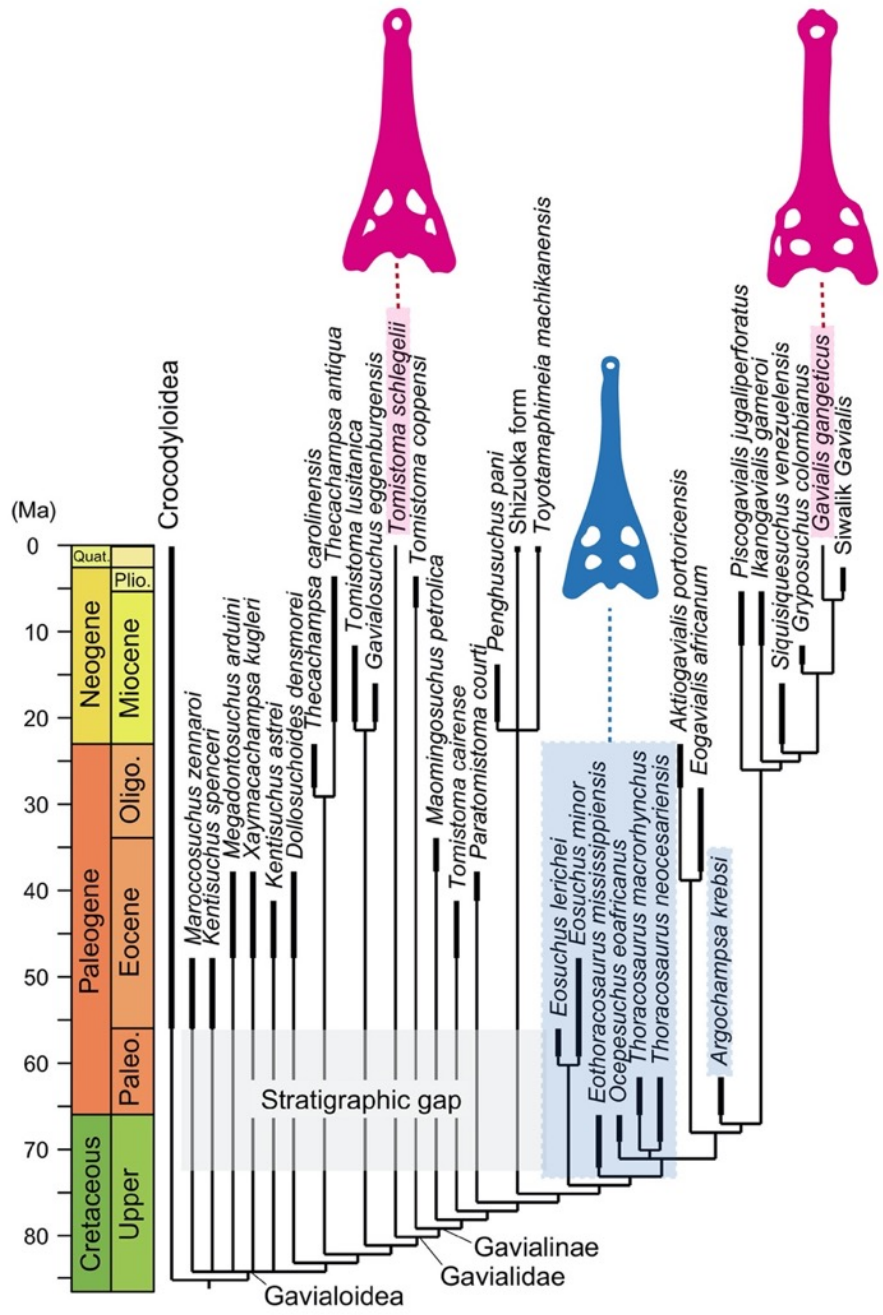

Figure 4. Time-scaled phylogeny of Gavialoidea using morphological and molecular data adapted from Iijima & Kobayashi (2019). Extant gavialoids are highlighted in pink. 'Thoracosaurs' are highlighted in blue. Grey shaded area indicates stratigraphic gap. Silhouettes are adapted from Lee & Yates (2018).

Total evidence tip-dating simultaneously generates phylogenetic inference (i.e. topology) and dating by explicitly considering stratigraphic age, likelihood-based clock-models, and substitution models applied to morphological and molecular data (Lee &

Palci, 2015). The method has been only recently implemented in crocodylian systematics (Turner et al., 2017; Lee & Yates, 2018; Salas-Gismondi et al., 2022), and is considered to be a promising approach for time-scaling phylogenies, for improvement of phylogenetic relationships and for the understanding of character evolution among lineages (Lee & Yates, 2018).

Although analyses using molecular data favour a common and distinct topology, phylogenetic studies focused on fossil crocodylians often continue to use morphology-only datasets (Bona et al., 2018; Cossette & Brochu, 2020; Godoy et al., 2021; Ristevski et al., 2020; Ristevski et al., 2021; Blanco et al., 2021; Puértolas-Pascual et al., 2023). DNA informed phylogenetic analyses are vital for interpreting the position of fossil taxa, as cladistic analyses on many groups (with extant representatives) have demonstrated that datasets based exclusively on morphological data are not sufficient to accurately understand the phylogenetic history of fossils considering incongruence between molecular and morphological topologies (Koepfli et al., 2007; Oyston et al., 2022), furthermore having implications on character polarization (Koepfli et al., 2007). Phylogenetic misleading effects of convergent evolution through cranial, dental and postacranial characters are commonly confounding cladistic analysis (Koepfli et al., 2007; Lee & Yates, 2018) and the use of an independent molecular phylogeny as a reference for deducing true phylogenetical signals from morphology has been broadly implemented (Gatesy et al., 2003; Asher et al., 2006; Koepfli et al., 2007; Springer et al., 2007; Havermans et al., 2010; Dávalos et al., 2014; Zou & Zhang, 2016; Iijima & Kobayashi, 2019; Kapli et al., 2020; Oyston et al., 2022). The addition of molecular data considerably changes the phylogenetic position of fossil taxa particularly close to the root of Crocodylia, and/or with *Gavialis*-like morphology, as the polarization and

optimization of key morphological characters are likely to shift. This in turn can affect their utility as age calibrations for molecular divergence age estimations.

Particularly, the origin of Crocodylia have been estimated to be around 81 – 100 Ma according to molecular clock studies and tip-dated analyses (Oaks, 2011; Pan et al., 2020; Lee & yates, 2018), estimates consistent with unambiguous oldest fossil representatives of the clade (i.e. *Brachychampsa*, Campanian of North America, *ca.* 80 Ma), furthermore supporting a North American origin of crocodylians. Conversely, species from the Late Cretaceous of Europe (i.e. Allodaposuchidae, *Acynodon*) have been tentatively suggested as alligatoroids (Buscalioni et al., 1997, 1999; Delfino et al., 2008; Martin & Buffetaut, 2008; Martin, 2007, 2010; Blanco, 2021), however phylogenetic analyses consistently recover those taxa as non-crocodylians (Narváez et al., 2015; Lee & Yates, 2018; Rio & Mannion, 2021; Ristevski et al., 2023; Puértolas-Pascual et al., 2023). Similarly, Orientalosuchina (a clade composed by species from the Late Cretaceous to the Eocene of Asia, Massonne et al., 2019) was primarily inferred as basal alligatoroids (Massonne et al., 2019), although its affinities with North American alligatoroids have been questioned (Wu et al., 2023), besides being furthermore recovered as early crocodyloids (Li et al., 2019; Rio & Mannion, 2021), or composing a clade with the Australasian mekosuchines (Ristevski et al., 2023). Finally, if thoracosaurs are considered gavialoids, it would suggest the presence of crown-crocodilians in the Late Cretaceous of Europe (Brochu, 1997; Brochu, 2004; Mateus et al., 2019), however as discussed above, the phylogenetic position of thoracosaurs within Crocodylia is highly controversial, and a phylogenetic interpretation of those taxa outside the crown is more consistent with the gavialoid fossil record and divergence age estimates (Lee & Yates, 2018). Thus, paleontological evidence of Crocodylia outside of North America before the Cretaceous-Paleogene boundary is weak.

A recently described taxon based on an incomplete skull from the upper Cenomanian (*ca* 95Ma) of Portugal, *Portugalosuchus azenhae* (Mateus et al., 2019) was inferred to represent the oldest known crocodylian, either as sister to all non-gavialoid crocodylians (Mateus et al., 2019), or in a clade with gavialoids (Ristevski et al., 2020; Ristevski et al., 2021; Rio and Mannion, 2021) according to previous morphological phylogenies. However, relying on morphology alone to interpret the putative position of *Portugalosuchus* as the oldest crocodylian is problematic as: (*i*) it would pre-date the previous oldest crown-crocodilian fossils (e.g., *Brachychampsa sealeyi* Williamson, 1996; 83.5–70.6 Ma) and imply substantial ghost lineage; (*ii*) topological conflict remains between morphological or molecular data in Crocodylia, and fossil taxa close to the root of the clade and/or with a *Gavialis*-like morphology (e.g. thoracosaurs), are particularly susceptible to considerable changes in phylogenetic position with the addition of molecular data as the polarization and optimization of key morphological characters are likely to shift; and (iii) *Portugalosuchus* would suggest the origin of Crocodylia in Europe, with a dispersal event to North America during the Late Cretaceous, which is poorly supported considering that phylogenies do not recover Cretaceous European taxa within the crown group.

Considering the extreme relevance of combining neontological and paleontological evidence as the best way to comprehend the phylogenetic relationships in Crocodylia, and the benefits of the newly implemented total evidence tip-dating method for generation of time-scaled topologies, a study focusing on the impact of the use of DNA informed analysis on the phylogenetic position of fossil crocodylians (specifically investigating the phylogenetic relationships of *P. azenhae* and the age of the crown group) is presented in Chapter 1.

2.2 Objectives of Chapter 1

- To investigate whether the phylogenetic position of basal crocodylian taxa, including *Portugalosuchus*, is altered under different phylogenetic analyses (Maxium Parsimony, undated and dated Bayesian Inference) by using DNA-informed datasets (either as a scaffold or combined with morphology);
- To estimate the age of Crocodylia by using total-evidence tip-dating analysis and compare the results with previously published divergence age estimates from molecular studies;
- To provide a comprehensive discussion on the impact of DNA for basal crocodylian relationships and age estimates in the clade.

2.3 Main findings and discussion

In all analyses in which molecular data is considered, either as scaffold or incorporated into a supermatrix approach (in both dated and undated analyses), *Portugalosuchus* is consistently recovered outside Crocodylia. Analyses using morphology-only datasets on the other hand recovered *Portugalosuchus* as a crocodylian (specifically near 'thoracosaurs'), although such result is questionable considering that total evidence tip-dating Bayesian analyses suggest that most, if not all 'thoracosaurs' are not crown crocodilians, but recovered outside of the crown-clade instead (Lee & Yates, 2018). Furthermore, as pointed out by Rio & Mannion (2021), *Portugalosuchus* does share exclusive character states with 'thoracosaurs', which in turn in combination with the results presented in the current study, *Portugalosuchus* likely represents a non-crocodylian eusuchian and should be avoided as a fossil age constraint for Crocodylia in calibration databases (e.g., Benton et al., 2015).

The age estimates for Crocodylia according to the total evidence tip-dated analysis in the present study is approximately 94 Ma (Cenomanian, Late Cretaceous), with a 95% highest posterior density interval (HPD) of approximately 87–104 Ma. These values are consistent with recent tip-dated estimates of Lee & Yates (2018; 100Ma) despite substantial differences in taxon and character sample. Furthermore, the results of the present study are consistent with molecular studies implicitly or explicitly following the best practices for justifying fossil calibrations (e.g., Parham et al., 2012; Turner et al., 2017; Detailed discussion on selection of fossil calibration is presented on chapter 2). The phylogenetic position of *Portugalosuchus* as a non-crocodylian is furthermore supported considering that if this taxon would have been interpreted as the oldest crown-crocodilian, its stratigraphic age (ca. 95Ma) would have been already older than the mean estimates of the present study (ca. 94Ma), which would lead to long ghost lineages that are inconsistent with the fossil record of Crocodylia by pulling the origin of the clade significantly back in time.

The results of this study furthermore show that analyses using DNA data as molecular scaffold generates topologies that are identical to those retrieved by combined datasets (morphology + DNA). These results are in turn consistent with discussions of previous studies regarding the mapping of morphology and fossils onto a molecular scaffold being highly comparable to the results of a simultaneous analysis where the DNA data essentially constrain the relationships among living taxa (Zhou and Rabi, 2015; Lee and Palci, 2015; Crawford et al., 2015). In addition to that, and considering the relevance of DNA in Crocodylia systematics, molecular scaffold represents a less demanding computational approach to inform molecular data into phylogenetic analysis, representing an efficient way to approximate more rigours supermatrix approaches (i.e. combined datasets).

2.4 Concluding remarks

- The mean age of Crocodylia is estimated as 94 Ma, consistent with those of molecular studies implicitly or explicitly following the best practices for justifying fossil calibrations;
- *Portugalouschus azenhae* most likely does not represent a crown-crocodilian and should be avoided as a fossil calibration for divergence age estimate studies;
- Macroevolutionary inferences in Crocodylia based exclusively on morphological data should be avoided, especially when morphology-only relationships among living taxa are highly contradicted by genomic data;
- Implementing DNA data into phylogenetic analysis as scaffold represents an efficient way to approximate more rigours supermatrix approaches in Crocodylia systematics, as results of phylogenetic analyses using molecular scaffold are consistent with those of analysis using combined datasets.

3. Summary of Chapter 2

3.1 Framework

Phylogeny of early alligatorids and implications for the age of Caimaninae

Alligatoroidea represents one of the main lineages in Crocodylia, including extant alligators and caimans, and presenting a fossil record tracing back to the Late Cretaceous Period (Bona et al., 208; Rio & Manion, 2021). Earliest divergent alligatoroids include *Leidyosuchus canadensis* (Campanian Age, Late Cretaceous of Canada), *Deinosuchus* (Campanian Age, Late Cretaceous of the United States and northern Mexico), and *Diplocynodon* spp. (i.e. Diplocynodontinae, Brochu, 1999; Bona et al., 2018; Cossette & Brochu, 2020; Paleocene to the Miocene of Europe), in which the presence of dentary teeth in occlusion in a notch at the premaxilla-maxilla suture, long, broad and flat skull compose a combination of morphological characters (plesiomorphic characters as similarly observed in early crocodyloids) common among these species (Brochu, 1999; Brochu, 2003; Cossette & Brochu, 2020). The phylogenetic position of these taxa is usually consistent, which are often recovered as the first divergent lineages in Alligatoroidea, especially the case for *Leidyosuchus* (Brochu, 1999; Brochu, 2004; Martin & Lauprasert, 2010; Wang et al., 2016). The monophyly of the Diplocynodontinae, on the other hand, and the interrelationships of *Diplocynodon* species have been extensively discussed, as well as challenged (Brochu, 1999; Martin, 2010; Brochu et al., 2012; Delfino & Smith, 2012; Martin et al., 2014; Groh et al., 2020; Rio & Mannion, 2021). The inclusion of *Deinosuchus* in phylogenetic analysis is furthermore introduce homoplasy and reduce resolution for the phylogenetic relationships at the base of Alligatoroidea, as species of *Deinosuchus* present convergent morphology with long-snouted forms (i.e. gavialoids) (Cossette & Brochu, 2020).

In a more derived phylogenetic position, crocodylians phylogenetically closer to *Alligator mississippiensis* than to *Diplocynodon ratelii* compose the clade Globidonta (*sensu* Brochu, 2003), which includes the crown clade Alligatoridae (i.e. composed by Caimaninae and Alligatorinae, Brochu, 1999; Figure 5). The definition of Globidonta although is dependent of phylogenetic context, and considering that the position of early globidontans have been recovered as unstable in relation to Alligatoridae (discussed below), Globidonta might appear as synonym of Alligatoridae (Bona et al., 2018; Rio & Mannion, 2021). Early globidontans include taxa such as Orientalosuchina, *Brachychampsa* spp., *Stangerochampsa mccabei*, and *Albertochampsa* spp. The recently erected clade Orientalosuchina (Massonne et al., 2019) includes extinct forms from the Late Cretaceous to the Late Eocene of southeastern Asia (Young, 1964; Martin & Lauprasert, 2010; Wang et al., 2016; Massonne et al., 2019; Shan et al., 2021; Wu et al., 2023), however besides being interpreted as an early divergent linage in Globidonta (Massonne et al., 2019; Shan et al., 2021; Wu et al., 2023), alternative phylogenetic positions of the clade have been suggested such as a crocodyloid (Rio & Mannion, 2021), and within the Australasian clade Mekosuchinae (i.e. longirostres crocodylians with inferred terrestrial habits, Ristevski, 2022; Ristevski et al., 2023). Future studies are essential to elucidate the relationships of orientalosuchines within Crocodylia, as it may play an important role on the understanding of alligatoroid origin and evolution. Similarly, the phylogenetic position of *Brachychampsa* spp.*, Stangerochampsa mccabei*, and *Albertochampsa* (taxa from the Cretaceous of North America) is critical for the fossil age of primary alligatoroid lineages (i.e. Globidonta and Alligatoroidea), as well as for the crown clades Caimaninae and Alligatorine (Alligatoridae).

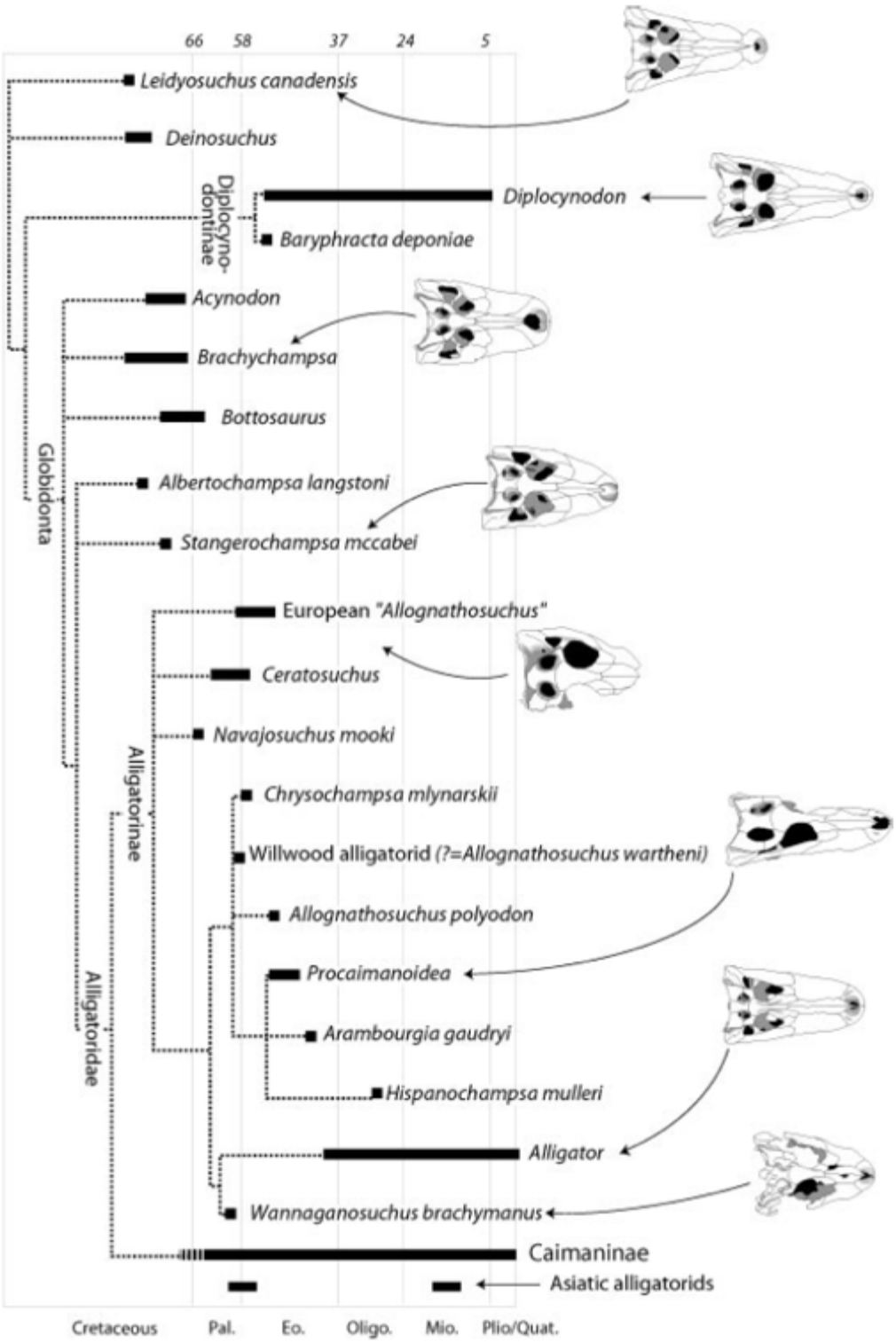

Figure 5. Topology indicating the phylogenetic relationships within Alligatoroidea. Removed from Brochu (2003).

The crown-group of Alligatoridae includes the alligators (Alligatorinae) and caimans (Caimaninae), species typically found in freshwater and coastal environments

of North, Central and South Americas with exception of a single species in Asia (i.e. *A. sinensis*, Brochu, 1999). Caimaninae is currently composed by six extant species including the black caiman *Melanosuchus niger*; the Paraguayan caiman *Caiman yacare,* the broad snouted caiman *Caiman latirostris*; the spectacled caiman *Caiman crocodilus* and finally the smallest living crocodilians Cuvier's dwarf caiman *Paleosuchus palpebrosus*, and the smooth-fronted caiman *Paleosuchus trigonatus* (Brochu, 1999; Grigg & Kirshner, 2015). Discovery of higher lineage diversity by molecular studies on the other hand supports the presence of more than 10 different lineages eligible for species recognition within the *Caiman* complex (*C.crocodilus*, *C. yacare*, and *C. latirostris*) and *P. trigonatus* (Bittencourt et al., 2019; Roberto et al., 2020).

On the other hand, the extinct diversity of Caimaninae is well-sampled along the Cenozoic Era, showing a remarkable morphological disparity particularly among caimanines From the Miocene of Western Amazonia (i.e. *Purussaurus* spp., *Mourasuchus* spp., *Gnatusuchus pebasensis*, Aureliano et al., 2015; Salas-Gismondi et al., 2015; Cidade et al., 2019). Although represented by specimens more fragmentary in nature, the fossil record of Caimaninae furthermore extends to the Paleocene of southern South America (i.e. *Eocaiman paleocenicus*, *Necrosuchus ionensis*, *Notocaiman stromeri*, and *Protocaiman peligrensis*), in which phylogenies strongly supports these species as the earliest unambiguous fossil caimanines (Bona 2007; Brochu, 2010, 2011; Hastings et al., 2013; Salas-Gismondi et al., 2015; Hastings et al., 2016; Bona et al., 2018; Cidade et al., 2020; Souza-Filho et al., 2018; Godoy et al., 2020; Cossette 2020; Stocker et al., 2021). However, Cretaceous North American taxa (i.e. *Brachychampsa* spp., *Stangerochampsa mccabei* and *Albertochampsa langstoni*) have been recovered in a basal position in Caimaninae in previous studies (Salas-

Gismondi et al., 2015; Bona et al., 2018; Cossette 2020, Stocker et al., 2021; Rio & Mannion, 2021), or unresolved relative to the clade (Hastings et al., 2016; Cossette & Brochu, 2018) (Figure 6). A complication regarding the phylogenetic position of these Cretaceous taxa arouses due to their use as fossil constraints (or calibrations) for divergence age estimates in published molecular studies (Bittencourt et al., 2019; Roberto et al., 2020). In particular, *Brachychampsa sealeyi* has been selected to calibrate crown-Caimaninae (Bittencourt et al., 2019; Roberto et al., 2020) despite the inconsistent placement of this taxon in published phylogenies, which in turn has major implications for character evolution within early Alligatoroidea. Estimates from these studies recover ages for the total-group Caimaninae (90.72 Ma, Bittencourt et al., 2019; 91.89 Ma, Roberto et al., 2020) that are significantly older than the earliest unambiguous fossils (i.e. *Necrosuchus ionensis*, *Protocaiman peligrensis,* early Paleocene, 66 – 61.6 Ma; Bona et al., 2018), whereas when *B. sealeyi* is used to calibrate Crocodylia instead, a more reasonable estimate albeit underestimating age for the origin of total-group Caimaninae is recovered (i.e. 53.39 Ma, Pan et al., 2020). Besides, all phylogenies agree that taxa from the paleocene of South America are caimanines (Bona 2007; Brochu, 2010, 2011; Hastings et al., 2013; Salas-Gismondi et al., 2015; Hastings et al., 2016; Bona et al., 2018; Cidade et al., 2020; Souza-Filho et al., 2018; Godoy et al., 2020; Cossette 2020; Stocker et al., 2021; Rio & Mannion, 2021), while many studies contradict the Caimaninae affinities of North American species (Brochu, 1999, 2011; Hastings et al., 2013; Hastings et al., 2016; Cossette & Brochu, 2018).

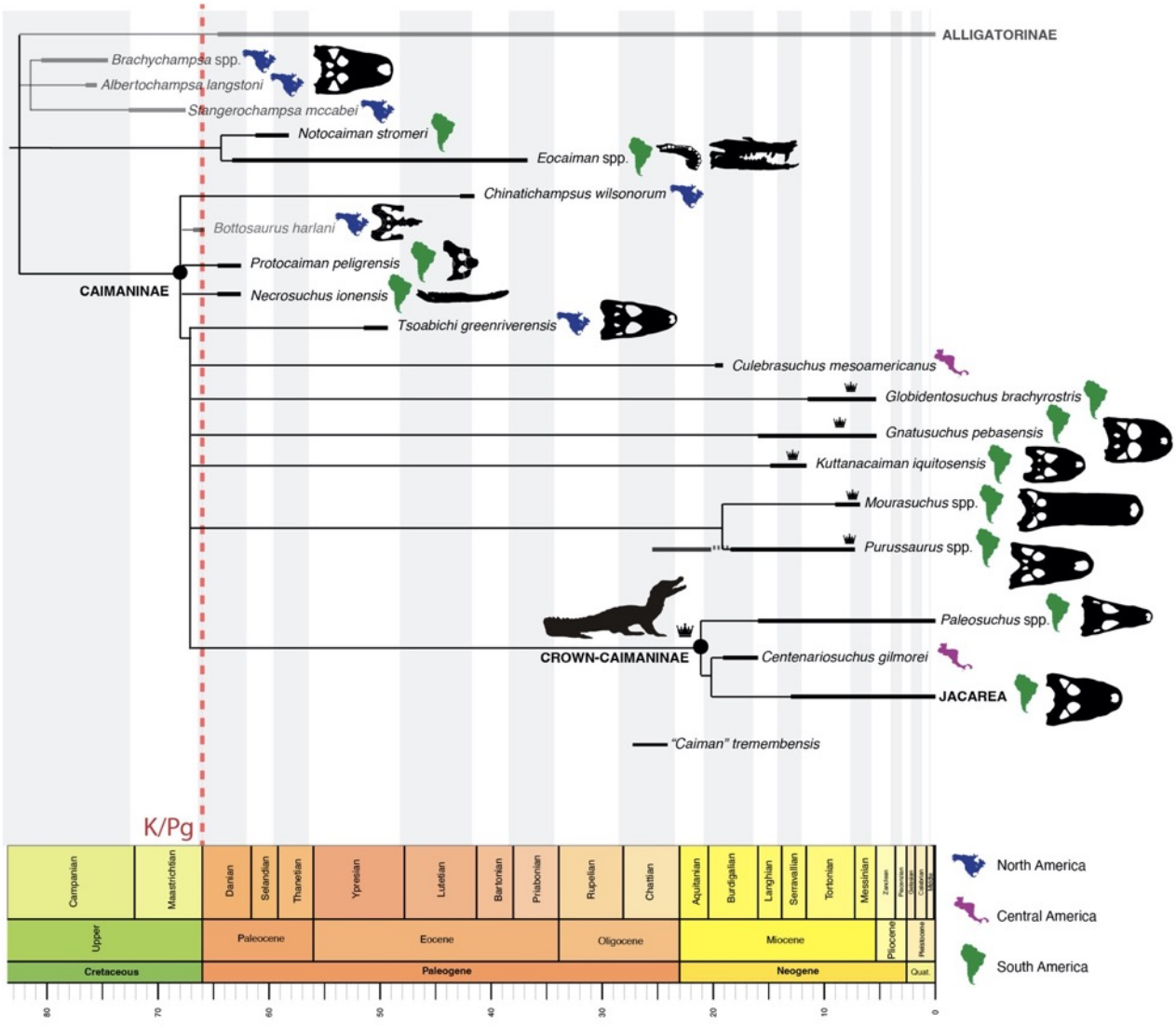

Figure 6. Time-calibrate phylogenetic consensus of Caimaninae modified from Walter et al. (2021) (Chapter 2), indicating the phylogenetic position of taxa as a composition from previously published studies. Crown silhouettes indicates preferred placements of species within crown-Caimaniane. Some silhouettes were modified from Rio & Mannion (2021). This topology is discussed in detail in chapter 2.

In order to avoid biased divergence age estimates based on the selection of fossils with ambiguous phylogenetic relationships, a five steps specimen-based protocol (best practices) have been proposed in order to promote well-justified fossil calibrations (Parham et al., 2012), which includes the following requirements: (i) museum number of specimens, where relevant characters and provenance are listed; (ii) an apomorphy-

based diagnosis of the specimen or explicit phylogenetic analysis including the specimen; (iii) explicit statement on the reconciliation of morphological and molecular data; (iv) specified locality and stratigraphic level from which the calibrating fossil was/were collected; and finally (v) reference to a published radioisotopic age and or/numeric timescale. This protocol accounts for the determination of the youngest possible age (hard minimum), and the soft maximum age, although the last can be rather subjective (Parham et al., 2012; Lee & Palci, 2015). Considering the instability of the Cretaceous taxa (i.e. *Brachychampsa* spp., *Stangerochampsa mccabei*, *Albertochampsa langstoni,* and Orientalosuchina) in respect to Caimaninae, a detailed discussion of the phylogenetic position of early globidontans and their use as fossil calibrations in molecular studies is presented in Chapter 2. A fossil calibration for the total-group Caimaninae is furthermore proposed based on the best-practices.

Regarding the crown-group Caimaninae, unambiguous fossil record traces back to the Miocene of Central and South Americas, including *Centenariosuchus gilmorei* from Panama (Hastings et al., 2013), and the remarkable Miocene diversity of caimanines of the complex aquatic environments of the Pebas Mega-Wetland System in western Amazonia (Hoorn et al., 2010), such as the giant predator *Purussaurus* spp. (Aguilera et al., 2006; Aureliano et al., 2015; Paiva et al., 2022), the platirostral *Mourasuchus* spp. (Bocquetin & Souza-Filho, 1990; Cidade et al., 2017; Cidade et al., 2019), and short snouted forms with crushing dentition *Kuttanacaiman iquitosensis*, and *Gnatusuchus pebasensis* (Salas-Gismondi et al., 2015). Further reports might indicate the presence of crown caimanines in the Oligocene of South America, as evidenced by putative *Purussaurus* specimens (Antoine et al., 2016; Solórzano et al., 2018) and "*Caiman*" *tremembensis* (Chiappe, 1988), although further analyses are required to evaluate the taxonomy and phylogenetic position of those specimens.

Phylogenetic analyses that are at some level derived from the dataset of Brochu (1999, 2010) have recovered Late Cretaceous to Eocene species from North and South America (*Orthogenysuchus olseni*, *Bottosaurus harlani*, *Necrosuchus ionensis*, and *Tsoabichi greenriverensis*) within the crown-group Caimaninae, particularly closely related to the dwarf caiman, *Paleosuchus* spp. (Bona, 2007; Brochu, 2011; Hastings et al., 2013; Pinheiro et al., 2013; Bona et al., 2018; Cossette & Brochu, 2018; Souza-Filho et al., 2018; Souza-Filho et al., 2020; Cidade et al., 2020; Cossette, 2020; Godoy et al., 2020; Stocker et al., 2021). Nonetheless, the position of these taxa has been reported as unstable with respect to the crown by other studies (Brochu, 2010, 2011; Cidade et al., 2020; Cossette, 2020). The phylogenetic context of these Late Cretaceous-Early Paleogene taxa is of extreme relevance for understanding the origin and biogeography of crown-Caimaninae, especially regarding those of North America provenance (i.e. *Orthogenysuchus olseni,* and *Tsoabichi greenriverensis*).

The distribution and age of outgroup taxa (i.e. Alligatorinae and early divergent alligatoroids) in combination with early stem-caimanine *Chinatichampsus wilsonorum* in North America (Middle Eocene, Stocker et al., 2021) suggests the origin and dispersal of Caimaninae from North to South America during the latest Stages of the Cretaceous Period, as furthermore evidenced by the presence of unambiguous early caimanines in the Paleocene of southern South America (i.e. *Eocaiman paleocenicus*, *Necrosuchus ionensis*, *Notocaiman stromeri*, and *Protocaiman peligrensis*; Brochu, 1999, 2020, 2011; Hastings et al., 2013; Bona et al., 2018; Rio & Mannion, 2021). Additionally, previous studies also suggest that a relict population derived from the first dispersal event of caimanines from North to South America would be present in Central America and/or northern South America based on a stem phylogenetic position of the Miocene *Centenariosuchus gilmorei, Culebrasuchus mesoamericanus*, and

Globidentosuchus brachyrostris, which in turn were suggested to be ancestral to South American Caimaninae (Hastings et al., 2013; Hastings et al., 2016). However, the origin and paleobiogeographical patterns in both total and crown groups are still uncertain considering (i) poor stratigraphic fit of phylogenies (and stratigraphic gap in the fossil record) (Salas-Gismondi et al., 2015; Hastings et al., 2016; Bona et al., 2018; Cidade et al., 2020; Cossette, 2020; Stocker et al., 2021; Rio & Mannion, 2021); (ii) poorly-justified selection of fossil as calibration for divergence age estimates in molecular studies (e.g. Bittencourt et al., 2019; Roberto et al., 2020); (iii) ambiguous divergence age estimates (Oaks, 2011; Pan et al., 2020); and (iv) conflicting phylogenetic position of relevant taxa such as *Brachychampsa* spp., *Necrosuchus ionensis*, *Tsoabichi greenriveresnsis*, *Bottosaurus* spp., *Globidentosuchus brachyrostris*.

Particularly, the phylogenetic position of *Tsoabichi greenriverensis* (Eocene of North America, Brochu, 2010) is highly relevant regarding the spatio-temporal origin of crown-caimanines, as *Tsoabichi greenriverensis* within the crown suggests a back dispersal from South to North America (Brochu, 2010, 2011; Hastings et al., 2013; Bona et al., 2018; Cossette, 2020), in order to justify the presence of the group already by the early Eocene of North America (Bona et al., 2018; Cossette and Brochu, 2018; Massonne et al., 2019; Cossette, 2020).

In Chapter 2, new specimens of *Tsoabichi greenriveresnsis* including a juvenile and a larger/subadult individual are described in order to investigate the morphology and phylogenetic relationships of the North American Eocene species in respect to crown-caimanines. The morphological knowledge of *Tsoabichi greenriverensis* is expanded in addition to a detailed revision of the character scoring of the species in the dataset. A comprehensive revision of the phylogenetic affitnities of fossil taxa to total and crown Caimaninae is provided, as well as new inputs on the pelobiogeography of

the group. Finally, well-justified fossil calibrations for both total and crown Caimaninae are provided by following the best practices specimen-based protocol.

3.2 Objectives of Chapter 2

- To describe and illustrate new specimens of *Tsoabichi greenriverensis* from the Eocene of North America;
- To revise the character scorings of *Ts. greenriverensis* in the dataset and perform a phylogenetic analysis under parsimony approach;
- To discuss the affinities of *Ts. greenriverensis* with crown-caimanines, including discussion on character support and character evolution;
- To provide in detail a review of the phylogenetic support for fossil caimanines in a composite approach, uniting the results of the present phylogenetic analysis with previously published data;
- To discuss the paleobiogeographical hypothesis of total and crown Caimaninae, also based in a composite approach of the new results of the present phylogenetic analysis in combination with hypothesis of previous published studies;
- To provide well-justified fossil calibrations for total and crown Caimaninae for divergence age estimates, in addition to discuss the impact of unreasonable selection fossil calibrations on the age of caimanines.

3.3 Main findings and discussion

Evidence for a placement of *Tsoabichi greenriveresnsis* in the crown-group Caimaninae is weak, as morphological characters drawing the species into the crown may in fact diagnose a more inclusive clade. Additionally, the results of the phylogenetic analysis

regarding Miocene taxa from Central and South America (i.e., *Centenariosuchus gilmorei*, *Kuttanacaiman iquitosensis*, *Globidentosuchus bachyrostris*) support the placement of these species in the crown-group. The study of chapter 2 reinforces that there is no clear evidence for Cretaceous taxa (*Stangerochampsa mccabei*, *Brachychampsa* spp., and *Albertochampsa langstoni*) belonging to the crown-Caimaninae as those taxa show weak caimanine affinities. Additionally, together with *Bottosaurus harlani* (Late Cretaceous/early Paleocene of North America), these taxa do not show unique Caimaninae synapomorphies, and *Brachychampsa* spp. should not be used to calibrate clades less inclusive than Crocodylia. A well-justified and reasonable fossil calibration is otherwise proposed by following the best practices of Parham et al. (2012): based on the presence of key-Caimaninae synapomorphies leading to a robust phylogenetic position in Caimaninae, *Necrosuchus ionensis* and *Protocaiman peligrensis*, both from the earliest Paleocene Salamanca Formation (Patagonia, Argentina) represent reasonable fossil calibrations for the total-group Caimaninae, setting a hard-minimum age constraint of 63.5Ma (early to middle Danian, early Paleocene) based on biostratigraphic, radioisotopic and paleomagnetic data (Clyde et al., 2014). This fossil constraint is explicitly justified and may play an important role in establishing age estimates of future divergence data analyses of Caimaninae, as well as Alligatoridae.

An obstacle on the selection of fossil calibrations is still setting a maximum possible age for a clade. The determination of soft-maximum age is rather subjective (Lee & Palci, 2015) as it relies on arbitrary selection of an older age than the oldest possible fossil record of the group, embracing the time when ecologic, biogeographic, geologic and taphonomic conditions met, but no fossils are known (Parham et al., 2012). In the case of a soft-maximum for the total-group Caimaninae, *Brachychampsa*

sealeyi cannot be excluded as it represents the oldest species ever considered a potential Caimaninae (e.g. Salas-Gismondi et al., 2015; Bona et al., 2018; Cossette, 2020; Sotcker et al., 2021), although it is more likely to occupy a basal position in Alligatoroidea. Thus, a conservative soft maximum for the total-group Caimaninae is set as 83 Ma (Santonian-Campanian boundary).

Regarding the crown-group Caimaninae, the oldest well-dated record of unambiguous crown-caimanine is represented by *Centenariosuchus gilmorei* from the early Miocene of Central America (Cucaracha Formation, Panama; Hastings et al., 2013), in which radioisotopic estimations based on 40 Ar/39Ar recovered an age of 18.96 ± 0.90 Ma, a value similar to U-Pb zircon estimates (18.81 ± 0.30 Ma) (MacFadden et al., 2014). Thus, a hard-minimum age of the crown-group can be set as 18.09 Ma. Considering that no convincing crown fossils are known from rocks older than the Neogene, a conservative soft-maximum age for crown-Caimaninae is suggested at the K-Pg boundary (66 Ma).

The new calibration is expected to provide considerably younger estimates for crown-Caimaninae compared to previously published estimates of 61.9 Ma (Roberto et al., 2020) and 60 Ma (Bittencourt et al., 2019), as these studies have unjustifiably used *Brachychampsa sealeyi* (77.9 – 83.6 Ma) to calibrate the crown-group. As discussed above, *Brachychampsa sealeyi* should not be used to calibrate clades less inclusive than Crocodylia considering the lack of caimanine affinities. On the other hand, more reasonable age estimates for crown-Caimanine have been suggested by the molecular studies of Roos et al. (2007) (crown-Caimaninae age estimate of 39Ma) and Oaks (2011) (crown-Caimaninae age estimate of 25.3 Ma), studies in which have calibrated Alligatoridae with an age interval of 71 – 66 Ma based on the relationships of the oldest known alligaotorinae *Stangerochampsa mccabei* in relation to Alligatoridae, as

proposed by Reisz (2005). Finally, when *Brachychampsa sealeyi* is used to calibrate Crocodylia (Pan et al., 2020), the age of the crown was estimated to 36.1 Ma, a similar result to those of the total-evidence tip-dating analysis of Lee & Yates (2018), which estimated ca. 35 Ma for crown Caimaninae. Regardless, molecular studies should employ *Centenariosuchus gilmorei* as the new well-justified calibration for crown-caimaninae, as the age of the crown remains poorly constrained.

The study of chapter 2 shows that unambiguous crown-caimanines have always been restricted to South and Central America, as well as the earliest unambiguous total-group caimanines are from the earliest Paleocene of South America. The origin of Caimaninae took place in North America as supported by the distribution of outgroup taxa and by the early stem-caimanine *Chinatichampsus wilsonorum*, followed by a rapid dispersal to South America during the Late Cretaceous/earliest Paleogene as evidenced by *Necrosuchus*, and *Protocaiman* in the Paleocene of Argentina. Previous phylogenies uniting *Tsoabichi* with the dwarf caimans (*Paleosuchus* spp.) suggested a back-dispersal from South to North America (Brochu, 2010, 2011; Hastings et al., 2013; Bona et al., 2018; Cossette, 2020) to explain the presence of *Tsoabichi* in the Eocene of North America. However, the comprehensive analysis in Chapter 2 (which finds weak support for *Tsoabichi* in the crown group) supports that a second dispersal of caimanines from North to South America during the Paleogene instead is necessary to explain the origin of crown-Caimaninae. This new inferred dispersal event does not exclude the previous "back-dispersal" of former hypotheses, but it suggests instead the presence of a remnant population of primary North American population to explain the presence of the Eocene caimanines *Tsoabichi greenriverensis*, and *Chinatichampsus wilsonorum*. Additionally, reinterpretation of Miocene Central and South American caimanines (*Centenariosuchus*, *Gnatusuchus*, *Kuttanacaiman*) in chapter 2 furthermore

suggest a crown position for these taxa, which represents a more consistent hypothesis considering the stratigraphic distribution and character evidence. Based on both extinct and extant diversity and previously published phylogenetic analyses, in addition to the results of chapter 2, a South American origin of the crown Caimaninae is supported with a dispersal to Central America no later than the early Miocene (contra previous hypotheses of Hastings et al., 2013; Hastings et al., 2016). However, a 24 Myr gap on Caimaninae fossil record (between middle Eocene to early Miocene) hampers more precise constraint of the origin of the crown group, and a revision of *Culebrasuchus mesoamericanus* is still in need. Finally, additional fossil caimanine from late Paleogene and early Neogene of South America are essential for a better constrained estimation of the origin of crown-Caimaninae.

3.4 Concluding remarks

- The study of Chapter 2 represents the most up-to-date review of the phylogenetic relationships of fossil caimanines;
- Taxa such as *Stangerochampsa mccabei, Brachychampsa* spp., *Albertochampsa langstoni,* and *Bottosaurus harlani* do not show unique Caimaninae morphology, and are recovered at the base of Alligatorinae in the analysis of Chapter 2. Phylogenetic support of those species as caimanines is weak, therefore they should not be used as fossil constraints for molecular divergence studies. Furthermore, the unstable phylogenetic position of these taxa occupying a basal position in major alligatorid clades compromises our understanding of charactered evolution in Alligatoroidea;

- The descriptions of new specimens of *Tsoabichi greenriveresnsis* contributed to confirm the taxonomic identity of the taxon and furthermore allowed the identification of additional character supporting its caimanine affinity;
- Phylogenetic support for *Tsoabichi greenriverensis* as a crown-caimanine on the other hand is weak, as synapomorphies responsible to drawing the species into the crown-group diagnose a more inclusive clade instead;
- In the phylogenetic analysis of chapter 2, Miocene Central American taxa (*Globidentosuchus gilmorei*, *Centenariosuchus gilmorei*) are reinterpreted as crown-caimanines instead of members of the stem-lineage, suggesting a northward expansion of the South American crown-Caimanine (contra the hypothesis of being interpreted as ancestral of South America caimanines of Hastings et al., 2013; Hastings et al. 2016);
- Well-justified fossil calibrations for the total and crown Caimaninae were selected by following the best practices specimen-based protocol of Parham et al. (2012): 1 – *Necrosuchus ionensis* and *Protocaiman peligrensis* from the early Paleocene of Argentina constraining a minimum age for the total group at 63.5 Ma, as similarly *Centenariosuchus gilmorei* from the early Miocene of Panama constrains the minimum age of the crown group at 18.09 Ma. These ages are consistent with some estimates of previously published molecular studies, however divergence ages in Caimaninae remains poorly constrained by both molecular estimates and fossil record. New fossil discoveries from the Eocene to Miocene and the use of the new proposed calibrations in molecular studies are essential for improving divergence age estimates and our understanding on the early Caimaninae evolution;

- Based on the phylogenetic analysis and review in chapter 2, two dispersal events of Caimaninae from North to South America (i.e. 1 – during the Late Cretaceous/earliest Paleogene based on North American outgroup caimaninae taxa and unambiguous caimanines from the early Paleocene of southern South America; and 2 – during the middle Paleocene from a remnant population of primarily North American caimanines) are proposed as equally likely hypothesis as back dispersal from South to North America (i.e. to explain the presence of Eocene caimanines in North America) adding to the paleobiogeography of total and crown Caimaninae.

4. Summary of Chapter 3

4.1 Framework

Evolutionary history of the Chinese alligator (*Alligator sinensis*)

Alligator species compose the major clade Alligatorinae (i.e. clade that includes *Alligator mississippiensis* (the American alligator) and all crocodylians closer to it than to *Caiman crocodilus*; *sensu* Brochu, 2003). The phylogenetic relationships of *Alligator* species are commonly resolved, representing a monophyletic group (Brochu 1997, 1999, 2004; Massonne et al., 2019; Rio & Mannion, 2019; Hastings et al., 2023; Figure 7). Whereas *Alligator* is currently represented by two species (the American and the Chinese alligators, *A. mississippiensis* and *A. sinensis*, respectively), a higher diversity were present in the past, as evidenced by the almost exclusive North American *Alligator* fossil record, including *A. prenasalis* (late Eocene- early Oligocene), *A. olseni* (early Miocene), and *A. mcgrewi* (middle Miocene), species often recovered in a basal position in *Alligator* (Brochu 1999, 2004; Stout, 2020; Rio & Mannion, 2021; Hastings et al., 2023), and *A. thomsoni* (middle Miocene), *A. mefferdi* (middle Miocene-Pliocene), and *A. hailensis* (Pliocene) (Brochu, 1999; Stout et al., 2020; Hastings et al., 2023), usually composing the crown-group *Alligator* (i.e. clade that includes the most common recent ancestor of *A. mississippiensis* and *A. sinensis* and all of its descendents) (Brochu, 1999; Stout, 2020; Rio & Mannion, 2021, Hastings et al., 2023). In marked contrast, the *Alligator* fossil record in Asia is scarce but no less important, including an articulated skeleton of *A. luicus* Li & Wang, 1987 from the Miocene of China; an altirostral short-snouted skull referred to *A*. cf. *sinensis* from the late Miocene/Pleistocene of Thailand (Claude et al., 2011); fragmentary remains of *A. sinensis* from the Pliocene of Japan (Iijima et al., 2016), and a near-complete skull from the Pleistocene of Taiwan referred to *A. sinensis* (‘Penghu’ alligator, Shan et al., 2013)

(Figs. 8–9). None of these fossils from Asia have been included in a phylogenetic framework, hence their relationships with the extant and extinct diversity of *Alligator* remain unknown (Brochu 1999, 2004; Massonne et al., 2019; Rio & Mannion, 2021).

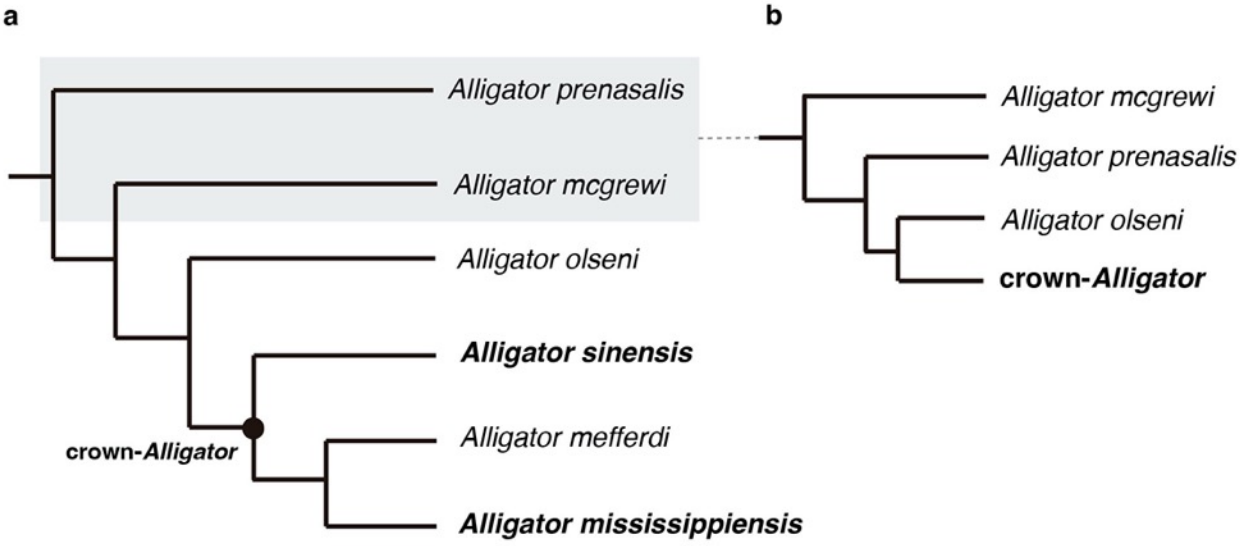

Figure 7. Phylogenetic relationships of *Alligator* based on the topology of (**a**) Brochu (1999), and (**b**) Rio & Mannion (2021), indicating the alternative position of early divergent taxa. Extant *Alligator* species are indicated in bold.

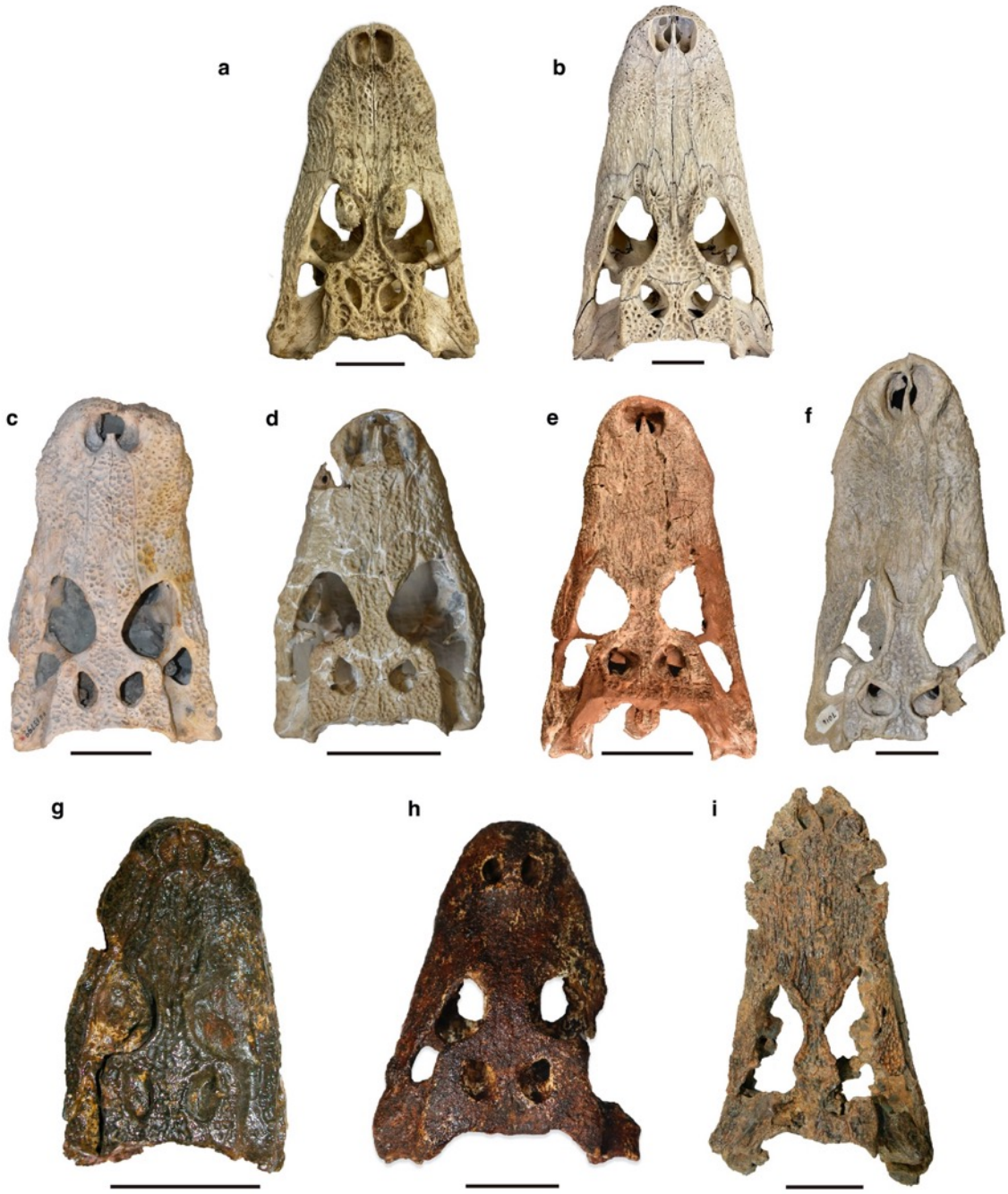

Figure 8. Skulls of *Alligator* species in dorsal view. (**a**) *Alligator sinensis* (SNSB 178/1947); (**b**) *Alligator mississippiensis* (SZ 1057)*;* (**c**) *Alligator prenasalis* (YPM PU 13799); (**d**) *Alligator mcgrewi* (holotype, FMNH P26242); I *Alligator olseni* (MCZ 1899); (**f**) *Alligator mefferdi* (holotype, AMNH 7016); (**g**) *Alligator luicus* (LPM, 850001); (**h**) 'Penghu' *Alligator* (NMNS006394-F051722)*;* (**i**) *Alligator* cf. *sinensis* (DMR-BSL-2011-2). Photos credits: Giovanne Cidade (c–f), Christopher Brochu (g), and Xiao-Chun Wu (i). Scale bars: 5 cm.

The timing and climatic context of *Alligator* dispersal from North America to Asia is poorly constrained (Brochu, 1999; Snyder, 2007; Oaks, 2011; Shan et al., 2013; Wang et al., 2016; Massonne et al., 2019). Early divergence age estimates between the American and Chinese alligator species by molecular clocks studies suggests ca. 58 – 31 Ma (Oaks, 2011; Pan et al., 2020), however the stratigraphic gap/lack of crown fossils earlier then 14 Ma. Is inconsistent with the molecular estimates (i.e. earliest crown-*Alligator* species *A. thomsoni* ca. 14 Ma Mook & Thomson, 1923; Brochu, 1997; Massonne et al., 2019. (Here, *A. thomsoni* and *A. hailensis* are not included in the phylogenetic analysis, however it will be incorporated in the future time-scaled analysis). The dispersal of *Alligator* from North America to Asia might have occurred via Beringia Land Bridge (Brochu, 1999; 2003; Massonne et al., 2019; Rio & Mannion, 2021), as the lack of salt glands in alligatorids weakens the hypothesis of overseas dispersal (Taplin & Grigg, 1989), in addition to weak support for phylogenetic relationships between European alligatorines and A*lligator* spp. (Brochu, 1999; Rio & Mannion, 2021). However, dispersal through Beringia might have occurred under favorable climatic conditions considering the crocodylian minimum limit of median annual temperature (MAT) of 14.2°C (Markwick, 1998). Despite the fact that populations of the Chinese alligator have a wider latitudinal range compared to other crocodylians (Thorbjarnarson & Wang, 2010), prolonged exposure to cold temperatures may still cause death (Brisbin et al., 1982; Thorbjarnarson & Wang, 2010; Grigg & Kirschner, 2015). Nevertheless, the timing of *Alligator* dispersal from North America to Asia via Beringia remains unclear and a time-scaled phylogeny including *Alligator* species from Asia are essential to better understand *Alligator* biogeography.

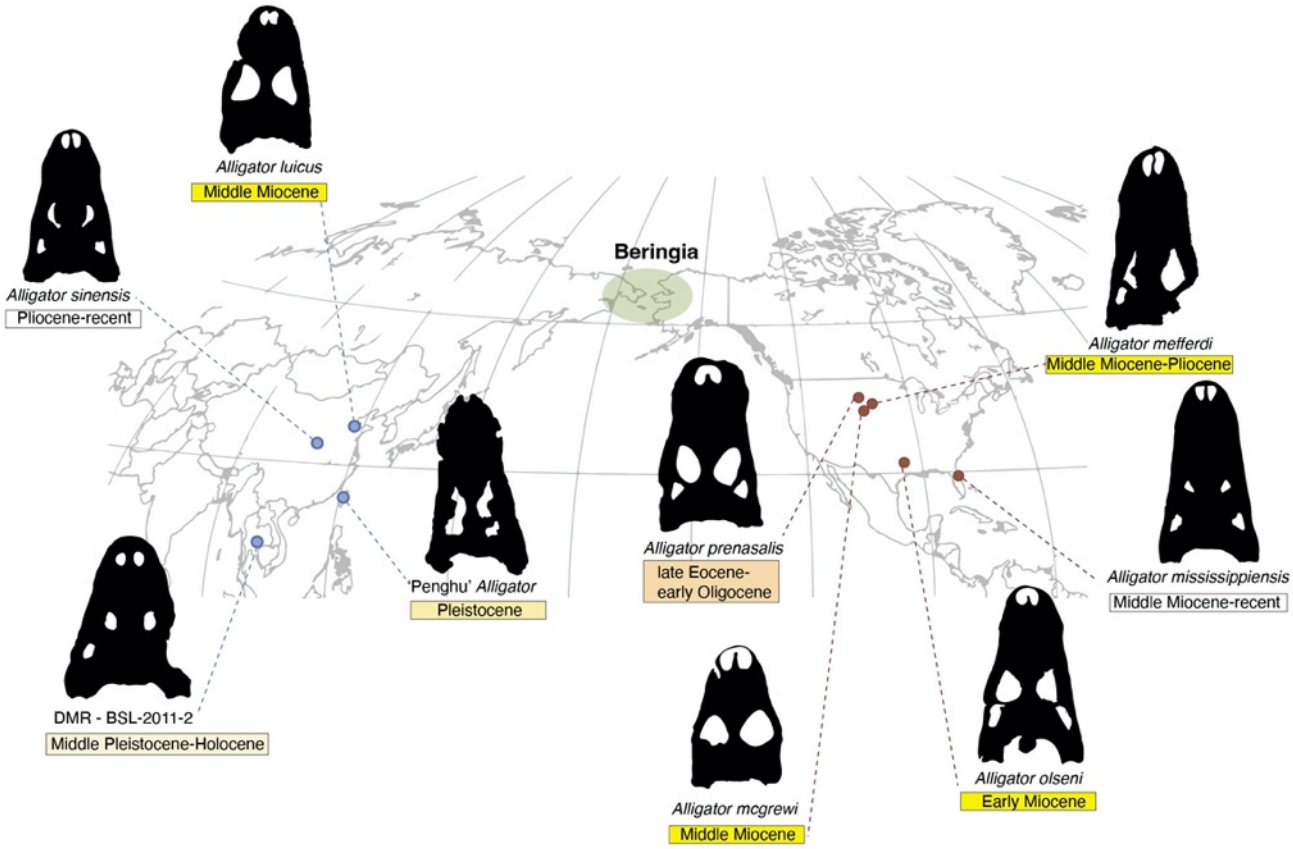

Figure 9. Distribution of extant and extinct *Alligator* species across North America (red dots) and Asia (blue dots). Age of the species are indicated below the silhouettes. Beringia Land Bridge is indicated by the green circle. World map modified from Wikimedia commons (under the license CC-BY-SA-3.0; https://shorturl.at/gzEJU).

Particularly, the skull refereed as *A*. cf. *sinensis* from northeastern Thailand preliminarily reported by Claude et al. (2011) (DMR-BSL-2011-2) is described in detail in Chapter 3 (including CT-scan imaging) and it is furthermore extensively compared with all *Alligator* species. Claude et al. (2011) noted similarities between the well-preserved skull with the extant *A. sinensis* as well as its distinctly robust and short snout, but the need for further preparation of the fossil (not possible at the time) precluded a detailed description at the time. Nevertheless, the occurrence in Thailand considerably expanded the previously known distribution of *Alligator* in Asia,

suggesting complex paleobiogeographic of history (Claude et al., 2011). The description of this material in Chapter 3 contributes significantly on expanding comparative morphological data for comprehensive phylogenetic study of *Alligator* species, critical for reconstructing the biogeographical history of the clade. Furthermore, fossil *Alligator* specimens from Asia (i.e. articulated skeleton of *A. luicus* from the Miocene of China; and the near-complete skull from the Pleistocene of Taiwan referred to *A. sinensis*), besides the *Alligator* skull from Thailand are for the first time incorporated into a phylogenetic analysis.

4.2 Objectives of Chapter 3

- to describe in detail the *Alligator* skull (DMR-BSL-2011-2) from the Quaternary of Thailand with assistance of computed tomography and 3D digital reconstruction, and compare it in detail with all extant and extinct *Alligator* species in order to determine the taxonomic identity of the specimen;
- to incorporate the specimen DMR-BSL-2011-2, in addition to other fossil *Alligator* from Asia (i.e. *A. luicus*, and 'Penghu' alligator) for the first time into a phylogenetic framework under Parsimony using the most recent and reviewed dataset for crocodylians (Rio & Mannion, 2021);
- to discuss the relationships within *Alligator* clade and how the new results of the phylogenetic analysis contribute to the paleobiogeographic inferences in *Alligator*, specifically regarding the dispersal of *Alligator* from North America to Asia;

4.3 Main findings and discussion

Based on an extensive morphological description of the well-preserved skull from the Quaternary of Thailand, several autapomorphic characters warrant the designation of a

new species of *Alligator* (*Alligator munensis* sp. nov.). Detailed morphological comparison among all *Alligator* species (extinct and extant) derived from the comparative description sheds light into previously unknown morphological affinities among species, specifically regarding the Asian *Alligator* fossil record with respect to the Chinese alligator. The phylogenetic analysis under parsimony approach for the first time retrieved a clade that includes *A. sinensis* and *Alligator* extinct species from Asia (*A. luicus*, *A. munensis*, and the 'Penghu' alligator), as well as Miocene taxa from North America, as *A. mcgrewi* and *A. olseni*. The Early Miocene *A. olseni* is recovered as the first divergence of the "*A. sinensis*-clade", followed by a subsequent phylogenetic position of the 'Penghu alligator' and *A. sinensis*. In a more derived position, the mid-Miocene *A.luicus* recovered as sister group to a clade composed by *A. mcgrewi* (Middle Miocene of North America) and *A. munensis* (Pleistocene to Holocene of Thailand). The close relationship between *A. munensis* and *A. munensis* is intriguing because of age discrepancy, although both taxa sharing clear synapomorphies (i.e. angle between the dorsal profile of the paroccipital process and dorsal margin of the cranial table more than °50; C109: 1→2). *A. olseni* at the base of the "*A. sinensis*-clade" suggests cladogenetic events taking place in North America in Early Miocene, preceding a dispersal to Asia, whereas the derived position of *A. mcgrewi* suggests a back dispersal of *Alligator* to North America still in early Stages of the Miocene, representing a complex biogeographic history for the lineage. However, the back dispersal suggested by the present phylogeny needs to be further tested under total-evidence tip dating analysis (in preparation), as the synapomorphy uniting *A. mcgrewi* and *A. munensis* might be optimized differently considering that tip-dating is expected to identify it as a homoplasy instead (Lee & Yates, 2018; Darlim et al., 2022). Thus, an early divergent

phylogenetic position of *A. mcgrewi* would be more likely to explain the relationships of this species within the "*A.sinensis*-clade".

Nevertheless, considering a dispersal of *Alligator* from North America to Asia via Beringia, climatic factors are still problematic as during most part of the Cenozoic global temperatures were too low therefore incompatible with crocodylian minimum limit of Mean Annual Temperature (MAT) of 14.2°C (Markwick, 1998). Available periods in which the temperatures of high latitudes are more consistent with a dispersal to Asia via Beringia, and with crocodylians minimum MAT limit, are evidenced during the Early Eocene artic (MAT variation of 17 – 14.1°C in Ellesmere Island, West et al., 2015); or during the Middle Miocene Climatic Optimum, as MAT in Alaska during this period was estimated to reach between 19.3 – 23.5°C (based on bivalve stable O isotopes, Oleinik et al., 2008). Particularly, a dispersal via Beringia during the Miocene Climatic Optimum represents a potential hypothesis to explain the *Alligator* dispersal to Asia, as this time window of warmer temperatures overlaps with the topology recovered in the present phylogenetic analysis, considering paleontological evidence of *Alligator* in Asia (*A. luicus*) during the Middle Miocene, in addition to with early divergent North American representatives (*A. olseni,* and potentially *A.mcgrewi*) showing phylogenetic affinities with *Alligator* species from Asia (i.e. compose the "*A. sinensis*-clade"). However, this hypothesis can only be further investigated after time-scaling the *Alligator* topology, specifically under total-evidence tip dating approach, as divergence age estimates retrieved from tip-dating analyses will provide better constrained divergence age estimates within the *Alligator* clade, which is essential to fit into the temporal and climatic factor to investigate *Alligator* dispersal.

Regarding the biogeography of *Alligator* within Asia, the unexpected presence of an alligatorid in northeastern Thailand requires explanation (Claude et al., 2011). The

tentative referral of DMR-BSL-2011-2 to *A.* cf *sinensis* posed a biogeographic enigma because the geographically closest historical occurrences of *A. sinensis* come from the Yangtze and Xi river systems (Thorbjarnarson and Wang, 2010; Pan et al., 2019) that only approach the Mekong and Chao Phraya systems of Thailand along their upper sections at high elevations, unfavourable for alligators (Claude et al., 2011). Nevertheless, as we here demonstrate, the specimen DMR-BSL-2011-2 confidently represents a separate species albeit with close affinities particularly to *A. mcgrewi* and *A. luicus*, as these species occupy a more derived position in comparison to *A. sinensis* (Fig. 9). The highly distinct morphology of *A. munensis* is furthermore consistent with relatively deep divergence from *A. sinensis*. If that is the case, the presence of *Alligator* in Thailand may be explained by the presence of a common ancestor of *A. munensis, A. luicus, A. mcgrewi,* and *A. sinensis* distributed in the lowlands of both the proto Yangtze-Xi and Mekong-Chao Phraya river systems that was subsequently split into separate, vicariant species due to the accelerated Miocene uplift of the eastern Tibetan Plateau, fully hindering dispersal between these drainage basins. The Mun river, the locality of the *A. munensis* specimen described herein, feeds the Mekong today but was connected to the proto-Chao Phraya river in the past (Hutchison, 1989; Brookfield, 1998; Breitfeld et al., 2022).

Although temporal inconsistency is present in the retrieved close relationship between *A. mcgrewi* and *A. munensis*, relevance of the results of the present phylogenetic analysis is acknowledged by the presence of Miocene taxa from both North America and Asia composing the "*A. sinensis*-clade", contributing on reducing the temporal gap otherwise inferred by the molecular estimates of the *A. mississippiensis–A. sinensis* split (Oaks, 2011; Pan et al., 2020). A time-scaled phylogeny is being prepared by the candidate of this thesis in order to evaluate the

dispersal of *Alligator* from North America to Asia. As discussed in chapter 1, total-evidence tip-dating analysis have the advantage of simultaneously generating divergence age estimates and topology by analysing morphological, molecular, and stratigraphical (age) data. As observed by the phylogenetic relationships of thoracosaurs being adjusted regarding the stratigraphic age of these taxa compared to fossil gavialines (Lee& Yates, 2018; Chapter 1), tip-dating approach is expected to similarly adjust the phylogenetic position of *A. mcgrewi* regarding the stratigraphic age of this species and test whether the synapomorphies uniting *A. mcgrewi* and *A. munensis* fulfill the homology criteria. Tip-dating analysis is furthermore expected to better constrain the divergence age estimates within *Alligator* (total and crown groups) allowing a more precise comparison between the divergence estimates with the available warm periods compatible with the minimum MAT tolerance of crocodylians (i.e. 14.2°C). As discussed above, special attention is drawn to the hypothesis of a dispersal during the Miocene Climatic Optimum, as it is most consistent with the *Alligator* fossil record (presence of *A. luicus* in the Middle Miocene of China), thus contributing to the understanding of *Alligator* paleobiogeography regarding both North America-Asia, and within-Asia dispersal events.

The study presented in chapter 3 is contributes significantly as an essential source of much needed morphological data, based on extensive morphological comparison among *Alligator* species. Furthermore, it highlights the importance of fossil material from Asia in order to the understand *Alligator* evolution, especially contributing to a better comprehension of the origin of the Chinese alligator, as for the first time, a phylogenetic analysis included species from Asia and recovered them composing a clade with *A. sinensis*.

4.4 Concluding remarks

- The specimen DMR-BSL-2011-2, a well-preserved skull from the Quaternary of Thailand, shows clear distinct morphology strongly supporting it to be assigned as a new species, *Alligator munensis*;
- The phylogenetic analysis of the study in chapter 3 represents a novelty in *Alligator* systematics as it includes for the first time extinct *Alligator* species from Asia, as *A. luicus* (Middle Miocene of China), *A. munensis* (middle Pleistocene-Holocene of Thailand) and the 'Penghu' alligator (Pleistocene of Taiwan), which in turn were recovered closely related composing a clade with *Alligator sinensis*. Furthermore, North American taxa as *Alligator olseni* (Early Miocene), and *Alligator mcgrewi* (Middle Miocene) are recovered more closely related to *Alligator* species from Asia then to the American alligator *A. mississippiensis*;
- *Alligator* species from North America and Asia composing a clade ("*A. sinensis*-clade"), contributes on reducing the temporal gap otherwise inferred by the molecular estimates of the *A. mississippiensis–A. sinensis* split (i.e. 31.3 Ma – 58.2 Ma);
- The presence of *A. olseni* at the base of the "*A. sinensis*-clade" suggests cladogenetic events taking place in North America in Early Miocene, preceding a dispersal to Asia, whereas the derived position of *A. mcgrewi* suggests a back dispersal of *Alligator* to North America still in early Stages of the Miocene, representing a complex biogeographic history for the lineage;
- A dispersal via Beringia during the Miocene Climatic Optimum (MAT in Alaska during this period was estimated to reach between 19.3 – 23.5°C, compatible with crocodylian minimum MAT limit of 14.2°C) represents a

potential hypothesis to explain the *Alligator* dispersal from North America to Asia, as this time window of warmer temperatures overlaps with the topology recovered in the present phylogenetic analysis, considering paleontological evidence of *Alligator* in Asia (*A. luicus*) during the Middle Miocene, in addition to with early divergent North American representatives (*A. olseni,* and potentially *A.mcgrewi*) showing phylogenetic affinities with *Alligator* species from Asia;

- The recovery of North American fossil taxa in the *A. sinensis* lineage is consistent with but not conclusive for a Miocene dispersal from the lineage to Asia;
- The highly distinct morphology and phylogeny of *A. munensis* is consistent with a deep-divergence from *A. sinensis*, as also evidenced by the new species being recovered in a clade with *A. mcgrewi* and *A. luicus* to the exclusion of *A. sinensis*. If that is the case, the presence of *A. munensis* in Thailand might be explained by a hypothetical common ancestor in the lowlands of the proto-Mekong and Yangtze River drainages, followed by their split after the uplift event of the Tibetan Plateau;
- The Mid Miocene *Alligator* dispersal to Asia and the dispersal events within Asia are going to be further explored under total-evidence tip dating analysis, currently under preparation by the candidate of this thesis. Tip-dating is expected to find a more suitable stratigraphical fit for *A. mcgrewi*, in addition to provide divergence age estimates in *Alligator*, allowing a more comprehensive evaluation of the hypothesized dispersal events discussed in the present thesis.

5. SUMMARY OF CONTRIBUTIONS AND OUTLOOK

The studies presented in chapters 1–3 have contributed to improving the paleontological evidence that are the base for topological inferences in Crocodylia, specifically contributing to the understanding of early divergent lineages of the clade and the interrelationships of the crown-clades in Alligatoridae.

In chapter 1, the incorporation of DNA-informed analysis (either by combining molecular and morphological data, or by reproducing the molecular topology as a scaffold) showed to be critical for understanding and interpreting evolutionary relationships in Crocodylia, directly impacting on the origin and age of the clade, as demonstrated by the results of the eleven performed analyses under different methodologies, including parsimony, undated and dated Bayesian inferences. Specially for dated analysis, the implementation of total evidence tip-dating provides a time-scaled phylogeny (essential for macroevolutionary studies) and is furthermore a promising method for inferring and interpreting crocodylian evolutionary relationships, as evidenced by resulting in more consistent topologies (in terms of stratigraphical age and morphological evolution) in contrast to analyses that otherwise are biased by being restricted to morphology-exclusive datasets.

Contributions of chapter 2 are evidenced by the most up-to-date review of the phylogenetic relationships of fossil caimanines, and a detailed discussion on the negative effects of the selection of fossils as calibrations in published molecular analyses in Caimaninae that does not follow the best practices for justifying such action. A major contribution of this chapter is the determination of the most suitable fossil caimanines (total and crown-groups) as fossil calibrations by following explicitly a specimen-based protocol, contributing to the understanding of major evolutionary patterns in the clade, including paleobiogeography.

Finally, the detailed comparative and alpha-taxonomic description of a new *Alligator* species from Thailand highlighted morphological affinities among certain fossil *Alligator* species with the Chinese alligator that were until now obscured. Additionally, the incorporation of fossil *Alligator* from Asia into a phylogenetic analysis resulted in those species composing the stem-lineage of *A. sinensis*, which represents a novelty in *Alligator* systematics, furthermore contributing to filling the temporal gap (inferred by molecular studies as Oaks, 2011) of the split between the *A. sinensis* and *A. mississippiensis* lineages. The findings of this chapter contribute to better understand the enigmatic origin of the critically endangered *A. sinensis*, as it is the only study to include the most updated paleontological evidence regarding *Alligator* fossils from Asia.

The studies presented in this thesis improve our understanding of crocodylian evolution and communicate with both paleontological and neontological researcher communities by expanding the knowledge of paleontological evidence as well as demonstrating the importance of incorporating molecular evidence into paleontological studies in Crocodylia. Many fossil crocodylian species are still in need of modern descriptions, and a detailed study of those extinct forms are critical for a more comprehensive understanding of morphological evolution and phylogenetic inferences. Furthermore, total evidence tip-dating analysis significantly improves divergence age estimates as it does not require subjective determination of age maxima for particular nodes, and it reasonably determines the position of fossil taxa in accordance with the simultaneous analysis of stratigraphic age and morphology in combination with molecular clock from living representatives. Implementation of tip dating in crocodylian systematics plays an essential role for macroevolutionary and paleobiogeographical

discussions, and should be addressed in future phylogenetic studies of crown crocodilians.

6. REFERENCES

Aguilera, O. A., Riff, D., & Bocquentin-Villanueva, J. (2006). A new giant *Purussaurus* (crocodyliformes, alligatoridae) from the upper Miocene Urumaco formation, Venezuela. *Journal of Systematic Palaeontology*, *4*(3), 221-232.

Antoine, P. O., et al. (2016). A 60-million-year Cenozoic history of western Amazonian ecosystems in Contamana, eastern Peru. *Gondwana Research*, *31*, 30-59.

Aoki, R. (1983). A new generic allocation of *Tomistoma machikanense*, a fossil crocodilian from the Pleistocene of Japan. *Copeia*, 89-95.

Asher, R. J., & Hofreiter, M. (2006). Tenrec phylogeny and the noninvasive extraction of nuclear DNA. *Systematic biology*, *55*(2), 181-194.

Aureliano, T., Ghilardi, A. M., Guilherme, E., Souza-Filho, J. P., Cavalcanti, M., & Riff, D. (2015). Morphometry, bite-force, and paleobiology of the Late Miocene Caiman *Purussaurus brasiliensis*. *PloS one*, *10*(2), e0117944.

Benton, M. J., Donoghue, P. C., Asher, R. J., Friedman, M., Near, T. J., & Vinther, J. (2015). Constraints on the timescale of animal evolutionary history. *Palaeontologia Electronica*, *18*(1), 1-106.

Bittencourt PS, et al. (2019). Evidence of cryptic lineages within a small South American crocodilian: the Schneider's dwarf caiman *Paleosuchus trigonatus* (Alligatoridae: Caimaninae). PeerJ. 7:e6580.

Blanco, A. (2021). Importance of the postcranial skeleton in eusuchian phylogeny: reassessing the systematics of allodaposuchid crocodylians. *Plos one*, *16*(6), e0251900.

Bocquentin, J. C., & De Souza Filho, J. P. (1990). O crocodiliano sul-americano *Carandaisuchus* como sinonímia de *Mourasuchus* (Nettosuchidae). *Brazilian Journal of Geology*, *20*(1), 230-233.

Bona P. (2007). Una nueva especie de *Eocaiman* Simpson (Crocodylia, Alligatoridae) del Paleoceno Inferior de Patagonia. Ameghiniana. 44(2):435–445.

Bona, P., Ezcurra, M. D., Barrios, F., & Fernandez Blanco, M. V. (2018). A new Palaeocene crocodylian from southern Argentina sheds light on the early history of caimanines. *Proceedings of the Royal Society B*, *285*(1885), 20180843.

Brisbin Jr, I. L., Standora, E. A., & Vargo, M. J. (1982). Body temperatures and behavior of American alligators during cold winter weather. *American Midland Naturalist*, 209-218.

Brochu, C. A. (1997). Morphology, fossils, divergence timing, and the phylogenetic relationships of *Gavialis*. *Systematic Biology*, *46*(3), 479-522.

Brochu, C. A. (1999). Phylogenetics, taxonomy, and historical biogeography of Alligatoroidea. *Journal of Vertebrate Paleontology*, *19*(S2), 9-100.

Brochu, C. A. (2003). Phylogenetic approaches toward crocodylian history. *Annual Review of Earth and Planetary Sciences*, *31*(1), 357-397.

Brochu, C. A. (2004). Alligatorine phylogeny and the status of *Allognathosuchus* Mook, 1921. *Journal of Vertebrate Paleontology*, *24*(4), 857-873.

Brochu CA. (2010). A new alligatoroid from the lower Eocene Green River Formation of Wyoming and the origin of caimans. Journal of Vertebrate Paleontology. 30(4):1109–1126.

Brochu CA. (2011). Phylogenetic relationships of *Necrosuchus ionensis* Simpson, 1937 and the early history of caimanines. Zoological Journal of the Linnean Society. 163:S228–S256

Brochu, C. A. (2012). Phylogenetic relationships of Palaeogene ziphodont eusuchians and the status of *Pristichampsus* Gervais, 1853. *Earth and Environmental Science Transactions of the Royal Society of Edinburgh*, *103*(3-4), 521-550.

Brochu, C. A., & Sumrall, C. D. (2020). Modern cryptic species and crocodylian diversity in the fossil record. *Zoological Journal of the Linnean Society*, *189*(2), 700-711.

Busbey, A. B., & Thomason, J. J. (1995). The structural consequences of skull flattening in crocodilians. *Functional morphology in vertebrate paleontology*, 173-192.

Buscalioni, A. D., Ortega, F., & Vasse, D. (1997). New crocodiles (Eusuchia: Alligatoroidea) from the Upper Cretaceous of southern Europe. *Comptes Rendus de l'Académie des Sciences-Series IIA-Earth and Planetary Science*, *325*(7), 525-530.

Buscalioni, A. D., Ortega, F., & Vasse, D. (1999). The Upper Cretaceous crocodilian assemblage from Laño (Northcentral Spain): implications in the knowledge of the finicretaceous European faunas. *Estudios del Museo de Ciencias Naturales de Alava*, *14*(1), 213-233.

Chiappe, L. M. (1988). Un nuevo Caiman (Crocodylia, Alligatoridae) de la Formación Tremembé (Oligoceno), Estado de São Paulo, Brasil, y su significado paleoclimático. *Paula-Coutiana*, *3*, 49-66.

Cidade, G. M., Solórzano, A., Rincón, A. D., Riff, D., & Hsiou, A. S. (2017). A new *Mourasuchus* (Alligatoroidea, Caimaninae) from the late Miocene of Venezuela, the phylogeny of Caimaninae and considerations on the feeding habits of Mourasuchus. *PeerJ*, *5*, e3056.

Cidade, G. M., Riff, D., & Hsiou, A. S. (2019). The feeding habits of the strange crocodylian *Mourasuchus* (Alligatoroidea, Caimaninae): a review, new hypotheses and perspectives. *Revista Brasileira de Paleontologia*, *22*(2), 106-119.

Cidade, G. M., Fortier, D., & Hsiou, A. S. (2020). Taxonomic and phylogenetic review of *Necrosuchus ionensis* (Alligatoroidea: Caimaninae) and the early evolution and radiation of caimanines. *Zoological Journal of the Linnean Society*, *189*(2), 657-669.

Claude, J., et al. (2011). Neogene reptiles of northeastern Thailand and their paleogeographical significance. In *Annales de Paléontologie* (Vol. 97, No. 3-4, pp. 113-131). Elsevier Masson.

Clyde, W. C., et al. (2014). New age constraints for the Salamanca Formation and lower Río Chico Group in the western San Jorge Basin, Patagonia, Argentina: Implications for Cretaceous-Paleogene extinction recovery and land mammal age correlations. *Bulletin*, *126*(3-4), 289-306.

Cossette, A. P., & Brochu, C. A. (2018). A new specimen of the alligatoroid *Bottosaurus harlani* and the early history of character evolution in alligatorids. *Journal of Vertebrate Paleontology*, *38*(4), 1-22.

Cossette, A. P. (2020). A new species of *Bottosaurus* (Alligatoroidea: Caimaninae) from the Black Peaks Formation (Palaeocene) of Texas indicates an early radiation of North American caimanines. *Zoological Journal of the Linnean Society*, *191*(1), 276-301.

Cossette, A. P., & Brochu, C. A. (2020). A systematic review of the giant alligatoroid *Deinosuchus* from the Campanian of North America and its implications for the relationships at the root of Crocodylia. *Journal of Vertebrate Paleontology*, *40*(1), e1767638.

Crawford NG, et al. (2015). A phylogenomic analysis of turtles. *Molecular Phylogenetics and Evolution*, **83**, 250–257. (doi.org/10.1016/j.ympev.2014.10.021)

Dávalos, L. M., Velazco, P. M., Warsi, O. M., Smits, P. D., & Simmons, N. B. (2014). Integrating incomplete fossils by isolating conflicting signal in saturated and non-independent morphological characters. *Systematic Biology*, *63*(4), 582-600.

Delfino, M., Martin, J. E., & Buffetaut, E. (2008). A new species of *Acynodon* (Crocodylia) from the upper cretaceous (Santonian–Campanian) of Villaggio del Pescatore, Italy. *Palaeontology*, *51*(5), 1091-1106.

Delfino, M., & Smith, T. (2012). Reappraisal of the morphology and phylogenetic relationships of the middle Eocene alligatoroid *Diplocynodon deponiae* (Frey, Laemmert, and Riess, 1987) based on a three-dimensional specimen. *Journal of Vertebrate Paleontology*, *32*(6), 1358-1369.

Dickinson, W. R., & Gehrels, G. E. (2009). Use of U–Pb ages of detrital zircons to infer maximum depositional ages of strata: a test against a Colorado Plateau Mesozoic database. *Earth and Planetary Science Letters*, *288*(1-2), 115-125.

Gatesy, J., & Amato, G. D. (1992). Sequence similarity of 12S ribosomal segment of mitochondrial DNAs of gharial and false gharial. *Copeia*, *1992*(1), 241-243.

Gatesy, J., Amato, G., Norell, M., DeSalle, R., & Hayashi, C. (2003). Combined support for wholesale taxic atavism in gavialine crocodylians. *Systematic Biology*, *52*(3), 403-422.

Godoy, P. L., Cidade, G. M., Montefeltro, F. C., Langer, M. C., & Norell, M. A. (2021). Redescription and phylogenetic affinities of the caimanine *Eocaiman cavernensis* (Crocodylia, Alligatoroidea) from the Eocene of Argentina. *Papers in Palaeontology*, *7*(3), 1205-1231.

Green, R. E., et al. (2014). Three crocodilian genomes reveal ancestral patterns of evolution among archosaurs. *Science*, *346*(6215), 1254449.

Grigg, G. (2015). Biology and Evolution of Crocodylians (Cornell University Press, 2015).

Groh, S. S., Upchurch, P., Barrett, P. M., & Day, J. J. (2020). The phylogenetic relationships of neosuchian crocodiles and their implications for the convergent evolution of the longirostrine condition. *Zoological Journal of the Linnean Society*, *188*(2), 473-506.

Harshman, J., Huddleston, C. J., Bollback, J. P., Parsons, T. J., & Braun, M. J. (2003). True and false gharials: a nuclear gene phylogeny of Crocodylia. *Systematic Biology*, *52*(3), 386-402.

Hastings, A. K., Bloch, J. I., Jaramillo, C. A., Rincon, A. F., & Macfadden, B. J. (2013). Systematics and biogeography of crocodylians from the Miocene of Panama. *Journal of Vertebrate Paleontology*, *33*(2), 239-263.

Hastings, A. K., Reisser, M., & Scheyer, T. M. (2016). Character evolution and the origin of Caimaninae (Crocodylia) in the New World Tropics: new evidence from the Miocene of Panama and Venezuela. *Journal of Paleontology*, *90*(2), 317-332.

Hastings, A. K., Schubert, B. W., Bourque, J. R., & Hulbert Jr, R. C. (2023). Oldest record of *Alligator* in southeastern North America. *Palaeontologia Electronica*, *26*(1), 1-19.

Havermans, C., Nagy, Z. T., Sonet, G., De Broyer, C., & Martin, P. (2010). Incongruence between molecular phylogeny and morphological classification in amphipod crustaceans: a case study of Antarctic lysianassoids. *Molecular Phylogenetics and Evolution*, *55*(1), 202-209.

Hoorn, C., Wesselingh, F. P., Hovikoski, J., & Guerrero, J. (2010). The development of the amazonian mega-wetland (Miocene; Brazil, Colombia, Peru, Bolivia). *Amazonia, landscape and species evolution: a look into the past*, *123*, 142.

Iijima, M., Takahashi, K., & Kobayashi, Y. (2016). The oldest record of *Alligator sinensis* from the Late Pliocene of Western Japan, and its biogeographic implication. *Journal of Asian Earth Sciences*, *124*, 94-101.

Iijima, M., & Kobayashi, Y. (2019). Mosaic nature in the skeleton of East Asian crocodylians fills the morphological gap between “Tomistominae” and Gavialinae. *Cladistics*, *35*(6), 623-632.

Janke, A., Gullberg, A., Hughes, S., Aggarwal, R. K., & Arnason, U. (2005). Mitogenomic analyses place the gharial (*Gavialis gangeticus*) on the crocodile tree and

provide pre-K/T divergence times for most crocodilians. *Journal of molecular evolution*, *61*, 620-626.

Kapli, P., Yang, Z., & Telford, M. J. (2020). Phylogenetic tree building in the genomic age. *Nature Reviews Genetics*, *21*(7), 428-444.

Kobayashi, Y., Tomida, Y., Kamei, T., & Eguchi, T. (2006). Anatomy of a Japanese tomistomine crocodylian, *Toyotamaphimeia machikanensis* (Kamei et Matsumoto, 1965), from the middle Pleistocene of Osaka Prefecture: the reassessment of its phylogenetic status within Crocodylia. *National Science Museum Monographs*, *35*, i-121.

Koepfli, K. P., Gompper, M. E., Eizirik, E., Ho, C. C., Linden, L., Maldonado, J. E., & Wayne, R. K. (2007). Phylogeny of the Procyonidae (Mammalia: Carnivora): molecules, morphology and the great American interchange. *Molecular Phylogenetics and Evolution*, *43*(3), 1076-1095.

Ksepka, D. T., et al. (2015). The fossil calibration database—a new resource for divergence dating. *Systematic Biology*, *64*(5), 853-859.

Langston, W. (1975). Ziphodont crocodiles, *Pristichampsus vorax* (Troxell), new combination, from the Eocene of North America.

Laurén, D. J. (1985). The effect of chronic saline exposure on the electrolyte balance, nitrogen metabolism, and corticosterone titer in the American alligator, *Alligator mississippiensis*. *Comparative Biochemistry and physiology. A, Comparative Physiology*, *81*(2), 217-223.

Lee, M. S., & Palci, A. (2015). Morphological phylogenetics in the genomic age. *Current Biology*, *25*(19), R922-R929.

Lee, M. S., & Yates, A. M. (2018). Tip-dating and homoplasy: reconciling the shallow molecular divergences of modern gharials with their long fossil record. *Proceedings of the Royal Society B*, *285*(1881), 20181071.

MacFadden, B. J., Bloch, J. I., Evans, H., Foster, D. A., Morgan, G. S., Rincon, A., & Wood, A. R. (2014). Temporal calibration and biochronology of the Centenario Fauna, early Miocene of Panama. *The Journal of Geology*, *122*(2), 113-135.

Martin, J. E. (2007). New material of the Late Cretaceous globidontan *Acynodon iberoccitanus* (Crocodylia) from southern France. *Journal of Vertebrate Paleontology*, *27*(2), 362-372.

Martin, J. E., & Lauprasert, K. (2010). A new primitive alligatorine from the Eocene of Thailand: relevance of Asiatic members to the radiation of the group. *Zoological Journal of the Linnean Society*, *158*(3), 608-628.

Martin, J. E., Smith, T., de Lapparent de Broin, F., Escuillié, F., & Delfino, M. (2014). Late Palaeocene eusuchian remains from Mont de Berru, France, and the origin of the alligatoroid *Diplocynodon*. *Zoological Journal of the Linnean Society*, *172*(4), 867-891.

Markwick, P. J. (1998). Fossil crocodilians as indicators of Late Cretaceous and Cenozoic climates: implications for using palaeontological data in reconstructing palaeoclimate. *Palaeogeography, Palaeoclimatology, Palaeoecology*, *137*(3-4), 205-271.

Massonne, T., Vasilyan, D., Rabi, M., & Böhme, M. (2019). A new alligatoroid from the Eocene of Vietnam highlights an extinct Asian clade independent from extant *Alligator sinensis*. *PeerJ*, *7*, e7562.

Mateus, O., Puértolas-Pascual, E., & Callapez, P. M. (2019). A new eusuchian crocodylomorph from the Cenomanian (Late Cretaceous) of Portugal reveals novel implications on the origin of Crocodylia. *Zoological Journal of the Linnean Society*, *186*(2), 501-528.

Miller, K. G., Fairbanks, R. G., & Mountain, G. S. (1987). Tertiary oxygen isotope synthesis, sea level history, and continental margin erosion. *Paleoceanography*, *2*(1), 1-19.

Mook, C. C., & Thomson, A. (1923). *A new species of Alligator from the Snake Creek beds*. By order of the Trustees of The American Museum of Natural History.

Müller J, Reisz RR. 2005. Four well-constrained calibration points from the vertebrate fossil record for molecular clock estimates. Bioessays. 27(10):1069–1075.

Narváez, I., Brochu, C. A., Escaso, F., Pérez-García, A., & Ortega, F. (2015). New crocodyliforms from southwestern Europe and definition of a diverse clade of European Late Cretaceous basal eusuchians. *PLoS One*, *10*(11), e0140679.

Norell, M. A. (1989). The higher level relationships of the extant Crocodylia. *Journal of Herpetology*, 325-335.

Norell, M., Clark, J. M., & Hutchison, J. H. (1994). The Late Cretaceous alligatoroid *Brachychampsa montana* (Crocodylia): new material and putative relationships. American Museum novitates; no. 3116.

Oaks, J. R. (2011). A time-calibrated species tree of Crocodylia reveals a recent radiation of the true crocodiles. *Evolution*, *65*(11), 3285-3297.

Oleinik, A., Marincovich Jr, L., Barinov, K. B., & Swart, P. K. (2009). Magnitude of Middle Miocene warming in North Pacific high latitudes: stable isotope evidence from Kaneharaia (Bivalvia, Dosiniinae). *Bulletin of the Geological Survey of Japan*, *59*(7-8), 339-353.

Ősi, A. (2014). The evolution of jaw mechanism and dental function in heterodont crocodyliforms. *Historical Biology*, *26*(3), 279-414.

Opdyke, N. D. (1990). Magnetic stratigraphy of Cenozoic terrestrial sediments and mammalian dispersal. *The Journal of Geology*, *98*(4), 621-637.

Oyston, J. W., Wilkinson, M., Ruta, M., & Wills, M. A. (2022). Molecular phylogenies map to biogeography better than morphological ones. *Communications Biology*, *5*(1), 521.

Paiva, A. L. S., Godoy, P. L., Souza, R. B., Klein, W., & Hsiou, A. S. (2022). Body size estimation of Caimaninae specimens from the Miocene of South America. *Journal of South American Earth Sciences*, *118*, 103970.

Pan, T. et al. (2020). Near-complete phylogeny of extant Crocodylia (Reptilia) using mitogenome-based data. *Zoological Journal of the Linnean Society*, *191*(4), 1075-1089.

Parham JF et al. 2012 Best practices for justifying fossil calibrations. *Syst. Biol.* **61**, 346–359. (doi.org/10.1093/sysbio/syr107)

Pinheiro AEP, Fortier DC, Pol D, Campos DA, Bergqvist LP. 2013. A new *Eocaiman* (Alligatoridae, Crocodylia) from the Itaboraí Basin, Paleogene of Rio de Janeiro. Braz Hist Biol. 25(3):327–337.

Piras, P. et al. (2010). The *Gavialis–Tomistoma* debate: the contribution of skull ontogenetic allometry and growth trajectories to the study of crocodylian relationships. *Evolution & development*, *12*(6), 568-579.

Puértolas-Pascual, E., Serrano-Martínez, A., Pérez-Pueyo, M., Bádenas, B., & Canudo, J. I. (2022). New data on the neuroanatomy of basal eusuchian crocodylomorphs (Allodaposuchidae) from the Upper Cretaceous of Spain. *Cretaceous Research*, *135*, 105170.

Puértolas-Pascual, E., Kuzmin, I. T., Serrano-Martínez, A., & Mateus, O. (2023). Neuroanatomy of the crocodylomorph *Portugalosuchus azenhae* from the late cretaceous of Portugal. *Journal of Anatomy*.

Rauhe, M. 1995. Die Lebensweise und Ökologie der Geiseltal-Krokodilier - Abschied von traditionellen Lehrmeinungen. *Hallesches Jahrbuch für Geowissenschaften* 17, 65-80.

Rio, J. P., & Mannion, P. D. (2021). Phylogenetic analysis of a new morphological dataset elucidates the evolutionary history of Crocodylia and resolves the long-standing gharial problem. *PeerJ*, *9*, e12094.

Ristevski, J., Yates, A. M., Price, G. J., Molnar, R. E., Weisbecker, V., & Salisbury, S. W. (2020). Australia's prehistoric 'swamp king': revision of the Plio-Pleistocene crocodylian genus *Pallimnarchus* de Vis, 1886. *PeerJ*, *8*, e10466.

Ristevski, J., Price, G. J., Weisbecker, V., & Salisbury, S. W. (2021). First record of a tomistomine crocodylian from Australia. *Scientific Reports*, *11*(1), 12158.

Ristevski, J., Weisbecker, V., Scanlon, J. D., Price, G. J., & Salisbury, S. W. (2023). Cranial anatomy of the mekosuchine crocodylian *Trilophosuchus rackhami* Willis, 1993. *The Anatomical Record*, *306*(2), 239-297.

Ristevski, J., et al. (2023). Migrations, diversifications and extinctions: the evolutionary history of crocodyliforms in Australasia. *Alcheringa: An Australasian Journal of Palaeontology*, 1-46.

Roberto, I.J., et al. (2020). Unexpected but unsurprising lineage diversity within the most widespread Neotropical crocodilian genus Caiman (Crocodylia, Alligatoridae). *Systematics and Biodiversity*, *18*(4), 377-395.

Roos, J., Aggarwal, R. K., & Janke, A. (2007). Extended mitogenomic phylogenetic analyses yield new insight into crocodylian evolution and their survival of the Cretaceous–Tertiary boundary. *Molecular phylogenetics and evolution*, *45*(2), 663-673.

Salas-Gismondi, R., Flynn, J. J., Baby, P., Tejada-Lara, J. V., Wesselingh, F. P., & Antoine, P. O. (2015). A Miocene hyperdiverse crocodylian community reveals peculiar trophic dynamics in proto-Amazonian mega-wetlands. *Proceedings of the Royal Society B: Biological Sciences*, *282*(1804), 20142490.

Salas-Gismondi, R., et al. (2022). Miocene fossils from the southeastern Pacific shed light on the last radiation of marine crocodylians. *Proceedings of the Royal Society B*, *289*(1974), 20220380.

Shan, H. Y., Wu, X. C., Cheng, Y. N., & Sato, T. (2009). A new tomistomine (Crocodylia) from the Miocene of Taiwan. *Canadian Journal of Earth Sciences*, *46*(7), 529-555.

Shan, H., Yen-nien, C., & Xiao-chun, W. (2013). The first fossil skull of *Alligator sinensis* from the Pleistocene, Taiwan, with a paleogeographic implication of the species. *Journal of Asian Earth Sciences*, *69*, 17-25.

Shan, H. Y., Wu, X. C., Sato, T., Cheng, Y. N., & Rufolo, S. (2021). A new alligatoroid (Eusuchia, Crocodylia) from the Eocene of China and its implications for the relationships of Orientalosuchina. *Journal of Paleontology*, *95*(6), 1321-1339.

Smith, K. T., Schaal, S. F., & Habersetzer, J. (2019). Messel-An ancient greenhouse ecosystem. *The Quarterly Review of Biology*, *94*(4).

Snyder, D. (2007). Morphology and systematics of two Miocene alligators from Florida, with a discussion of Alligator biogeography. *Journal of Paleontology*, *81*(5), 917-928.

Solórzano, A., Rincón, A. D., Cidade, G. M., Núñez-Flores, M., & Sánchez, L. (2019). Lower Miocene alligatoroids (Crocodylia) from the Castillo Formation, northwest of Venezuela. *Palaeobiodiversity and Palaeoenvironments*, *99*, 241-259.

Souza-Filho JP, et al. (2018). A new caimanine (Crocodylia, Alligatoroidea) species from the Solimões Formation of Brazil and the phylogeny of Caimaninae. J Vertebr Paleontol. 38(5):e1528450.

Souza-Filho JP, et al. (2020). On a new *Melanosuchus* species (Alligatoroidea: Caimaninae) from Solimões Formation (Eocene-Pliocene), Northern Brazil, and evolution of Caimaninae. Zootaxa. 4894(4):561–593.

Springer, M. S., et al. (2007). The adequacy of morphology for reconstructing the early history of placental mammals. *Systematic Biology*, *56*(4), 673-684.

Stocker MR, Brochu CA, Kirk EC. (2021). A new caimanine alligatorid from the Middle Eocene of Southwest Texas and implications for spatial and temporal shifts in Paleogene crocodyliform diversity. PeerJ. 9:e10665.

Stout, J. B. (2020). New early Pleistocene *Alligator* (Eusuchia: Crocodylia) from Florida bridges a gap in Alligator evolution. *Zootaxa*, *4868*(1), 41-60.

Taplin, L. E., & Grigg, G. C. (1989). Historical zoogeography of the eusuchian crocodilians: a physiological perspective. *American Zoologist*, *29*(3), 885-901.

Thorbjarnarson, J., & Wang, X. (2010). *The Chinese alligator: ecology, behavior, conservation, and culture*. JHU Press.

Trueman, J. W. (1998). Reverse successive weighting. *Systematic biology*, 733-737.
Turner, A. H., Pritchard, A. C., & Matzke, N. J. (2017). Empirical and Bayesian approaches to fossil-only divergence times: a study across three reptile clades. *PloS one*, *12*(2), e0169885.

Turner, A. H., Pritchard, A. C., & Matzke, N. J. (2017). Empirical and Bayesian approaches to fossil-only divergence times: a study across three reptile clades. *PloS one*, *12*(2), e0169885.

Walter, J., Darlim, G., Massonne, T., Aase, A., Frey, E., & Rabi, M. (2022). On the origin of Caimaninae: insights from new fossils of *Tsoabichi greenriverensis* and a review of the evidence. *Historical Biology*, *34*(4), 580-595.

Young, C. C. (1964). New fossil crocodiles from China. *Vertebrata Palasiatica*, *8*(2), 189-208.

Wang, Y. Y., Sullivan, C., & Liu, J. (2016). Taxonomic revision of *Eoalligator* (Crocodylia, Brevirostres) and the paleogeographic origins of the Chinese alligatoroids. *PeerJ*, *4*, e2356.

West, C. K., Greenwood, D. R., & Basinger, J. F. (2015). Was the Arctic Eocene 'rainforest'monsoonal? Estimates of seasonal precipitation from early Eocene megafloras from Ellesmere Island, Nunavut. *Earth and Planetary Science Letters*, *427*, 18-30.

Wilberg, E. W., Turner, A. H., & Brochu, C. A. (2019). Evolutionary structure and timing of major habitat shifts in Crocodylomorpha. *Scientific reports*, *9*(1), 514.

Williamson TE. 1996. *Brachychampsa sealeyi*, sp. nov., (Crocodylia, Alligatoroidea) from the Upper Cretaceous (lower Campanian) Menefee Formation, northwestern New Mexico. J Vertebr Paleontol. 16(3):421–431.

Willis, R. E., McAliley, L. R., Neeley, E. D., & Densmore III, L. D. (2007). Evidence for placing the false gharial (*Tomistoma schlegelii*) into the family Gavialidae: inferences from nuclear gene sequences. *Molecular Phylogenetics and Evolution*, *43*(3), 787-794.

Willis, R. E. (2009). Transthyretin gene (TTR) intron 1 elucidates crocodylian phylogenetic relationships. *Molecular Phylogenetics and Evolution*, *53*(3), 1049-1054.

Wu, X. C., Wang, Y. C., You, H. L., Zhang, Y. Q., & Yi, L. P. (2023). New brevirostrines (Crocodylia, Brevirostres) from the Upper Cretaceous of China. *Cretaceous Research*, *144*, 105450.

Zachos, J., Pagani, M., Sloan, L., Thomas, E., & Billups, K. (2001). Trends, rhythms, and aberrations in global climate 65 Ma to present. *science*, *292*(5517), 686-693.

Zhou, C. F., & Rabi, M. 2015 A sinemydid turtle from the Jehol Biota provides insights into the basal divergence of crown turtles. *Scientific Reports* **5**, 1–12. (doi.org/10.1038/srep16299)

Zou, Z., & Zhang, J. (2016). Morphological and molecular convergences in mammalian phylogenetics. *Nature Communications*, *7*(1), 12758.

Part II: chapters (manuscripts)

Chapter 1

The impact of molecular data on the phylogenetic position of the putative oldest crown crocodilian and the age of the clade

Explanation of candidate contribution to collaborative work

This chapter is based on collaborative work. The text represents the published version of the following manuscript:

Darlim, G., Lee, M. S., Walter, J., & Rabi, M. (2022). The impact of molecular data on the phylogenetic position of the putative oldest crown crocodilian and the age of the clade. *Biology Letters*, *18*(2), 20210603. (https://doi.org/10.1098/rsbl.2021.0603).

Author contributions
Darlim, G. conceptualization, data curation, formal analysis, investigation, project administration, writing—original draft; Lee, M.S.Y. conceptualization, data curation, formal analysis, methodology, software, writing—review and editing; Walter, J. conceptualization, data curation, formal analysis, writing—review and editing; Rabi, M. conceptualization, funding acquisition, investigation, project administration, supervision, visualization, writing—original draft.

The impact of molecular data on the phylogenetic position of the putative oldest crown crocodilian and the age of the clade

Abstract

The use of molecular data for living groups is vital for interpreting fossils, especially when morphology-only analyses retrieve problematic phylogenies for living forms. These topological discrepancies impact on the inferred phylogenetic position of many fossil taxa. In Crocodylia, morphology-based phylogenetic inferences differ fundamentally in placing Gavialis basal to all other living forms,whereasmolecular data consistently unite it with crocodylids. The Cenomanian *Portugalosuchus azenhae* was recently described as the oldest crown crocodilian, with affinities to Gavialis, based on morphology-only analyses, thus representing a potentially important new molecular clock calibration. Here, we performed analyses incorporating DNA data into these morphological datasets, using scaffold and supermatrix (total evidence) approaches, in order to evaluate the position of basal crocodylians, including *Portugalosuchus*. Our analyses incorporating DNA data robustly recovered *Portugalosuchus* outside Crocodylia (as well as thoracosaurs, planocraniids and *Borealosuchus* spp.), questioning the status of *Portugalosuchus* as crown crocodilian and any future use as a node calibration in molecular clock studies. Finally, we discuss the impact of ambiguous fossil calibration and how, with the increasing size of phylogenomic datasets, the molecular scaffold might be an efficient (though imperfect) approximation of more rigorous but demanding supermatrix analyses.

INTRODUCTION

In phylogenetic analyses, DNA data for living groups are often vital for interpreting the position of fossil taxa, as adaptive convergence in morphological characters can strongly mislead phylogenetic analyses (Gatesy et al., 2003; Asher & Hofreiter, 2006; Koepfli et al., 2007; Havermans et al., 2010; D;Avalos et al., 2014; Zou & Zhang, 2016; Zhou & Rabi, 2015). Although molecular analysis in Crocodylia using both mitochondrial and nuclear DNA has consistently favoured a common topology (Gatesy et al., 2003; Harshman et al., 2003; Roos et al., 2007; Oaks, 2011; Lee & Yates, 2018; Pan et al., 2020), analyses focused on fossil crocodylians often continue to use morphology-only datasets, which do not retrieve the molecular tree for living crocodilians (e.g. Bona et al., 2018; Cossette & Brochu, 2020; Godoy et al., 2021; Ristevski et al., 2020; Ristevski et al., 2021). Phylogenetic inference based on morphology alone places Gavialis gangeticus sister to all other living crocodilians (i.e. alligators and crocodiles) (Norell, 1989; Borchu, 1997; Piras et al., 2010; Iijima & Kobayashi, 2019), while molecular data unite *Gavialis* with *Tomistoma* as sister to Crocodylidae alone (Gatesy et al., 2003; Harshman et al., 2003; Roos et al., 2007; Oaks, 2011; Gatesy & Amado, 1992; Janke et al., 2005; Willis et al., 2007; Willis, 2009). Recent morphological studies, however, have presented strong evidence that numerous apparently plesiomorphic character states in *Gavialis* are instead atavistic, consistent with the molecular tree (Ristevski et al., 2020; Iijima & Kobayashi, 2019; Rio & Mannion, 2021). Fossil taxa close to the root of Crocodylia, and/or with a *Gavialis* like morphology, are particularly susceptible to considerable changes in phylogenetic position with the addition of molecular data as the polarization and optimization of key morphological characters are likely to shift. This in turn can affect their utility as age calibrations for molecular divergence age estimations. *Portugalosuchus azenhae*,

recently described from an incomplete skull from the upper Cenomanian (ca 95 Ma) of Portugal, represents a notable example of this phenomenon. Based on morphology alone, *Portugalosuchus* was potentially the oldest member of Crocodylia (i.e. the crown group; the least-inclusive clade that contains all living crocodilians) (Mateus et al., 2019). This would pre-date the previous oldest crown crocodilian fossils (e.g. *Brachychampsa sealeyi*, Williamson, 1996) and imply substantial ghost lineages. Furthermore, it would influence the age of Crocodylia if used as a node calibration for molecular divergence dating (e.g. Benton et al., 2015). Considering the topological conflict between morphological and molecular data in Crocodylia, relying on morphology alone to interpret the putative position of *Portugalosuchus* as the oldest crocodylian is potentially problematic, and indeed the original description acknowledged this conclusion had some uncertainty (Mateus et al., 2019). Here, we use DNA-informed analyses to investigate whether molecular data substantially alters the phylogenetic interpretation of *Portugalosuchus*. We added molecular data into the original, and updated, morphological datasets of Mateus et al. (2019) using different phylogenetic analytical approaches, including parsimony, undated Bayesian and tip-dating Bayesian analyses. All analyses robustly exclude *Portugalosuchus* from Crocodylia, instead placing it as a non-crocodylian eusuchian. We highlight the importance of DNA-informed phylogenetic inference for basal crocodylian relationships and divergence age estimates together with the use of well-justified fossil calibrations.

MATERIAL AND METHODS

Morphological, molecular and stratigraphic data

The morphological datasets analysed here include (i) Narváez et al (2016) as modified by Mateus et al (2019) (abbreviated as NM), and (ii) Turner (2015) as modified by Mateus et al (2019) (TM). In addition, we analysed a modified version of NM (mNM) by changing 16 characters scorings of *Portugalosuchus* to 'unknown' that cannot be confirmed using published information (see electronic supplementary material, file S1 for a list of modified characters scorings). For total evidence analyses of the NM and mNM datasets, we added molecular data for all 16 living species: a total of 9284 base pairs of mtDNA and nucDNA compiled from published data, especially (Gatesy et al., 2003; Oaks, 2011); details of sources and alignment are in a previous study Lee & Yates (2018). For tip-dated analyses, stratigraphic data for the taxa were collected from the literature. A table with ages of taxa and references is provided in the electronic supplementary material, file S2.

Phylogenetic analyses

We performed eleven additional phylogenetic analyses (table 1) employing the NM and mNM morphological datasets using different approaches: maximum-parsimony and Bayesian analyses, both with and without molecular information, either as a molecular scaffold Springer et al. (2001) using the topology of Oaks (2010) or added as a DNA alignment in a supermatrix de Queiroz & Gatesy (2007). Tip-dating Bayesian analysis was also performed on the morphology + molecular supermatrices. We also re-analysed the TM matrix under parsimony and undated Bayesian approaches (but did not add DNA information as this dataset only included three living species). Furthermore, the taxon and character sampling for the TM dataset were not aimed at resolving crown

crocodylian relationships, so we focused on the NM and mNM datasets. All parsimony analyses were conducted in TNT v. 1.5 (Goloboff & Catalano, 2016) following the same search settings as Mateus et al. (2019); undated and tip-dated Bayesian analyses were performed, respectively, in MrBayes (Ronquist et al., 2012) and BEAST 2.5 (Bouckaert et al., 2019). The optimal partitioning scheme and substitution models for the molecular data were obtained by PartitionFinder (Lanfear et al., 2012). The tip-dating analysis co-estimated topologies, branch lengths, divergence dates and evolutionary rates. The divergence age estimations for the nodes incorporate the phenotypic and stratigraphic information contained in the fossil taxa (tips). A full description of all analyses is provided in the electronic supplementary material (electronic supplementary material, file S3).

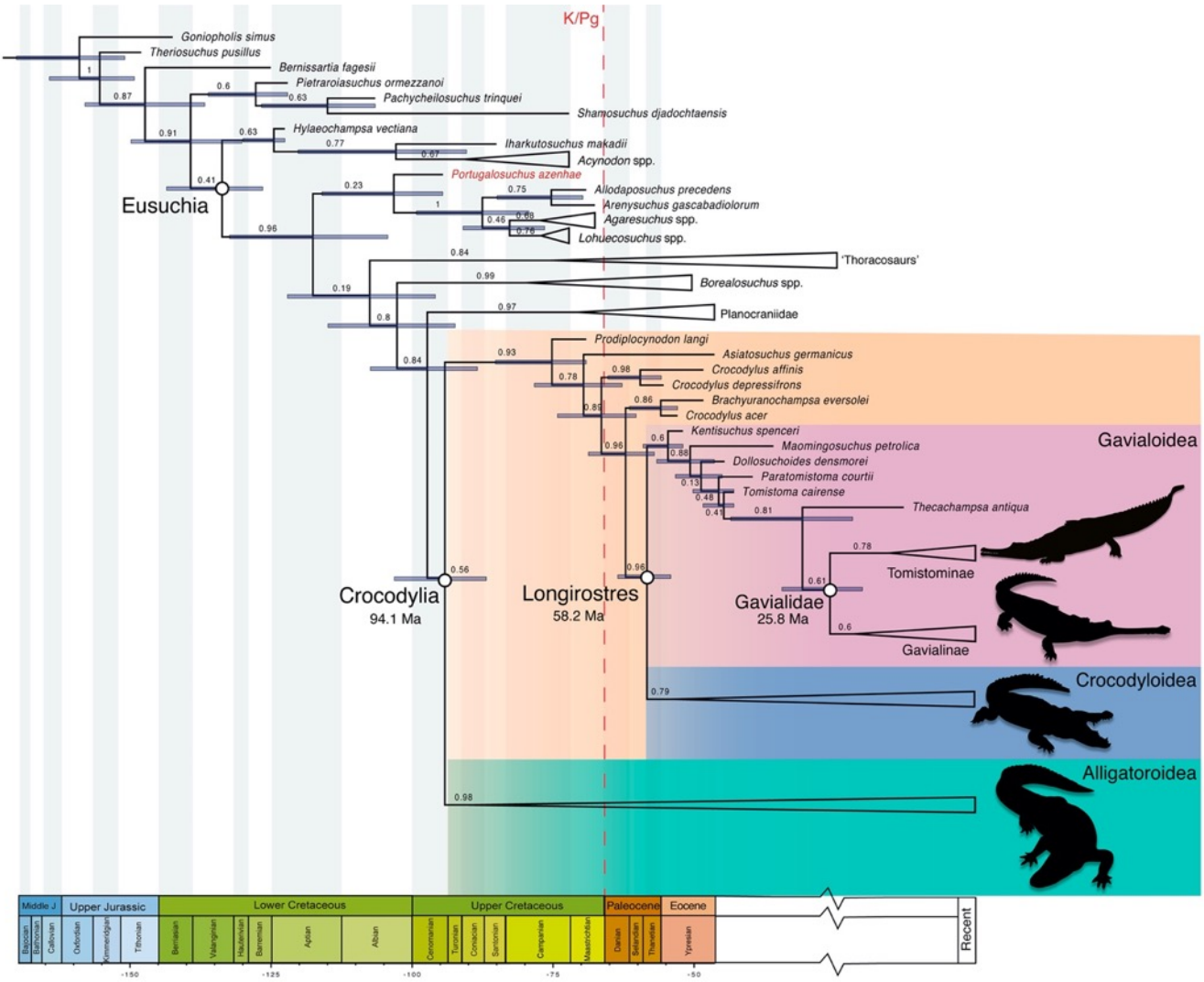

Figure 1. Simplified phylogeny of crocodylians based on total evidence tip-dated Bayesian analysis using the original morphology dataset (NM) of Mateus et al. (2019). Numbers indicate posterior probability support values for the clades. Horizontal blue–grey bars indicate 95% highest posterior density interval (HPD) for age estimate. Full phylogeny is available in electronic supplementary material, figure S10.

RESULTS

Parsimony analysis of the original morphological dataset (NM) reproduces Mateus et al. 2019 by placing *Portugalosuchus* within Crocodylia, but the modified dataset with some character state-codings re-scored to unknown (mNM) finds *Portugalosuchus*

forming a polytomy with Crocodylia (electronic supplementary material, figure S1). The (undated)Bayesian analyses of morphology alone (NM and mNM) also place *Portugalosuchus* within Crocodylia, along the *Gavialis* lineage (electronic supplementary material, figures S2 and S3).

However, these two morphological datasets (NM, mNM) consistently place *Portugalosuchus* outside Crocodylia when molecular data are considered, either as a scaffold or incorporated in a supermatrix in a total evidence framework. These results hold under scaffold + parsimony (electronic supplementary material, figures S4 and S5), total evidence parsimony (electronic supplementary material, figures S6 and S7), total evidence undated Bayesian (electronic supplementary material, figures S8 and S9) and total evidence tip-dated Bayesian (figure 1; electronic supplementary material, figures S10 and S11). In all analyses employing molecular data (scaffold or total evidence), Planocraniidae and *Borealosuchus* spp. are likewise recovered outside Crocodylia. Finally, our tip-dated analysis estimate ca 95 Ma (Cenomanian, early Late Cretaceous) as the age for Crocodylia.

For the TM dataset, parsimony analysis found *Portugalosuchus* as part of a large polytomy that included living crocodylians (again in agreement with Mateus et al., 2019); however, we note that in several most parsimonious trees, *Portugalosuchus* was outside of crown Crocodylia (electronic supplementary material, figure S14). All supplementary figures can be found in the electronic supplementary material, file S4.

Table 1. Phylogenetic position of *Portugalosuchus azenhae* related to Crocodylia according to different data types and analytical approaches.

Data type	**Analytic method**	**Position of *Portugalosuchus***	**Referred phylogenies**

Morphology, original (NM)	Parsimony	crown	Figure 11 in Mateus et al., 2019
Morphology, modified (mNM)	Parsimony	unresolved	Figure S1
Morphology, original (NM)	Bayesian undated	crown	Figure S2
Morphology, modified (mNM)	Bayesian undated	crown	Figure S3
Scaffold+Morphology, original (NM+DNA)	Parsimony	stem	Figure S4
Scaffold+Morphology, modified (mNM+DNA)	Parsimony	stem	Figure S5
DNA+Morphology, original (NM+DNA)	Parsimony	stem	Figure S6
DNA+Morphology, modified (mNM+DNA)	Parsimony	stem	Figure S7
DNA+Morphology, original (NM+DNA)	Bayesian undated	stem	Figure S8
DNA+Morphology, modified (mNM+DNA)	Bayesian undated	stem	Figure S9
DNA+Morphology, original (NM+DNA)	Bayesian tip-dated	stem	Figure S10, Figure 1
DNA+Morphology, modified (mNM+DNA)	Bayesian tip-dated	stem	Figure S11

DISCUSSION

The impact of DNA data on the phylogenetic position of *Portugalosuchus*

Previous morphological phylogenies inferred the Cenomanian *P. azenhae* to represent the oldest known crown crocodilian, either as sister to all other non-gavialoid crocodylians (Mateus et al., 2019) or in a clade with gavialoids (Ristevski et al., 2020; Ristevski et al., 2021; Rio & Mannion, 2021). In each case, ghost lineages are inferred extending into the mid to latest Early Cretaceous. The addition of molecular data abruptly moves *Gavialis* from a basal to a nested position with respect to other living crocodilans and is thus expected to most affect taxa around the 'gavialoid' region of the morphological tree. For instance, putative synapomorphies placing *Portugalosuchus* closer to Alligatoridae + Crocodylidae (to the exclusion of gavialoids) are likely to reoptimize as symplesiomorphies for all Crocodylia under the molecular topology (e.g. Gatesy et al., 2003). Indeed, in our analyses (both dated and undated), *Portugalosuchus* together with Borealosuchidae and Planocraniidae are consistently recovered outside Crocodylia when we add molecular information to the morphological dataset of Mateus et al. (2019), either under total evidence or under a scaffold (figure 1; electronic supplementary material, figures S4–S13; cf. also electronic supplementary material, figure S15 with Blanco, 2021). In the total evidence tip-dated tree (NM), *Portugalosuchus* and its sister group, Allodaposuchidae, are excluded from the clade formed by Borealosuchidae, Planocraniidae and Crocodylia owing to the absence of an enlarged external mandibular fenestra (63 : 0–1). The slit-like condition score for *P. azenhae* instead (Mateus et al., 2021) was acquired four times independently according to this topology but never within Crococodylia, except for *Deinosuchus riograndensis*. Additionally, the presence of a postorbital process divided into two spines (134 : 0) and

postorbital bar flush with lateral jugal surface (135 : 0) (both reversed in Gavialinae, electronic supplementary material, file S5) contributes in placing *P. azenhae* outside the crown and more
inclusive clades.

Phylogenies finding Portugalosuchus inside Crocodylia place it near 'thoracosaurs' (in either a clade or a grade) and are questionable given that tip-dating Bayesian analyses (Lee & Yates, 2018; this study) suggest that most if not all 'thoracosaurs' are not crown crocodylians related to gavialids, but are outside crown Crocodylia. As pointed out by Rio & Mannion (2021), *Portugalosuchus* does exclusively share character states with 'thoracosaurs' that distinguish these taxa from gavialids. *Portugalosuchus* therefore likely represents a non-crocodylian eusuchian and should be avoided as a fossil age constraint for Crocodylia in calibration databases (e.g. Benton et al., 2015).

Supermatrix ('combined', 'total evidence') approaches are the most rigorous way to integrate multiple sources of phylogenetic data, such as morphology and DNA (e.g. de Queiroz & Gatesy, 2007). However, the increasing size of phylogenomic datasets is making these approaches harder to implement, owing to computational demands as well as additional bioinformatic expertise required. However, this trend also means that phylogenetic relationships between living taxa are increasingly dictated by DNA (e.g. Lee & Palci, 2015); this asymmetry means that interactions between morphological and molecular datasets that manifest themselves in a supermatrix framework (e.g. Gatesy et al., 1999) might be less important. If so, molecular scaffolds might be an efficient way forward. In this study, the molecular scaffold analysis generated topologies identical to those retrieved by combined morphological and molecular data with respect to the placement of both fossil and extant taxa (electronic

supplementary material, figures S4–S7); in accordance with expectation, mapping morphology and fossils onto a molecular scaffold will be highly comparable to the results of a simultaneous analysis where the DNA data essentially constrain the relationships among living taxa (e.g. Zhou & Rabi, 2015; Lee & Palci, 2015; Crawford et al., 2015). As phylogenomic data become commonplace, molecular scaffolds therefore comprise an increasingly pragmatic way of integrating molecular information into fossil phylogenies.

The age of Crocodylia and the impact of ambiguous fossil calibrations

In our tip-dated analyses (using both original and modified datasets), the age for Crocodylia is approximately 94 Ma (Cenomanian, Late Cretaceous), with a 95% highest posterior density interval (HPD) of approx. 87–104 Ma. If *Portugalosuchus* were assumed to be a crown crocodilian, tip- or node dated molecular divergence dating would estimate a substantially older age for the clade; the age of *Portugalosuchus* (95 Ma) would form the hard minimum age for the clade. The present estimate is consistent with recent tip-dating estimates of approximately 100 Ma (Lee & Yates, 2018) despite substantial differences in taxon and character sampling. Our estimate is also broadly consistent with molecular studies implicitly or explicitly following best practices for fossil calibrations (Parham et al., 2012) (table 2) as well as fossil divergence age estimates (e.g. Bona et al., 2018; Turner et al., 2017). All these converge upon an interval between 90 and 100 Ma for the age of Crocodylia. On the other hand, controversial choices for fossil calibrations of some published molecular divergence studies have led to much earlier inferred ages for Crocodylia. *Brachychampsa sealeyi*, a taxon conventionally regarded as a basal alligatoroid (e.g. Williamson, 1996; Norell et al., 1994; Brochu, 1999; Brochu, 2010; Brochu, 2011; Massonne et al., 2019; Walter et

al., 2021), has been used as a constraint for a much smaller clade, Caimaninae, following some weakly supported phylogenies (see Walter et al., 2021 for a review), resulting in inflated age estimations for Alligatoridae (split between Caimaninae and Alligatorinae, 71.61–129.7 Ma; Bittencourt et al., 2019; Roberto et al., 2020). Similarly, the same studies overlooked that some crocodylian clades have stembased definitions and therefore include stem fossils (Brochu, 1999; de Queiroz & Gautier, 1992) and thus calibrated crown-Alligatorinae (*Alligator mississippiensis–A. sinensis* split) with the stem-alligatorine *Navajosuchus mooki* (Bona et al., 2018; Brochu, 1999; Brochu, 2004); this leads to overestimating crown-alligatorine divergence ages.

Table 2. Compilation of divergence age estimations for Crocodylia. Except for Roos et al. (2007), all the age intervals represent the 95% highest posterior densities (HPD).

	Crocodylia divergence age estimations intervals (Ma)	**Time-calibrated technique**	**Clock model**	**Tree model**
Roos et al., 2007	101 ± 3.0	Molecular clock (node calibration)	r8s non-parametric rate smoothing NPRS	
Oaks, 2011	81.08–90.00	Molecular clock (node calibration)	Relaxed uncorrelated lognormal	Bayesian Dirichlet process
Turner et al., 2017	81.02–114.25	Tip-dating (morphology-only)	Relaxed uncorrelated lognormal	Birth-Death Process

Lee & Yates, 2018	90.0–110.0	Tip-dating (total-evidence)	Relaxed uncorrelated lognormal	Birth-Death Process
Pan et al., 2020	83.6–90.02	Molecular clock (node calibration)	Relaxed uncorrelated lognormal	Yule Process
* This work	86.77–103.09	Tip-dating (total-evidence)	Relaxed uncorrelated lognormal	Birth-Death Process

Our analyses demonstrate how the integration of molecular and morphological data/topologies plays an important role in interpreting the phylogenetic position of basal crocodylians and suggest avoiding inferences based exclusively on morphological data, especially when morphology-based relationships among living taxa are robustly contradicted by genomic data. While it is intriguing that a recent morphological phylogeny resolved the Tomistoma–Gavialis conflict (Rio & Mannion, 2021), its use of quantitative characters in turn resulted in unconventional placement of some extant and fossil taxa (e.g. polyphyletic Jacarea as opposed to all previous morphological and molecular phylogenies). Integrating DNA and morphological data/topologies therefore remains a vital approach for phylogenetic inference as well as reconstruction of character evolution and divergence ages, and molecular scaffolds can be an efficient way to approximate more rigorous supermatrix approaches.

References

Asher RJ, Hofreiter M. 2006 Tenrec phylogeny and the noninvasive extraction of nuclear DNA. *Syst*. *Biol*. **55**, 181–194. (doi.org/10.1080/10635150500433649)

Benton MJ, Donoghue PC, Asher RJ, Friedman M, Near TJ, Vinther J. 2015 Constraints on the timescale of animal evolutionary history. *Palaeontol Electron*, **18**, 1–106. (https://doi.org/10.26879/424)

Bittencourt PS, Campos Z, Muniz FL, Marioni B, Souza BC, Da Silveira R, De Thoisy B, Hrbek B, Farias IP. 2019 Evidence of cryptic lineages within a small South American crocodilian: the Schneider's dwarf caiman *Paleosuchus trigonatus* (Alligatoridae: caimaninae). *PeerJ*. 7:e6580. (doi:10.7717/peerj.6580)

Blanco A. 2021 Importance of the postcranial skeleton in eusuchian phylogeny: Reassessing the systematics of allodaposuchid crocodylians. *PloS ONE* **16**, e0251900. (doi.org/10.1371/journal.pone.0251900)

Bona P, Ezcurra MD, Barrios F, Fernandez Blanco MV. 2018. A new Palaeocene crocodylian from southern Argentina sheds light on the early history of caimanines. *Proc. R. Soc. B* **285**, 20180843. (doi:10.1098/rspb.2018.0843)

Bouckaert R,et al. 2019 BEAST 2.5: An advanced software platform for Bayesian evolutionary analysis. *PLoS Comput. Biol.* **15**, e1006650. (https://doi.org/10.1371/journal.pcbi.1006650)

Brochu CA. 1997 Morphology, fossils, divergence timing, and the phylogenetic relationships of *Gavialis*. *Syst. Biol*. **46**, 479–522. (doi.org/10.1093/sysbio/46.3.479)

Brochu CA. 1999 Phylogenetics, taxonomy, and historical biogeography of Alligatoroidea. *J. Vertebr. Paleontol.* **19**, 9–100. (doi.org/10.1080/02724634.1999.10011201)

Brochu CA. 2004 Alligatorine phylogeny and the status of *Allognathosuchus* Mook, 1921. *J. Vertebr. Paleontol.* **24**, 857–873. (https://doi.org/10.1671/0272-4634(2004)024[0857:APATSO]2.0.CO;2)

Brochu CA. 2010 A new alligatorid from the lower Eocene Green River Formation of Wyoming and the origin of caimans. *J. Vertebr. Paleontol.* **30**, 1109–1126. (doi.org/10.1080/02724634.2010.483569)

Brochu CA. 2011 Phylogenetic relationships of *Necrosuchus ionensis* Simpson, 1937 and the early history of caimanines. *Zool. J. Linn. Soc.* **163**, S228–S256. (doi.org/10.1111/j.1096-3642.2011.00716.x)

Cossette AP, Brochu CA. 2020 A systematic review of the giant alligatoroid *Deinosuchus* from the Campanian of North America and its implications for the relationships at the root of Crocodylia. *J. Vertebr Paleontol.* **40**, e1767638. (https://doi.org/10.1080/02724634.2020.1767638)

Crawford NG, Parham JF, Sellas AB, Faircloth BC, Glenn TC, Papenfuss TJ, Henderson JB, Hansen MH, Simison, WB. 2015 A phylogenomic analysis of turtles. *Mol. Phyl. Evol.* **83**, 250–257. (doi.org/10.1016/j.ympev.2014.10.021)

Dávalos LM, Velazco PM, Warsi OM, Smits PD, Simmons NB. 2014. Integrating incomplete fossils by isolating conflicting signal in saturated and non-independent morphological characters. *Syst. Biol.* **63**, 582–600. (https://doi.org/10.1093/sysbio/syu022)

de Queiroz A, Gatesy J. 2007 The supermatrix approach to systematics. *Trends Ecol. Evol*. **22**, 34–41. (https://doi.org/10.1016/j.tree.2006.10.002)

deQueiroz KD, Gauthier J. 1992 Phylogenetic taxonomy. *Annu. Rev. Ecol. Syst.* **23**, 449–480.

Gatesy J, Amato G, Norell M, DeSalle R, Hayashi C. 2003 Combined support for wholesale taxic atavism in gavialine crocodylians. *Syst. Biol.* **52**, 403–422. (doi.org/10.1080/10635150390197037)

Gatesy J, Amato GD. 1992 Sequence similarity of 12S ribosomal segment of mitochondrial DNAs of gharial and false gharial. *Copeia* **1992**, 241–243. (doi.org/10.2307/1446560)

Gatesy J, O'Grady P, Baker RH. 1999 Corroboration among data sets in simultaneous analysis: hidden support for phylogenetic relationships among higher level artiodactyl taxa. *Cladistics*, **15**, 271–313. (https://doi.org/10.1111/j.1096-0031.1999.tb00268.x)

Godoy PL, Cidade GM, Montefeltro FC, Langer MC, Norell MA. 2021 Redescription and phylogenetic affinities of the caimanine *Eocaiman cavernensis* (Crocodylia,

Alligatoroidea) from the Eocene of Argentina. *Pap. Palaeontol.*, **7**, 1205–1231. (https://doi.org/10.1002/spp2.1339)

Goloboff PA, Catalano SA. 2016 TNT version 1.5, including a full implementation of phylogenetic morphometrics. *Cladistics*, **32**, 221–238. (doi.org/10.1111/cla.12160)

Harshman J, Huddleston CJ, Bollback JP, Parsons TJ, Braun MJ. 2003 True and false gharials: a nuclear gene phylogeny of Crocodylia. *Syst. Biol.* **52**, 386–402. (doi.org/10.1080/10635150390197028)

Havermans C, Nagy ZT, Sonet G, De Broyer C, Martin P. 2010 Incongruence between molecular phylogeny and morphological classification in amphipod crustaceans: a case study of Antarctic lysianassoids. *Mol. Phylogenet. Evol.* **55**, 202–209. (doi.org/10.1016/j.ympev.2009.10.025)

Iijima M, Kobayashi Y. 2019 Mosaic nature in the skeleton of East Asian crocodylians fills the morphological gap between "Tomistominae" and Gavialinae. *Cladistics* **35**, 623–632. (doi.org/10.1111/cla.12372)

Janke A, Gullberg A, Hughes S, Aggarwal RK, Arnason U. 2005 Mitogenomic analyses place the gharial (*Gavialis gangeticus*) on the crocodile tree and provide pre-K/T divergence times for most crocodilians. *J. Mol. Evol.* **61**, 620–626. (doi.org/10.1007/s00239-004-0336-9)

Koepfli KP, Gompper ME, Eizirik E, Ho CC, Linden L, Maldonado JE, Wayne RK. 2007 Phylogeny of the Procyonidae (Mammalia: Carnivora): molecules, morphology and the

great American interchange. *Mol. Phylogenet. Evol.* **43**, 1076–1095. (doi.org/10.1016/j.ympev.2006.10.003)

Lanfear R, Calcott B, Ho SYW, Guindon S. 2012 PartitionFinder: Combined Selection of Partitioning Schemes and Substitution Models for Phylogenetic Analyses. *Mol. Biol. Evol.* **6**, 1695–1701. (doi.org/10.1093/molbev/mss020)

Lee MS, Palci A. 2015 Morphological phylogenetics in the genomic age. *Curr. Biol.* **25**, R922–R929. (doi.org/10.1016/j.cub.2015.07.009)

Lee MSY, Yates AM. 2018 Tip dating and homoplasy: reconciling the shallow molecular divergences of modern gharials with their long fossil record. *Proc. R. Soc. B*. **285**, 20181071. (doi.org/10.1098/rspb.2018.1071).

Massonne T, Vasilyan D, Rabi M, Böhme M. 2019 A new alligatoroid from the Eocene of Vietnam highlights an extinct Asian clade independent from extant *Alligator sinensis*. *PeerJ*, **7**, e7562. (doi.org/10.7717/peerj.7562)

Mateus O, Puértolas-Pascual E, Callapez PM. 2019 A new eusuchian crocodylomorph from the Cenomanian (Late Cretaceous) of Portugal reveals novel implications on the origin of Crocodylia. *Zool. J. Linn. Soc.* **186**, 501–528. (doi.org/10.1093/zoolinnean/zly064)

Narváez I, Brochu CA, Escaso F, Pérez-García A, Ortega F. 2016 New Spanish Late Cretaceous eusuchian reveals the synchronic and sympatric presence of two allodaposuchids. *Cretac. Res.* **65**, 112–125. (doi.org/10.1016/j.cretres.2016.04.018)

Norell M, Clark JM, Hutchison JH. 1994 The Late Cretaceous alligatoroid *Brachychampsa montana* (Crocodylia): new material and putative relationships. Am. Mus. Novit. **3116**. 1–26.

Norell MA. 1989 The higher level relationships of the extant Crocodylia. *J. Herpetol.* 325–335. (doi.org/10.2307/1564042)

Oaks JR, 2011. A time-calibrated species tree of Crocodylia reveals a recent radiation of the true crocodiles. *Evolution*. **65**, 3285–3297. (doi.org/10.1111/j.1558-5646.2011.01373.x)

Pan T et al. 2020 Near-complete phylogeny of extant Crocodylia (Reptilia) using mitogenome-based data. *Zool. J. Linn. Soc*. **191**, 1075–1089. (doi.org/10.1093/zoolinnean/zlaa074)

Parham JF et al. 2012 Best practices for justifying fossil calibrations. *Syst. Biol.* **61**, 346–359. (doi.org/10.1093/sysbio/syr107)

Piras P, Colangelo P, Adams DC, Buscalioni A, Cubo J, Kotsakis T, Meloro C, Raia, P. 2010. The *Gavialis–Tomistoma* debate: the contribution of skull ontogenetic allometry

and growth trajectories to the study of crocodylian relationships. *Evol*. *dev*. **12**, 568–579. (doi.org/10.1111/j.1525-142X.2010.00442.x)

Rio JP, Mannion PD. 2021 Phylogenetic analysis of a new morphological dataset elucidates the evolutionary history of Crocodylia and resolves the long-standing gharial problem. *PeerJ* **9**, e12094. (doi.org/10.7717/peerj.12094)

Ristevski J, Price GJ, Weisbecker V, Salisbury SW. 2021 First record of a tomistomine crocodylian from Australia. *Sci*. *Rep*. **11**, 1–14. (doi.org/10.1038/s41598-021-91717-y)

Ristevski J, Yates AM, Price GJ, Molnar RE, Weisbecker V, Salisbury SW. 2020 Australia's prehistoric 'swamp king': revision of the Plio-Pleistocene crocodylian genus *Pallimnarchus* de Vis, 1886. *PeerJ* **8**, e10466. (doi.org/10.7717/peerj.10466)

Roberto IJ et al. 2020 Unexpected but unsurprising lineage diversity within the most widespread Neotropical crocodilian genus Caiman (Crocodylia, Alligatoridae). *Syst. Biodivers.* **18**, 377–395. (doi.org/10.1080/14772000.2020.1769222)

Ronquist F, Teslenko M, van der Mark P, Ayres DL, Darling A, Höhna S, Larget B, Liu L, Suchard MA, Huelsenbeck JP. 2012 MrBayes 3.2: efficient Bayesian phylogenetic inference and model choice across a large model space. *Syst. Biol*. **61**, 539–542. (doi: 10.1093/sysbio/sys029)

Roos J, Aggarwal RK, Janke A. 2007 Extended mitogenomic phylogenetic analyses yield new insight into crocodylian evolution and their survival of the Cretaceous-Tertiary boundary. *Mol Phyl. Evol*. **45**, 663–673. (doi.org/10.1016/j.ympev.2007.06.018)

Springer MS, Teeling EC, Madsen O, Stanhope MJ, de Jong WW. 2001 Integrated fossil and molecular data reconstruct bat echolocation, *Proc. Natl Acad. Sci*. **98**, 6241–6246. (https://doi.org/10.1073/pnas.111551998)

Turner AH, Pritchard AC, Matzke NJ. 2017 Empirical and Bayesian approaches to fossil-only divergence times: a study across three reptile clades. *PLoS One* **12**, e0169885. (doi.org/10.1371/journal.pone.0169885)

Turner AH. 2015 A review of *Shamosuchus* and *Paralligator* (Crocodyliformes, Neosuchia) from the Cretaceous of Asia. *PLoS ONE*. **10**, e0118116. (doi.org/10.1371/journal.pone.0118116)

Walter J, Darlim G, Massonne T, Aese A, Frey E, Rabi, M. 2021 On the origin of Caimaninae: insights from new fossils of *Tsoabichi greenriverensis* and a review of the evidence. *Hist. Biol*. 1–16. (doi.org/10.1080/08912963.2021.1938563)

Williamson TE. 1996 ? *Brachychampsa sealeyi*, sp nov.,(Crocodylia, Alligatoroidea) from the Upper Cretaceous (lower Campanian) Menefee Formation, northwestern New Mexico. *J. Vertebr. Paleontol.* **16**, 421–431. (doi.org/10.1080/02724634.1996.10011331)

Willis RE, McAliley LR, Neeley ED, Densmore III LD. 2007 Evidence for placing the false gharial (*Tomistoma schlegelii*) into the family Gavialidae: inferences from nuclear gene sequences. *Mol. Phylogenet. Evol.* **43**, 787–794. (doi.org/10.1016/j.ympev.2007.02.005)

Willis RE. 2009 Transthyretin gene (TTR) intron 1 elucidates crocodylian phylogenetic relationships. *Mol. Phylogenet. Evol.* **53**, 1049–1054. (dx.doi.org/10.1016%2Fj.ympev.2009.09.003)

Zhou, C. F., & Rabi, M. 2015 A sinemydid turtle from the Jehol Biota provides insights into the basal divergence of crown turtles. *Sci*. *Rep*. **5**, 1–12. (doi.org/10.1038/srep16299)

Zou Z, Zhang J. 2016 Morphological and molecular convergences in mammalian phylogenetics. *Nat*. *Commun*. **7**, 1–9. (doi.org/10.1038/ncomms12758)

SUPPORTING INFORMATION

All Supplementary files can be found in the following link of Dryad Digital reporsitory:

Darlim G, Lee MSY, Walter J, Rabi M. 2022 Data from: The impact of molecular data on the phylogenetic position of the putative oldest crown crocodilian and the age of the clade. Dryad Digital Repository. (doi:10.5061/dryad.q2bvq83mf)

Supplementary Material 1. List of modified scorings of *Portugalosuchus azenhae*

Supplementary Material 2. Age of taxa for tip-dating analysis

Supplementary Material 3. Phylogenetic analyses, paramters and resuls

Supplementary Material 4. Supplementary figures.

Supplementary Materials 5 and 6. Datasets available at:

doi:10.5061/dryad.q2bvq83mf

Supplementary Material 1

List of modified scorings of *Portugalosuchus azenhae* Mateus, Puértolas-Pascal and Callapez, 2019

The following character codifications for *Portugalosuchus* could not be confirmed using the published information of Mateus et al. (2019), therefore being re-scored here as 'unknown' for the species. In order to test the impact of the new scorings, the modified dataset was analyzed under different phylogenetic approaches (e.g., parsimony, undated and total evidence tip-dated Bayesian analyses; see supplementary files 1 and 2 for detail).

(65). 0→? Angular extends dorsally toward or beyond anterior end of foramen intermandibularis caudalis; anterior tip acute (0) or does not extend dorsally beyond anterior end of foramen intermandibularis caudalis; anterior tip very blunt (1).

(98). 1→? Antorbital fenestra present (0) or absent (1).

(100) 0→? Vomer entirely obscured by maxillae and palatines (0) or exposed on palate between palatines (1).

(106) 0→? Penultimate maxillary alveolus less than (0) or more than (1) twice the diameter of the last maxillary alveolus.

(108) 1→? Dorsal half of prefrontal pillar narrow (0) or expanded anteroposteriorly (1).

(115) 0→? Palatine process extends (0) or does not extend (1) significantly beyond anterior end of suborbital fenestra.

(127) 1→? Ectopterygoid extends (0) or does not extend (1) to posterior tip of lateral pterygoid flange at maturity.

(131) 0→? Anterior tip of frontal (0) forms simple acute point or (1) forms broad, complex sutural contact with the nasals

(157) 0→? Posterolateral margin of squamosal horizontal or nearly so (0) or upturned to form a discrete horn (1).

(161) 0→? Anterior foramen for palatine ramus of cranial nerve VII ventrolateral (0) or ventral (1) to basisphenoid rostrum.

(162) 1→? Sulcus on anterior braincase wall lateral to basisphenoid rostrum (0) or braincase wall lateral to basisphenoid rostrum smooth; no sulcus (1).
(170)1→? External surface of basioccipital ventral to occipital condyle oriented posteroventrally (0) or posteriorly (1) at maturity.

(171) 0→? Posterior pterygoid processes tall and prominent (0) or small and project posteroventrally (1) or small and project posteriorly (2).

(173) 1→? Basisphenoid not broadly exposed ventral to basioccipital at maturity; pterygoid short ventral to median eustachian opening (0) or basisphenoid exposed as broad sheet ventral to basioccipital at maturity; pterygoid tall ventral to median eustachian opening (1).

(180) 0→? Attachment scar for posterior mandibular adductor muscle on ventral surface of quadrate ramus forms modest crests (0) or prominent knob (1).

(187) 0→? Palatine-maxillary suture intersects suborbital fenestra at its anteromedial margin (0) or nearly at its anteriormost limit (1).

References

Mateus O, Puértolas-Pascual E, Callapez PM. 2019 A new eusuchian crocodylomorph from the Cenomanian (Late Cretaceous) of Portugal reveals novel implications on the origin of Crocodylia. *Zool. J. Linn. Soc.* **186**, 501–528. (doi.org/10.1093/zoolinnean/zly064)

Supplementary Material 2

Age of taxa for tip-dating analysis.

Taxon	Age older	Age younger	Stage	Source
Goniopholis simus	145	139.8	Cretaceous (Berriasian)	Salisbury et al., 1999
Theriosuchus pusillus	157	139	Late Jurassic (Kimmerdian) - Early Cretaceous (Berriasian)	Young et al., 2016
Bernissartia fagesii	125	125	Cretaceous (latest Barremian/earliest Aptian)	Clark and Norell, 1992
Alligator mississippiensis	0	extant	-	
Alligator sinensis	0	extant	-	

Caiman crocodilus	0	extant
Caiman latirostris	0	extant
Caiman yacare	0	extant
Crocodylus niloticus	0	extant
Crocodylus porosus	0	extant
Crocodylus rhombifer	0	extant
Gavialis gangeticus	0	extant
Mecistops cataphractus	0	extant
Melanosuchus niger	0	extant
Osteolaemus osborni	0	extant
Osteolaemus tetraspis	0	extant
Paleosuchus palpebrosus	0	extant

Paleosuchus trigonatus	0	extant		
Tomistoma schlegelii	0	extant		
Acynodon adriaticus	83.6	83.6	Cretaceous (Santonian/Campanian)	Delfino et al., 2008
Acynodon iberoccitanus	72.1	72.1	Cretaceous (Campanian/Maastrichtian)	Martin, 2007
Agaresuchus fontisensis	72.1	72.1	Cretaceous (Campanian/Maastrichtian)	Narváez et al., 2016
Agaresuchus subjuniperus	69	66	Cretaceous (Late Maastrichtian)	Puértolas-Pascual et al., 2013
Alligator mcgrewi	19	17	Miocene (Hemingfordian NALMA)	Whiting et al 2016
Alligator mefferdi	12	10	Miocene (Clarendonian NALMA)	Whiting et al 2016
Alligator olseni	19	17	Miocene (Hemingfordian NALMA)	Whiting et al 2016

Alligator prenasalis	33.9	33.9	Eocene: Priabonian/Rupelian (Chadronian/Orellan NALMA)	Whiting et al 2016
Alligator thomsoni	16.3	13.6	Miocene: Burdigalian/Langhian (Barstovian NALMA)	Whiting et al 2016
Allodaposuchus precedens	72.1	66	Cretaceous (Maastrichtian)	Delfino et al., 2008
Allognathosuchus polyodon	50.3	46.2	Eocene: Ypresian/Lutetian (Bridgerian NALMA)	Brochu 1999, 2004
Allognathosuchus wartheni	55.4	55.4	Eocene: Thanetian/Ypresian (Clarkforkian/Wasatchian NALMA)	Brochu, 1999, 2004
Arambourgia gaudryi	35	35	late Eocene (MP 18/19)	Kälin 1939
Arenysuchus gascabadiolorum	68	67	Cretaceous (Maastrichtian)	Puértolas et al., 2011

Asiatosuchus germanicus	48.2	44.4	Eocene (Ypresian-Lutetian)	Brochu & Miller-Camp 2018, Hastings & Hellmund 2017
Australosuchus clarkae	26	24	Late Oligocene (Chattian)	Yates, 2017
Baryphracta deponiae	48.2	48	Eocene (Ypresian)	Delfino et al. 2012
Borealosuchus acutidentatus	60.2	56.8	Paleocene: Selandian/Thanetian (Tiffanian NALMA)	Brochu et al., 2012
Borealosuchus formidabilis	60.2	56.8	Paleocene: Selandian/Thanetian (Tiffanian NALMA)	Brochu et al., 2012
Borealosuchus sternbergii	66	66	Late Cretaceous/Early Paleocene	Brochu, 1997
Borealosuchus threeensis	66	66	Late Cretaceous/Early Paleocene	Brochu et al., 2012

Borealosuchus wilsoni	50.3	50.3	Eocene (Wasatchian/Bridgerian NALMA)	Brochu et al., 2012
Boverisuchus magnifrons	48.2	44.4	Eocene (Ypresian-Lutetian)	Brochu & Miller-Camp 2018, Hastings & Hellmund 2017
Boverisuchus vorax	50.3	46.2	Eocene: Ypresian/Lutetian (Bridgerian NALMA)	Brochu, 2012
Brachychampsa montana	67.2	66	Cretaceous (Maastrichtian)	Norell et al., 1994
Brachychampsa sealeyi	82	74	Cretaceous (Campanian)	Williamson, 1996
Brachyuranochampsa eversolei	50.3	46.2	Eocene: Ypresian/Lutetian (Bridgerian NALMA)	Stout, 2012
Brochuchus pigotti	20.4	20.4	Miocene (Aquitainian/Burdigalian)	Conrad et al. 2013

Caiman lutescens	13.8	11.6	Miocene (Serravalian)	Brochu, 1999
Ceratosuchus burdoshi	56.8	55.4	Paleocene: Thanetian (Clarkforkian NALMA)	Bartels, 1984
Crocodylus acer	55.4	50.3	Eocene: Ypresian (Wasatchian NALMA)	Brochu, 2000
Crocodylus affinis	50.3	46.2	Eocene: Ypresian-Lutetian (Bridgerian NALMA)	Brochu, 2000
Crocodylus depressifrons	55.8	54.8	Eocene (Ypresian)	Delfino and Smith, 2009
Crocodylus megarhinus	37	36.6	Eocene (Priabonian)	Brochu 1997
Deinosuchus riograndensis	83.6	72.1	Cretaceous (Campanian)	Cossette and Brochu, 2020
Diplocynodon darwini	48.2	44.4	Eocene (Ypresian-Lutetian)	Brochu & Miller-Camp 2018, Hastings &

				Hellmund 2017
Diplocynodon hantoniensis	37.8	33.9	Eocene (Priabonian)	Rio et al, 2019
Diplocynodon muelleri	33.9	27.8	Oligocene (Rupelian)	Piras and Buscalioni, 2006; Martin, 2010
Diplocynodon ratelii	23	20.4	Miocene (Aquitanian)	Martin, 2010
Diplocynodon tormis	41.2	37.8	Middle Eocene (Bartonian)	Buscalioni et al, 1992; Macaluso et al, 2019
Dollosuchoides densmorei	47.8	41.2	Eocene (Lutetian)	Brochu, 2007a
Eocaiman cavernensis	41.6	39	Eocene: Lutetian/Bartonian (Barrancan SALMA)	Godoy et al, 2020; Ré et al, 2010
Eogavialis africanus	33.9	33.9	Eocene (Priabonian)/Oligocene (Rupelian)	Buffetaut, 1982

Eosuchus lerichei	59.2	56	Paleocene (Thanetian)	Delfino, 2005
Eosuchus minor	56	56	Paleocene (Thanetian)/ Eocene (Ypresian)	Brochu, 2006
Eothoracosaurus mississippiensi	72.1	72.1	Cretaceous (Campanian/Maastrichtian)	Brochu, 2004
Euthecodon arambourgii	20.4	15.9	Miocene (Burdigalian)	Ginsburg and Buffetaut 1978
Gavialis lewisi	5.3	2.5	Pliocene	Martin, 2018
Gavialosuchus eggenbergensis	18.2	20.4	Middle Miocene (lower Burdigalian)	Toula and Kail, 1885
Gryposuchus colombianus	13.8	11.6	Miocene (Serravallian)	Langston, 1997; Salas-Gismondi et al., 2016
Hassiacosuchus haupti	48.2	44.4	Eocene (Ypresian-Lutetian)	Brochu & Miller-Camp 2018,

				Hastings & Hellmund 2017
Hylaeochampsa vectiana	125	120	Cretaceous (Early Aptian)	Clark and Norell 1992
Iharkutosuchus makadii	86.3	83.6	Cretaceous (Santonian)	Ösi et al., 2007
Kambara implexidens	56	47.8	Eocene (Ypresian)	Salisbury and Willis, 1996
Kentisuchus spenceri	56	47.8	Eocene (Ypresian)	Brochu, 2007a
Leidyosuchus canadensis	83.6	72.1	Cretaceous (Campanian)	Wu, Russell and Brinkman 2001
Lohuecosuchus mechinorum	72.1	72.1	Cretaceous (Campanian/Maastrichtian)	Narváez et al., 2015
Lohuecosuchus megadontos	72.1	72.1	Cretaceous (Campanian/Maastrichtian)	Narváez et al., 2015
Melanosuchus fisheri	3.6	2.6	Pliocene (Piacenzian)	Medina, 1976

Mourasuchus atopus	13.8	11.8	Miocene (Laventan)	Langston, 1965
Navajosuchus mooki	65	60.2	Paleocene Danian (Puercan-Torrejonian NALMA)	Brochu, 2004
Orthogenysuchus olseni	55.4	50.3	Eocene Ypresian (Wasatchian NALMA)	Brochu, 1999
Pachycheilosuchus trinquei	113	100	Cretaceous (Albian)	Rogers, 2003
Paratomistoma courtii	41.2	37.8	Middle Eocene (Bartonian)	Brochu and Gingerich, 2000
Pietraroiasuchus ormezzanoi	125	119	Cretaceous (Aptian)	Buscalioni et al., 2011
Piscogavialis jugaliperforatus	7.2	5.3	Miocene (Messinian)	Kraus, 1998
Planocrania datangensis	61.6	59.2	Paleocene (Selandian)	Brochu 2012
Planocrania hengdongensis	59.2	56	Paleocene (Thanetian)	Brochu 2012; Ting 2003
Portugalosuchus azenhae	95	93.9	Cretaceous (Cenomanian)	Mateus et al., 2019

Procaimanoidea kayi	50.3	46.2	Ypresian/Lutetian (Bridgerian NALMA)	Brochu, 1999
Procaimanoidea utahensis	46.2	42	Lutetian (Uintan NALMA)	Gilmore, 1946
Prodiplocynodon langi	72.1	66	Cretaceous (Maastrichtian)	Mook, 1941
Purussaurus neivensis	13.8	11.8	Miocene (Serravalian)	Mook, 1941; Langston, 1965
Quinkana spp.	27.8	0.011	Late Oligocene-Pleistocene	Willis, 1997
Rimasuchus lloydi	18	17	Miocene (Burdigalian)	Storrs 2003; Brochu, 2007
Shamosuchus djadochtaensis	72.1	72.1	Cretaceous (Campanian/Maastrichtian)	Pol et al., 2009
Stangerochampsa mccabei	72.1	68	Cretaceous (Maastrichtian)	Wu et al., 1996
Thecachampsa antiqua	13.8	11.6	Miocene (Serravalian)	Leidy, 1852
Thoracosaurus macrorhynchus	66	61.6	Paleocene (Danian)	Brochu, 2004

Thoracosaurus neocesariensis	66	66	Maastrichtian/Paleocene	Brochu, 2004
Tomistoma cairense	44.5	41.2	Eocene (late Lutetian)	Müller, 1927; Brochu, 1997; Jouve, 2016
Tomistoma lusitanica	13.8	11.6	Miocene (Serravalian)	Brochu, 1997
Tomistoma petrolica	37.8	33.9	Late Eocene (Priabonian)	Shan et al., 2017
Toyotamaphimaea machikanensis	0.7	0.3	Pleistocene	Ijima et al., 2018
Trilophosuchus rackhami	14	13	Middle Miocene (late Langhian - early Serravalian)	Willis, 1993
Tsoabichi greenriverensis	55.4	50.3	Ypresian (Wasatchian NALMA)	Brochu, 2010
Voay robustus	0.1	0.011	Pleistocene-Holocene	Brochu, 2007
Wannaganosuchus brachymanus	60.2	56.8	Selandian/Thanetian(Tiffanian NALMA)	Brochu, 2004

Supplementary Material 3

PHYLOGENETIC ANALYSES PARAMETERS AND RESULTS

All of our analyses using molecular data either as a scaffold or combined with discrete morphological characters retrieved *Portugalosuchus azenhae*, as well as *Borealosuchus* spp., Planocraniidae and Allodaposuchidae, outside the crown-group Crocodylia. All the main results including number of most parsimonious trees and bootstrap support for the nodes are provided in the caption for each analysis on the figures from the electronic supplementary material (see file "Supplementary File 4"). For each analytical approach, we analysed both the 'original' and the modified dataset.

The data matrices and analysis files used in all analyses below are in Supplementary File 6.

1. Morphological data alone

1.1 Parsimony Analyses

The morphological datasets analyzed here include *i)* Narváez et al. (2016) as modified by Mateus et al. (2019) (NM), *ii)* Turner (2015) as modified by Mateus et al. (2019) (TM), and *iii)* Blanco (2021). We analyzed a modified version of NM by changing 16 characters scorings of *Portugalosuchus azenhae* to 'unknown' that are irreproducible based on the preservation of the fossil (see Supplementary File 1).

The parsimony analyses of modified NM and TM performed on TNT 1.5 (Goloboff and Catalano, 2016) followed the same parameters of Mateus et al. (2019), which is also the same parameters employed by Blanco (2021): The taxon *Goniopholis simus* was used as the outgroup taxon, tree-space was searched using a heuristic search

algorithm (traditional search method), with tree-bisection-reconnection (TBR) branch swapping, random seed set to 1 and 1000 random addition replicates holding 10 most parsimonious trees for each replicate. To recover all trees, a second search using the overflowed trees retained in the memory was performed. All characters were equally weighted and multistate characters were unordered. bootstrap frequencies (1000 bootstrap replicates searched) were calculated to assess the robustness of the nodes.

1.2 Undated Bayesian Analyses

Undated Bayesian analyses used MCMC as implemented in MrBayes 3.2.7 (Ronquist et al. 2012). The morphological characters were analyzed using the Lewis (2000) model, with correction for non-sampling of constant characters. Stepping-stone sampling favoured the inclusion of gamma parameter for rate variation across characters (Bayes Factor *sensu* Kass and Raftery 1995 > 400). For rooting, *Goniopholis* was the outgroup to all other taxa. Four independent runs (each with 4 incrementally-heated chains) were performed, each of length 50M with sampling every 5000, resulting in 10000 samples/run. Burnin (50%) and convergence in numerical parameters was confirmed by superimposed traces and high (>>100) effective sample sizes in Tracer (Rambaut et al. 2014) as well as similar within- and between-run variances in MrBayes (PSRF or potential scale reduction factor was ~1). Convergence in topology was confirmed via MrBayes (standard deviation of split ie clade frequencies between runs was low, <0.05). The post-burnin samples were combined in MrBayes to generate summary statistics and a majority-rule consensus tree with posterior probabilities. The full MrBayes file with all MCMC run settings can be found on Supplementary File 6.

2. Morphological and molecular data combined.

The supermatrix contained 9473 characters, in which characters 1–9284 are from molecular data, and the remaining (9285–9473) are discrete morphological characters. The molecular data of the 16 living taxa included in the analyses was taken from the supermatrix in Lee and Yates (2018); this was obtained from the dataset of Oaks (2011) combined with an alignment (7283–9284) from Gatesy et al. (2003), and with the addition of *Osteolaemus orborni* sequence from GenBank (JX627164 JX62722). All accession codes for the species are provided in the .mrb files on the Supplementary File 6.

The molecular scaffold was constructed manually on TNT based on the phylogenetic relationship of crocodylians according to the molecular hypothesis of Oaks (2011). The living taxa were set as non-floating taxa and the function 'enforce constraints' was activated before running the analyses, allowing all the fossil taxa to rearrange through the topology.

2.1 Parsimony Analysis.

Parsimony analysis used TNT, with all morphological and molecular character changes assigned unit weight (i.e. "unweighted"). Heuristic searches with multiple (20) random starting points were used, saving only 5000 trees per tree island (to avoid memory overflow on large tree island). Run files available on Supplementary File 6.

Bootstrapping (200 reps) was used to evaluate clade support; to reduce computation time to weeks rather than months, the above search setting was used but the number of random starting points was reduced to 10, and the number of saved trees per island was reduced to 1000. Bootstrap frequencies for each of the clades on the strict consensus are shown on Figures S1 and S2 (Supplementary File 4).

2.2 Undated Bayesian Analyses

Undated Bayesian analyses used MCMC as implemented in MrBayes (Ronquist et al. 2012), with settings for the morphological data as discussed in the Morphology Only analyses above. For the molecular data, partitioning schemes and substitution models were selected using PartitionFinder (Lanfear et al. 2012). Candidate partitions evaluated were: each codon for each locus (exons), each locus (introns, tRNAs and D-loop). BIC with unlinked branch lengths and common ("MrBayes") substitution models were used to ascertain the appropriate number of partitions; these settings were used to avoid selecting overly complex partitioning schemes and models, which might be analytically unnecessary and also cause problems with achieving convergence in Bayesian analysis. The favoured partition scheme involved 5 partitions with the following substitution models.

Subset	Best Model	Sites	Partition names
1	HKY+I	2387	LDHB_exon_6, ACTC_exon_4, aTROP_exon_6, rag1_1, cmos_1, ACTC_exon_5, LDHA_exon_7, LDHB_exon_7, rag1_2, GAPDH_exon_12, ACTB_exon_4, GAPDH_exon_11, LDHA_exon_8, cmos_2, RHO_exon_3, ACTB_exon_3, AChR_exon_8
2	K80+G	3562	GAPDH_intron_11, cmos_3, aTROP_intron_5, ACTB_intron_3, AChR_intron_7, LDHA_intron_7, LDHB_intron_6, AChR_exon_7, ACTC_intron_4, aTROP_exon_5, RHO_exon_2, rag1_3, RHO_intron_2
3	GTR+G	1581	tRNAarg, CYTB_1, DLOOP, ND2_1, tRNAmet, tRNAglu, tRNAgly, ND3_1

4	HKY+G	887	ND2_2, ND3_2, tRNAtrp, CYTB_2
5	GTR+I+G	867	CYTB_3, ND3_3, ND2_3

The combined analyses used 6 independent partitions (morphology and the 5 molecular partitions), with above models. For rooting, *Goniopholis* was the outgroup to all other taxa.

Four independent runs with 6 incrementally-heated chains were performed, initially each of length 50M with sampling every 5000, resulting in 10000 samples/run. Burnin (20%) and convergence in numerical parameters was confirmed by superimposed traces and high (>100) effective sample sizes in Tracer (Rambaut et al. 2014) as well as similar within- and between-run variances in MrBayes (PSRF or potential scale reduction factor was ~1). Convergence in topology was confirmed via MrBayes (standard deviation of split ie clade frequencies between runs was low, <0.05).

2.3 Tip-Dated Bayesian Analyses

The tip-dated Bayesian analyses used MCMC as implemented in BEAST 2.6 and related packages. The morphological characters were analyzed using the Lewis (2000) model, with correction for non-sampling of constant characters. The molecular data were analyzed using the same (PartitionFinder) models as in above undated analysis.

The Sampled Ancestor Birth-Death tree prior was used. Separate relaxed (uncorrelated lognormal: Drummond et al. 2006) clocks were allocated to the morphological and molecular partitions. For rooting, *Goniopholis* was again the outgroup to all other taxa. Tip dates were as presented in Supplementary File 2.

Four independent runs were performed, each of length 100M with sampling every 10000, resulting in 10000 samples/run. Burnin and convergence was confirmed by

superimposed traces and high (>100) effective sample sizes in Tracer (Rambaut et al. 2014). The post-burnin samples were combined in LogCombiner, and TreeAnnotator was used to generate a consensus tree (maximum clade credibility) and associated summary statistics. In contrast to the other analyses, this analysis robustly retrieved thoracosaurs as stem crocodylians, far removed from living gavials, as also recovered by Lee and Yates (2018) (Figure S10, supplementary file 4).

References

Blanco A. 2021 Importance of the postcranial skeleton in eusuchian phylogeny: Reassessing the systematics of allodaposuchid crocodylians. *PloS ONE* **16**, e0251900. doi.org/10.1371/journal.pone.0251900

Drummond AJ, Ho SYW, Phillips MJ, Rambaut A. 2006 Relaxed phylogenetics and dating with confidence. *PLoS Biology*. **4**, e88. (doi:10.1371/journal.pbio.0040088)

Gatesy J, Amato G, Norell M, DeSalle R, Hayashi C. 2003 Combined support for wholesale Taxic atavism in gavialine crocodylians. *Syst. Biol*. **52**, 403–422. (doi.org/10.1080/10635150390197037)

Goloboff PA, Catalano SA. 2016. TNT version 1.5, including a full implementation of phylogenetic morphometrics. *Cladistics*, **32**, 221–238. (doi.org/10.1111/cla.12160)

Lanfear R, Calcott B, Ho SYW, Guindon S. 2012. PartitionFinder: Combined Selection of Partitioning
Schemes and Substitution Models for Phylogenetic Analyses. *Mol. Biol. Evol*. **6**, 1695–1701. (doi.org/10.1093/molbev/mss020)

Lee MSY, Yates AM. 2018 Tip dating and homoplasy: reconciling the shallow molecular divergences of modern gharials with their long fossil record. *Proc. R. Soc. B*. **285**, 20181071. (doi.org/10.1098/rspb.2018.1071).

Mateus O, Puértolas-Pascual E, Callapez PM. 2019. A new eusuchian crocodylomorph from the Cenomanian (Late Cretaceous) of Portugal reveals novel implications on the origin of Crocodylia. *Zool. J. Linn. Soc.* **186**, 501–528. (doi.org/10.1093/zoolinnean/zly064)

Oaks JR, 2011. A time-calibrated species tree of Crocodylia reveals a recent radiation of the true
crocodiles. *Evolution*. **65**, 3285–3297. (doi.org/10.1111/j.1558-5646.2011.01373.x)

Rambaut A., Suchard MA, Xie D & Drummond AJ. 2014 Tracer v1.6, Available from http://beast.bio.ed.ac.uk/Tracer

Ronquist F, Teslenko M, van der Mark P, Ayres DL, Darling A, Höhna S, Larget B, Liu L, Suchard MA, Huelsenbeck JP. 2012 MrBayes 3.2: efficient Bayesian phylogenetic inference and model choice across a large model space. *Syst. Biol*. **61**, 539–542. (doi: 10.1093/sysbio/sys029)

Turner AH. 2015 A review of *Shamosuchus* and *Paralligator* (Crocodyliformes, Neosuchia) from the Cretaceous of Asia. *PLoS ONE*. **10**, e0118116. (doi.org/10.1371/journal.pone.0118116)

Supplementary Material 4

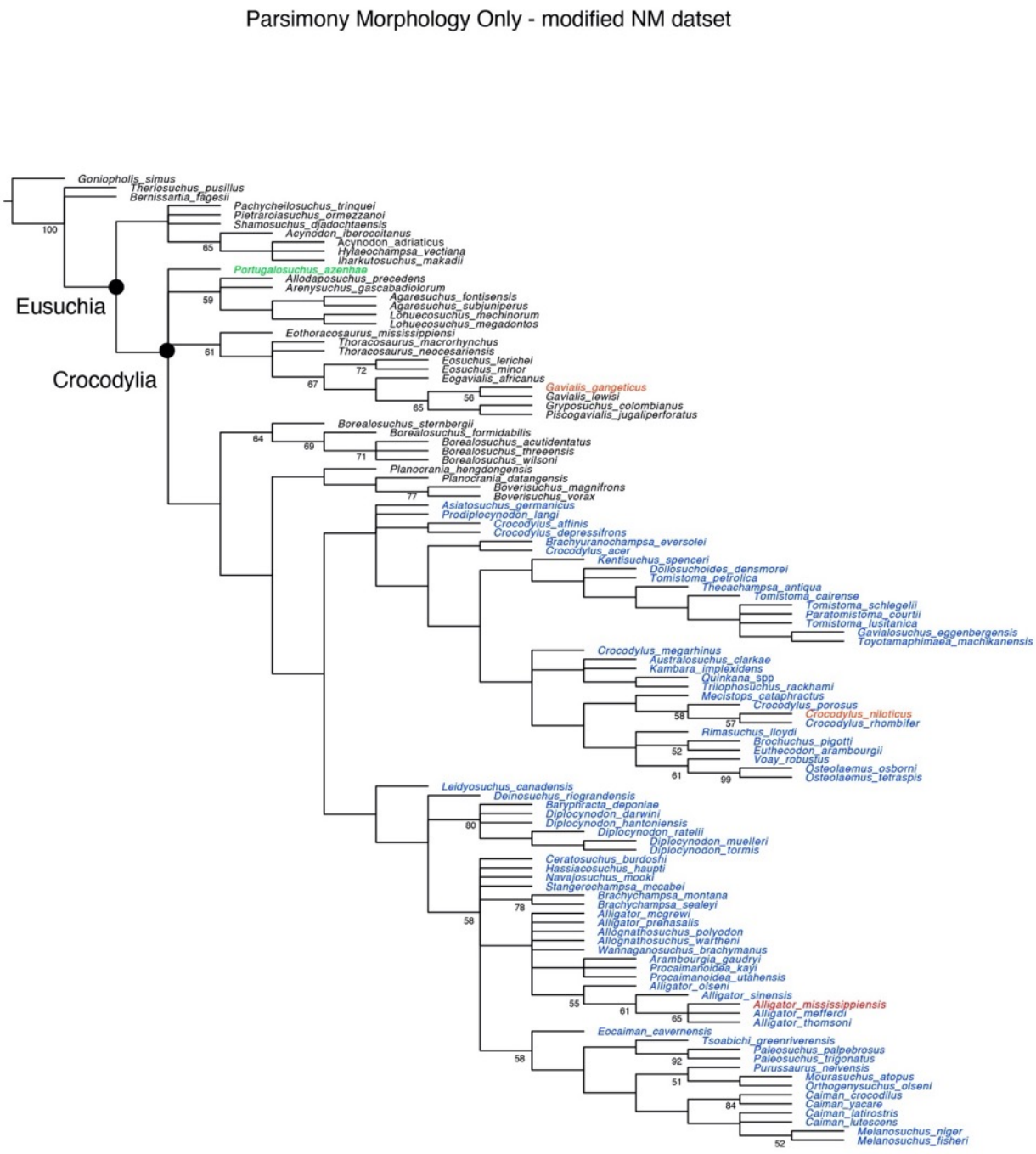

Figure S1. Parsimony Analysis Morphology Only, modified NM dataset. Strict consensus of 11160 most-parsimonious trees. Numbers on nodes indicate GC Bootstrap values (50% cut).

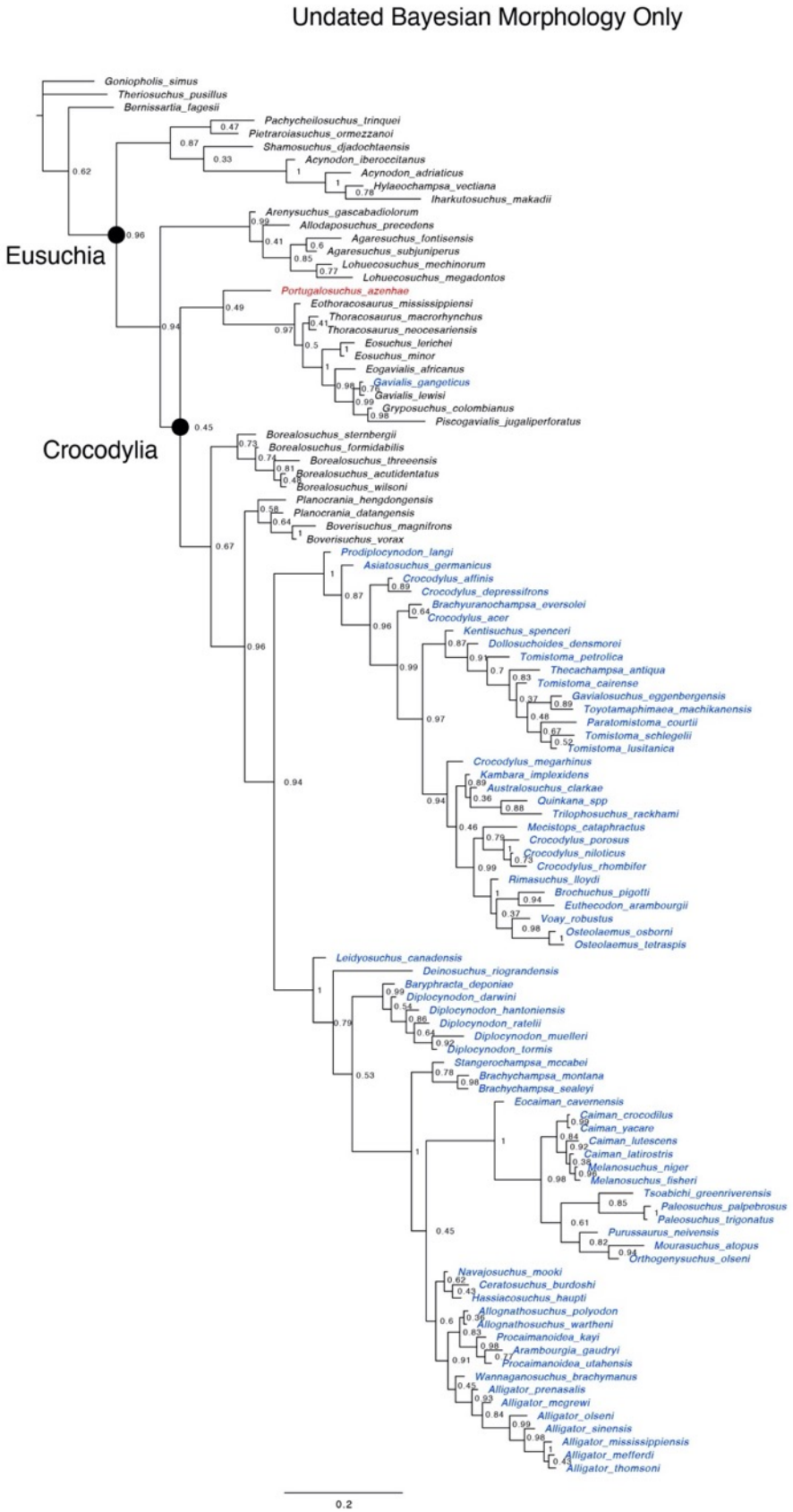

Figure S2. Morphology Only, Undated Bayesian Analysis. Original NM dataset. Majority-rule consensus of sampled post-brunin trees, with clade posterior probabilities at nodes.

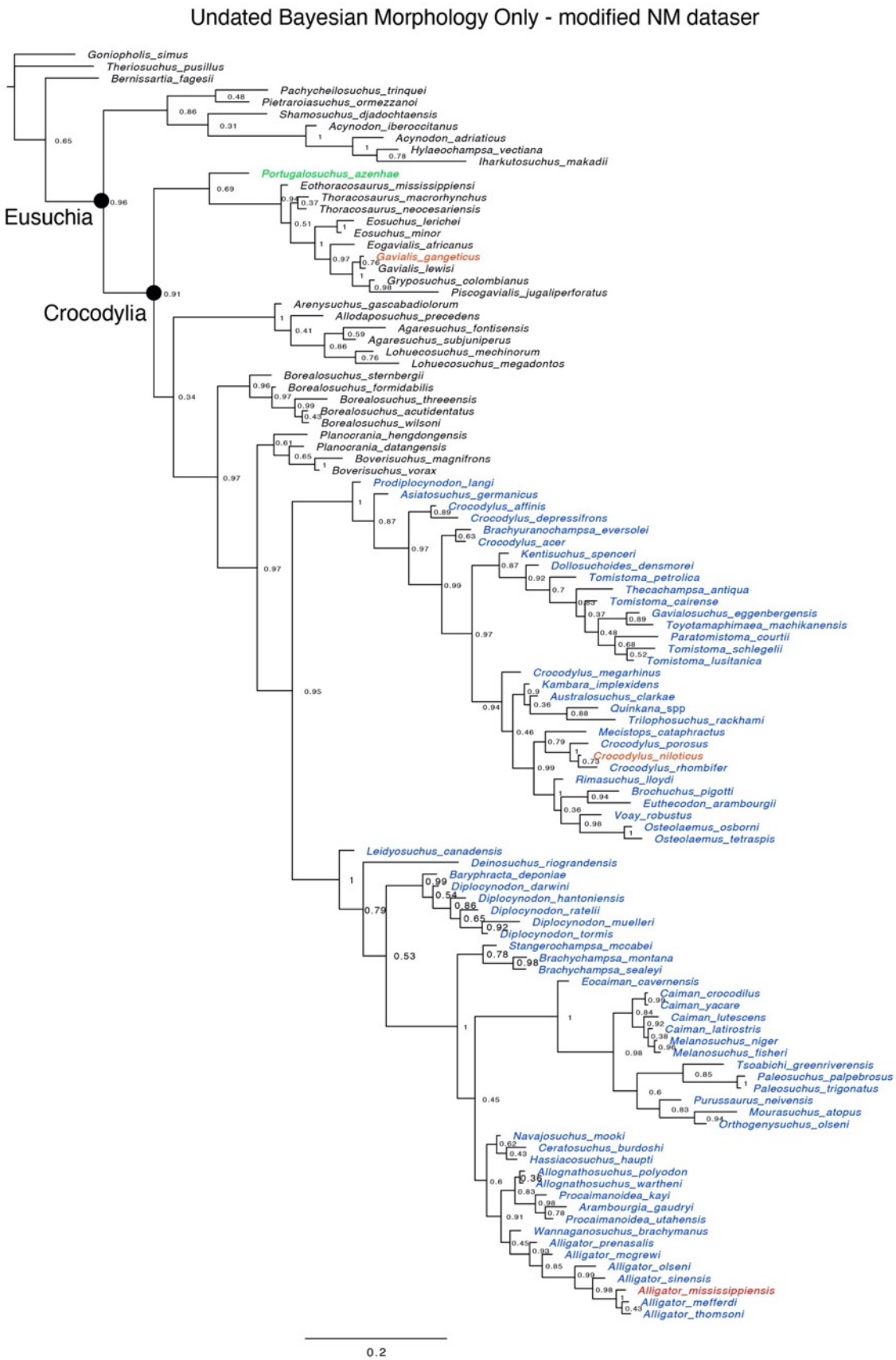

Figure S3. Morphology Only, Undated Bayesian Analysis. Modified NM dataset. Majority-rule consensus of sampled post-brunin trees, with clade posterior probabilities at nodes.

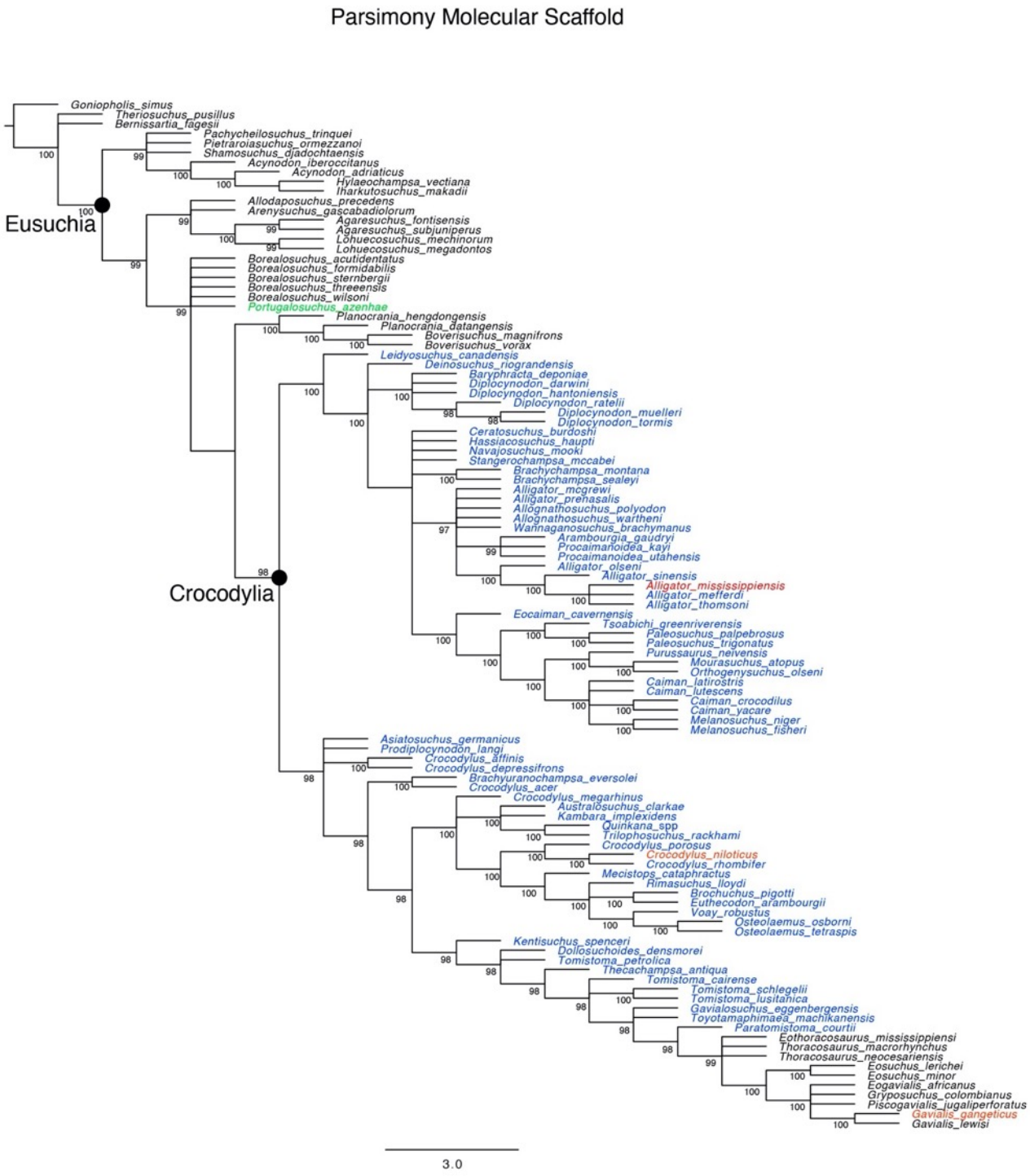

Figure S4. Parsimony Analysis, Molecular Scaffold on original NM dataset. Strict consensus of 10000 most-parsimonious trees. Numbers on nodes indicate GC Bootstrap values (50% cut).

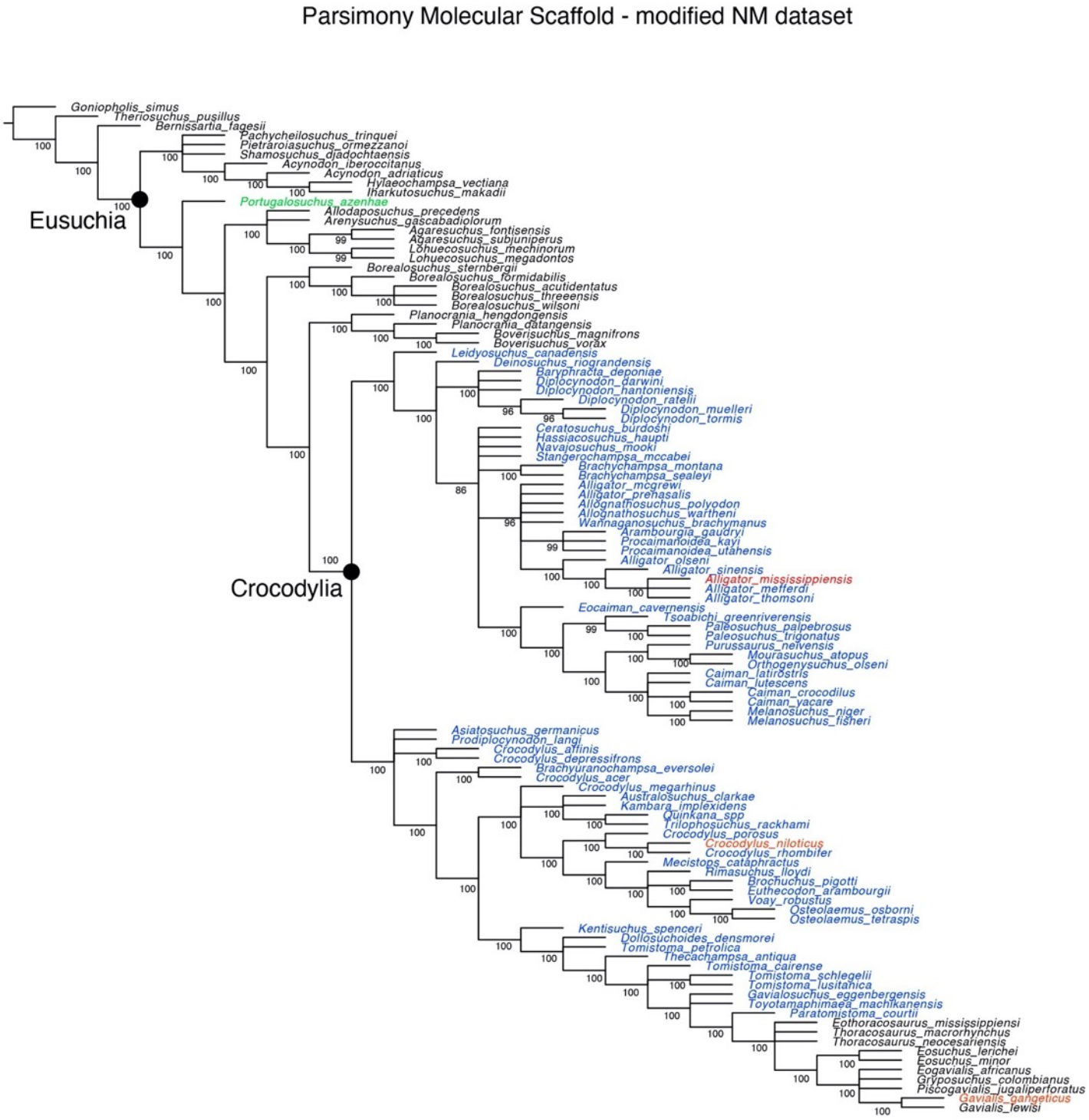

Figure S5. Parsimony Analysis, Molecular Scaffold on modified NM dataset. Strict consensus of 10000 most-parsimonious trees. Numbers on nodes indicate GC Bootstrap values (50% cut).

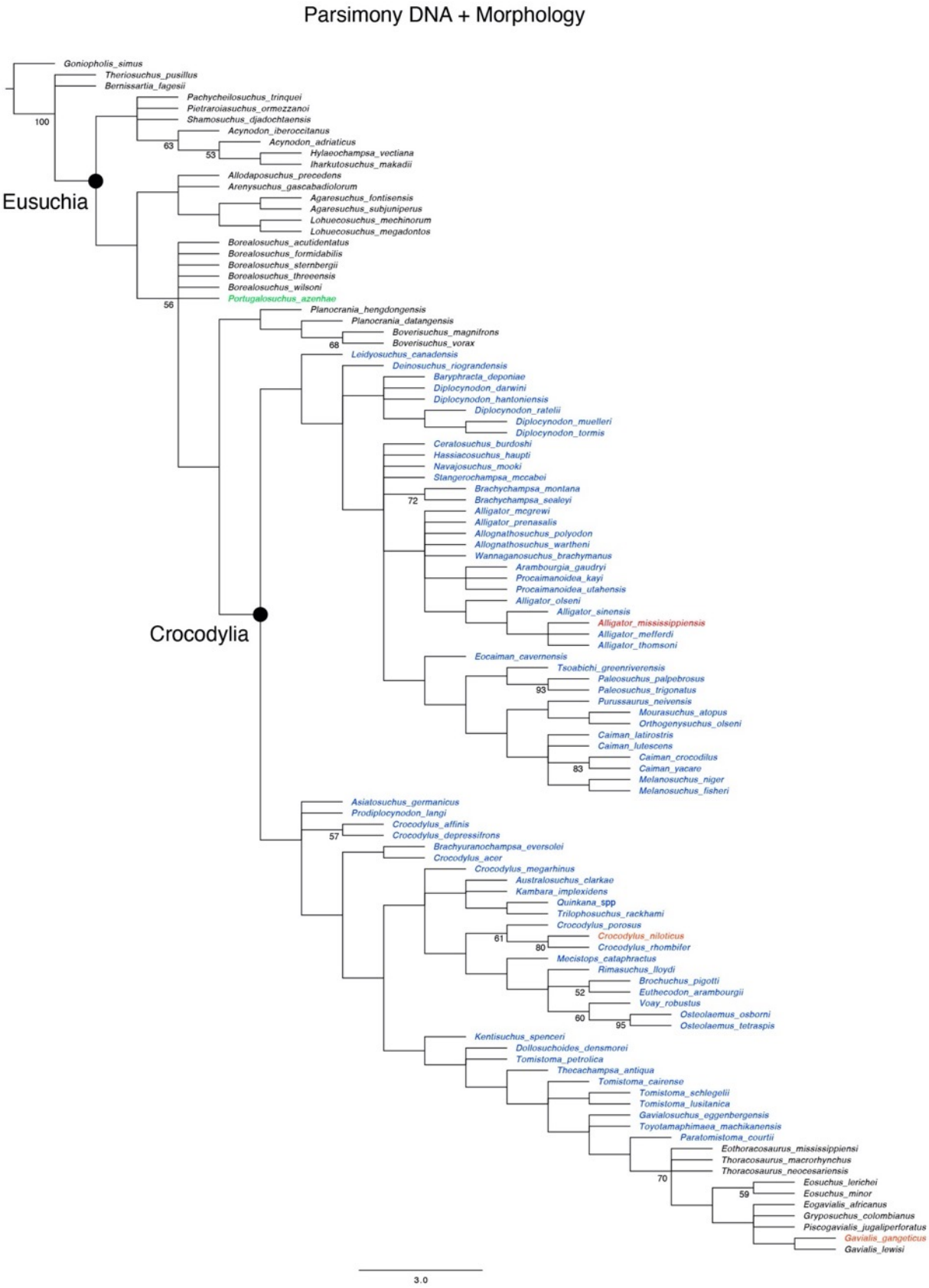

Figure S6. Morphology and Molecules, Parsimony Analysis of original NM dataset. Strict consensus of 10000 most-parsimonious trees of lenght 5485. Numbers on nodes indicate GC Bootstrap values (50% cut).

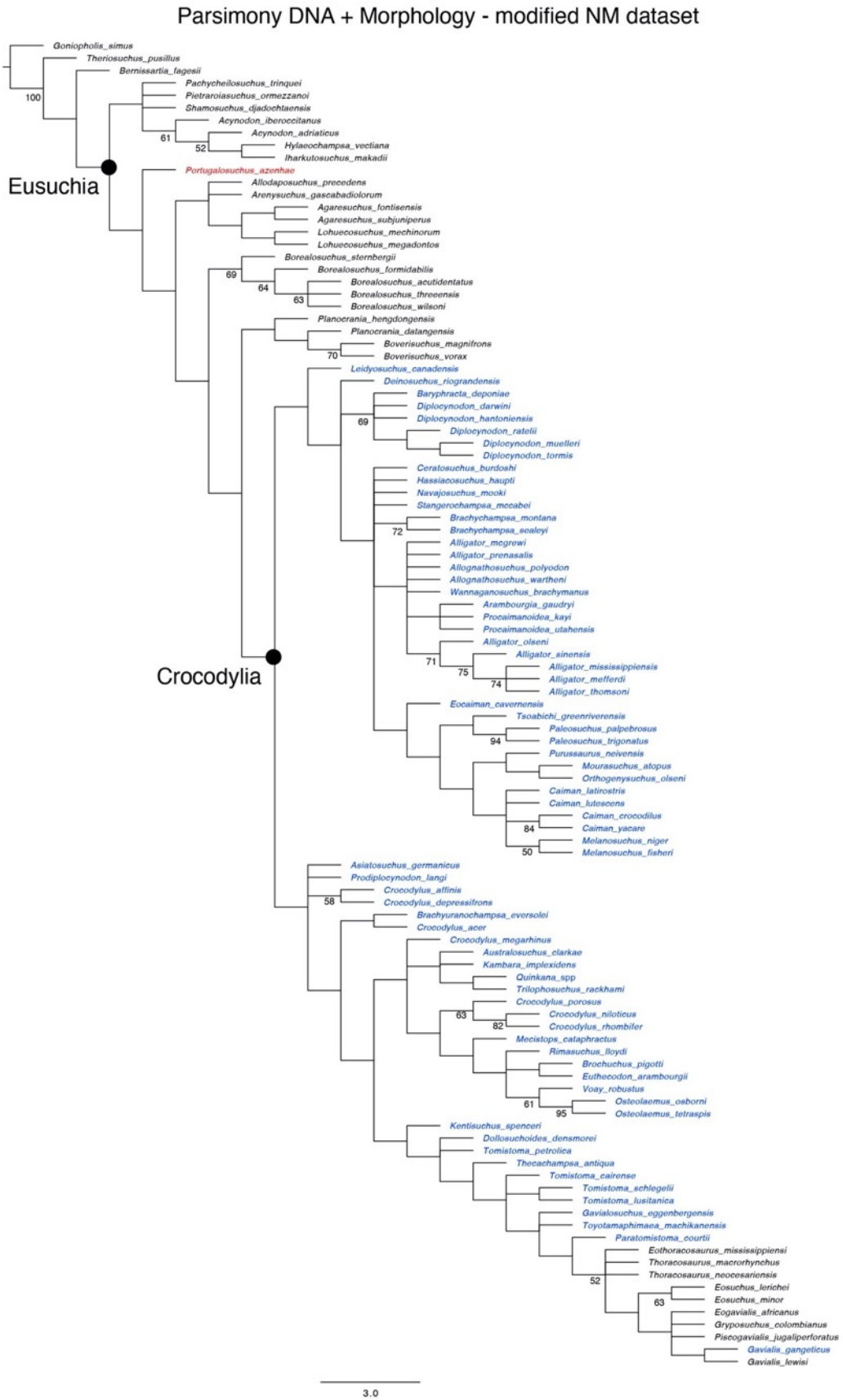

Figure S7. Morphology and Molecules, Parsimony Analysis of modified NM dataset. Strict consensus of 10000 most-parsimonious trees of lenght 5483. Numbers on nodes indicate GC Bootstrap values (50% cut).

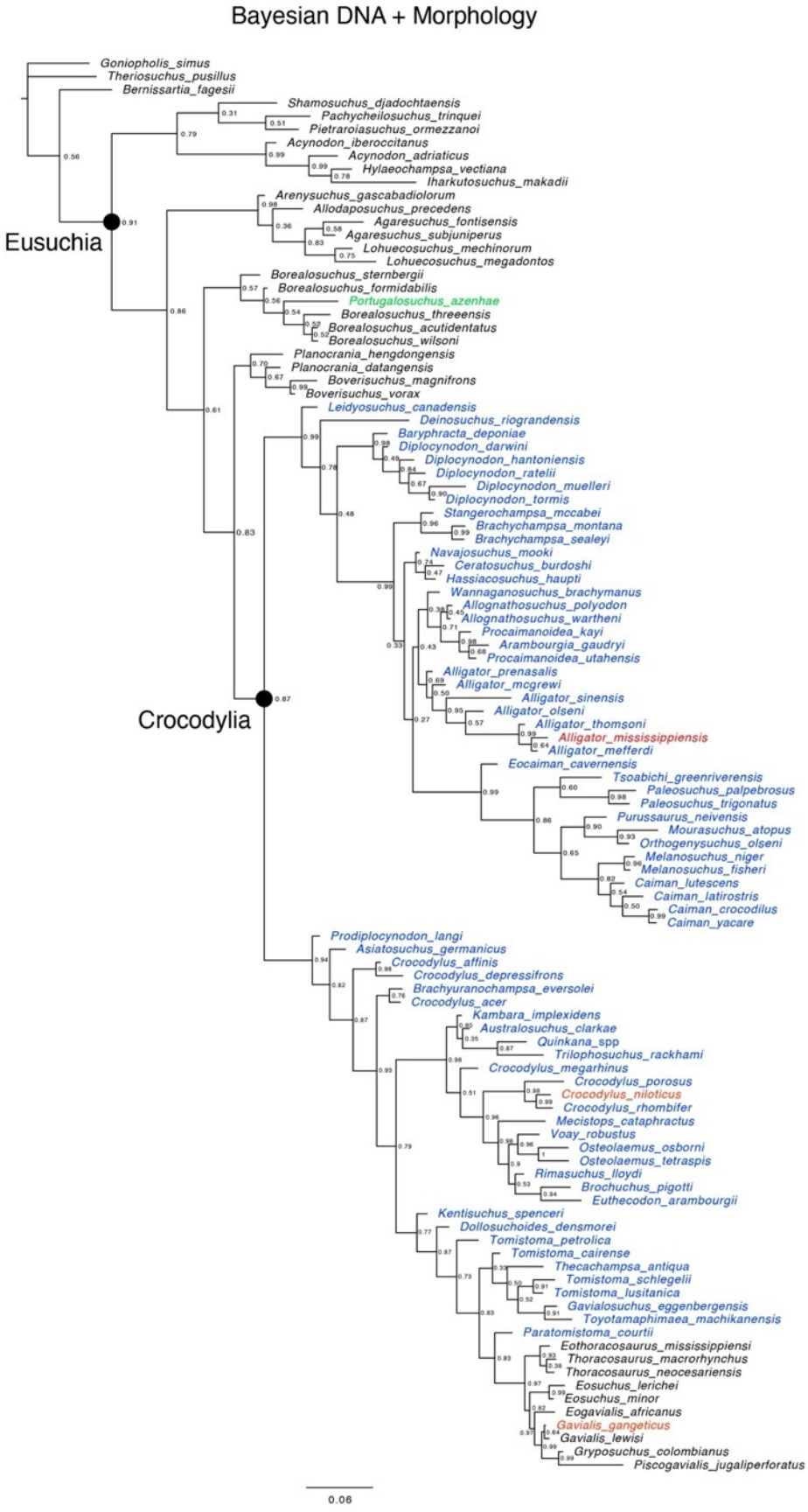

Figure S8. Morphology and Molecules, Undated Bayesian Analysis of original NM dataset. Majority-rule consensus of sampled post-burnin trees, with clade posterior probabilities at nodes.

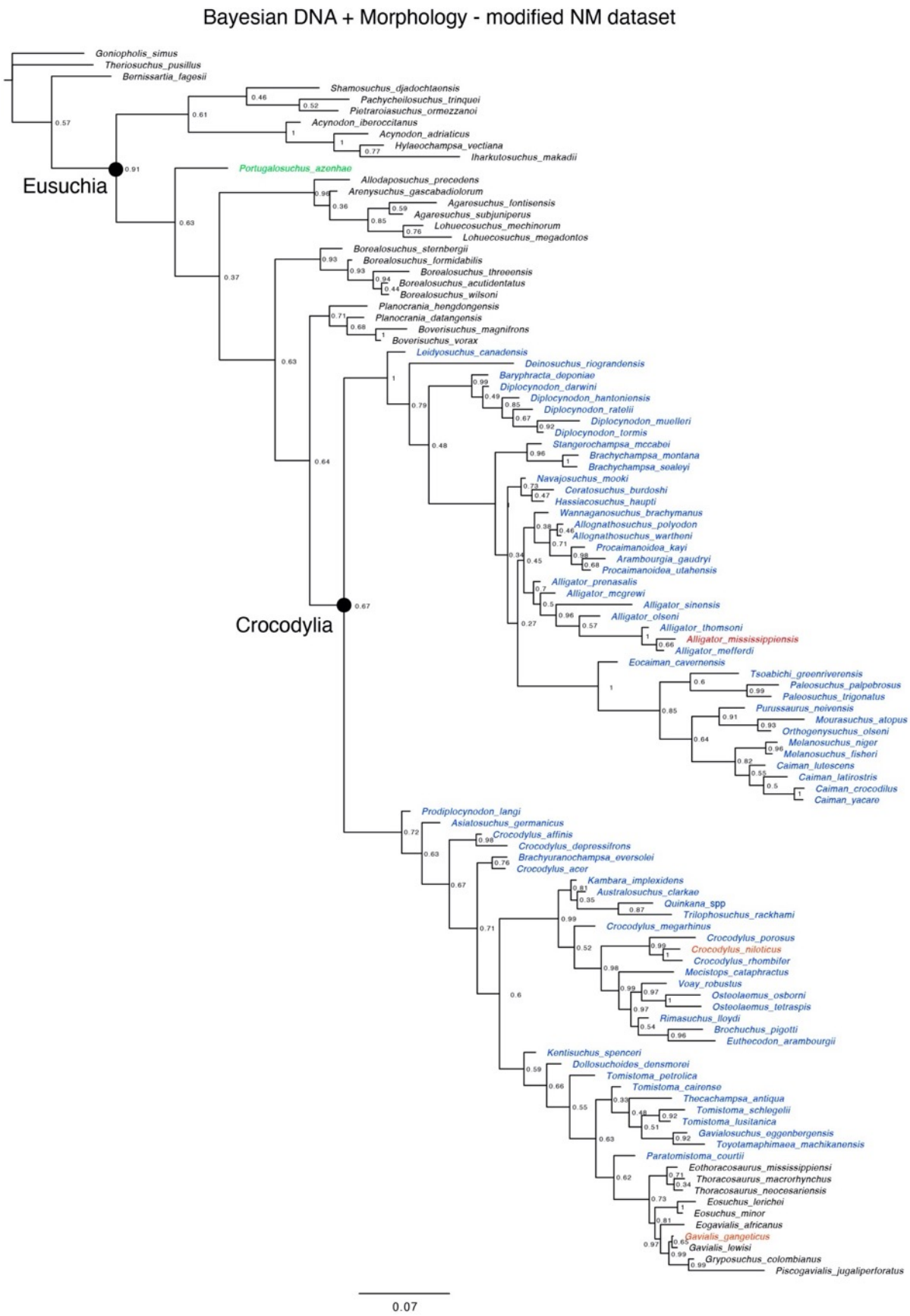

Figure S9. Morphology and Molecules, Undated Bayesian Analysis of modified NM dataset. Majority-rule consensus of sampled post-burnin trees, with clade posterior probabilities at nodes.

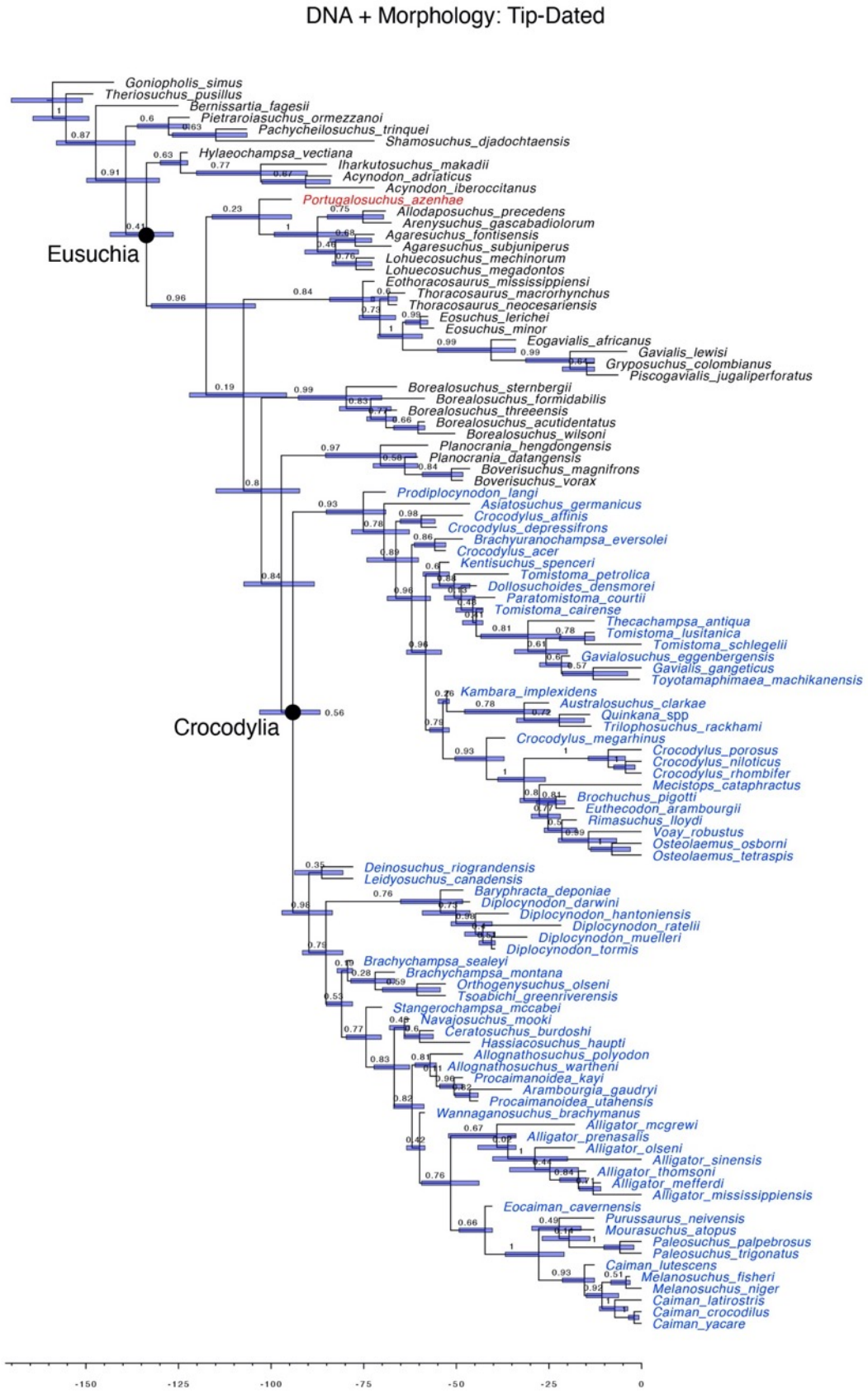

Figure S10. Morphology and Molecules, Tip-Dated Bayesian Analysis. Original NM dataset. Maximum clade credibility consensus of sampled post-burnin trees. Node information includes clade posterior probability (number) and 95% HPD for age estimate (blue bar).

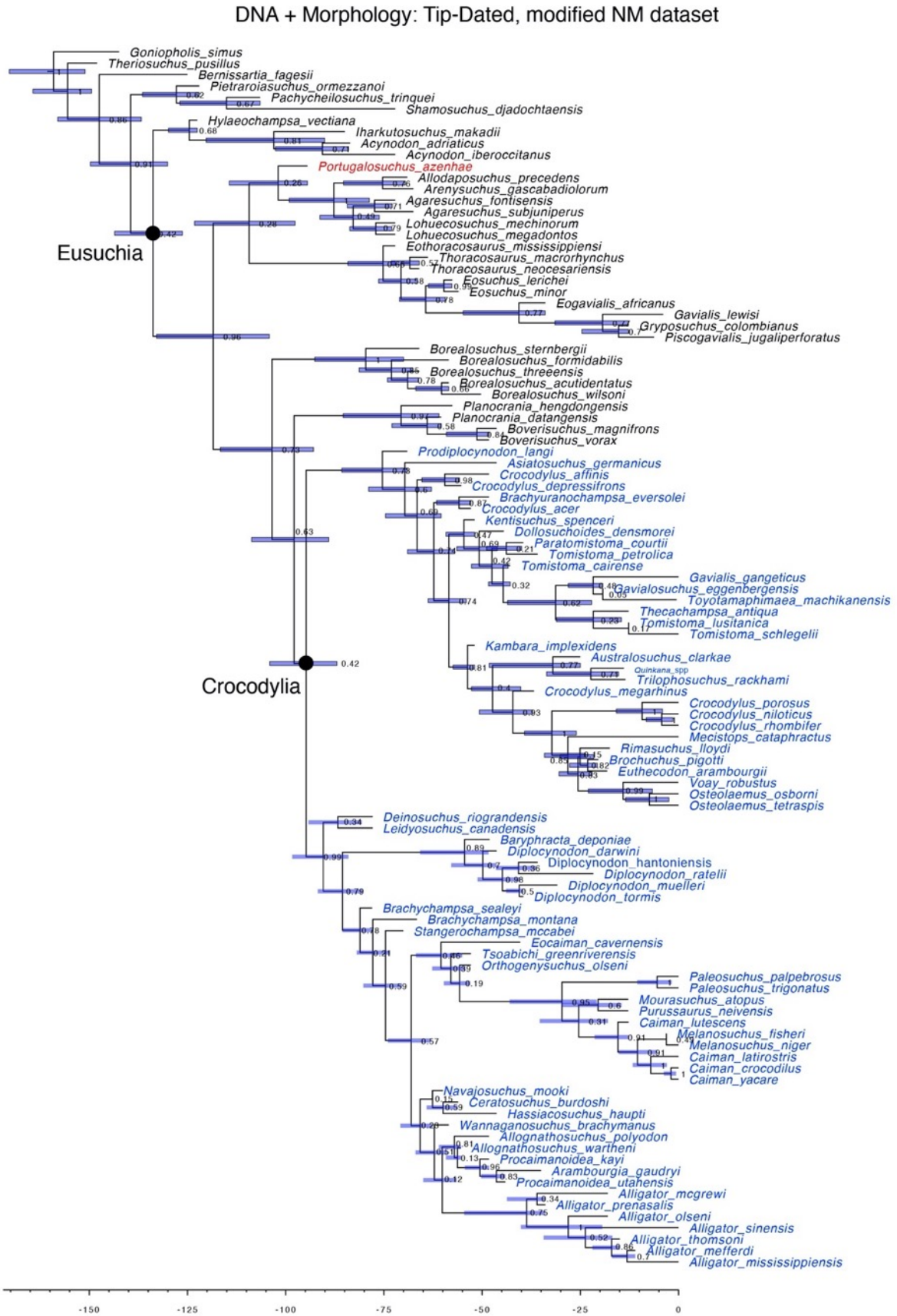

Figure S11. Morphology and Molecules, Tip-Dated Bayesian Analysis. Modified NM dataset. Maximum clade credibility consensus of sampled post-burnin trees. Node information includes clade posterior probability (number) and 95% HPD for age estimate (blue bar).

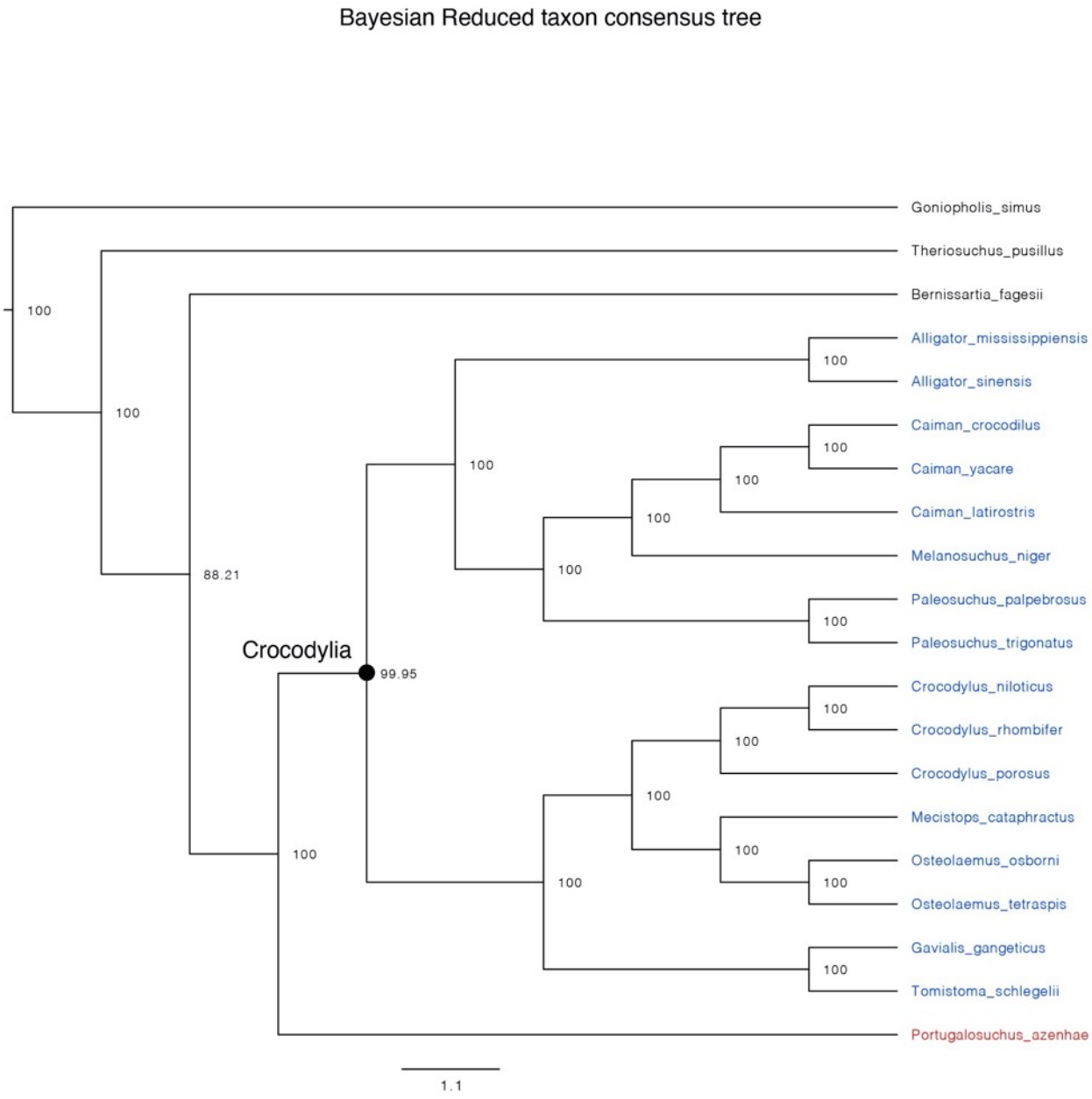

Figure S12. Reduced taxon majority-rule consensus tree, Undated Bayesian Analysis, original NM dataset. Values indicate node support based on posterior probality, showing high support of *Portugalosuchus azenhae* outisde Crocodylia.

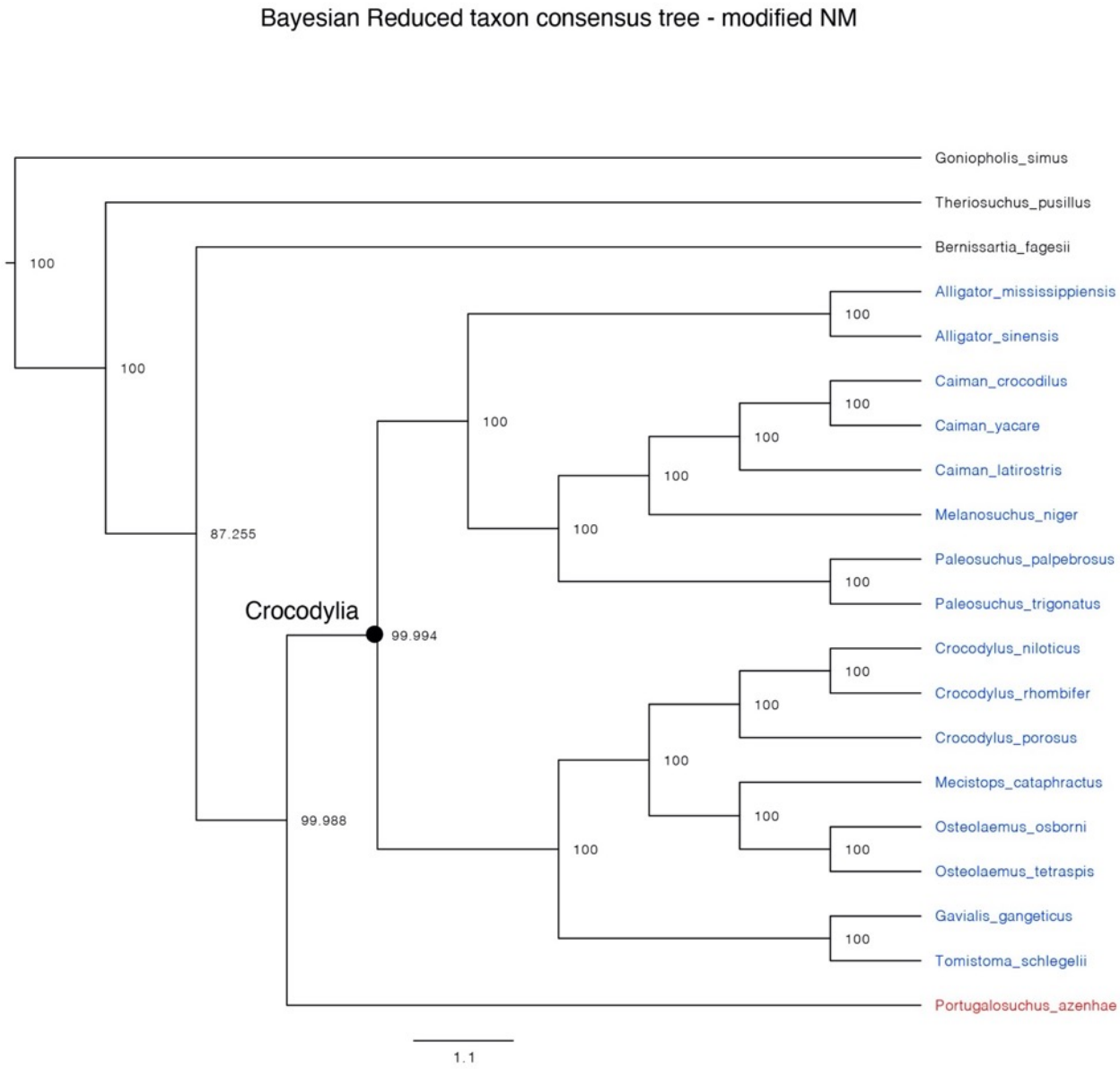

Figure S13. Reduced taxon majority-rule consensus tree, Undated Bayesian Analysis, modified NM dataset. Values indicate node support based on posterior probality, showing high support of *Portugalosuchus azenhae* outisde Crocodylia.

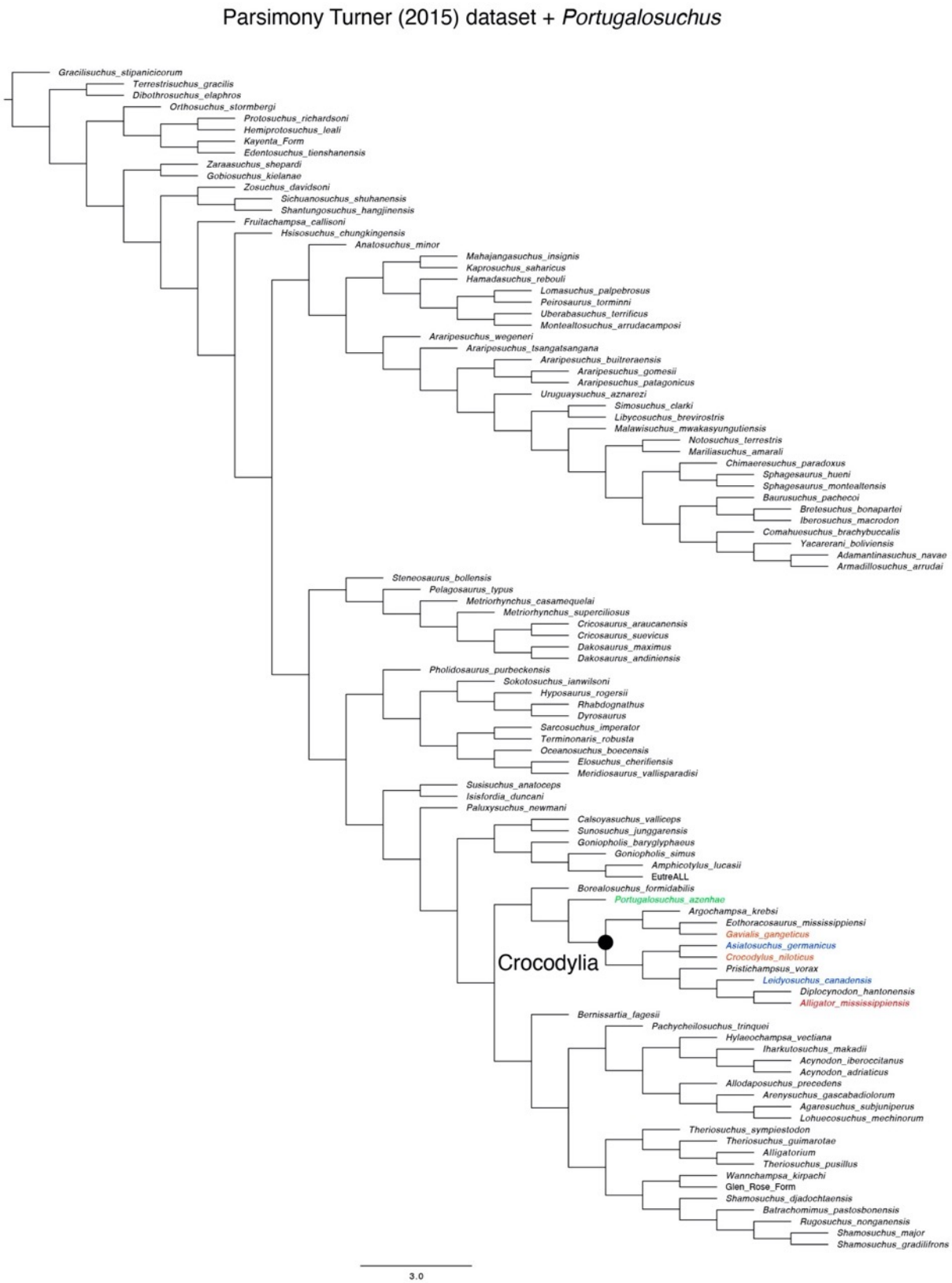

Figure S14. Parsimony Analysis, addition of Portugalosuchus azenhae to Turner (2015) dataset (as in Mateus et al., 2019). One of the 660 most-parsimonious trees.

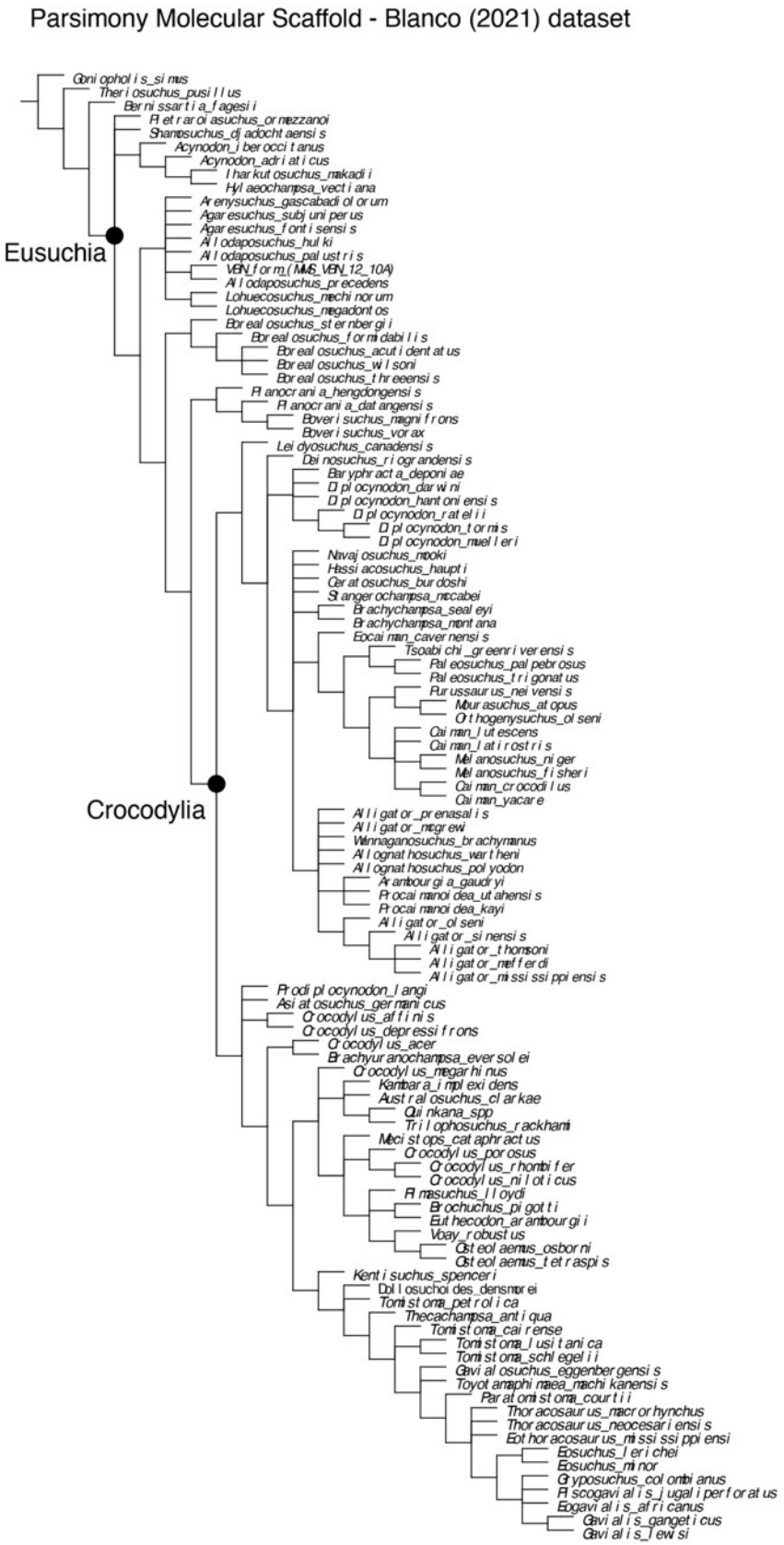

Figure S15. Parsimony Analysis, Molecular Scaffold on Blanco (2021) dataset. Strict consensus of 3600 most-parsimonious trees.

Chapter 2

On the origin of Caimaninae: insights from new fossils of *Tsoabichi greenriverensis* and a review of the evidence

Explanation of candidate contribution to collaborative work

This chapter is based on collaborative work. The text represents the published version of the following manuscript:

Walter, J., **Darlim, G.**, Massonne, T., Aase, A., Frey, E., & Rabi, M. (2022). On the origin of Caimaninae: insights from new fossils of *Tsoabichi greenriverensis* and a review of the evidence. *Historical Biology*, *34*(4), 580-595. (https://doi.org/10.1080/08912963.2021.1938563)

Author contributions

Walter. J. conceptualization, visualization, investigation, formal analysis, writing (original draft); **Darlim, G.** conceptualization, investigation, formal analysis, writing (original draft); Massonne, T. visualization, investigation, formal analysis; Aase, A investigation, visualization; Frey, E. data curation; Rabi, M. conceptualization writing (review and editing).

On the origin of Caimaninae: insights from new fossils of *Tsoabichi greenriverensis* and a review of the evidence

Abstract

An incomplete fossil record and unstable phylogenies of extinct taxa hamper reconstructing the early evolution of Caimaninae. We describe previously unpublished articulated fossils of a key species, *Tsoabichi greenriverensis* from the early Eocene Green River Formation of North America, exhibiting further character evidence for the caimanine affinities of this taxon. Parsimony analysis of modified morphological taxon-character datasets coupled with a critical review of character evolution and published phylogenies reveals that fossil evidence for Palaeogene crown group and Late Cretaceous total-group representatives is unreliable due to uncertain character evolution in early Alligatoridae. The earliest unambiguous fossil age for total and crown-group Caimaninae are 63.5 Ma and 18.06 Ma, respectively. These calibration points follow best practices and are vital for better constrained estimates of time calibrated analyses. Phylogeny continues to imply two separate Caimaninae dispersals between North and South America, but instead of a northward back-dispersal, we find two Palaeogene dispersals to South America an equally likely hypothesis. Miocene taxa of Central America previously assigned to the stem lineage ancestral to South American Caimaninae are reinterpreted as part of a Neogene northward expansion of the crown group.

INTRODUCTION

Caimaninae represents the stem-based group including *Caiman crocodilus* and all crocodylians more closely related to it than to *Alligator mississippiensis* (Brochu 2003).

The oldest unambiguous fossils of the clade are known from the early Palaeocene of South America (Bona 2007; Brochu 2011; Bona et al. 2018; Cidade et al. 2020), but Late Cretaceous taxa from North America, otherwise usually considered basal alligatoroids (*Stangerochampsa mccabei* and *Brachychampsa* spp.), have been recovered as basal caimanines in some studies (Salas-Gismondi et al. 2015; Bona et al. 2018; Cossette 2020; Stocker et al. 2021). Regardless of the uncertainty around the Late Cretaceous fossil record of Caimaninae, the spatio-temporal distribution of the outgroups (Alligatorinae and basal alligatoroids) suggests an origin and dispersal to South America at latest around the K/Pg boundary (e.g., Brochu 1999, 2010, 2011; Hastings et al. 2013; Bona et al. 2018). The timing of total and crown-group Caimaninae origin and details of early biogeographic history nevertheless remains uncertain due to gaps in the fossil record, poor stratigraphic fit of phylogenies (e.g., Salas-Gismondi et al. 2015; Hastings et al. 2016; Bona et al. 2018; Cidade et al. 2020; Cossette 2020; Stocker et al., 2021), conflicting divergence date estimates (Oaks 2011; Pan et al. 2020), *ad hoc* fossil calibrations (Bittencourt et al. 2019; Godoy et al. 2020), and lack of consensus regarding the placement of key taxa (e.g., *Brachychampsa* spp., *Necrosuchus ionensis, Tsoabichi greenriverensis, Bottosaurus* spp., *Globidentosuchus brachyrostris*). The North American *Tsoabichi greenriverensis* Brochu (2010) is a species of particular interest owing to its geographic occurrence, early Eocene age, and potential affinities with the crown group.

Tsoabichi greenriverensis is one of the few caimanine species found in North America. It was described based on rare but complete cranial and postcranial remains from the deposits in the Green River Formation (Brochu 2010), Wyoming, dated to the Wasatchian North American Land Mammal Age (NALMA). Previous phylogenies have either recovered the species in an unresolved position relative to the crown group

(Brochu 2010, 2011; Pinheiro et al. 2013; Salas- Gismondi et al. 2015; Bona et al. 2018; Cidade et al. 2020; Godoy et al. 2020), within the crown as sister to extant dwarfcaimans, *Paleosuchus* spp. (Fortier et al. 2014; Salas- Gismondi, 2015; Cidade et al. 2017; Bona et al. 2018; Cossette and Brochu 2018; Massonne et al. 2019) or sister to crown-group Caimaninae (Hastings et al. 2013). The phylogenetic position of *Ts. greenriverensis* is therefore highly relevant regarding the spatio-temporal origin of crown caimanines, as it may attest the presence of the group already by the early Eocene (Bona et al. 2018; Cossette and Brochu 2018; Massonne et al. 2019; Cossette 2020). *Tsoabichi greenriverensis* as a crown-group Caimaninae would suggest a rather complex palaeobiogeography, involving a back-dispersal from South to North America (Brochu 2010, 2011; Hastings et al. 2013; Bona et al. 2018; Cossette 2020). We here describe previously unpublished articulated specimens of *Ts. greenriverensis* from the Green River Formation and report additional morphological evidence for both the caimanine affinities of the species and its phylogenetic position within the group. In the light of these new data and through modifications of published character-taxon matrices, we provide a comprehensive and critical review of the Caimaninae fossil phylogeny with novel insights into divergence timing and early biogeographic history. Furthermore, we propose previously lacking explicit fossil calibrations for total and crown-group Caimaninae following best practices (Parham et al. 2012).

Institutional abbreviations

FMNH – Field Museum of Natural History, USA, Chicago; SMNK - Staatliches Museum für Naturkunde, Germany, Karlsruhe; TMM – Texas Memorial Museum, USA, Austin; UCM – University of Colorado Museum of Natural History, USA, Boulder; UNSM – University of Nebraska State Museum, USA, Lincoln.

MATERIAL AND METHODS

Geologic settings

Lacustrine sediments comprising the Green River Formation were deposited in three basins by intermittently interconnected lakes over a span of 8 Myr (Smith et al. 2008, and references cited therein). Lake Gosiute (Figure 1) extended eastward from the leading edge of Wyoming's thrust sheet to the Wind River Mountains in the north and the Washakie Basin near Wamsutter, Wyoming in the south. The basal Tipton Member is dominated by siliciclastic sediments typical of an overfilled lake, followed by underfilled evaporites of the Wilkins Peak Member. The terminal Laney Member is primarily balanced-fill sediments (Carroll and Bohacs 1999) with beds containing abundant fossil fish. The Farson Fish Beds and Eighteen-Mile Canyon are two areas well-known for their abundant fish fossils. Rocks in the Farson Fish Beds tend to split irregularly along weak parting plains. The fish species are diverse but commonly the bones were dissolved leaving a mould. Rocks of the Eighteen-Mile Canyon area split into large sheets containing mass-mortality assemblages of *Gosiutichthys parvus*, a small freshwater herring that swam in large schools. At both localities, the freshly split rock is yellow, with a brighter yellow colour typical of the Eighteen-Mile Canyon area.

The Layered Tuff below the Laney Member was dated at 50.1 ± 0.09 Ma and the Analcine Tuff near the top was dated at 49.25 ± 0.12 Ma (Smith et al. 2008, 2010). These dates place Laney Member deposition at the waning end of the Early Eocene Climatic Optimum (EECO) (Inglis et al. 2020; Figure 1 in Birgenheier et al., 2019). Fossil Basin (Figure 1), the smallest of the three basins, formed behind the leading edge of the Wyoming thrust sheet. Lacustrine deposits in the Fossil Basin are approximately 200 m thick with over a hundred air-fall ashes documented. Only the K-spar Tuff has

suitably large phenocrysts for radiometric dating, which produced an age of 51.98 ± 0.09 Ma (Smith et al. 2008, 2010). The K-spar Tuff, located 178 m above the section base, is 6 m and 7 m, respectively, above the 18-in. Layer and Sandwich Beds that have produced specimens of *Tsoabichi greenriverensis*. Although deposition rates are unknown, the placement of the K-spar Tuff 1.32 million years after the onset of the EECO at 53.3 Ma (Inglis et al. 2020) clearly places the 18-in. Layer and Sandwich Bed deposits within this warm period.

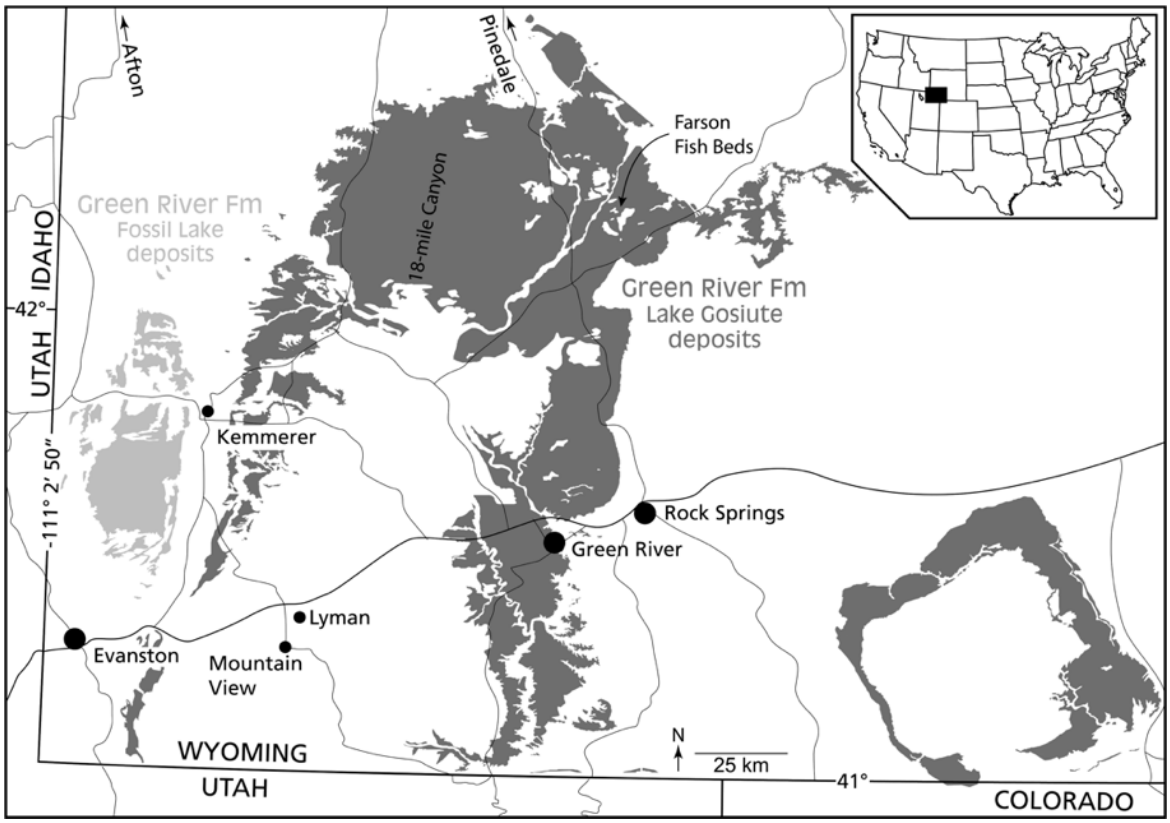

Figure 1. Multiple specimens of *Tsoabichi greenriverensis* are known from the Fossil Lake deposits (51.98 Ma) of the Green River Formation in southwest Wyoming, USA. The exact localities for specimens at SMNK are unknown. The presence of *Gosiutichthys parvus* fossil fish on specimen SMNK-PAL 2334 confirms the specimen came from the Laney member (49.25 Ma) of the Lake Gosiute deposits of the Green River

Formation. The yellow matrix of both specimens and quality of preservation of the fossil fish suggest they were found in 18-mile Canyon area of Lake Gosiute deposits although it is possible they came from the Farson Fish Beds.

RESULTS

Systematic paleontology

CROCODYLIA Gmelin, 1789, *sensu* Benton and Clark, 1988

ALLIGATORIDAE Cuvier, 1807, *sensu* Norell et al., 1994

CAIMANINAE Brochu, 2003

Tsoabichi greenriverensis Brochu, 2010

(Figures 2-4)

Holotype–TMM 42509-1; Wasatchian beds (NALMA), Green River Formation, lower Eocene of Wyoming, USA (Brochu, 2010).

Referred specimens–SMNK-PAL 2333a–SMNK-PAL 2333b, articulated skeleton of a single juvenile individual recovered in two slabs (Figure 2A-B); SMNK-PAL 2334, articulated skeleton of a juvenile individual (Figure 2C), Green River Formation, Lake Gosiute deposits, Laney Member. TMM 42509-1, holotype, skull in dorsal view and lacking premaxilla; AMNH 3666, anterior half of skull; FMNH PR 1793, cast of complete, articulated juvenile in private collection; UNSM 9301, skull in dorsal view; UCM 101064, disarticulated skeletal material; Wasatchian beds in the Green River Formation, Wyoming, USA (previously described by Brochu, 2010). FMNH PR 3050, cast of complete, articulated juvenile in private collection; Fossil Butte Member in the Green River Formation, Wyoming, USA (Grande, 2013).

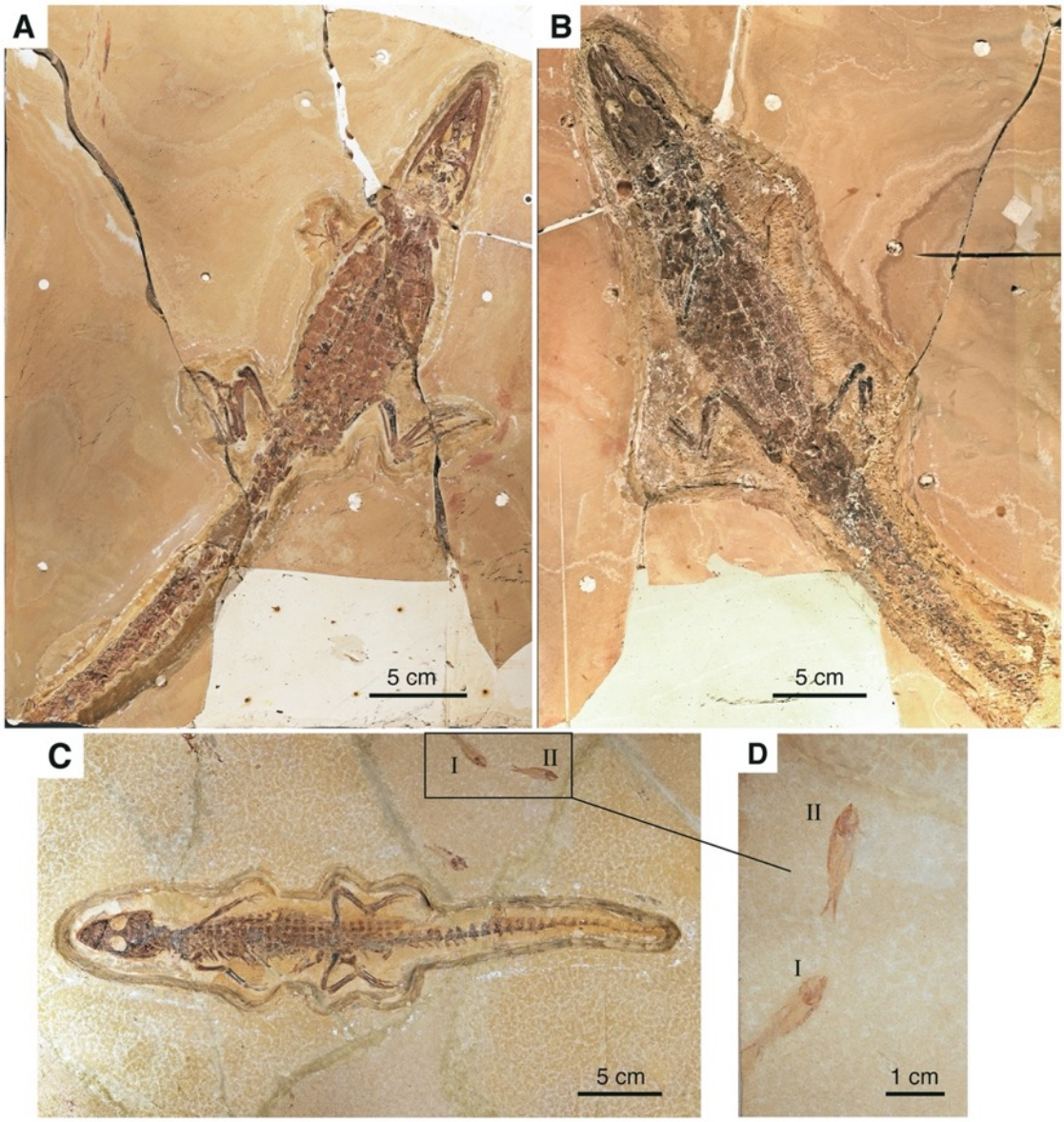

Figure 2. Specimens of *Tsoabichi greenriverensis* described in this study; from Green River Formation, Lake Gosiute deposits, Wyoming, USA. (A) SMNK-PAL 2333b, (B) SMNK-PAL 2333a, (C) SMNK-PAL 2334. (D) *Gosiutichthys parvus* specimens on SMNK-PAL 2334 slab.

Amended diagnosis–We continue the diagnosis of Brochu (2010) with the following additions. Caimanine crocodylian based on bipartite ventral osteoderms, abrupt supratemporal fenestral rim, a large supraoccipital exposure on the skull table, presence

of foramina in the medial wall of the parietal in the supratemporal fenestra, and the posterior rim of the internal choana is deeply notched. A deeply concave margin of the lacrimal as a diagnostic feature for *Tsoabichi greenriverensis* was a typo in Brochu (2010), and the morphology of the new specimen herein described, together with the previously published specimens, agree with an anteriorly convex margin of the lacrimal (see description).

Description

The following morphological description expands that of Brochu (2010). Several differences from his description are attributable to the juvenile ontogenetic stage of the specimens here described (see '*Ontogeny*' section below). The new material (Figure 2) confirms previous diagnostic characters of *Tsoabichi greenriverensis* and allows a partial description of the palatal anatomy for the first time. We directly studied SMNK specimens and a cast of FMNH PR 1793 (Fossil Butte National Monument by MR); all other comparisons with *Ts. greenriverensis* were via the description of Brochu (2010).

Cranium

The premaxillae in SMNK-PAL 2333a share a similar shape to UNSM 9301 (Figure 3A-Figure 3B in Brochu 2010), with an acute process projecting posteriorly between the maxilla and nasal (Figure 3A-Figure 3B). As in larger specimens (e.g., UNSM 9301 and AMNH 3666, Figure 3C-Figure 3D in Brochu 2010), the external nares are also anteroposteriorly oriented in SMNK-PAL 2333a. The diagnostic thin crest encircling the external naris of this species (Brochu 2010) is present in SMNK-PAL 2333a and SMNK-PAL 2334 (Figure 3A-Figure 3B and Figure 4A-Figure 4B), but is thicker and more prominent compared to that of larger specimens (e.g., UNSM 9301). Moreover,

the premaxillary contribution to the posterior wall of the nares through this crest is more pronounced in juveniles (SMNK-PAL 2333a, SMNK-PAL 2334 and FMNH PR1793) than in adults (UNSM 9301, AMNH 3666). Other caimanines also bear posteromedial processes of the premaxillae entering the external naris aperture, but very modestly, lateral to the nasals (e.g., *Caiman crocodilus, Paleosuchus* spp.). The incisive foramen is partially visible and small in SMNK-PAL 2333a, as in most alligatorids (Figure 3A-Figure 3B).

The maxillae are narrower in SMNK-PAL 2333a and SMNK-PAL 2334 compared to the holotype TMM 42509–1 and UNSM 9301 (Figure 3A-Figure 3B in Brochu 2010). The maxillae interact anteriorly with the premaxillae by a posteromedially oriented suture, and posteriorly the lacrimals and jugals Figure 3A-Figure 3B and Figure 4A-Figure 4B). The contact between the maxilla and lacrimal is not as deeply concave as in the holotype TMM 42509–1 (Figure 2A-Figure 2B in Brochu 2010), but rather undulated as in some older specimens (e.g., UNSM 9301). SMNK-PAL 2333a exposes the lacrimal foramina and they are notably large on both sides (Figure 3). The area surrounding the left lacrimal is crushed medially, making the foramen to appear slightly larger than the one on the right side. The lacrimal presents a convex anterior margin at the contact with the maxilla, in contrast to the condition seen in the diagnosis of *Ts. greenriverensis*: 'Lacrimal with deeply concave anterior margin' (pp. 1110, Brochu 2010). Brochu (2010) contradicted his diagnosis in his description: 'Its dorsal expression is roughly rectangular, with a convex anterior margin where it contacts the maxilla' and 'Because of the convexity of the anterior margin of the lacrimal, the maxilla extends posteriorly between the lacrimal and nasal for a short distance.' (pp. 1112, Brochu 2010). The condition was misstated in the diagnosis of that paper (C.A. Brochu, pers. com.). We modify the diagnosis by simply omitting

‘Lacrimal with deeply concave anterior margin’ as otherwise a convex margin is not diagnostic for the species. The prefrontals in SMNK-PAL 2333a and SMNK-PAL 2334 bear a nearly V-shaped ridge (Figure 3A-Figure 3B and Figure 4A-Figure 4B). Such ridges seem to be absent from larger specimens (e.g., TMM 42509–1, UNSM 9301). A prefrontal ridge is common in many crocodylians and it is different from the canthi rostralii seen in other caimanine taxa (e.g., *Melanosuchus niger*), which usually occur on the lacrimals and can reach the maxillae when very prominent.

The frontal terminates slightly anterior to the anterior margins of the orbits in SMNK-PAL 2333a and SMNK-PAL 2334, comparably to the holotype, TMM 42509–1. The frontal-nasal suture is oriented mediolaterally. Three thin antero-posteriorly oriented ridges extend on the dorsal surface of the anterior part of the frontal, beginning slightly anterior to the level where the prefrontal-frontal suture reaches the medial orbital margin (Figure 3A-Figure 3B and Figure 4A-Figure 3B). These ridges are diagnostic for *Ts. greenriverensis* (Brochu 2010) and confirm their presence already during early ontogeny. The absence of this feature in FMNH PR 1793 is likely due to the imprecise cast print as already stated by Brochu (2010). The posteromedial margins of the orbits are flush with the skull surface in SMNK-PAL 2333a and SMNK-PAL 2334. This condition was also observed previously in other older specimens of *Ts. greenriverensis* (UNSM 9301, UCM 10,164) by Brochu (2010) and seems to be a general condition for the species. An exception was noticed by Brochu (2010) in the holotype (TMM 42509–1), which appears to present an upturned posteromedial margin of the orbits, however he argued that it probably represents preservational artefact. Nevertheless, Brochu (2010) scored this character as unknown for *Ts. greenriverensis*. The two individuals herein described allow a clear observation of the dorsal surface of the frontal and an upturned orbital margin is again absent, which reinforces that this is

the typical condition for *Ts. greenriverensis*. We therefore rescored this character as orbit margins flush with the skull surface (137:?>0), a condition not seen in crown camanines (Brochu 1999; with the exception of *Kuttanacaiman iquitosensis* and *Globidentosuchus brachyrostris*, taxa recovered in the crown by the present study).

The parietal in SMNK-PAL 2333a and SMNK-PAL 2334 bears a thin midline ridge reaching from the anterior border of the supraoccipital exposure to approximately mid-length of the parietal (Figure 3A-Figure 3B and Figure 4A-Figure 4B). Such a ridge is barely visible in the holotype TMM 42509–1 (Figure 2A-Figure 2B in Brochu 2010) or UNSM 9301 (Figure 3A-Figure 3B in Brochu 2010) and is absent in UCM 101,064 (Figure 8A-B in Brochu 2010). Expansion of the ornamentation on the skull table in later ontogenetic stages might have caused this ridge to fade. The supratemporal fenestrae are less covered by the parietal, squamosal, and postorbital in SMNK-PAL 2333a and SMNK-PAL 2334, compared to larger individuals (e.g., TMM 42509–1, UNSM 9301 and UCM 101,064). Unlike in previously published specimens, it is therefore possible to observe the medial parietal wall of the fenestrae: although relatively smooth along most of its surface, the parietal medial walls of supratemporal fenestrae are perforated by small foramina in SMNK-PAL 2333a and 2334.

Palatal anatomy–The palatal anatomy has not been described for previously published specimens of *Tsoabichi greenriverensis*. It is only preserved in SMNK-PAL 2333b and a private specimen (a cast is in the Field Museum: FMNH PR3050). Grande (2013) figures this specimen with the skull exposed in dorsal view and the rest of the skeleton in ventral view (the skull was removed and subsequently refitted upside down (C.A. Brochu, pers. com.). In SMNK-PAL 2333b, the palatines project far anteriorly along the medial margin of the suborbital fenestrae, and form a generally broad nearly rectangular anterior process, similar to most crocodylians. The palatal bridge becomes

slightly narrower at mid-length. Preservation does not allow us to trace a potential posterior flaring nor precise projection of the palatine-pterygoid suture. No suture was, however, observed on the palatal bridge.

The ectopterygoids form the posterolateral borders of the suborbital fenestrae. The ectopterygoid-pterygoid suture appears to be straight and lacking a flexure, comparable to modern *Caiman* species, but confidence is low as the anteriormost part of the suture is missing. Actual contact between the ectopterygoid and the maxillary tooth row is also missing in the specimen, but based on the dorsal view of SMNK-PAL 2333a (Figure 3A-Figure 3B), the ectopterygoid seems to project anteromedially away from the toothrow, as in other alligatorids. The posterior extension of the ectopterygoid does not reach the posterior end of the pterygoid in SMNK-PAL 2333b.

The pterygoids of *Ts. greenriverensis* were only known from a small dorsal exposure in UNSM 9301. The pterygoids are ventrally exposed in SMNK-PAL 2333b (Figure 3C-Figure 3D). The pterygoid wings consist of subtriangular-shaped elements, slightly posteriorly oriented at its ventralmost acute tip, and being overlapped by the ectopterygoid on part of its anterior margin. The posterior midline contact of the pterygoids with one another can be observed positioned dorsally in relation to the pterygoid wings, at the level of the palatal region. Anteriorly to this contact, the internal choana is visible, presenting a notched posterior rim. This is important as the notched posterior rim of the internal choana is a synapomorphy of Caimaninae (Brochu 1999; Stocker et al. 2021; this work). The septum in the internal choana is not preserved.

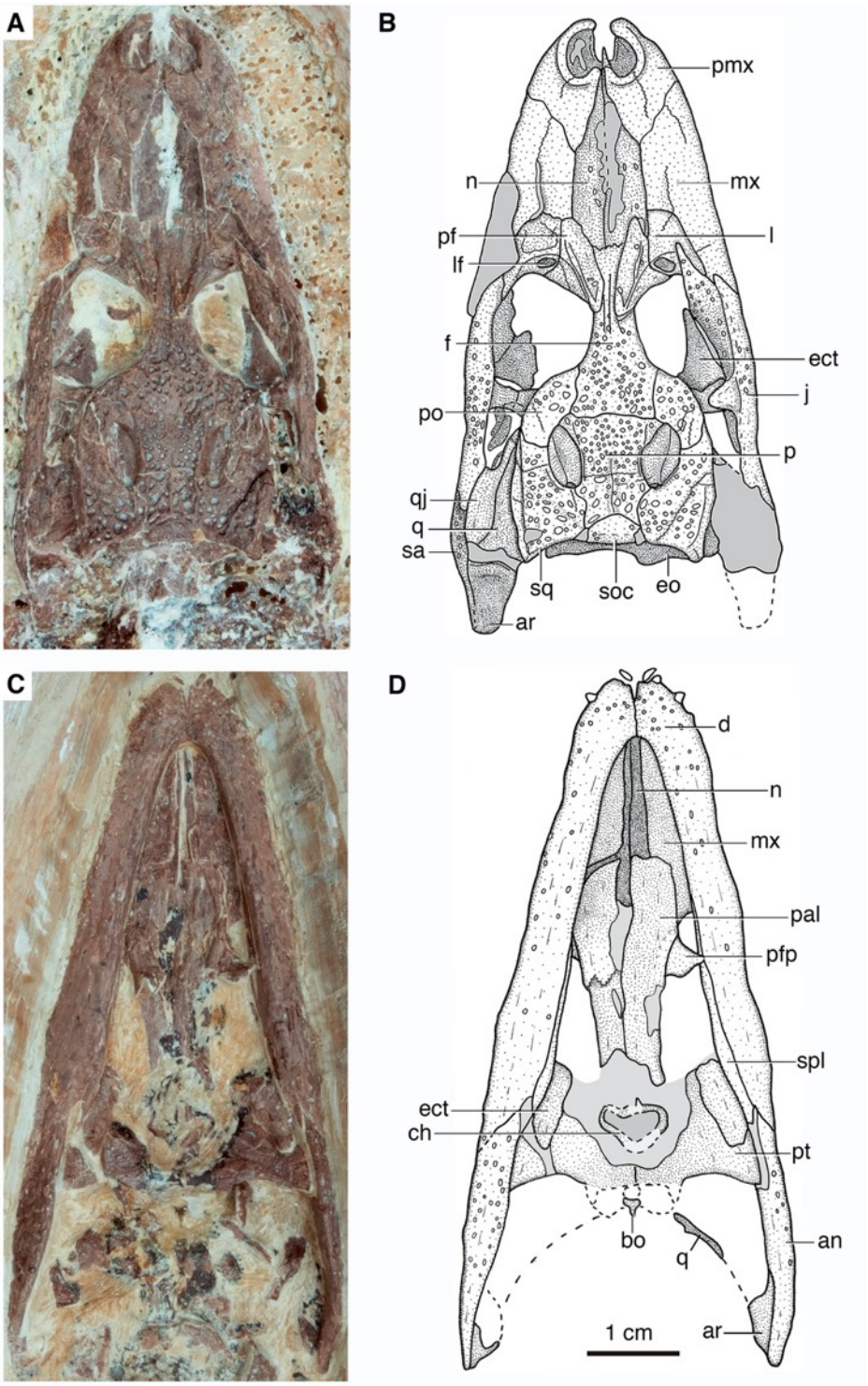

Figure 3. *Tsoabichi greenriverensis*, Green River Formation, Lake Gosiute deposits. (A) SMNK-PAL 2333a, skull in dorsal view, (B) interpretative outline (C) SMNK-PAL 2333b, skull and mandible in ventral view. (D) Interpretative outline of C. Abbreviations: **an**, angular; **ar**, articular; **bo**, basioccipital; **ch**, internal choana; **d**, dentary; **ect**,

ectopterygoid; **eo**, exoccipital; **f**, frontal; **j**, jugal; **l**, lacrimal; **lf**, lacrimal foramen; **mx**, maxilla; **n**, nasal; **p**, parietal; **pal**, palatine; **pf**, prefrontal; **pfp**, prefrontal pillar; **pmx**, premaxilla; **po**, postorbital; **pt**, pterygoid; **q**, quadrate; **qj**, quadratojugal; **sa**, surangular; **soc**, supraoccipital; **spl**, splenial; **sq**, squamosal.

Mandible–The mandible is only exposed in SMNK-PAL 2333b in ventral view (Figure 3, Figure 3C-Figure 3D) and does not contribute significantly to our understanding of the mandible anatomy in *Ts. greenriverensis*. Important questions still remain unclear, such as the participation of the splenial in the mandibular symphysis (see Brochu 2010), as the anterior extension of the splenial is not exposed in SMNK-PAL 2333b.

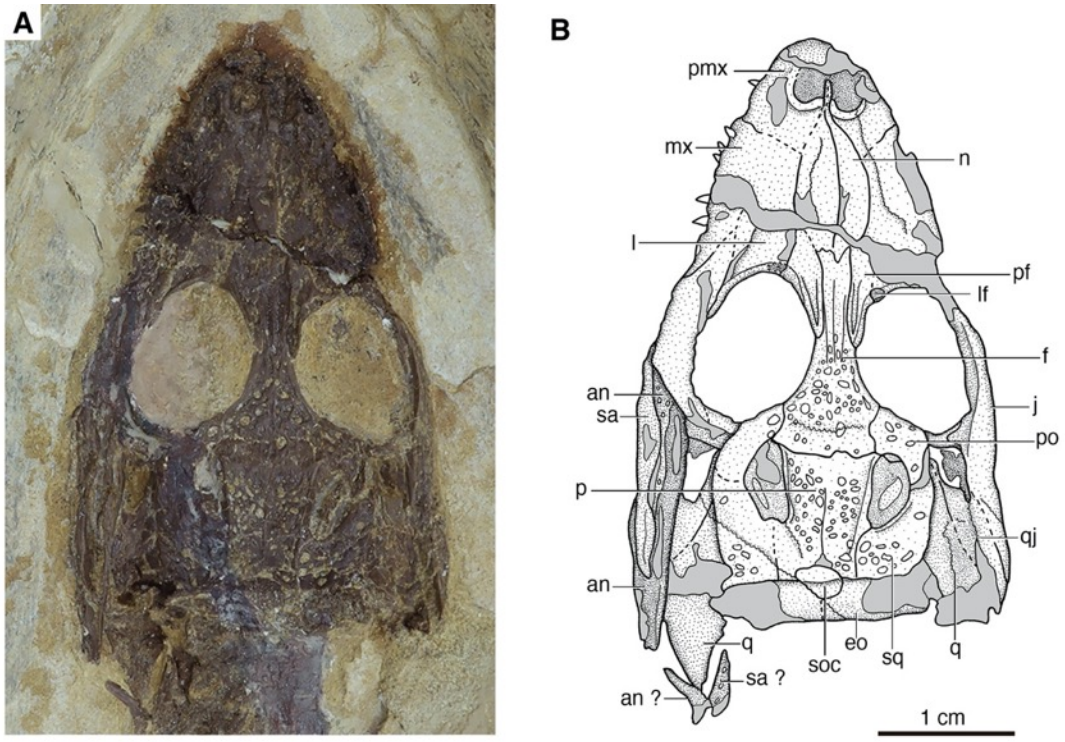

Figure 4. SMNK-PAL 2334, *Tsoabichi greenriverensis*, Green River Formation, Lake Gosiute deposits. (A) Skull in dorsal view, (B) interpretative outline. Abbreviations: **an**,

angular; **eo**, exoccipital; **f**, frontal; **j**, jugal; **l**, lacrimal; **lf**, lacrimal foramen; **mx**, maxilla; **n**, nasal; **p**, parietal; **pf**, prefrontal; **pmx**, premaxilla; **po**, postorbital; **q**, quadrate; **qj**, quadratojugal; **sa**, surangular; **soc**, supraoccipital; **sq**, squamosal.

Postcranium

The postcranial material is partially preserved in SMNK specimens. Most of the postcranial bones, such as vertebrae and ribs, are however covered by osteoderms. The pectoral girdle is partially visible in SMNK-PAL 2333b (Figure 2A), with only the scapula being preserved. The scapula blade looks dorsally broad, unlike in modern *Caiman* species, but resembling the morphology of *Paleosuchus* spp. This differs from the general growth pattern of this bone in living caimanines as juveniles show unflared blades which grow dorsally in later ontogenetic stages. A broad scapular blade early in the ontogeny implies that adults probably retained this morphology for their whole life (Brochu 1996). New material from the pectoral girdle of adult specimens would further confirm the flared condition of the scapular blade in *Ts. greenriverensis*.

The pelvic girdle is also partially visible in SMNK-PAL 2333b (Figure 2A). The ischia and pubis are exposed in ventral view and have a typical alligatorid morphology. The left ilium is partially preserved in SMNK-PAL 2333a (Figure 2B). The posterior tip of the iliac blade seems to be relatively narrow, but the overall preservation of the ilium margins does not allow an accurate assessment. Slender forelimbs and hindlimbs seen in SMNK-PAL 2333a, 2333b and 2334 (Figure 2) are comparable to FMNH PR 1793 (Figure 5 in Brochu 2010), accounting for a juvenile stage in specimens described in our study. Limb bones (humerus, radius, ulna in SMNK-PAL 2334; femur, tibia, fibula in SMNK-PAL 2333b) as well as metacarpalia and metatarsalia are consistent with extant *Caiman* species and alligatorid morphology in general.

Osteoderms–The dorsal armour is partially preserved in SMNK-PAL 2333a and 2334, and ventral armour in SMNK-PAL 2333b (Figure 2A-Figure 2C). The dorsal armour consists of at least six contiguous rows, with the medial elements being rectangular and single keeled, similar to previously published specimens (e.g., Figure 6B in Brochu 2010). The ventral shield in SMNK-PAL 2333b is made of bipartite osteoderms, with anterior and posterior medial elements being approximately similar in width, a diagnostic feature of the species (Brochu 2010). This condition is present in *Caiman* species and *Paleosuchus* spp., but also in other alligatoroid taxa such as *Diplocynodon* spp. and *Procaimanoidea kayi*. Double keeled osteoderms were reported by Brochu (2010) in the nuchal region of UNSM 9301, but such elements are not preserved in SMNK-PAL 2333a or 2334.

Ontogeny

The available specimens of *Tsoabichi greenriverensis* can be ordered into an ontogenetic series according to increasing skull length: SMNK-PAL 2334 (ca. 4.5 cm), SMNK-PAL 2333a (ca. 6.1 cm), FMNH PR 1793 (ca. 7 cm), TMM 42509-1 (ca. 17.5 cm), UNSM 9301 (ca. 20.4 cm). The neurocentral sutures are fully closed in visible caudal vertebrae in SMNK-PAL 2333a-b and SMNK-PAL 2334, including vertebrae immediately caudal to the pelvic girdle. Closure of the neurocentral suture follows a caudal to cranial sequence (Brochu, 1996) and most presacral vertebrae are either damaged and/or covered by osteoderms, making the closure of neurocentral sutures impossible to observe anterior to the pelvic girdle in the SMNK specimens. SMNK-PAL 2334 is nevertheless no doubt a juvenile based on its relative body length, large orbits and pointed snout. SMNK-PAL 2333a-b probably also corresponds to a juvenile given its body and orbit size relative to SMNK-PAL 2334; far from that of UNSM

9301, the largest known specimen of the species. TMM 42509-1 and UNSM 9301 likely represent adults based on their size and the broadness and more pronounced sculpturing of the snout.

Phylogenetic analyses

Phylogenetic analyses were conducted using a modified matrix of Bona et al. (2018; mB, Supplementary material S2) and a modified matrix of Massonne et al. (2019; mM, Supplementary material S3), including 95 and 113 taxa respectively. Both datasets contain 202 characters based on Brochu (2011) and subsequent expansions (e.g., Narváez et al., 2015; Salas-Gismondi et al., 2015) but have slightly different character sampling. We increased the taxon sampling of Bona et al. (2018) by adding four taxa: *Bottosaurus harlani* and *Chinatichampsus wilsonorum* with the character coding from Stocker et al. (2021); and *Orientalosuchus naduongensis* and *Jiangxisuchus nankangensis* with the character coding from Massonne et al. (2019). The following changes were made to both datasets: we ordered two characters that form a clear morphocline (see Supplementary material S1 for details): character (152), overhang of supratemporal fenestra by dermal bones (intermediate state added + ordered) and (160), supraoccipital exposure on dorsal skull table and character (redefined + ordered). All other characters were treated as unordered. A number of character scores were updated for *Eocaiman cavernensis*, *Globidentosuchus brachyrostris*, *Tsoabichi greenriverensis* in both datasets as well as for *Centenariosuchus gilmorei*, *Chinatichampsus wilsonorum*, and *Crocodylus niloticus* of Bona et al. (2018). A full list of changes applied to the datasets, along with matrix files and additional trees, is available in Supplementary material S1-S3.

Culebrasuchus mesoamericanus was excluded from both datasets, as we noticed several inconsistencies in the scoring of this taxon relative to the description of Hastings et al. (2013, 2016; see Supplementary material S1) and following Stocker et al. (2021), who likewise chose to exclude *Cu. mesoamericanus* from their analysis following preliminary first-hand observations of the material. This species is known to be a wildcard taxon: previous phylogenies either recovered it as the earliest branching caimanine, predicting ghost lineages into the early Paleocene of Central America (Hastings et al., 2013; Cidade et al., 2017, 2020; Cossette, 2020), or nesting in Alligatorinae with *Alligator* spp. (Salas-Gismondi et al., 2015 and Bona et al., 2018).

Operational taxonomic units were managed in Mesquite version 3.6 (Maddison & Maddison, 2015). Analyses were run using Tree search using New Technology software (TNT 1.5, standard version. Goloboff et al., 2016). We applied a molecular scaffold for each analysis based on the phylogeny of Oaks (2011) and let the morphological data place each fossil species within this topology. A first round of traditional search using 1000 replicates of Wagner trees was performed and a second round was then conducted using tree bisection reconnection (TBR) on trees saved from the first round, with 10 saves per replication.

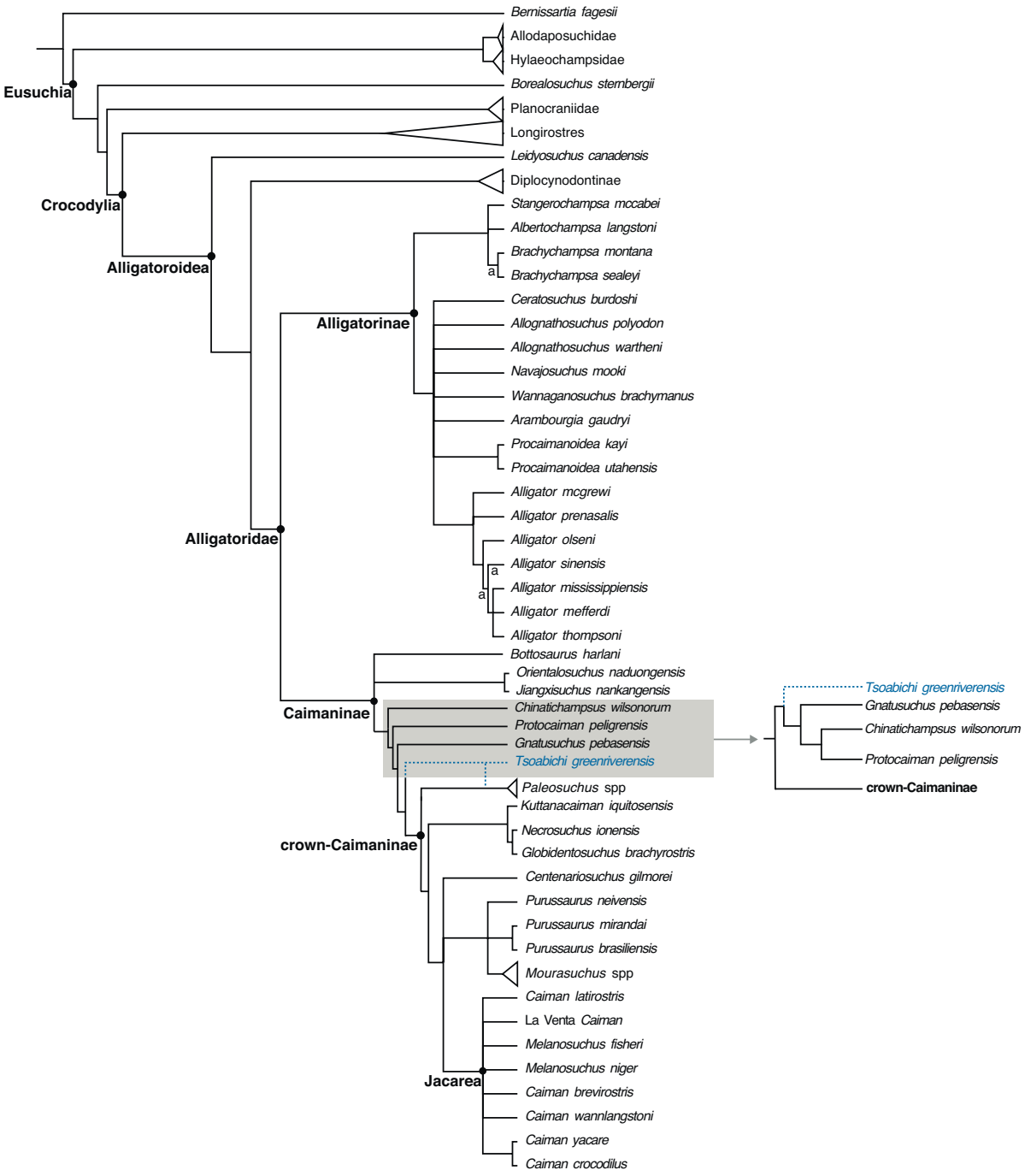

Figure 5. Reduced strict consensus tree obtained from the maximum parsimony analysis of the modified Bona et al. (2018) dataset (mB). Letter "a" shows the alternative placements of the unresolved clade including *Eocaiman* spp. and *Notocaiman stromeri*.

The mB analysis recovered 99,999+ equally optimal trees. Unexpectedly, *Eocaiman* spp. and *Notocaiman stromeri* was recovered in Alligatorinae in all trees.

Stem-group Caimaninae is largely unresolved in the consensus tree, with *Paleosuchus* spp. taking part in this polytomy (Figure 5). Removing the backbone constraints from the analysis did recover the same topology for Alligatoroidea, but Caimaninae is largely unresolved. *Eocaiman* spp., *No. stromeri* and *Necrosuchus ionenesis* have an additional alternative position as the sister clade to *Paleosuchus* spp.

The mM analysis recovered 99,999+ equally optimal trees. Compared to the mB analysis, the main topological differences relevant to this study include *Stangerochampsa mccabei* and *Brachychampsa* spp. as stem-alligatorids, *Procaimanoidea* spp. is found in stem-group Caimaninae, *Globidentosuchus brachyrostris* is the sister taxon to remaining caimanines forming an unresolved clade, *Eocaiman cavernensis* is recovered either in Alligatorinae (sister to *Alligator sinensis*) or in Caimaninae (sister to *Mourasuchus atopus*; see Supplementary material, Figure S1).

DISCUSSION

Phylogenetic relationships of early caimanines

Evidence for caimanine affinity of *Brachychampsa* spp. is weak

The extent of the caimanine stem lineage is subject to considerable uncertainty. *Stangerochampsa mccabei*, *Brachychampsa* spp. and *Albertochampsa langstoni* usually formed the immediate outgroup to Alligatoridae in previous phylogenies (e.g., Norell et al., 1994; Williamson, 1996a; Brochu, 1999, 2010, 2011; Massonne et al., 2019), but several more recent phylogenies recovered these taxa in a clade forming the basal-most Caimaninae lineage (e.g., Salas-Gismondi et al., 2015; Bona et al., 2018; Cossette, 2020; Stocker et al., 2021). On the other hand, other recent phylogenies of comparable taxon sampling keep finding the same taxa in their "conventional" phylogenetic position

as basal alligatoroids (e.g., Massonne et al., 2019; Souza-Filho et al., 2019; Cossette and Brochu, 2018) or unresolved relative to Caimaninae (e.g., Hastings et al., 2016; Cossette & Brochu, 2018).

With the mB dataset, our phylogeny recovered *St. mccabei*, *Brachychampsa spp*. and *Al. langstoni* as the basal-most alligatorines (Figure 5), unlike in any previous studies, including Bona et al. (2018). This relationship is based on three synapomorphies, either exclusively shared with alligatorines among Crocodylia (51:1>0, largest dentary alveolus immediately caudal to 4th is the 13th or 14th), or shared with most crown caimanines as well (118:1>0, palatine-pterygoid suture lies near the posterior angle of suborbital fenestra; and 129:0>1, prefrontals separated by the frontal and nasals with anterior process of frontal around the same level or posterior to anterior margin of orbit). Our analysis using the mM dataset, however, found *St. mccabei*, *Brachychampsa* spp. in a polytomy with other basal alligatorids, at the base of Alligatoridae (see Supplementary material, Figure S1). The uncertainty regarding the placement of basal alligatorids in our mM analysis pulls Orientalosuchina (Massonne et al., 2019) in stem-group Caimaninae. Most of the synapomorphies responsible for this relationship are not even scored for most orientalosuchines or *Bo. harlani* (e.g., 66:1, surangular-angular suture meets articular lingually dorsal to the tip; 72:0, surangular extension reaches the posterior end of retroarticular process). Notably, our modifications to the dataset of Bona et al. (2018) and Massonne et al. (2019) did not involve *St. mccabei*, *Brachychampsa* spp. or *Al. langstoni*, yet our analyses altered their placement, including a position never before recovered (Alligatorinae). These taxa are highly sensitive to minor modifications of the datasets, which is furthermore illustrated by their inconsistent placements in previous phylogenies using roughly identical

matrices. Together, these highlight our poor understanding of the ancestral morphology of major alligatoroid clades.

Because of their Late Cretaceous age, the phylogenetic position of *Brachychampsa* spp. and similar taxa is critically important for the fossil age of primary alligatoroid lineages. For instance, recent molecular divergence date analyses have previously employed the early Campanian *Brachychampsa sealeyi* to calibrate crown-Caimaninae (Bittencourt et al., 2019; Roberto et al., 2020), despite the apparent inconsistent placement of this taxon in published phylogenies. Additionally, regardless of their placement within Alligatoroidea, these taxa are invariably recovered in a basal position and therefore directly affect the topologies of successive less inclusive clades. This further highlights our inadequate understanding of character evolution within early Alligatoroidea.

Protocaiman peligrensis **and** ***Chinatichampsus wilsonorum*** **are unambiguous stem caimanines**

We recovered *Protocaiman peligrensis* and *Chinatichampsus wilsonorum* as part of the stem-group (mB; Figure 5). While in most trees we found them as basal-most caimanines, in accordance with Bona et al. (2018) and Stocker et al. (2021), a few trees recover them in a stem-group clade including *Gnatusuchus pebasensis*. This latter topology results from character states optimized as independent secondary acquisitions for this clade (112:0>1, maxillary margins adjacent to the suborbital fenestra bears a broad shelf extending into the fenestra, making the lateral margin concave; 151:1>0, the frontoparietal suture between the supratemporal fenestrae is linear). *Protocaiman peligrensis*, however, is only scored for one of these synapomorphies (ch.151). On the other hand, trees recovering *Ch. wilsonorum* and *Pr. peligrensis* as basal caimanines are based on similar synapomorphies as in Bona et al. (2018) and Stocker et al. (2021): *Ch.*

wilsonorum and remaining caimanines are united by lateral edges of palatines with lateral process projecting into the suborbital fenestrae (112:0>1, maxillary margins adjacent to the suborbital fenestra bears a broad shelf extending into the fenestra, making the lateral margin concave (new synapomorphy in this study); lateral edges of palatines with lateral processes projecting into suborbital fenestrae (117:0>1; new synapomorphy in this study), posterior rim of internal choana is deeply notched (124:0>1), medial parietal wall of the supratemporal fenestra bears foramina (154:0>1; unique to Caimaninae, previously uniting *Pr. peligrensis* and remaining caimanines), and the exoccipitals send a slender process ventrally to the basioccipital tubera (176:0>2). The latter synapomorphy is unique to Caimaninae (excluding *Bottosaurus harlani* + Orientalosuchina), as is a deeply notched posterior rim of the internal choana except for the allodaposuchid *Agaresuchus fontisensis*. *Protocaiman peligrensis* and remaining caimanines are united by a single synapomorphy: parietal, squamosal and postorbital overhang the rim of supratemporal fenestra near maturity (152:0>2; otherwise only present in *Diplocynodon deponiae*). The ancestral condition of the supraoccipital exposure (160:0, supraoccipital exposure on the skull table is small) places *Ch. wilsonorum* and *Pr. peligrensis* at the base of Caimaninae (all more crownward taxa bears a large supraoccipital exposure; 160:2/3).

Is *Bottosaurus harlani* a caimanine?

Bottosaurus harlani from the Late Cretaceous/early Paleocene of North America and Orientalosuchinae from the Late Cretaceous-Paleogene of Asia are recovered as basal caimanines in our analyses (mB, Figure 5; mM, see Supplementary material, Figure S1). Under implied weighting, orientalosuchines are recovered sister to Alligatoridae (see Supplementary material, Figure S2). In the mB analysis, most trees find *Bo.*

harlani forming the basal-most caimanine clade with *Orientalosuchus naduongensis* and *Jiangxisuchus nankangensis*, branching to all remaining caimanines. Alternatively, a few trees recover *Bo. harlani* sister to the clade uniting *Chinatichampsus wilsonorum* and remaining caimanines. This is in contrast with the crown-caimanine position (sister to *Paleosuchus* spp.) of previous studies, which had been questioned given the low nodal support, homoplastic synapomorphies, and large spatio-temporal gap (Cossette & Brochu, 2018; Massonne et al., 2019; Cossette, 2020; Stocker et al., 2021). *Bo. harlani* and Orientalosuchinae are lacking key unique synapomorphies of Caimaninae (i.e., 124:1, posterior rim of internal choana is deeply notched; 176:2, the exoccipitals send slender process ventrally to the basioccipital tubera; 152:2, parietal, squamosal and postorbital overhang the rim of supratemporal fenestra near maturity; and 154:01, medial parietal wall of the supratemporal fenestra bears foramina). Most of the synapomorphies supporting the inclusion of these taxa into Caimaninae are lower jaw characters unknown in the only unambiguous stem-caimanines *Protocaiman peligrensis* and *Chinatichampsus wilsonoroum* and therefore may have evolved independently (dorsal margin of iliac blade is narrow with dorsal indentation, 34:0>3; splenial lacks an anterior perforation for mandibular ramus of cranial nerve V, 52:0>1; dentary symphysis extends to fourth or fifth alveolus, 49:1>0; surangular/angular suture meets the articular dorsal to tip, 66:0>1; surangular extends to posterior end of retroarticular process, 72:1>0). Considering *Eocaiman* spp. as plausible stem caimanines (e.g., Bona, 2007; Cidade et al., 2020; Godoy et al., 2020) would alter the ancestral condition of character 49 (dentary symphysis extension) and 60 (angular/surangular suture position relative to the external mandibular fenestra), therefore potentially impacting the placement of *Bo. harlani* and orientalosuchines in our dataset. Additional material of

Bo. harlani and basal-most caimanines would be beneficial for a more rigorous test of the caimanine affinities of this taxon.

Eocaiman spp. and *Necrosuchus ionensis*

The South American taxa *Eocaiman* spp., *Notocaiman stromeri* were recovered in the stem-group Caimaninae in previous studies (e.g., Bona, 2007, 2018; Brochu, 2011; Pinheiro et al., 2013; Cidade et al., 2017, 2020). This phylogenetic position is congruent with their Paleocene age and biogeographical distribution. Our mB analysis nevertheless recovers *Eocaiman* spp. and *Notocaiman stromeri* in Alligatorinae, either sister to living species (e.g., *Alligator sinensis*) or sister to *Brachychampsa* spp. (Figure 5). This is partly due to 1) our partial rescoring of *Eocaiman cavernensis* (see Supplementary material S1); 2) a missing skull table or basicranium for these species, an anatomical region where most unique Caimaninae synapomorphies are found, and 3) to a few lower jaw characters, which are otherwise widely shared with crown caimanines too (e.g., 54:0>2, splenial excluded from the dentary symphysis with dorsal tip passing dorsal to the Meckelian groove).

Previous studies usually recovered *Necrosuchus ionensis* from the early Paleocene of Argentina in an unresolved position relative to the crown-group Caimaninae (Brochu, 2010, 2011; Hastings et al., 2016), although recent phylogenies found it as part of the crown, either sister to *Tsoabichi greenriverensis* and *Paleosuchus* spp. (Salas-Gismondi et al., 2015; Bona et al., 2018) or even part of Jacarea (Cidade et al., 2020). Our results (mB) find *Ne. ionensis* part of the crown-group Caimaninae, sister to *Globidentosuchus brachyrostris*, in all most parsimonious trees (Figure 5). Synapomorphies uniting crown-group Caimaninae are not scored for *Ne. ionensis*, however, and a single character pulls it into the crown-group, sister to *Gl. brachyrostris*

(51:1>0, largest dentary alveolus immediately caudal to 4th is the 13th or 14th; also shared with all alligatorines). This support is problematic for several reasons. First, the ancestral condition in Caimaninae is unknown in our topology, as basal caimanines do not preserve any lower jaw. However, if we regard *Eocaiman* spp. (51:0) as basal caimanines, the plesiomorphic state for crown-group Caimaninae would be the largest dentary alveolus immediately caudal to 4th being the 13th or 14th (51:0), potentially drawing *Ne. ionensis* to the stem-group. Second, the condition found in *Gl. brachyrostris* is a reversal likely induced by its highly specialized globidont dentition, which questions the homology with *Ne. ionensis*. Finally, *Ne. ionensis* occurs in the Paleocene, which implies an extensive ghost lineage for crown-group Caimaninae, in conflict with molecular divergence date analyses (e.g., Oaks, 2011; Pan et al., 2020; see below).

Tsoabichi greenriverensis **may not belong to the crown group**

Tsoabichi greenriverensis can be confidently recognised as part of Caimaninae based on several characters shared with other caimanines (e.g., bipartite ventral osteoderms, a significant overhang of the supratemporal fenestrae rim, and a large supraoccipital exposure; Brochu, 2010). New specimens described in this study confirm the presence of aforementioned features, but also bear additional unique caimanine traits: presence of foramina on the medial parietal wall of the supratemporal fenestra, and a deeply notched posterior rim of the internal choana. Most phylogenies since the description of *Ts. greenriverensis* found the taxon in Caimaninae, with the exception of Rio et al. (2019; Diplocynodontinae, using implied weights). Other previous phylogenies recovered *Ts. greenriverensis* either in an unresolved position relative to crown-group

Caimaninae (Brochu, 2010, 2011; Souza-Filho et al., 2019; Cossette, 2020; Cossette & Brochu, 2020), or in the crown as sister to extant dwarf-caimans, *Paleosuchus* spp. (Fortier et al., 2014; Salas-Gismondi, 2015; Bona et al., 2018; Cossette & Brochu, 2018; Massonne et al., 2019), or sister to the crown-group (Hastings et al., 2013). Considering *Ts. greenriverensis* as part of the crown group infers extensive ghost lineages for *Paleosuchus* spp. into the early Eocene (inconsistent with most molecular divergence time estimates; Roos, 2007; Oaks, 2011; Pan et al., 2020) and complex paleobiogeography (Brochu, 2010).

Our mB analysis found *Ts. greenriverensis* in an unresolved position relative to crown-group Caimaninae. When in the stem group, *Ts. greenriverensis* is either alone the sister taxon of the crown group, or forming a clade (no synapomorphies) with *Gnatusuchus pebasensis*, *Ch. wilsonorum* and *Protocaiman peligrensis* (Figure 5). *Ts. greenriverensis* in the stem group has two alternatives: 1) no synapomorphies unite the crown group; 2) synapomorphies uniting the crown group are unknown for *Ts. greenriverensis* (68:0>2, articular/surangular suture, articular bears an anterior lamina ventral to lingual foramen; 126:0>1 ectopterygoid/pterygoid flexure remains during ontogeny). The reason why *Ts. greenriverensis* is recovered outside the crown group in these trees (Figure 5) is due to the ordering of character 160 in the present study (size of the supraoccipital exposure on the skull roof; see Phylogenetic analyses and Supplementary material S1). Ordering this character recovered several equally longer topologies compared to unordering. Unordering character 160 finds *Ts. greenriverensis* in the crown, sister to *Paleosuchus* spp., in the consensus tree of mB dataset, as this placement provides the only parsimonious result.

Brochu (2010) found *Ts. greenriverensis* sister to *Paleosuchus* spp. in the Adams consensus, based on a large supraoccipital exposure allowing the parietal to

reach the posterior margin of the skull table (160:2). In this previous phylogeny, the basal-most caimanine (i.e., *Eocaiman cavernensis*) was scored as bearing a large supraoccipital exposure excluding the parietal from the posterior margin of the skull table (160:3), which made the latter state the primitive condition for Caimaninae. However, the recent revision of *Eo. cavernensis* by Godoy et al. (2020) highlighted the absence of confident skull table material for this taxon. Recently described basal caimanines from the Paleogene (i.e., *Pr. peligrensis*, Bona et al., 2018; *Ch. wilsonorum*, Stocker et al., 2021) now suggest that a small supraoccipital exposure is the basal condition for the Caimaninae. This alone, however, would not impact the placement of *Ts. greenriverensis* as the change in the character state remains a single step (without ordering).

In those most parsimonious trees where *Ts. greenriverensis* is in the crown in our mB analysis, it forms a clade with *Paleosuchus* spp. (Figure 5), but this is not supported with synapomorphies. The inclusion of *Ts. greenriverensis* in the crown group therefore results from synapomorphies uniting the crown in these trees (54:0>2, splenial is excluded from the mandibular symphysis with the anterior tip passing dorsal to Meckelian groove; 68:0>2, articular/surangular suture, articular bears an anterior lamina ventral to lingual foramen; 126:0>1 ectopterygoid/pterygoid flexure during ontogeny; and 151:0>1, frontoparietal suture is linear), and of which only two are scored for *Ts. greenriverensis* (54:2 and 151:1). However, even these two characters are of questionable support as they may diagnose a more inclusive clade. Character 54 (splenial participation in symphysis) is unknown for the unambiguous stem-caimanines *Ch. wilsonorum* and *Pr. peligrensis* and a linear frontoparietal suture (151) diagnoses *Ts. greenriverensis* + crown-Caimaninae in other trees of our analysis. If we consider *Eocaiman* spp., *Notocaiman stromeri* and *Necrosuchus ionensis* as plausible stem

caimanines (see above), the basal condition would be a splenial excluded from the mandibular symphysis with the anterior tip passing dorsal to the Meckelian groove (54:2; instead of a synapomorphy of the crown-group). The mM analysis recovers *Ts. greenriverensis* unresolved relative to the crown-group Caimaninae, both under ordering and unordering character 160. The exclusion of *Ts. greenriverensis* from the crown-group in some trees is driven by the absence of upturned margins of the orbits in the taxon (character rescored in both datasets of the present study, see Description). However, under the broader taxonomic sample of the mB dataset, this character state is independently acquired twice in the crown.

Our results highlight the limited support for the inclusion of *Ts. greenriverensis* into the crown-group as synapomorphies responsible for drawing *Ts. greenriverensis* into the crown (54:0>2; 151:0>1) may in fact diagnose a more inclusive clade. A stem-group placement is more consistent with the early Eocene age of *Ts. greenriverensis* in light of the fossil record (no older fossils of *Paleosuchus* spp. than Miocene; Salas-Gismondi et al.; 2015) and molecular divergence date estimates (Roos, 2007; Oaks, 2011; Pan et al., 2020).

Miocene taxa from Panama and Peru may belong to the crown

Instead of being placed along the stem lineage of Caimaninae in previous studies (Hastings et al., 2013, 2016; Salas-Gismondi et al., 2015; Bona et al., 2018; Souza-Filho, 2019; Godoy et al., 2020), the Miocene taxa from Panama, *Kuttanacaiman iquitosensis* and *Globidentosuchus bachyrostris,* are recovered in crown-group Caimaninae in our analyses (mB, Figure 5). Three synapomorphies unite them with a clade formed by Nettosuchidae + *Centenariosuchus gilmorei* + Jacarea: 118:1>0,

palatine/pterygoid suture is located far anteriorly from the posterior angle of suborbital fenestra; 129:0>2, prefrontals meet medially with anterior process of frontal around the same level of the anterior margin of the orbit (present in most crown caimanines and otherwise only in *Hylaeochampsa vectiana*); and 160:2>3, large supraoccipital excluding the parietal from the posterior margin of the skull table. These synapomorphies are unique to the crown-group (with the exception of *Paleosuchus* spp.) The crown-group placement of these Miocene taxa resolves the extensive ghost lineage otherwise inferred by a position in the stem group (Hastings et al, 2013 and all subsequent works).

Gnatusuchus pebasensis, a peculiar, broad-snouted taxon from the Miocene of Peru, is recovered in the stem-group in our mB analysis and previous works (Salas-Gismondi et al., 2015 and subsequent studies) but this is questionable. Character states placing it outside crown-group Caimaninae may rather represent secondary losses due to adaptation to a durophagous ecology with an extremely short and broad, specialized snout in this species (e.g., 54, presence instead of absence of a splenial symphysis; 93, largest maxillary alveolus is 3rd instead of 4th). Future analyses should rescore these and perhaps other characters correlated with the snout shape and globidont dentition as inapplicable for *Gn. pebasensis*. This taxon otherwise shows characters that are unique to the crown (e.g., 160:3, large supraoccipital exposure excluding the parietal from the posterior margin of the skull table). In addition, a crown-group placement would be more consistent with the Miocene age of this taxon.

Fossil constraints for time calibrated Caimaninae phylogenies

Total-group Caimaninae

Below we provide explicit fossil calibrations for time calibrated phylogenies of total and crown-group Caimaninae following best practices of Parham et al. (2012).. For composite phylogeny of published consensus trees and spatio-temporal distribution of fossil Caimaninae see Figure 6 and Table 1. Most phylogenies agree that the oldest unambiguous caimanines are from the Paleocene of South America. These include *Eocaiman paleocenicus*, *Necrosuchus ionensis*, *Notocaiman stromeri* and *Protocaiman peligrensis* (e.g., Bona, 2007; Brochu, 2010, 2011; Hastings et al., 2013; Salas-Gismondi et al., 2015; Hastings et al., 2016; Bona et al., 2018; Cidade et al., 2020; 2020; Souza-Filho et al., 2019; Godoy et al., 2020; Cossette, 2020; Stocker et al., 2021). Of these species, *Eocaiman* spp. and *No. stromeri* are less robustly placed among Caimaninae, as shown by our own phylogeny in which they are placed within Alligatorinae (Figure 5 and 6). The instability of these taxa is due to the lack of posterior cranial material, a region bearing several Caimaninae synapomorphies (e.g., parietal excluded from posterior edge of table by supraoccipital; exoccipitals sending slender process ventrally to basioccipital tubera). In contrast, key caimanine synapomorphies robustly place *Ne. ionensis* and *Pr. peligrensis* in the group (i.e., splenial excluded from the mandibular symphysis, with a projection dorsal to the Meckelian groove, an angular-surangular suture contacting the ventral margin of the external mandibular fenestra, a dentary symphysis extending back to a level just behind the fourth dentary alveolus, and presence of a slender process of exoccipital ventral to the basioccipital tubera for *Ne. ionensis*; and dermal bones of skull roof overhanging the rim of the supratemporal fenestrae, and medial parietal wall of supratemporal fenestra bearing foramina in *Pr. peligrensis* (Simpson, 1937; Brochu, 2011; Bona et al., 2018; Cidade et al., 2020). Both species come from the earliest Paleocene Salamanca Fm. (Patagonia, Argentina) where a multidisciplinary geochronologic study including

biostratigraphic, radioisotopic and paleomagnetic data determined an age of 65.7–63.5 Ma, early to middle Danian, early Paleocene (Clyde et al., 2014; Table 1). This age is consistent with the earliest alligatorine, *Navajosuchus mooki* from the early Paleocene of New Mexico (65.68–65.22 Ma, Williamson, 1996b; Lucas & Estep, 2000; Brochu, 2004b; Flynn et al., 2020). Even though coming from older rocks than the South American caimanines, *Na. mooki* is not consistently recovered in Alligatorinae (see Farke et al., 2014; Whiting & Hastings, 2015; Lee & Yates, 2018; Massonne et al., 2019), comprising an unstable taxon to be set as a fossil constraint for total-group Alligatorinae (which by definition would imply the age of Caimaninae as well; Brochu, 2003). Following the best practices protocol of Parham et al. (2012) for time calibrated analyses, *Ne. ionensis* and *Pr. peligrensis* therefore provide a hard minimum fossil age of 63.5 Ma for the total-group Caimaninae as well as total-group Alligatorinae (divergence of Alligatorinae and Caimaninae). This fossil constraint is explicitly justified and may play an important role in stabilizing age estimations of future divergence date analyses of Alligatoridae. We set the soft-maximum age with *Brachychampsa sealeyi*, the oldest species ever considered a potential Caimaninae (e.g., Salas-Gismondi et al., 2015; Bona et al., 2018; Cossette, 2020; Stocker et al., 2021) even though it more likely represents a basal alligatoroid (see discussion and references above; Figure 6). *Br. sealeyi* comes from the Menefee Formation, San Juan Basin, in north-western New Mexico, and the locality was dated with high-precision U-Pb estimation, recovering an depositional age of 81–75 Ma (Dickinson & Gehrels, 2009; Table 1). Considering that *i)* the soft maximum should be set to an older age than the oldest possible fossil record of the group embracing the time when ecologic, biogeographic, geologic, and taphonomic conditions met, but no fossils are known (Parham et al., 2012), and *ii)* that *Br. sealeyi* is probably not even a caimaninae, we

suggest a conservative soft maximum for total-group Caimaninae as 83 Ma, at the Santonian-Campanian boundary.

Table 1. Stratigraphic age ranges of species for time-scaling the composite tree in Figure 6. Alligatorinae and Jacarea are based on the phylogenetic position and stratigraphic age of *Wannaganosuchus brachymanus* (Brochu, 2004b, 2013; Archibald & Gingerich, 1987; Erickson, 1991), and *Caiman wannlangstoni* (Salas-Gismondi et al., 2015; Bona et al., 2018; Wesselingh et al., 2006), respectively. Question mark indicates a possible age range for *Purussaurus* sp. This list is more up to date and rigorous than the data found in the Paleobiology Database (used by e.g., Bona et al., 2018). Symbol " · " denotes corrected maximum duration of depositional age in Ma.

Species	Age range (Mya)	References
Albertochampsa langstoni	77 – 76	Gilbert et al., 2018
Alligatorinae *	65 – 0	Archibald & Gingerich, 1987
Bottosaurus harlani	66 – 65	Miller et al., 2010
Brachychampsa sealeyi	82 – 74 •	Dickinson & Gehrels, 2009
Jacarea *	13.0 – 0	Salas-Gismondi et al., 2015/ Wesselingh et al., 2006
Centenariosuchus gilmorei	19.86 – 18.06	Hastings et al., 2013/ MacFadden et al., 2014
Chinatichampsus wilsonorum	42.8 – 41.5	Stocker et al., 2021/ Atwater, et al., 2020
Culebrasuchus mesoamericanus	19.83 – 19.12	Hastings et al., 2013

Eocaiman spp.	63.8 – 39	Clyde et al., 2014 / Godoy et al., 2020
Globidentosuchus brachyrostris	11.6 – 5.3	Scheyer et al., 2013
Gnatusuchus pebasensis	15.9 – 5.3	Salas-Gismondi et al., 2015/ Wesselingh et al., 2006
Kuttanacaiman iquitosensis	15 – 12.3	Salas-Gismondi et al., 2015/ Wesselingh et al., 2006
Mourasuchus amazonensis	9 – 6.8	Cidade et al., 2019
Necrosuchus ionensis	65.7 – 63.5	Clyde et al., 2014
Notocaiman stromeri	61.6 – 58.7	Kreuse, et al., 2017
Paleosuchus sp.	13.8 – 0	Salas-Gismondi et al., 2015
Purussaurus spp.	26.63(?) – 7.24	Solórzano et al., 2019/ Rincón et al., 2014
Protocaiman peligrensis	63.8 – 61.7	Bona et al., 2018
Stangerochampsa mccabei	73.1 – 68	Eberth & Kamo, 2020
Tsoabichi greenriverensis	51.4 – 49.23	Smith et al., 2010

Some recent mitogenomic divergence date studies used *Br. sealeyi* as a calibration point for crown-Caimaninae and recovered significantly older age estimations for the total-group than the earliest unambiguous fossils (Bittencourt et al., 2019; Roberto et al., 2020; mean of 90.72 Ma, and 91.89 Ma, respectively; Turonian, early Late Cretaceous; Table 2). We emphasize that *Br. sealeyi* should not be used to calibrate clades less inclusive than Crocodylia and that the practice of these authors cannot be justified. When *Br. sealeyi* was used as a fossil constraint for Crocodylia instead (Pan et al., 2020), a more reasonable albeit underestimating age for the origin of

total-group Caimaninae was recovered, with a mean of 53.39 Ma. This estimation is more reasonable, however it is still not consistent with the fossil record, being younger than the oldest South American caimanines, such as *Ne. ionensis* and *Pr. peligrensis*. Other molecular divergence date studies employed a calibration interval proposed by Müller & Reisz (2005) for the Alligatorinae-Caimaninae split: 66–71 Ma (e.g., Roos, 2007; Oaks, 2011). Both studies used mitogenomic data (Table 2) for the analysis (plus some loci from nuclear DNA; Oaks, 2011), and recovered ages that are consistent with the fossil record of total-group Caimaninae (mean age of 70 Ma and 65.48 Ma, respectively). A similar estimation was reported by Brochu (2004a) in a mitogenomic analysis (64 Ma), but fossil constraints used were not explicitly reported.

Although the tip-dating fossilized birth-death analysis of Godoy et al. (2020) recovered *Brachychampsa* spp., *St. mccabei,* and *Al. langstoni* as basal alligatoroids, their analysis still reconstructed an unusually old, Campanian age for total-group Caimaninae. This can be explained by their questionable calibration choice for Crocodylia, *Portugalosuchus azanhae* from the Cenomanian, as the crocodylian affinity of this species is poorly supported (see Supplementary material of Mateus et al., 2019) and unjustifiably pulls back the age of Caimaninae.

Table 2. Compilation of divergence timing estimates for the total and crown-group Caimaninae.

	MRCA	Mean age (Mya)	Fossil constraint	Genome	Sequence
Brochu (2004)	Total group	64.0 54.0	?	mtDNA	12s, 16s, cytb, ctrl, nd6

	Crown-group				
Janke et al. (2005)	Total-group Crown-group	110 -	Outgroup constraints	mtDNA	Trp, HtGly, LtGly, Phe, Thr
Roos (2007)	Total-group Crown-group	70.0 39.0	Interval of Müller & Reisz (2005)	mtDNA	12H strand encoded protein-coding sequence
Oaks (2011)	Total-group Crown-group	65.48 25.37	Interval of Müller & Reisz (2005) -	mtDNA & nDNA	Cyt b, tRNAGlu, tRNATrp, tRNAMet, tRNAGly, tRNAArg, tRNAPhe; Nuclear loci: ACTC, aTROP, ACTB, AChR, GAPDH, LDH-B, LDH-A, RHO
Bittencourt et al. (2019)	Total-group Crown-group	90.72 60.08	- *Brachychampsa sealeyi*	mtDNA	Cyt b
Pan et al. (2020)	Total-group Crown-group	53.39 36.18	*Brachychampsa sealeyi* for Alligatoridae	mtDNA	Complete mt genome
		91.89	-	mtDNA	Cyt b

Roberto et al. (2020)	Total-group Crown-group	61.93	*Brachychampsa sealeyi*	

Crown-group Caimaninae

Multiple phylogenetic analysis, using expanded versions of the dataset of Brochu (1999, 2010), recovered Late Cretaceous to Eocene species from North and South America (*Tsoabichi greenriverensis, Necrosuchus ionensis*, *Orthogenysuchus olseni*, and *Bottosaurus harlani*) within the crown-group of Caimaninae, mostly related to extant *Paleosuchus* spp. (Bona, 2007; Brochu, 2011; Hastings et al., 2013; Pinheiro, 2013; Bona et al., 2018; Cossette & Brochu, 2018; Souza-Filho et al., 2019, 2020; Cidade et al., 2020; Godoy et al., 2020; Stocker et al., 2021; Cossette, 2020). However, the position of those species is unstable with respect to the crown (Brochu, 2010, 2011; Cidade et al., 2020; Cossette, 2020; see discussion above; Figure 6), and should be avoided as calibration points. *Orthogenysuchus olseni* is consistently recovered closely related to *Purussaurus* spp., *Mourasuchus* spp., and *Paleosuchus* spp. in several studies (Bona, 2007; Brochu, 2010; Brochu, 2011; Pinheiro et al., 2013; Hastings et al., 2013; Fortier et al., 2014; Hastings et al., 2016; Massone et al., 2019) but recent re-preparation of the type and only known specimen resulted in the reinterpretation of key morphological features (Salas-Gismondi et al., 2015) and the taxon awaits revision. Therefore, *Or. olseni* should not be used to calibrate crown-Caimaninae.

The oldest well-dated record of unambiguous crown caimanines, *Centenariosuchus gilmorei*, come from the early Miocene of Central America (Hastings et al., 2013; Table 1). Hastings et al. (2016) recovered *Ce. gilmorei* in a crown-group polytomy including Nettosuchidae and *Paleosuchus* spp. Stocker et al. (2021) and the

present study obtained comparable results. Other studies have recovered *Ce. gilmorei* as closely related to Jacarea (Hastings et al., 2013; Salas-Gismondi et al., 2015; Bona et al., 2018; Godoy et al., 2020; Cidade et al., 2020), demonstrating different phylogenetic affinities of the species but consistently within the crown-group.

Ce. gilmorei is known from reasonably complete cranial and few postcranial material (Hastings et al., 2013, 2016) coming from the upper Cucaracha Formation of Panama. Radioisotopic estimations based on $^{40}Ar/^{39}Ar$ recovered an age of 18.96 ± 0.90 Ma, similarly to estimations based on U-Pb zircon, which recovered an age of 18.81 ± 0.30 Ma (Table 1), both indicating an early Miocene age for the Cucaracha Formation (MacFadden et al., 2014). This establishes the minimum age of crown-group Caimaninae to 18.06 Ma. Other taxa such as *Mourasuchus* spp. and *Purussaurus* spp. are often recovered within the crown-group as well (Bona, 2007; Brochu, 2010; Hastings et al., 2013; Pinheiro et al., 2013; Fortier et al., 2014; Hastings et al., 2016; Cidade et al., 2017; Cidade et al., 2020; Cossette, 2020), but sometimes recovered in a polytomy with stem taxa and *Paleosuchus* spp. (Brochu, 2011; Cossette & Brochu, 2018; Souza-Filho et al., 2019; Souza-Filho et al., 2020; Stocker et al., 2021), or even outside the crown (Salas-Gismondi et al., 2015; Bona et al., 2018). Fragmentary material of *Purussaurus* sp. is dated as old as the late Oligocene (Antoine et al., 2016; Solórzano et al., 2019), however new fossil discoveries are needed in order to provide additional morphological evidence to the identification of *Purussaurus* sp. in late Oligocene rocks. The late Oligocene "*Caiman*" *tremembensis* from the Tremembé Formation of Brazil, represented by a fragmentary dentary (Chiappe, 1988) does show a splenial excluded from the mandibular symphysis with its anterior tip passing dorsal to the Meckelian groove, but this character may not diagnose the crown alone, as it is also

present in taxa usually associated with stem-Caimaninae (e.g., *Eocaiman* spp., *Ne. ionensis*; Fortier et al., 2014).

For a soft maximum age of the crown-group we suggest 66 Ma (K-Pg boundary), a conservative date as no convincing crown fossils are known from rocks older than the Neogene. Molecular divergence date studies variously estimate the origin of the crown-group into the late Oligocene (Oaks, 2011), Eocene (Brochu, 2004a; Roos, 2007; Pan et al., 2020), and early Paleocene (Bittencourt, et al., 2019; Roberto et al., 2020; Table 2). Of these, Bittencourt et al. (2019) and Roberto et al. (2020) calibrated crown-group Caimaninae with *Brachychampsa sealeyi* (77.9–83.6 Ma), an unjustifiable practice given the potential basal alligatoroid affinity of this taxon (e.g., Norell and Clark, 1994; Brochu, 1999, 2004b, 2010; 2011; Hastings, et al. 2013; Pinheiro, et al., 2013; Cossette & Brochu, 2018; Lee & Yates, 2018; Cidade et al., 2020; Godoy et al., 2020; Souza-Filho et al., 2020). This calibration (together with other calibration points) resulted in age estimates notably older than the oldest known unambiguous fossil record of the crown-group (mean age of 60 Ma for Bittencourt et al., 2019; and 61.93 Ma for Roberto et al., 2020; Table 2). More reasonable ages (according to the current fossil record) were recovered by Roos (2007), and Oaks (2011). Both works used the age interval (71 – 66 Ma) suggested by Müller & Reisz (2005), which was proposed based on the oldest known alligatorine and the sister-relationship of *Stangerochampsa mccabei* and Alligatoridae , to calibrate the Alligatoridae node. Yet, the recovered ages of these two studies differ by more than 10 Myr (39 Ma for Roos, 2007; and 25.37 Ma for Oaks, 2011). Such discrepancies could be due to different mitogenomic data used for each analysis (Table 2). Pan et al. (2020) employed *Br. sealeyi* as a calibration for Crocodylia and estimated the age of crown-group Caimaninae to the late Eocene (36.18 Ma). The age of the crown remains poorly constrained but future analyses should

nevertheless now employ *Ce. gilmorei* as a well-justified minimum age fossil calibration point (18.06 Ma).

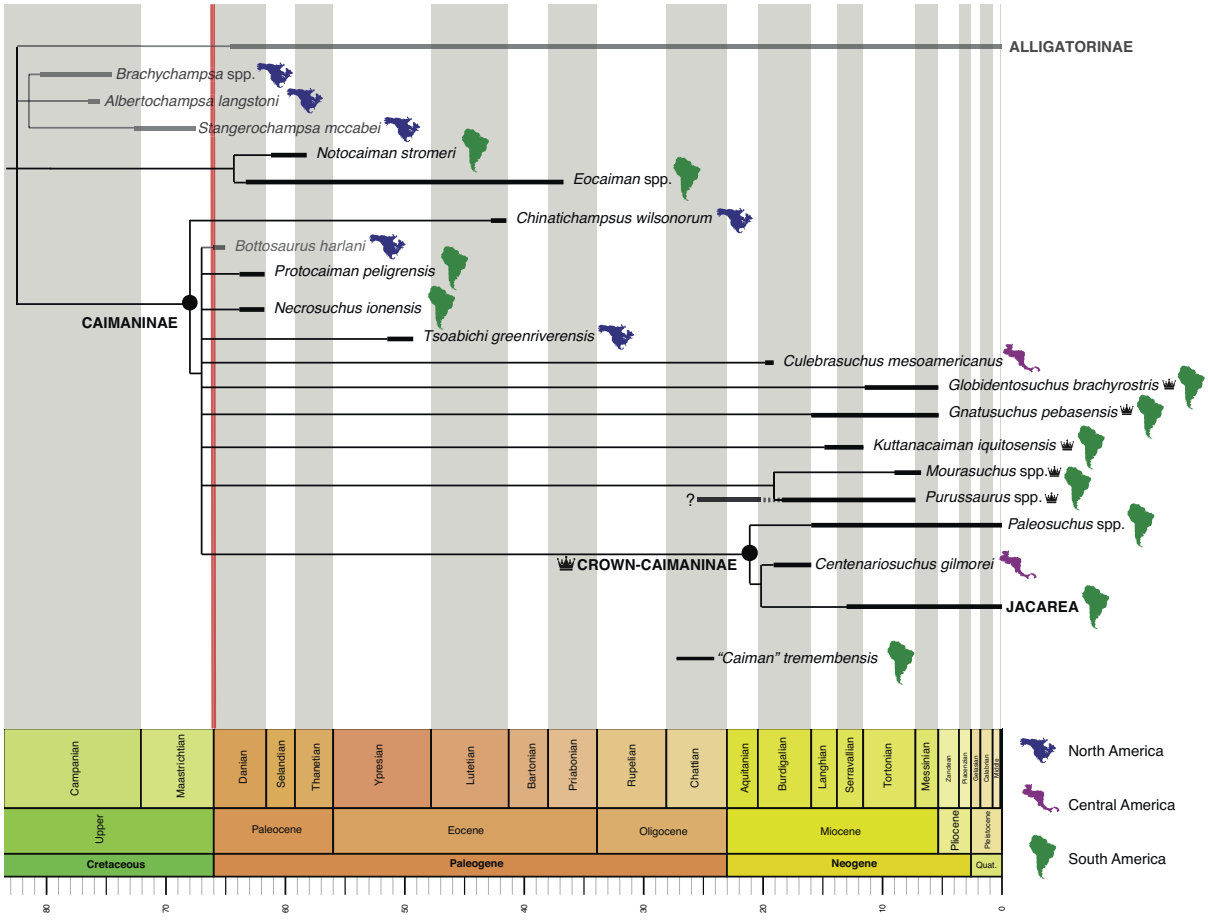

Figure 6. Time calibrated composite phylogenetic consensus of Caimaninae relationships using published consensus trees as well as the present study (see text for references on published topologies and Table 1 for stratigraphic ages). Crown silhouette indicates preferred placement of species within crown-Caimaninae following the present study (see Discussion). Question mark indicates possible age range (see Table 1 and discussion). Red line marks the K-Pg boundary.

Paleobiogeographic implications

Instead of literal interpretation of a single phylogeny to reconstruct historical biogeography (i.e., most previous studies), we provide a balanced discussion based on

the consensus and critical review of all previous phylogenies (Figure 6; see discussion above). Our study demonstrates that unambiguous crown taxa have always been restricted to South and Central America as well as that the earliest unambiguous total-group caimanines are from the earliest Paleocene of South America. The origin of total-group Caimaninae, however, took place in North America based on the distribution of outgroup taxa and the recently discovered basal-caimanine, *Chinatichampsus wilsonorum*, and was followed by a rapid dispersal to South America around the Cretaceous/Paleogene boundary (Brochu, 1999, 2010, 2011; Hastings et al., 2013; Bona et al., 2018; Cossette & Brochu, 2018; Cidade et al., 2020; Godoy et al., 2020; Stocker et al., 2021), regardless the phylogenetic placement of *Brachychampsa* spp., *Stangerochampsa mccabei* and *Albertochampsa langstoni*. The North American middle Eocene *Chinatichampsus wilsonorum* is considered the most basal but not the oldest unambiguous caimanine; Late Cretaceous and Paleocene representatives of the group are yet to be discovered/identified in the continent (Stocker et al., 2021; this study; Figure 6). The earliest alligatorids in South America are taxa usually recovered in Caimaninae, (*Necrosuchus ionensis*, Cidade et al., 2020; *Notocaiman stromeri*, Rusconi, 1937; *Protocaiman peligrensis*, Bona et al., 2018; *Eocaiman palaeocenicus*, Bona, 2007; and *Eocaiman itaboraiensis*; Pinheiro et al., 2013), which accounts for a dispersal of the clade from northern latitudes prior to the earliest Paleocene. Dispersal to South America must have occurred via island-hopping through the Antillean volcanic arc system that formed around the Late Cretaceous (Proenza et al., 2006). This connection was primarily consisting of islands divided by shallow marine waters, and subject to dynamic geological reconfiguration along most of the Paleogene (figures 5 to 7 of Iturralde-Vinent et al., 2006). Despite the absence of salt glands in alligatorids (Taplin et al., 1989), they do tolerate saltwater to some extent and crossing narrow

shallow marine barriers is unproblematic (Grigg, 1998; Brochu, 1999 and references therein; Mazzotti et al., 2019; Somaweera et al., 2020).

Previous phylogenies uniting *Ts. greenriverensis* and *Paleosuchus* spp. suggested a second Paleogene dispersal from South to North America (e.g., Brochu, 2010; Bona et al., 2018). However, our study reveals that *Ts. greenriverensis* was more likely near but still outside crown-Caimaninae (see Discussion above), which does not exclude the possibility of back-dispersal but raises the alternative explanation of a remnant member of primary North American caimanines. In that case (no back-dispersal), a second North to South America dispersal during the Paleogene is necessary to explain the origin of the crown-group because *Ts. greenriverensis* is apparently more derived (e.g., large supraoccipital exposure, skull roof partially covering supratemporal fenestra) than the basalmost species in South and North America (*Protocaiman peligrens*is and *Chinatichampsus wilsoni*, respectively). On the other hand, most Paleogene species from South America are too fragmentary (e.g., skull table is missing for *Eocaiman* spp., *Necrosuchus ionensis*) and if more material will place them in a more crownward position, a back dispersal is necessary to explain the presence of *Ts. greenriverensi*s in North America. Regardless of which of these two alternative hypotheses will stand the test of time, the past distribution of Caimaninae requires two intercontinental dispersals to resolve.

In light of the phylogenetic reinterpretation of the present study, Central American taxa from the Miocene belong to the crown and were not ancestral to South American Caimaninae (Figure 6; contra phylogenies of Hastings et al., 2013, 2016). While *Culebrasuchus mesoamericanus* still awaits revision (Stocker et al., 2021; this study), phylogeny and diversity of both extant and fossil taxa (Scheyer et al., 2013; Hastings et al., 2016; Scheyer and Delfino, 2016) rather support a South American

origin of crown-Caimaninae with a dispersal to Central America no later than the early Miocene. The age of the crown remains poorly constrained by fossils owing to a nearly 24 Myr gap in the Caimaninae record between the middle Eocene and the early Miocene. Molecular divergence estimations are yet unable to close this gap and reasonable dates range from the early Eocene to late Oligocene (54 Ma, Brochu, 2004a; 39 Ma, Roos, 2007; 36.18 Ma, Pan et al., 2020; 25.37 Ma, Oaks, 2011). Additional fossils from the late Paleogene and early Neogene of South America will be crucial for providing a more precise estimation and improved understanding of Caimaninae paleobiogeography.

CONCLUSION

A review of published fossil Caimaninae phylogenies combined with the preferred hypothesis of the present study is provided together with the spatio-temporal distributions in Figure 6. This composite tree represents a state of the art of early Caimaninae systematics and paleobiogeography to serve as a useful source for discussions on caimanine evolution and origins. A list of published stratigraphic ranges of taxa is found in Table 1; this is more up to date and rigorous than the data currently found in the Paleobiology Database (e.g., used by Bona et al., 2018).

1) Evidence for the previous caimanine affinity of *Stangerochampsa mccabei*, *Brachychampsa* spp. and *Albertochampsa langstoni* is feeble: changes we applied to the dataset of Bona et al. (2018) did not involve these taxa, yet they are recovered at the base of Alligatorinae, in contrast to the basal caimanine result of Bona et al. (2018). These taxa, together with *Bottosaurus harlani*, do not show unique caimanine synapomorphies. The invariably basal placement of these taxa in each major alligatorid clades highlights the uncertainty of character

evolution in Alligatoroidea. As such, there is no clear evidence for Cretaceous caimanines.

2) New specimens of *Tsoabichi greenriverensis* allowed us to confirm previous diagnostic features of the taxon, and additional characters demonstrating its caimanine affinity: posterior rim of internal choana is deeply notched and medial wall of supratemporal fenestra bears foramina. Evidence for a placement in crown-group Caimaninae is weak, as synapomorphies responsible for drawing *Ts. greenriverensis* into the crown may in fact diagnose a more inclusive clade.

3) Our results show that South and Central American Miocene taxa, previously recovered as basal caimanines (*Globidentosuchus brachyrostris*, *Kuttanacaiman iquitosensis*), belong to the crown-group. The persistent placement of *Gnatusuchus pebasensis* in the stem-group is driven by the peculiar morphology of this taxon, despite otherwise showing crown-caimanine synapomorphies. A crown placement of these taxa resolves the extensive ghost lineage previously inferred by their basal position.

4) The oldest unambiguous crown-Caimaninae is *Centenariosuchus gilmorei*, from the early Miocene of Panama, and fulfils best practices criteria (Parham et al., 2012) for minimum age calibration (18.06 Ma). *Ne. ionensis* and *Pr. peligrensis* set the minimum age of the total-group at 63.5 Ma, which approximates some but not all published molecular divergence date estimates that used reasonable calibration points. The herein proposed calibration points will nevertheless allow more rigorous time calibrated analyses. The age of the crown remains poorly constrained both by fossils and molecular divergence date estimates other than the late Paleogene. More comprehensive genetic data and fossils from the Late

Cretaceous and late Eocene-early Miocene would be vital for improved understanding of divergence times and early evolution of Caimaninae.

5) We found two Paleogene dispersals of stem-Caimaninae from North to South America an equally likely hypothesis as a previously proposed northward back-dispersal. The phylogeny however continues to imply at least two Caimaninae dispersals between North and South America. Miocene taxa of Central America previously assigned to the stem-lineage ancestral to South American Caimaninae (*Globidentosuchus brachyrostris*, *Centenariosuchus gilmorei*) are reinterpreted as part of a Neogene northward expansion of the otherwise ancestrally South American crown-group.

REFERENCES

Antoine PO, Abello MA, Adnet S, Sierra AJA, Baby P, Billet G, Boivina M, Calderón Y, Candela A, Chabain J, et al. 2016. A 60-million-year Cenozoic history of western Amazonian ecosystems in Contamana, eastern Peru. Gondwana Res. 31:30–59.

Atwater AL, Thomson KD, Kirk EC, Emery-Wetherell M, Wetherell L, Stocki DF. 2020. Geochronology of the middle Eocene Purple Bench locality (Devil's Graveyard Formation), Trans-Pecos Texas, USA. Palaeontol. Electronica. 23(1):a06.

Archibald JD, Gingerich, PD 1987. First North American land mammal ages of the Cenozoic Era. In: Woodburne MO, editor. Cenozoic mammals of North America: Geochronology and Biostratigraphy. University of California Press, Berkley, California. p. 24–76.

Benton MJ, Clark JM. 1988. The Phylogeny and Classification of the Tetrapods. Vol. 1, Amphibians, Reptiles, Birds. In: Benton MJ, editor. Archosaur phylogeny and the relationships of the Crocodylia. Clarendon Press, Oxford. p. 295–338.

Birgenheier LP, Vanden Berg MD, Plink-Björklund P, Gall RD, Rosencrans R, Rosenberg J, Toms LC, Morris J. 2019. Climate impact on fluvial-lake system evolution, Eocene Green River Formation, Uinta Basin, Utah, USA. Geol Soc Am Bull. 132(3–4):562–587.

Bittencourt PS, Campos Z, de Lima Muniz F, Marioni B, Souza BC, Da Silveira R, de Thoisy B, Hrbek B, Farias IP. 2019. Evidence of cryptic lineages within a small South American crocodilian: the Schneider's dwarf caiman *Paleosuchus trigonatus* (Alligatoridae: Caimaninae). PeerJ. 7:e6580.

Bona P. 2007. Una nueva especie de *Eocaiman* Simpson (Crocodylia, Alligatoridae) del Paleoceno Inferior de Patagonia. Ameghiniana. 44(2):435–445.

Bona P, Ezcurra MD, Barrios F, Fernandez Blanco MV. 2018. A new Palaeocene crocodylian from southern Argentina sheds light on the early history of caimanines. Proc R Soc B. 285(1885):20180843.

Brochu CA. 1996. Closure of neurocentral sutures during crocodilian ontogeny: implications for maturity assessment in fossil archosaurs. J Vertebr Paleontol. 16(1):49–62.

Brochu CA. 1999. Phylogenetics, taxonomy, and historical biogeography of Alligatoroidea. J Vertebr Paleontol. 19(S2):9–100.

Brochu CA. 2003. Phylogenetic approaches toward crocodylian history. Annu Rev Earth Planet Sci. 31:357–397.

Brochu CA. 2004a. Calibration age and quartet divergence date estimation. Evolution. 58(6):1375–1382.

Brochu CA. 2004b. Alligatorine phylogeny and the status of *Allognathosuchus* Mook, 1921. J Vertebr Paleontol. 24(4):857–873.

Brochu CA. 2010. A new alligatoroid from the lower Eocene Green River Formation of Wyoming and the origin of caimans. J Vertebr Paleontol. 30(4):1109–1126.

Brochu CA. 2011. Phylogenetic relationships of *Necrosuchus ionensis* Simpson, 1937 and the early history of caimanines. Zool J Linn Soc. 163:S228–S256.

Brochu CA. 2013. Phylogenetic relationships of Palaeogene ziphodont eusuchians and the status of *Pristichampsus* Gervais, 1853. Earth Environ Sci Transact R Soc Edinb. 103(3–4):521–550.

Carroll AR, Bohacs KM. 1999. Stratigraphic classification of ancient lakes: balancing tectonic and climatic controls. Geology. 27(2):99–102.

Chiappe LM. 1988. Un nuevo *Caiman* (Crocodylia, Alligatoridae) de la Formación Tremembé (Oligoceno), Estado de São Paulo, Brasil, y su significado paleoclimático. Paula-Coutiana. 3:49–66.

Cidade GM., Solórzano A, Rincón AD, Riff D, Hsiou AS. 2017. A new *Mourasuchus* (Alligatoroidea, Caimaninae) from the late Miocene of Venezuela, the phylogeny of Caimaninae and considerations on the feeding habits of *Mourasuchus*. PeerJ. 5:e3056.

Cidade GM, Fortier DC, Hsiou AS. 2020. Taxonomic and phylogenetic review of *Necrosuchus ionensis* (Alligatoroidea: Caimaninae) and the early evolution and radiation of caimanines. Zool J Linn Soc. 189(2):657–669.

Clyde WC, Wilf P, Iglesias A, Slingerland RL, Barnum T, Bijl PK, Timothy J, Bralower TJ, Brinkhuis H, Comer EE, et al. 2014. New age constraints for the Salamanca Formation and lower Río Chico Group in the western San Jorge Basin, Patagonia, Argentina: implications for Cretaceous-Paleogene extinction recovery and land mammal age correlations. Geol Soc Am Bull. 126(3–4):289–306.

Cossette AP, Brochu CA. 2018. A new specimen of the alligatoroid *Bottosaurus harlani* and the early history of character evolution in alligatorids. J Vertebr Paleontol. 38(4):1–22.

Cossette AP. 2020. A new species of *Bottosaurus* (Alligatoroidea: Caimaninae) from the Black Peaks Formation (Palaeocene) of Texas indicates an early radiation of North American caimanines. Zool J Linn Soc. 191(1):276–301.

Cossette AP, Brochu CA. 2020. A systematic review of the giant alligatoroid *Deinosuchus* from the Campanian of North America and its implications for the relationships at the root of Crocodylia. J Vertebr Paleontol. 40(1):e1767638.

Cuvier G. 1807. Sur les différentes espèces de crocodiles vivants et sur leurs caractères distinctifs [On the different living crocodile species and their distinctive characters]. Annales du Muséum d'Histoire Naturelle de Paris. 10:8–66.

Dickinson WR, Gehrels GE. 2009. Use of U–Pb ages of detrital zircons to infer maximum depositional ages of strata: a test against a Colorado Plateau Mesozoic database. Earth Planet Sci Lett. 288(1-2):115–125.

Eberth DA, Kamo SL. 2020. High-precision U–Pb CA–ID–TIMS dating and chronostratigraphy of the dinosaur-rich Horseshoe Canyon Formation (Upper Cretaceous, Campanian–Maastrichtian), Red Deer River valley, Alberta, Canada. Can J Earth Sci. 57(10):1220–1237.

Erickson BR. 1991. Flora and Fauna of the Wannagan Creek Quarry: Late Paleocene of North America. Sci Publ Sci Mus Minn. 7(3):1–19

Farke AA., Henn, MM, Woodward, SJ, Xu, HA 2014. *Leidyosuchus* (Crocodylia: Alligatoroidea) from the Upper Cretaceous Kaiparowits Formation (late Campanian) of Utah, USA. PaleoBios. 30(3):72–88.

Flynn AG, Davis, AJ, Williamson, TE, Heizler, M, Fenley IV, CW, Leslie, CE, Secord, R, Brusatte, SL, Peppe, DJ. 2020. Early Paleocene magnetostratigraphy and revised biostratigraphy of the Ojo Alamo Sandstone and lower Nacimiento Formation, San Juan Basin, New Mexico, USA. Geol Soc Am Bull. 132(9-10):2154–2174.

Fortier DC, Souza-Filho JP, Guilherme E, Maciente A, Schultz CL. 2014. A new specimen of *Caiman brevirostris* (Crocodylia, Alligatoridae) from the Late Miocene of Brazil. J Vertebr Paleontol. 34(4): 820–834.

Gilbert MM, Bamforth EL, Buatois LA, Renaut RW. 2018. Paleoecology and sedimentology of a vertebrate microfossil assemblage from the easternmost Dinosaur Park Formation (Late Cretaceous, Upper Campanian,) Saskatchewan, Canada: Reconstructing diversity in a coastal ecosystem. Palaeogeogr, Palaeoclimatol, Palaeoecol. 495:227–244.

Gmelin J. 1789. Linnei Systema Naturae. Leipzig. p.1057.

Godoy PL, Cidade GM, Montefeltro FC, Langer MC, Norell MA. 2020. Redescription and phylogenetic affinities of the caimanine *Eocaiman cavernensis* (Crocodylia, Alligatoroidea) from the Eocene of Argentina. Pap Palaeontol. 1–27.

Goloboff PA, Catalano SA. 2016. TNT version 1.5, including a full implementation of phylogenetic morphometrics. Cladistics. 32(3):221–238.

Grande L. 2013. The lost world of Fossil Lake: snapshots from deep time. Chicago (IL): The University of Chicago Press.

Grigg GC, Beard LA, Moulton T, Melo MTQ, Taplin LE. 1998. Osmoregulation by the broad-snouted caiman, *Caiman latirostris*, in estuarine habitat in southern Brazil. J Comp Physiol. 168:445–452.

Hastings AK, Bloch JI, Jaramillo CA, Rincon AF, MacFadden BJ. 2013. Systematics and biogeography of crocodylians from the Miocene of Panama. J Vertebr Paleontol. 33(2):239–263.

Hastings AK, Reisser M, Scheyer TM. 2016. Character evolution and the origin of Caimaninae (Crocodylia) in the New World Tropics: new evidence from the Miocene of Panama and Venezuela. J Paleontol. 90(2):317–332.

Inglis GN, Bragg F, Burls NJ, Cramwinckel MJ, Evans D, Foster GL, Huber M, Lunt DJ, Siler N, Steinig S, et al. 2020. Global mean surface temperature and climate sensitivity of the early Eocene Climatic Optimum (EECO), Paleocene–Eocene Thermal Maximum (PETM), and latest Paleocene. Clim Past. 16(5):1953–1968.

Krause JM, Clyde WC, Ibañez-Mejía M, Schmitz MD, Barnum T, Bellosi ES, Wilf P. 2017. New age constraints for early Paleogene strata of central Patagonia, Argentina:

Implications for the timing of South American Land Mammal Ages. Geol Soc Am Bull. 129(7–8):886–903.

Lee MSY, Yates AM. 2018. Tip-dating and homoplasy: reconciling the shallow molecular divergences of modern gharials with their long fossil record. Proc R Soc B. 285(1881):20181071.

Li C, Wu X-C, Rufolo S. 2019. A new crocodyloid (Eusuchia: Crocodylia) from the Upper Cretaceous of China. Cretac Res. 94:25–39.

Lucas SG, Estep, JW 2000. Osteology of *Allognathosuchus mooki* Simpson, a Paleocene crocodilian from the San Juan Basin, New Mexico, and the monophyly of Allognathosuchus. N M Mus Nat Hist Sci Bull. 16:155–168.

MacFadden BJ, Bloch JI, Evans H, Foster DA, Morgan GS, Rincon A, Wood AR. 2014. Temporal calibration and biochronology of the Centenario Fauna, early Miocene of Panama. J Geol. 122(2):113–135.

Massonne T, Vasilyan D, Rabi M, Böhme M. 2019. A new alligatoroid from the Eocene of Vietnam highlights an extinct Asian clade independent from extant *Alligator sinensis*. PeerJ. 7(Ser.2):e7562

Mateus O, Puertolas-Pascual E, Callapez PM. 2019. A new eusuchian crocodylomorph from the Cenomanian (Late Cretaceous) of Portugal reveals novel implications on the origin of Crocodylia. Zool J Linn Soc. 186(2):501–528.

Mazzotti FJ, Smith BJ, Squires MA, Cherkiss MS, Farris SC, Hackett C, Hart KM, Briggs-Gonzalez V, Brandt LA. 2019. Influence of salinity on relative density of American crocodiles (Crocodylus acutus) in Everglades National Park: Implications for restoration of Everglades ecosystems. Ecol Indic. 102:608–616.

Miller KG, Sherrell RM, Browning JV, Field MP, Gallagher W, Olsson RK, Sugarman PT, Tuorto S, Wahyudi H. 2010. Relationship between mass extinction and iridium across the Cretaceous-Paleogene boundary in New Jersey. Geology. 38(10):867–870.

Montes C, Cardona A, McFadden R, Morón SE, Silva CA, Restrepo-Moreno S, Ramírez DA, Hoyos N, Wilson J, Farris D, et al. A. 2012. Evidence for middle Eocene and younger emergence in Central Panama: implications for Isthmus closure. Geol Soc Am Bull. 124(5-6):780–799.

Mook CC. 1924. A new crocodilian from the Wasatch Beds. Am Mus Novit. 137:1–4.

Müller J, Reisz RR. 2005. Four well-constrained calibration points from the vertebrate fossil record for molecular clock estimates. Bioessays. 27(10):1069–1075.

Narváez I, Brochu CA, Escaso F, Pérez-Garcia A, Ortega F. 2015. New crocodyliforms from southwestern Europe and definition of a diverse clade of European Late Cretaceous basal eusuchians. PLoS One. 10(11):e0140679.

Norell MA, Clark JM, Hutchison JH. 1994. The Late Cretaceous alligatoroid *Brachychampsa montana* (Crocodylia): new material and putative relationships. Am Mus Novit. 3116:1–26.

Oaks JR. 2011. A time-calibrated species tree of Crocodylia reveals a recent radiation of the true crocodiles. Evolution. 65(11):3285–3297.

Pan T, Miao J-S, Zhang H-B, Yan P, Lee P-S, Jiang X-Y, Ouyang J-H, Deng Y-P, Zhang B-W, Wu X-B. 2020. Near-complete phylogeny of extant Crocodylia (Reptilia) using mitogenome-based data. Zool J Linn Soc. 191(4):1075–1089.

Parham JF, Donoghue PCJ, Bell CJ, Calway TD, Head JJ, Holroyd PA, Inoue JG, Irmis RB, Joyce WG, Ksepka DT, et al. 2012. Best practices for justifying fossil calibrations. Syst Biol. 61(2):346–359.

Pinheiro AEP, Fortier DC, Pol D, Campos DA, Bergqvist LP. 2013. A new *Eocaiman* (Alligatoridae, Crocodylia) from the Itaboraí Basin, Paleogene of Rio de Janeiro. Braz Hist Biol. 25(3):327–337.

Raigemborn MS, Krause JM, Bellosi E, Matheos SD. 2010. Redefinición estratigráfica del Grupo Río Chico (Paleógeno inferior), en el norte de la Cuenca del Golfo San Jorge, Chubut. Rev Asoc Geol Argent. 67(2):239–256.

Rincón AD, Solórzano A, Benammi M, Vignaud P, McDonald HG. 2014. Chronology and geology of an Early Miocene mammalian assemblage in North of South America,

from Cerro La Cruz (Castillo Formation), Lara State, Venezuela: implications in the changing course of Orinoco River hypothesis. Andean Geol. 41(3): 507–528.

Roberto IJ, Bittencourt PS, Muniz FL, Hernández-Rangel SM, Nóbrega YC, Ávila RW, Souza BC, Alvarez G, Miranda-Chumacero G, Campos Z, et al. 2020. Unexpected but unsurprising lineage diversity within the most widespread Neotropical crocodilian genus *Caiman* (Crocodylia, Alligatoridae). Syst Biodiver. 18(4):377–395.

Roos J, Aggarwal RK, Janke A. 2007. Extended mitogenomic phylogenetic analyses yield new insight into crocodylian evolution and their survival of the Cretaceous–Tertiary boundary. Mol Phyl Evol. 45(2):663–673.

Salas-Gismondi R, Flynn JJ, Baby P, Tejada-Lara JV, Wesselingh FP, Antoine PO. 2015. A Miocene hyperdiverse crocodylian community reveals peculiar trophic dynamics in proto-Amazonian mega-wetlands. Proc R Soc B: Biol Sci. 282(1804):20142490.

Scheyer TM, Aguilera OA, Delfino M, Fortier DC, Carlini AA, Sánchez R, Carrillo-Briceño JD, Quiroz L, Sánchez-Villagra MR. 2013. Crocodylian diversity peak and extinction in the late Cenozoic of the northern Neotropics. Nat Commun. 4(1):1–9.

Scheyer T, Delfino M. 2016. The late Miocene caimanine fauna (Crocodylia: Alligatoroidea) of the Urumaco Formation, Venezuela. Palaeo Electron. 19(3.48A):1–57.

Smith ME, Carroll AR, Singer B. 2008. Synoptic reconstruction of a major ancient lake system: Eocene Green River Formation, western United States. Geolo Soc Am Bull. 120(1-2):54–84.

Smith ME, Chamberlain KR, Singer BS, Carroll AR. 2010. Eocene clocks agree: Coeval 40Ar/39Ar, U-Pb, and astronomical ages from the Green River Formation. Geology. 38(6):527–530.

Solórzano A, Rincón AD, Cidade GM, Núñez-Flores M, Sánchez L. 2019. Lower Miocene alligatoroids (Crocodylia) from the Castillo Formation, northwest of Venezuela. Palaeo Palaeo. 99(2):241–259.

Somaweera R, Nifong J, Rosenblatt A, Brien ML, Combrink X, Elsey RM, Grigg G, Magnusson WE, Mazzotti FJ, Pearcy A, Platt SG. 2020. The ecological importance of crocodylians: towards evidence-based justification for their conservation. Biol Rev. 95(4):936–59.

Souza-Filho JP, Souza RG, Hsiou AS, Riff D, Guilherme E, Negri FR, Cidade GM. 2018. A new caimanine (Crocodylia, Alligatoroidea) species from the Solimões Formation of Brazil and the phylogeny of Caimaninae. J Vertebr Paleontol. 38(5):e1528450.

Souza-Filho JP, Guilherme E, De Toledo PM, Carvalho IDS, Negri FR, Maciente AADR, Cidade GM, Da Silva Lacerda MB, De Souza LG. 2020. On a new *Melanosuchus* species (Alligatoroidea: Caimaninae) from Solimões Formation (Eocene-Pliocene), Northern Brazil, and evolution of Caimaninae. Zootaxa. 4894(4):561–593.

Stocker MR, Brochu CA, Kirk EC. 2021. A new caimanine alligatorid from the Middle Eocene of Southwest Texas and implications for spatial and temporal shifts in Paleogene crocodyliform diversity. PeerJ. 9:e10665.

Taplin LE, Grigg GC. 1989. Historical zoogeography of the eusuchian crocodilians: a physiological perspective. Am Zool. 29(3):885–901.

Wegner W, Wörner G, Harmon ME, Jicha BR. 2011. Magmatic history and evolution of the Central American land bridge in Panama since the Cretaceous times. Geol Soc Am Bull. 123(3/4):703–724.

Wesselingh FP, Hoorn MC, Guerrero J, Räsänen ME, Romero Pittman L, Salo JS. 2006. The stratigraphy and regional structure of Miocene deposits in western Amazonia (Peru, Colombia and Brazil), with implications for late Neogene landscape evolution. Scr Geol. 133:291–322.

Whiting ET, Hastings, AK 2015. First fossil *Alligator* from the late Eocene of Nebraska and the Late Paleogene record of alligators in the Great Plains. J Herpetol. 49(4):560–569.

Williamson TE. 1996a. *Brachychampsa sealeyi*, sp. nov., (Crocodylia, Alligatoroidea) from the Upper Cretaceous (lower Campanian) Menefee Formation, northwestern New Mexico. J Vertebr Paleontol. 16(3):421–431.

Williamson TE. 1996b. The beginning of the age of mammals in the San Juan Basin, New Mexico: biostratigraphy and evolution of Paleocene mammals of the Nacimiento Formation. Albuquerque (NM): Bull N M Mus Nat Hist Sci.

SUPPORTING INFORMATION

Supplementary material S1. Character definition and parsimony model changes to the datasets of Bona et al. (2018) and Massonne et al. (2019)

Supplementary material S2. Supplementary figures.

Supplementary Material S1

CHARACTER DEFINITION AND PARSIMONY MODEL CHANGES TO THE DATASETS OF Bona et al. (2018) AND Massonne et al. (2019)

152. [Supratemporal fenestra with fossa; dermal bones of skull roof do not overhang rim at maturity (0) or dermal bones of skull roof overhang rim of supratemporal fenestra near maturity (1) or supratemporal fenestra closes during ontogeny (2).]

This character is coding the overhang of the supratemporal fenestrae rims at maturity by the dermal elements of the skull roof. The previous version of this character only scored the presence or absence of an overhang and the closure of the fenestra. We add an intermediate state to reflect the morphology of some taxa (e.g., *Bottosaurus harlani*, *Chinatichampsus wilsoni*) where the overhang is only consisting of the parietal. As this character forms a morphocline, it is ordered in the analysis.

Redefinition: 152. Supratemporal fenestra with fossa; dermal bones of skull roof do not overhang rim at maturity (0), or parietal overhangs the rim at maturity (1), or postorbital, squamosal and parietal overhang the rim at maturity (2), or fenestra is closed at maturity (3). [**ordered**]

160. [Supraoccipital exposure on dorsal skull table small (0), absent (1), large (2), or large such that parietal is excluded from posterior edge of table (3).]

We ordered the states into a morphocline by flipping state 0 and 1 and ordered the character in the analyses as this character otherwise forms a clear morphocline.

Redefinition: 160. Supraoccipital exposure on dorsal skull table absent (0), small (1), large (2), or large such that parietal is excluded from posterior edge of table (3). [**ordered**]

CHANGES APPLIED TO Bona et al. (2018) DATASET

FURTHER CHANGES APPLIED TO THE DATASET OF Bona et al. (2018)

Addition of taxa

4 taxa were added to the dataset: *Bottosaurus harlani* and *Chinatichampsus wilsonorum* from Stocker et al. (2021) and *Orientalosuchus naduongensis* and *Jiangxisuchus nankangensis* from Massonne et al. (2019).

Character changes for *Eocaiman cavernensis*

49. Dentary symphysis extends to fourth or fifth alveolus (0) or sixth through eighth alveolus (1) or behind eighth alveolus (2).

The dentary symphysis clearly extends to the 5th alveoli on dentary and not beyond (AMNH 3158, holotype; Godoy, 2020 – Figure 7A-B). We rescore this character from state 1 to 0.

62. Surangular with spur bordering the dentary toothrow lingually for at least one alveolus length (0) or lacking such spur (1).

This character is coding the surangular spur found in some crocodylids (e.g: *Crocodylus acutus*; Brochu, 1997). Such feature is not present in *Eocaiman cavernensis* (Godoy, 2020 – Figure 7A-B). We rescore this character from state ? to 1.

64. Surangular-dentary suture intersects external mandibular fenestra anterior to posterodorsal corner (0) or at posterodorsal corner (1).

The surangular meets the dentary anterior to the posterodorsal corner of the external mandibular fenestra (Godoy, 2020 – Figure 8A-B). We rescore this character from state ? to 0.

94. Maxillary tooth row curved medially or linear (0) or curves laterally broadly (1) posterior to first six maxillary alveoli.

We consider the maxillary tooth row to be linear in *Eocaiman cavernensis* based on the left part of the snout (Godoy, 2020 – Figure 4A-B and 5A-B). We rescore this character from state ? to 0.

96. Canthi rostralii absent or very modest (0) or very prominent (1) at maturity.

These ridges usually appear on the lacrimal and extend onto the maxilla. These features are typically found in some alligatorids, notably in *Melanosuchus niger*. They are absent in *Eocaiman cavernensis* (Godoy, 2020 – Figure 1A and 3A-B). We rescore this character from state ? to 0.

104. Ectopterygoid abuts maxillary tooth row (0) or maxilla broadly separates ectopterygoid from maxillary tooth row (1).

This character is coding the ectopterygoid lateral contact with the maxillary tooth row (Brochu, 1997). In the present species, the ectopterygoid borders the two posteriormost alveoli, and the maxilla does not send any process in between (Godoy, 2020 – Figure 4A-B). We rescore this character from state 1 to 0.

113. Anterior face of palatine process rounded or pointed anteriorly (0) or notched anteriorly (1).

Palatines in *Eocaiman cavernensis* are notched anteriorly (Godoy, 2020 – Figure 4A-B). We rescore this character from state ? to 1.

118. Palatine-pterygoid suture nearly at (0) or far from (1) posterior angle of suborbital fenestra.

This region of the skull is poorly preserved on the fossil and one could not trace the suture accurately. We rescore this character from state 0 to ?.

119. Pterygoid ramus of ectopterygoid straight, posterolateral margin of suborbital fenestra linear (0) or ramus bowed, posterolateral margin of fenestra concave (1).

The posterolateral border of the suborbital fenestra is noticeably concave (Godoy, 2020 – Figure 4A-B). We rescore this character from state ? to 1.

126. Ectopterygoid-pterygoid flexure disappears during ontogeny (0) or remains throughout ontogeny (1).

Given the scarce recognised material referred to *Eocaiman cavernensis*, it is impossible to give any accurate scoring for this character, as no ontogenetic sequence can be reconstructed. We rescore this character from state 0 to ?.

The following characters were changed to unknown, as these features are missing from the holotype and only known specimen confidently referable to *E. cavernensis* following Godoy et al. (2020):

85. External naris (0) opens flush with dorsal surface of premaxillae or (1) circumscribed by thin crest. Changed from 0 to ?.

144. Quadratojugal bears long anterior process along lower temporal bar (0) or bears modest process, or none at all, along lower temporal bar (1). Changed from 0 to ?.

158. Mature skull table with broad curvature; short posterolateral squamosal rami along paroccipital process (0) or with nearly horizontal sides; significant posterolateral squamosal rami along paroccipital process (1). Changed from 1 to ?.

160. Supraoccipital exposure on dorsal skull table absent (0), small (1), large (2), or large such that parietal is excluded from posterior edge of table (3). Changed from 3 to ?.

171. Posterior pterygoid processes tall and prominent (0) or small and project posteroventrally (1) or small and project posteriorly (2). Changed from 0 to ?.

174. Exoccipital with very prominent boss on paroccipital process; process lateral to cranioquadrate opening short (0) or exoccipital with small or no boss on paroccipital process; process lateral to cranioquadrate opening long (1). Changed from 1 to ?.

176. Exoccipitals terminate dorsal to basioccipital tubera (0) or send robust process ventrally and participate in basioccipital tubera (1) or send slender process ventrally to basioccipital tubera (2). Changed from 2 to ?.

Character changes for *Globidentosuchus brachyrostris*

49. Dentary symphysis extends to fourth or fifth alveolus (0) or sixth through eighth alveolus (1) or behind eighth alveolus (2).

The dentary symphysis extension was previously scored as 1, reaching the 7th dentary alveolus (AMU-CURS-222; Scheyer et al., 2013), but the termination is not evident. Material from Scheyer & Delfino (2016) does not bring additional information for this character. We would expect the dentary symphysis to extend to 5th or 6th alveolus. We advise caution here and rescore this character from state 1 to 0&1.

60. Angular-surangular suture contacts external mandibular fenestra at posterior angle at maturity (0) or passes broadly along ventral margin of external mandibular fenestra late in ontogeny (1).

In order to score this character as state 0, we would consider the suture to contact the external mandibular fenestra to a more dorsal point (Scheyer & Delfino, 2016; Figure 9). Here, the suture is deflected ventrally from the posterior most angle. We rescore this character from state 0 to 1.

151. Frontoparietal suture concavoconvex (0) or linear (1) between supratemporal fenestrae.

Based on specimen AMU-CURS-222 (Scheyer et al., 2013; Hastings et al., 2016), the frontoparietal suture was scored as concavoconvex. We rescore this character from state 0 to 1, as this suture appears evidently linear.

Character changes for *Tsoabichi greenriverensis*

Following scorings are based on first-hand observations of the new specimens described in this paper.

23. Scapular blade flares dorsally at maturity (0), or sides of scapular blade subparallel with minimal dorsal flare at maturity (1)

We rescore this character state from ? to 0 based on SMNK-PAL 2334.

88. Incisive foramen is small with less than half the greatest width of premaxillae (0), is extremely reduced and thin (1), is large with more than half the greatest width of premaxillae (2), or is large and intersects premaxillary/maxillary suture (3).

We rescore this character from state ? to 0 based on SMNK-PAL 2333a.

116. The palatine process is generally broad (0), or in form of a thin wedge (1).

We rescore this character from state ? to 0 based on SMNK-PAL 2333b.

124. Posterior rim of the choana is not deeply notched (0), or is deeply notched (1).

We rescore this character from state ? to 1 based on SMNK-PAL 2333b.

137. Margin of orbit flush with skull surface (0) or dorsal edges of orbits upturned (1) or orbital margin telescoped (2).

Based on the new specimens described in this paper, we can confidently rescore this character from state ? to 0 based on SMNK-PAL 2333a, 2334.

The posteromedial margins of the orbits are flush with the skull surface in SMNK-PAL 2333a and SMNK-PAL 2334. This condition was also observed previously in other specimens of *Ts. greenriverensis* (UNSM 9301, UCM 10164) by Brochu (2010) and seems to be a general condition for the species. An exception was noticed by Brochu (2010) in the holotype (TMM 42509-1), which appears to present an upturned posteromedial margin of the orbits, however he argued that it probably represents preservational artifact Nevertheless, Brochu (2010) scored this character as unknown for *Ts. greenriverensis*. The two individuals herein described allow a clear observation of the dorsal surface of the frontal and an upturned orbital margin is again absent, which reinforces that this is the typical condition for *Ts. greenriverensis*. We therefore rescored this character as orbit margins flush with the skull surface (137: ? > 0), a condition not seen in crown camanines (Brochu, 1999; with the exception of *Kuttanacaiman iquitosensis* and *Globidentosuchus brachyrostris*, taxa recovered in the crown by the present study).

154. Medial parietal wall of supratemporal fenestra imperforate (0) or bearing foramina (1).

Based on first hand observation of the new specimens described in this paper, we can confidently change this character from state ? to 1 based on SMNK-PAL 2333a, 2334.

Character changes for *Chinatichampsus wilsonorum*

152. Supratemporal fenestra with fossa; dermal bones of skull roof do not overhang rim at maturity (0), or parietal overhangs the rim at maturity (1), or postorbital, squamosal and parietal overhang the rim at maturity (2), or fenestra is closed at maturity (3).

The parietal slightly overhangs the supratemporal fenestra anteromedial corner (Stocker et al., 2021). We rescore this character from 0 to 1.

154. Medial parietal wall of supratemporal fenestra is imperforate (0), bearing foramina (1).

The description of this character in Stocker et al. (2021) mentions the presence of foramina on the medial wall of the supratemporal fenestrae, while this character was scored as absent in their dataset. We rescore this character from 0 to 1.

93. Largest maxillary alveolus is 3rd (0), 5th (1), 4th (2), 4th and 5th are same size (3), 6th (4), maxillary teeth are homodont (5), or maxillary alveoli gradually increase in diameter posteriorly (6).

The description of this character and Fig. 5 in Stocker et al. (2021) show a polymorphic condition in *Chinatichampsus wilsonorum*, with 3rd and 4th maxillary teeth being the largest. We therefore rescore this character from state 0 to 0&2.

Character changes for *Centenariosuchus gilmorei*

Scoring changes for *Centenariosuchus gilmorei* followed scorings applied by Stocker et al. (2021).

Character changes for *Crocodylus niloticus*

124. Posterior rim of internal choana is not deeply notched (0), or is deeply notched (1).

After revising collection material of *Crocodylus niloticus* (e.g., SMNK 6663) we observed that the posterolateral shape of the internal choana shows a different morphology from Caimaninae. We therefore decided to change the scoring to 0.

FURTHER CHANGES APPLIED TO THE DATASET OF Massonne et al. (2019)

Character changes for *Eocaiman cavernensis*

49. Dentary symphysis extends to fourth or fifth alveolus (0) or sixth through eighth alveolus (1) or behind eighth alveolus (2).

The dentary symphysis clearly extends to the 5th alveoli on dentary and not beyond (AMNH 3158, holotype; Godoy, 2020 – Figure 7A-B). We rescore this character from state 1 to 0.

51. Largest dentary alveolus immediately caudal to fourth is (0) 13 or 14, (1) between 11 and 14 and a series behind it, (2) 11 or 12, (3) no differentiation, (4) behind 14, (5)

The largest dentary alveolus immediately caudal to fourth is alveolus 13 (Godoy, 2020 – Figure 4A-B). We rescore this character from state ? to 0.

60. Angular-surangular suture contacts external mandibular fenestra at posterior angle at maturity (0) or passes broadly along ventral margin of external mandibular fenestra late in ontogeny (1).

Surangular/angular suture reaches the external mandibular fenestra at posterior angle (Godoy, 2020; Figure 8A-B), as seen in *Alligator mississippiensis*, and unlike *Caiman* spp. We rescore this character from state 1 to 0.

62. Surangular with spur bordering the dentary toothrow lingually for at least one alveolus length (0) or lacking such spur (1).

This character is coding the surangular spur found in some crocodylids (e.g: *Crocodylus acutus*; Brochu, 1997). Such feature is not present in *Eocaiman cavernensis* (Godoy, 2020 – Figure 7A-B). We rescore this character from state ? to 1.

64. Surangular-dentary suture intersects external mandibular fenestra anterior to posterodorsal corner (0) or at posterodorsal corner (1).

The surangular meets the dentary anterior to the posterodorsal corner of the external mandibular fenestra (Godoy, 2020 – Figure 8A-B). We rescore this character from state ? to 0.

94. Maxillary tooth row curved medially or linear (0) or curves laterally broadly (1) posterior to first six maxillary alveoli.

We consider the maxillary tooth row to be linear in *Eocaiman cavernensis* based on the left part of the snout (Godoy, 2020 – Figure 4A-B). We rescore this character from state ? to 0.

96. Canthi rostralii absent or very modest (0) or very prominent (1) at maturity.

These ridges usually appear on the lacrimal and extend onto the maxilla. These features are typically found in some alligatorids, notably in *Melanosuchus niger*. They are absent in *Eocaiman cavernensis* (Godoy, 2020 – Figure 1A and 3A-B). We rescore this character from state ? to 0.

104. Ectopterygoid abuts maxillary tooth row (0) or maxilla broadly separates ectopterygoid from maxillary tooth row (1).

This character is coding the ectopterygoid lateral contact with the maxillary tooth row (Brochu, 1997). In the present species, the ectopterygoid borders the two posteriormost alveoli, and the maxilla does not send any process in between (Godoy, 2020 – Figure 4A-B). We rescore this character from state 1 to 0.

113. Anterior face of palatine process rounded or pointed anteriorly (0) or notched anteriorly (1).

Palatines in *Eocaiman cavernensis* are notched anteriorly (Godoy, 2020 – Figure 4A-B). We rescore this character from state ? to 1.

118. Palatine-pterygoid suture nearly at (0) or far from (1) posterior angle of suborbital fenestra.

This region of the skull is poorly preserved on the fossil and one could not trace the suture accurately. We rescore this character from state 0 to ?.

119. Pterygoid ramus of ectopterygoid straight, posterolateral margin of suborbital fenestra linear (0) or ramus bowed, posterolateral margin of fenestra concave (1).

The posterolateral border of the suborbital fenestra is noticeably concave (Godoy, 2020 – Figure 4A-B). We rescore this character from state ? to 1.

126. Ectopterygoid-pterygoid flexure disappears during ontogeny (0) or remains throughout ontogeny (1).

Given the scarce recognised material referred to *Eocaiman cavernensis*, it is impossible to give any accurate scoring for this character, as no ontogenetic sequence can be reconstructed. We rescore this character from state 0 to ?.

135. Ventral margin of postorbital bar flush with lateral jugal surface (0) or inset from lateral jugal surface (1).

The ventral margin of the postorbital bar insets from the lateral jugal surface (Godoy, 2020 -Figure 3A-B). We rescore this character from state ? to 1.

The following characters were changed to unknown, as these features are missing from the holotype and only known specimen confidently referable to *E. cavernensis* following Godoy et al. (2020):

85. External naris (0) opens flush with dorsal surface of premaxillae or (1) circumscribed by thin crest. Changed from 0 to ?.

144. Quadratojugal bears long anterior process along lower temporal bar (0) or bears modest process, or none at all, along lower temporal bar (1). Changed from 0 to ?.

152. Supratemporal fenestra with fossa; dermal bones of skull roof do not overhang rim at maturity (0) or dermal bones of skull roof overhang rim of supratemporal fenestra near maturity (1) or supratemporal fenestra closes during ontogeny (2). Changed from 0 to ?.

158. Mature skull table with broad curvature; short posterolateral squamosal rami along paroccipital process (0) or with nearly horizontal sides; significant posterolateral squamosal rami along paroccipital process (1). Changed from 1 to ?.

160. Supraoccipital exposure on dorsal skull table small (0), absent (1), large (2), or large such that parietal is excluded from posterior edge of table (3). Changed from 3 to ?.

171. Posterior pterygoid processes tall and prominent (0) or small and project posteroventrally (1) or small and project posteriorly (2). Changed from 0 to ?.

174. Exoccipital with very prominent boss on paroccipital process; process lateral to cranioquadrate opening short (0) or exoccipital with small or no boss on paroccipital process; process lateral to cranioquadrate opening long (1). Changed from 1 to ?.

176. Exoccipitals terminate dorsal to basioccipital tubera (0) or send robust process ventrally and participate in basioccipital tubera (1) or send slender process ventrally to basioccipital tubera (2). Changed from 2 to ?.

Character changes for *Globidentosuchus brachyrostris*

49. Dentary symphysis extends to fourth or fifth alveolus (0) or sixth through eighth alveolus (1) or behind eighth alveolus (2).

The dentary symphysis extension was previously scored as 1, reaching the 7th dentary alveolus (AMU-CURS-222; Scheyer et al., 2013), but the termination is not evident. Material from Scheyer & Delfino (2016) does not bring additional information for this character. We would expect the dentary symphysis to extend to 5th or 6th alveolus. We advise caution here, and rescore this character state as 0&1.

60. Angular-surangular suture contacts external mandibular fenestra at posterior angle at maturity (0) or passes broadly along ventral margin of external mandibular fenestra late in ontogeny (1).

In order to score this character as state 0, we would consider the suture to contact the external mandibular fenestra to a more dorsal point (Scheyer & Delfino, 2016; Figure 9). Here, the suture is deflected ventrally from the posterior most angle. We rescore this character from 0 to 1.

151. Frontoparietal suture concavoconvex (0) or linear (1) between supratemporal fenestrae.

Based on specimen AMU-CURS-222 (Scheyer et al., 2013; Hastings et al., 2016), the frontoparietal suture was scored as concavoconvex. We rescore this character from state 0 to 1, as this suture appears evidently linear.

Character changes for *Tsoabichi greenriverensis*

Following scorings are based on first-hand observations of the new specimens described in this paper.

23. Scapular blade flares dorsally at maturity (0), or sides of scapular blade subparallel with minimal dorsal flare at maturity (1)

We rescore this character state from ? to 0 based on SMNK-PAL 2334.

88. Incisive foramen is small with less than half the greatest width of premaxillae (0), is extremely reduced and thin (1), is large with more than half the greatest width of premaxillae (2), or is large and intersects premaxillary/maxillary suture (3).

We rescore this character from state ? to 0 based on SMNK-PAL 2333a.

116. The palatine process is generally broad (0), or in form of a thin wedge (1).

We rescore this character from state ? to 0 based on SMNK-PAL 2333b.

124. Posterior rim of the choana is not deeply notched (0), or is deeply notched (1).

We rescore this character from state ? to 1 based on SMNK-PAL 2333b.

137. Margin of orbit flush with skull surface (0) or dorsal edges of orbits upturned (1) or orbital margin telescoped (2).

Based on the new specimens described in this paper, we can confidently rescore this character from state ? to 0 based on SMNK-PAL 2333a, 2334.

154. Medial parietal wall of supratemporal fenestra imperforate (0) or bearing foramina (1).

Based on first hand observation of the new specimens described in this paper, we can confidently change this character from state ? to 1 based on SMNK-PAL 2333a, 2334.

Supplementary Material 2

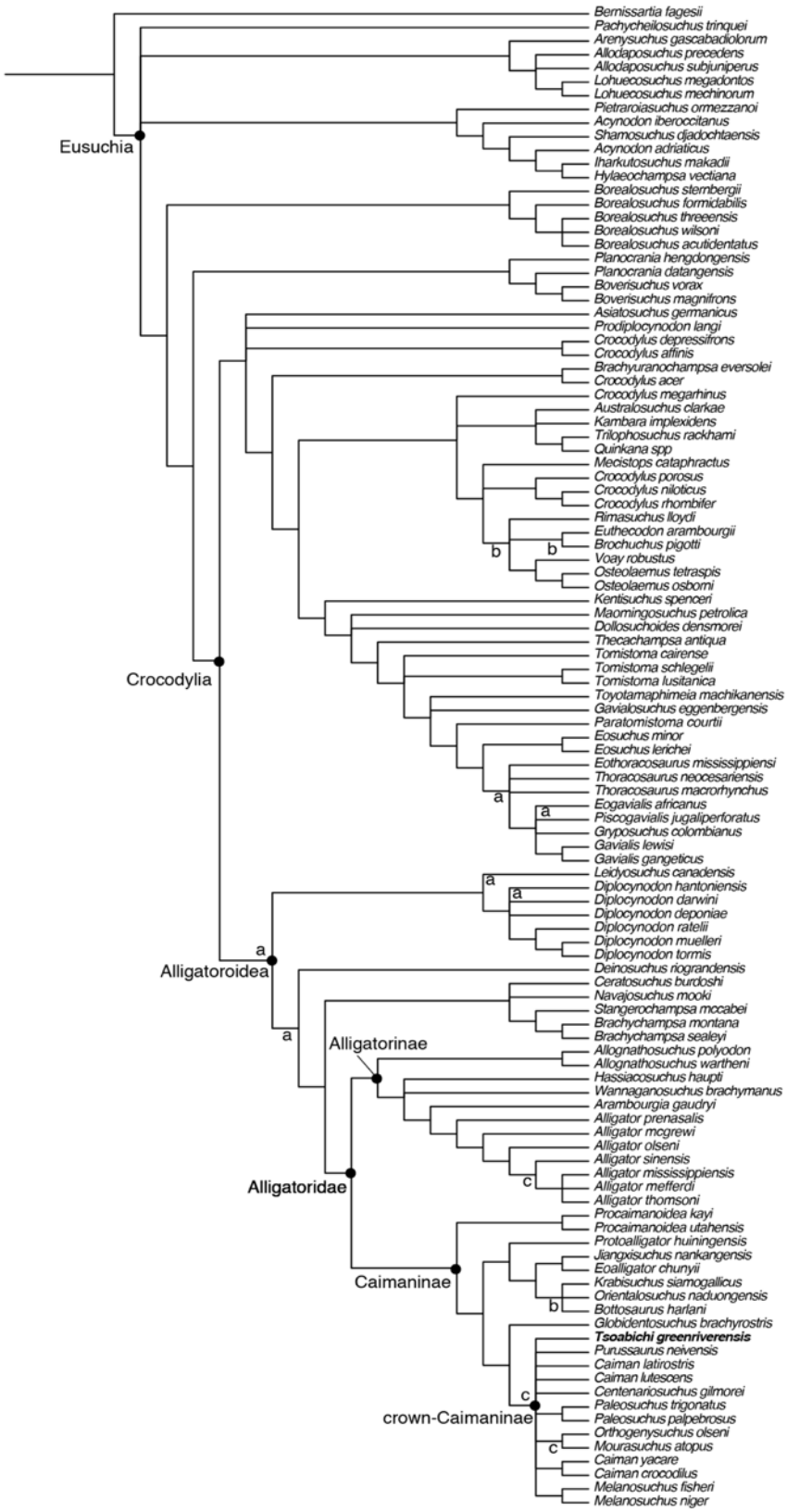

Figure S1. Reduced strict consensus tree obtained from the maximum parsimony analysis of the modified Massonne et al. (2019) dataset (mM). Letters show the alternative

placements of: “a”, *Asiatosuchus nanligensis*; “b”, Maoming crocodylian; “c”, *Eocaiman cavernensis*.

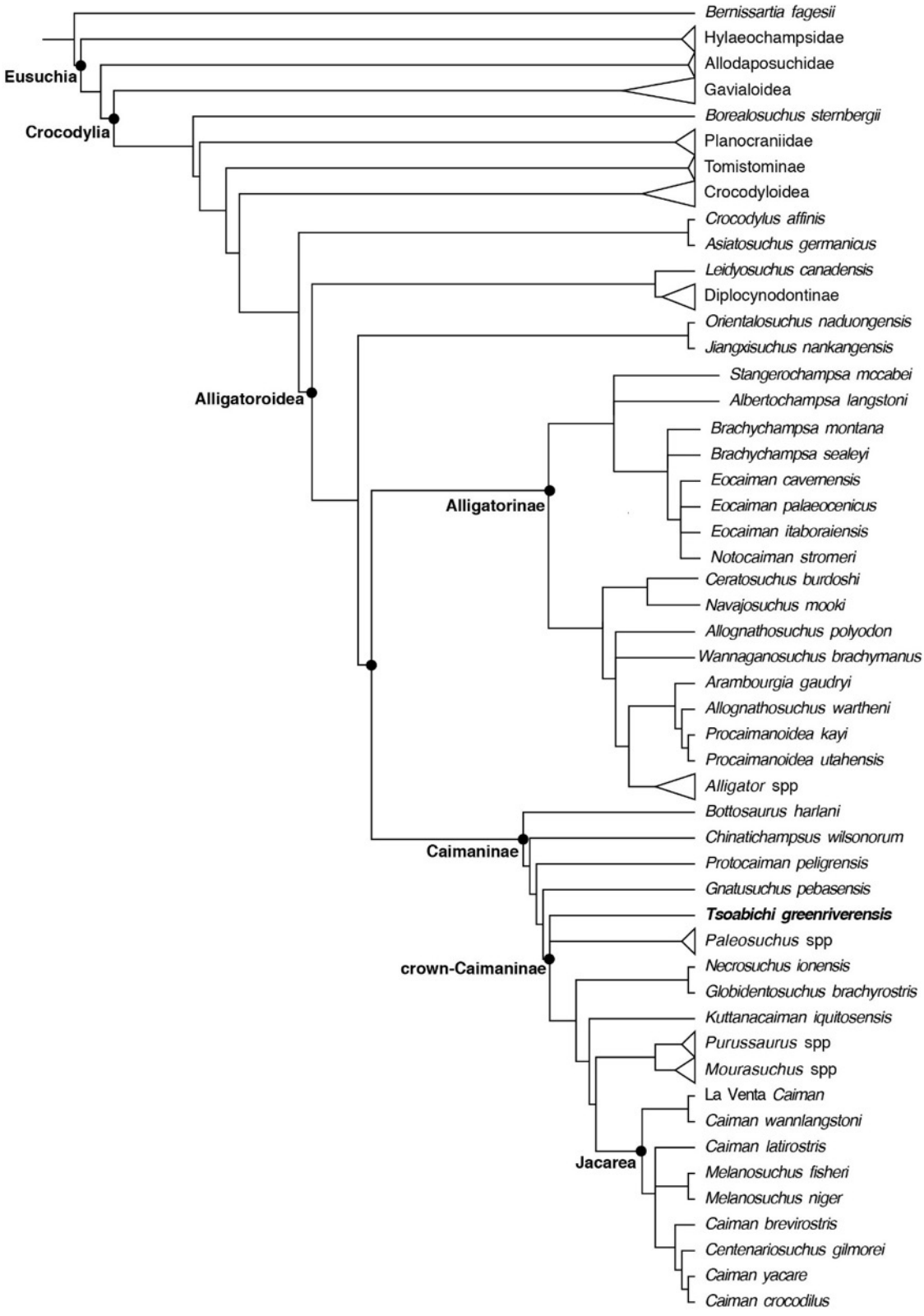

Figure S2. Reduced strict consensus tree of 99,999+ equally optimal trees obtained from the implied weight analysis of mB dataset. Concavity (k) value = 12. TNT 1.5 was not able to recover trees fulfilling molecular backbone constraints under implied weight search. This resulted in recovering Gavialoidea at the base of the tree, and not sister to Tomistominae, as opposed to the topology suggested by molecular data. *Eocaiman* spp. and *No. stromeri* are part of the alligatorine clade formed by the Cretaceous taxa *Brachychampsa* spp., *Stangerochampsa mccabei* and *Albertochampsa langstoni*, a result also recovered in some trees from the mB analysis. Unlike in the equal weight analysis, orientalosuchines are recovered as basal globidontans, making *Bo. harlani* the basal most caimanine under this topology.

REFERENCES

Bona P, Ezcurra MD, Barrios F, Fernandez Blanco MV. 2018. A new Palaeocene crocodylian from southern Argentina sheds light on the early history of caimanines. Proc R Soc B. 285(1885):20180843.

Brochu CA. 2010. A new alligatoroid from the lower Eocene Green River Formation of Wyoming and the origin of caimans. J Vertebr Paleontol. 30(4):1109–1126.

Hastings AK, Reisser M, Scheyer TM. 2016. Character evolution and the origin of Caimaninae (Crocodylia) in the New World Tropics: new evidence from the Miocene of Panama and Venezuela. J Paleontol. 90(2):317–332.

Godoy PL, Cidade GM, Montefeltro FC, Langer MC, Norell MA. 2020. Redescription and phylogenetic affinities of the caimanine *Eocaiman cavernensis* (Crocodylia, Alligatoroidea) from the Eocene of Argentina. Pap Palaeontol. 1–27.

Massonne T, Vasilyan D, Rabi M, Böhme M. 2019. A new alligatoroid from the Eocene of Vietnam highlights an extinct Asian clade independent from extant Alligator sinensis. PeerJ. 7(Ser.2):e7562

Scheyer TM, Aguilera OA, Delfino M, Fortier DC, Carlini AA, Sánchez R, Carrillo-Briceño JD, Quiroz L, Sánchez-Villagra MR. 2013. Crocodylian diversity peak and extinction in the late Cenozoic of the northern Neotropics. Nat Commun. 4:1907.

Scheyer TM, Delfino M. 2016. The late Miocene caimanine fauna (Crocodylia: Alligatoroidea) of the Urumaco Formation, Venezuela. Palaeontol Electronica. 19.3.48A: 1–57.

Stocker MR, Brochu CA, Kirk EC. 2021. A new caimanine alligatorid from the Middle Eocene of Southwest Texas and implications for spatial and temporal shifts in Paleogene crocodyliform diversity. PeerJ. 9:e10665.

Chapter 3

Evolutionary history of the Chinese alligator (*Alligator sinensis*)

Explanation of candidate contribution to collaborative work

This chapter is based on collaborative work. Parts of the text represent a modified version of the manuscript published in *Scientific Reports* (doi: 10.1038/s41598-023-36559-6). The chapter furthermore includes content in preparation, thus unpublished.

Darlim G., Suraprasit K., Chaimanee Y., Tian P., Yamee C., Rugbumrung M., Kaweera A., Rabi M. An extinct deep-snouted *Alligator* species from the Quaternary of Thailand and comments on the evolution of crushing dentition in alligatorids. *Scientific Reports,* 13 (1), 10406. doi: 10.1038/s41598-023-36559-6

Author contributions
Darlim, G. designed the project, collected data, wrote the main manuscript text, conducted the comparative analysis and phylogenetic analysis, prepared all the figures, and produced 3D reconstruction; Rabi, M. designed the project, collected data, extensively reviewed the manuscript, wrote parts of manuscript text, supervised the project, acquired funding, and conceptualised the manuscript; Suraprasit, K. facilitated project design and organisation, study of specimens, collected data, identified mammal specimens, organised the CT-scan, and wrote parts of the manuscript; Chaimanee, Y., Tian, P., Yamee, C., Rugbumrung, M., Kaweera, A. acquired and gathered the geological data. All authors reviewed and have approved the final version of the manuscript.

Evolutionary history of the Chinese alligator (*Alligator sinensis*)

ABSTRACT

Fossil *Alligator* remains from Asia are critical for tracing the enigmatic evolutionary origin of the Chinese alligator, *Alligator sinensis*, the only living representative of Alligatoridae outside the New World. The Asian fossil record is extremely scarce and it remains unknown whether *A. sinensis* is an anagenetic lineage or alternatively, extinct divergent species were once present. We provide a detailed comparative description of a morphologically highly distinct *Alligator* skull from the Quaternary of Thailand, and several autapomorphic characters warrant the designation of a new species. The presence of enlarged posterior alveoli in *Alligator munensis* is most consistent with a reversal to the alligatorine ancestral condition of having crushing dentition, a morphology strikingly absent among living alligatorids. Results of a phylogenetic analysis that for the first time employed *Alligator* fossil material from Asia, including the enigmatic *A. luicus* from the Miocene of China, retrieved a close relationship of those species with *A. sinensis* in addition to the North American Miocene *A. olseni* and *A. mcgrewi*. Particularly, *A. munensis* is recovered closely related to *A. luicus* and *A. mcgrewi*, which in combination with the presence of many autapomorphies of the new species, a cladogenetic split possibly driven by the uplift of the southeastern Tibetan plateau is suggested to explain the split between *A. munensis* and *A. sinensis*. The presence of intercontinental Miocene taxa in the clade in the phylogenetic analysis supports the hypothesis of a cladogenetic event in North America that precedes a dispersal event through Beringia during Middle Miocene Climatic Optimum, although future time-scaled analyses are necessary to better elucidate our understanding on *Alligator* paleobiogeography.

INTRODUCTION

The Chinese alligator, *Alligator sinensis* Fauvel, 1879 is the only extant representative of Alligatoridae (the crown-group of caimans and alligators) outside the Americas. Early divergence age estimates between the American and Chinese alligator species by molecular clocks studies suggests ca. 58 – 31 Ma (Oaks, 2011; Pan et al., 2020), although inconsistent with the earliest crown-*Alligator* species *A. thomsoni* (ca. 14 Ma Mook & Thomson, 1923; Brochu, 1997; Massonne et al., 2019). The dispersal of *Alligator* from North America to Asia might have occurred via Beringia, although under favorable climatic conditions given the crocodylian minimum limit of Mean Annual Temperature (MAT) of approximately 14.2°C (Markwick, 1998). Despite the fact that populations of the Chinese alligator have a wider latitudinal range compared to other crocodylians (Thorbjarnarson & Wang, 2010), prolonged exposure to cold temperatures may still cause death (Brisbin et al., 1982; Thorbjarnarson & Wang, 2010; Grigg & Kirschner, 2015). However, phylogenetic relationships of fossil *Alligator* from Asia are essential to better understand the biogeography of the group.

Owing to a preservational and research bias of the *Alligator* fossil record towards North America (see Hastings et al., 2023 for a review), description of fossil material from Asia is essential and much needed comparative morphological data. Previously published *Alligator* fossil material from Asia include an articulated skeleton of *A. luicus* Li & Wang, 1987 from the Miocene of China; an altirostral short-snouted skull referred to *A*. cf. *sinensis* from the late Miocene/Pleistocene of Thailand (Claude et al., 2011); fragmentary remains of *A. sinensis* from the Pliocene of Japan (Iijima et al., 2016), and a near-complete skull from the Pleistocene of Taiwan referred to *A. sinensis* (Shan et al., 2013).

The subject of this contribution is the DMR-BSL2011-2 *A*. cf. *sinensis* skull from northeastern Thailand preliminarily reported by Claude et al. (2011). Claude et al. (2011) noted similarities with *A. sinensis* as well as its distinctly robust and short snout, but the need for further preparation of the fossil precluded a detailed description at the time. Nevertheless, the occurrence in Thailand considerably expanded the previously known distribution of *Alligator* in Asia, suggesting complex paleobiogeographic of history (Claude et al., 2011). Following preparation of DMR-BSL2011-2, we present a comparative description utilising CT-scan imaging data and demonstrate that its specimen is highly distinct morphology warrants naming a new species and at the same time several shared several derived characteristics suggest close relationship to *Alligator sinensis*. In addition, we discuss the evolutionary implications of the inferred enlarged posterior dentition of the new species.

This new species highlights previously unsampled comparative morphological data that was furthermore included in a phylogenetic analysis, representing a novelty in *Alligator* systematic. The specimen DMR-BSL2011-2 is included in a phylogenetic framwework, in addition to the complete skull of the *Alligator* from the Pleistocene of Taiwan, and the enigmatic *A. luicus* from the Miocene of China. Morphological support in *Alligator*, and implications on the evolution of *Alligator* and the dispersal from North America to Asia is explored based on the new results of the phylogenetic analysis.

Geological settings

The fossil site (UTM coordinates: 102°15'02.4"E, 15°08'33.1"N) is located at Ban Si Liam, Non Sung district, Nakhon Ratchasima Province in northeastern Thailand (Fig. 1a,b). In 2005, the square-shaped pond with an area of 8 m long x 8.4 m wide x 2 m deep was dug out by the villagers and yielded some vertebrate fossils (see

Supplementary Information). Regarding the stratigraphic profile of Ban Si Liam (Fig. 1c), the dark-colored topsoil is 30 cm in thickness and organic-rich in content, underlain by yellowish medium- to fine-grained sands with the thickness of 2 m (Supplementary Fig. 1). Some fragments of ancient pottery and ceramics were collected from the topsoil but vertebrate fossils (nine specimens) were entirely found from the yellowish sandy layer that overlies a thin layer of indurated iron oxide (10 cm thick), followed by the yellowish clay at the lowermost part of the pond. Three reptile fossils included a fragment of a turtle carapace (DMR-BSL2011-1) and a nearly complete cranium of an alligator (DMR-BSL2011-2), both of which have been previously described by Claude et al. (2011), as well as a crocodylian vertebra (DMR-BSL2011-3; Supplementary Fig. 2).

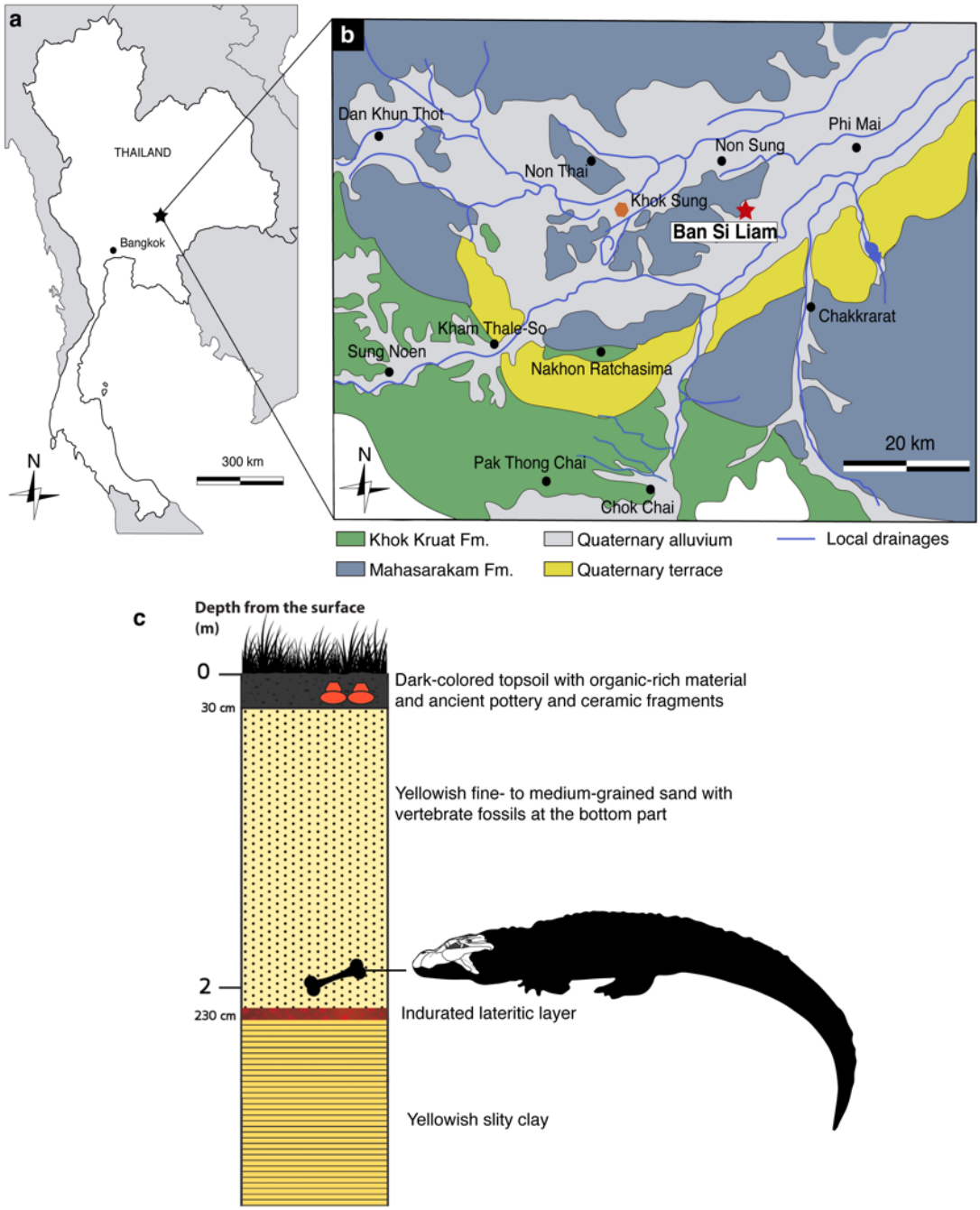

Figure 1. Locality of the *Alligator munensis* sp. nov. holotype (DMR-BSL-2011-2). (a) schematic drawing of the map of Thailand. (b) geological map of Nakhon Ratchasima province modified after Suraprasit et al. (2015). Red star indicates the type locality of *Alligator munensis* sp. nov. Orange polygon indicates Quaternary fossil site of Khok Sung; (c) stratigraphic profile of the fossil site of Ban Si Liam in Non Sung district (Nakhon Ratchasima) showing the level where *Alligator munensis* sp. nov. was found as indicated by the bone and alligator silhouette.

In addition to the alligator's skull described here in this study, fossils of two mammalian species collected from the same layer were identified as belonging to a wild water buffalo (*Bubalus arnee*) and a sambar deer (*Rusa unicolor*) (Supplementary Fig. 3) based on the comparisons of morphological features and dimensions with extant comparative specimens and fossils recovered nearby (i.e. the late Middle Pleistocene fauna from Khok Sung, Suraprasit et al., 2016). We find no evidence for the presence of giraffids (otherwise known from the Late Miocene of Thailand) in contrast to the report of Claude et al. (2011). The presence of *Bubalus arnee* and *Rusa unicolor*, on the other hand suggests a younger and narrower age range than the previously proposed Late Miocene to Pleistocene (Claude et al., 2011) as these taxa are typical for late Middle Pleistocene faunas of Thailand like that of Tham Wiman Nakin (dated to >169 ka Esposito et al., 1998; Esposito et al., 2003; Suraprasit et al., 2021) or Khok Sung (dated to either 217 or 130 ka (Suraprasit et al., 2016; Duval et al., 2019). Moreover, the stratigraphic position of a fossiliferous layer at Ban Si Liam is quite shallow (around 2 m below the surface, Fig. 1c), compared to other Late Miocene sedimentary deposits along the Mun River systems (i.e. around 10 to 20 m deep in Tha Chang sandpits, Chaimanee et al., 2006) (see Supplementary Information for detailed geological settings). A Holocene age of the locality cannot be excluded at the moment.

Institutional abbreviations. AMNH–American Museum of Natural History, New York, New York, USA; DMR–Department of Mineral Resources, Bangkok, Thailand; FMNH–Field Museum of Natural History, Chicago, Illinois, USA; IRScNB–Institut Royal des Sciences Naturelles de Belgique, Brussels, Belgium; MCZ–Museum of Comparative Zoology, Harvard University, Cambridge, Massachusetts, USA; SNSB–Staatliche Naturwissenschaftliche Sammlungen Bayerns, Munich, Germany; SZ–

Museum der Universität Tübingen, Zoologisches Schausammlung, Tübingen, Germany; YPM–PU–Princeton University collection housed at Peabody Museum, New Haven, Connecticut, USA.

Material and methods

Comparative material. The comparative analysis of the present study was conducted using the following specimens: *Alligator mcgrewi* AMNH 7905, FMNH P26242; *Alligator mefferdi* AMNH 7016; *Alligator mississippiensis* SNSB 4/1921*, 2530/0*; SZ 1057*; *Alligator olseni* MCZ 1887, 1899; *Alligator prenasalis* YPM–PU 13799, MCZ 1014, 1015; *Alligator sinensis* AMNH 23899, 23901, 139673, 140775, IRScNB 13904; R23898; SNSB 178/1947*; and *Caiman crocodilus* SZ 10276*; in addition to published data (Brochu, 1999). Specimen numbers indicated with an asterisk were first hand studied, whereas the remaining specimens were studied through photographs.

Digitalisation and imaging. Photographs were personally taken by G.D and M.R**.** CT scan image stacks were acquired using CT scanner Philips IQon Spectral CT (Advanced Diagnostic Imaging Center (AIMC), Mahidol University in Thailand), with voltage of 120 Kv and current of 562 µA. A total of 1272 slices with thickness of 0.80 mm were generated and voxel size of 0.234375 x 0.234375 x 0.4 mm. Digital reconstructions and CT scan image stacks were analysed using a Working Station equipped with Amira software 3D 2021.1 (https://www.thermofisher.com/order/catalog/product/AMIRA) in the 2D/3D imaging/digitisation lab of the Centre of Visualisation, Digitalisation and Replication at the Eberhard Karls Universität Tübingen, Germany. Additional photographs of 3D models were made using the software MeshLab 2021.07 (https://www.meshlab.net/).

Images were further processed in Adobe Photoshop CC (https://www.adobe.com/products/photoshop.html) and all drawings and figures were produced using Adobe Illustrator CC (https://www.adobe.com/products/illustrator.html).

Phylogenetic analysis. Parsimony analysis was conducted using the re-discretised morphological dataset of Rio & Mannion (2021). Three taxa were added (i.e. *Alligator* cf. *sinensis*, *A.luicus*, and *A. munensis*) as well as the proposal of three new morphological characters, resulting in a total of 148 taxa and 333 characters. Multistate characters were treated as ordered (17, 37, 47, 48, 58, 65, 72, 75, 78, 81, 87, 88, 102, 109, 110, 137, 142, 151, 162, 175, 181, 188, 210, 214, 220, 221, 222, 224, 235, 243, 284, 293, 297, 308, 323, and 324). The analysis was performed using the New Technology Search in TNT 1.6 (Goloboff et al., 2016; Goloboff & Morales, 2023), with all algorithms enabled and the consensus tree stabilized five times with a factor of 75. Following the parameters of analysis 2.3 and general recommendations of Rio & Mannion (2021), the analysis was performed employing extended implied weighting with a *k*-value of 12 (EIW12) considering that measures of phylogenetic accuracy, internal consistency, higher values for stratigraphic congruence were achieved when setting higher *k*-values using extended implied weighing (Rio & Mannion, 2021).

Trees recovered from the analysis were furthermore used as starting trees for a second round under tradition search using tree bisection and reconnection (TBR). A molecular constraint was not applied as the used dataset is able to retrieve the molecular topology (Oaks, 2011; Pan et al., 2020; Rio & Mannion, 2021).

Nomenclatural acts. This work and the nomenclatural acts it contains have been registered in the proposed online registration system (ZooBank) for the International

Code of Zoological Nomenclature. The ZooBank Life Science Identifier can be resolved and the associated information viewed through any standard web browser by appending the LSID to the prefix http://zoobank.org/. The LSID for this publication is: [urn:lsid:zoobank.org:pub:844D9DB3-98B2-40B6-9AE9-666B6B9C8DE5].

RESULTS

Systematic Palaeontology.

Eusuchia Huxley, 1875 *sensu* Brochu, 2003

Crocodylia Gmelin, 1789 *sensu* Benton & Clark, 1988

Alligatoroidea Gray, 1844 *sensu* Brochu, 2003

Globidonta Brochu, 1999

Alligatoridae Cuvier, 1807 *sensu* Brochu, 2003

Alligatorinae Kälin, 1940

Alligator Cuvier, 1807 *sensu* Brochu, 1999

Alligator munensis sp. nov. (Figs. 2–10)

Alligator cf. *sinensis* Fauvel, 1879: Claude et al. (2011), page 126, plate 3

Etymology. The specific name *munensis* refers to the Mun River, close to the locality where the specimen was found in northeastern Thailand.

Holotype. DMR-BSL-2011-2 comprises a nearly complete skull, missing only a few elements of the right side, such as the jugal and quadratojugal, and the dentition.

Horizon and locality. Ban Si Liam locality, Non Sung district, Nakhon Ratchasima Province, Thailand, sandy layer 2 meters below the surface (Fig. 1c).

Diagnosis. *Alligator munensis* is diagnosed as an *Alligator* based on the external nares bisected by the nasals and the presence of a notch lateral to the external nares; *Alligator munensis* can be distinguished from all other extinct and extant *Alligator* species (i.e. *A. mcgrewi*, *A. mefferdi*, *A. mississippiensis*, *A. olseni*, *A. prenasalis*, and *A. sinensis*) by the following combination of characters (autapomorphies marked with asterisk): anteroposteriorly compressed skull; significant posterior retraction of the external nares on the dorsal surface of the snout*; mediolaterally thick internarial bar resulting in small and circular external nares*; reduced maxillary dentition containing only 12 alveoli; dorsal surface of the nasals markedly concave on its anterior portion immediately posterior to the external nares*; presence of a smooth sagittal midline crest on the nasals*; presence of a sagittal midline crest on the posterior portion of frontal; frontal slightly convex and lacking upturned margins*; presence of a smooth midline crest on the parietal; presence of acute dorsal indentation on the parietal in occipital view; small and elliptical shaped incisive foramen; lateral process of the palatine not reaching the anterior margin of the suborbital fenestra; lateral palatine shelf forming a pointed tip; pterygoid excluded from the posterior margin of the suborbital fenestra by broad ectopterygoid-palatine suture*; absence of pterygoid “neck” around the posterior margin of the choana; bisected choana; posterior rims of the choana mediolaterally constricted; prominent quadrate condyles*.

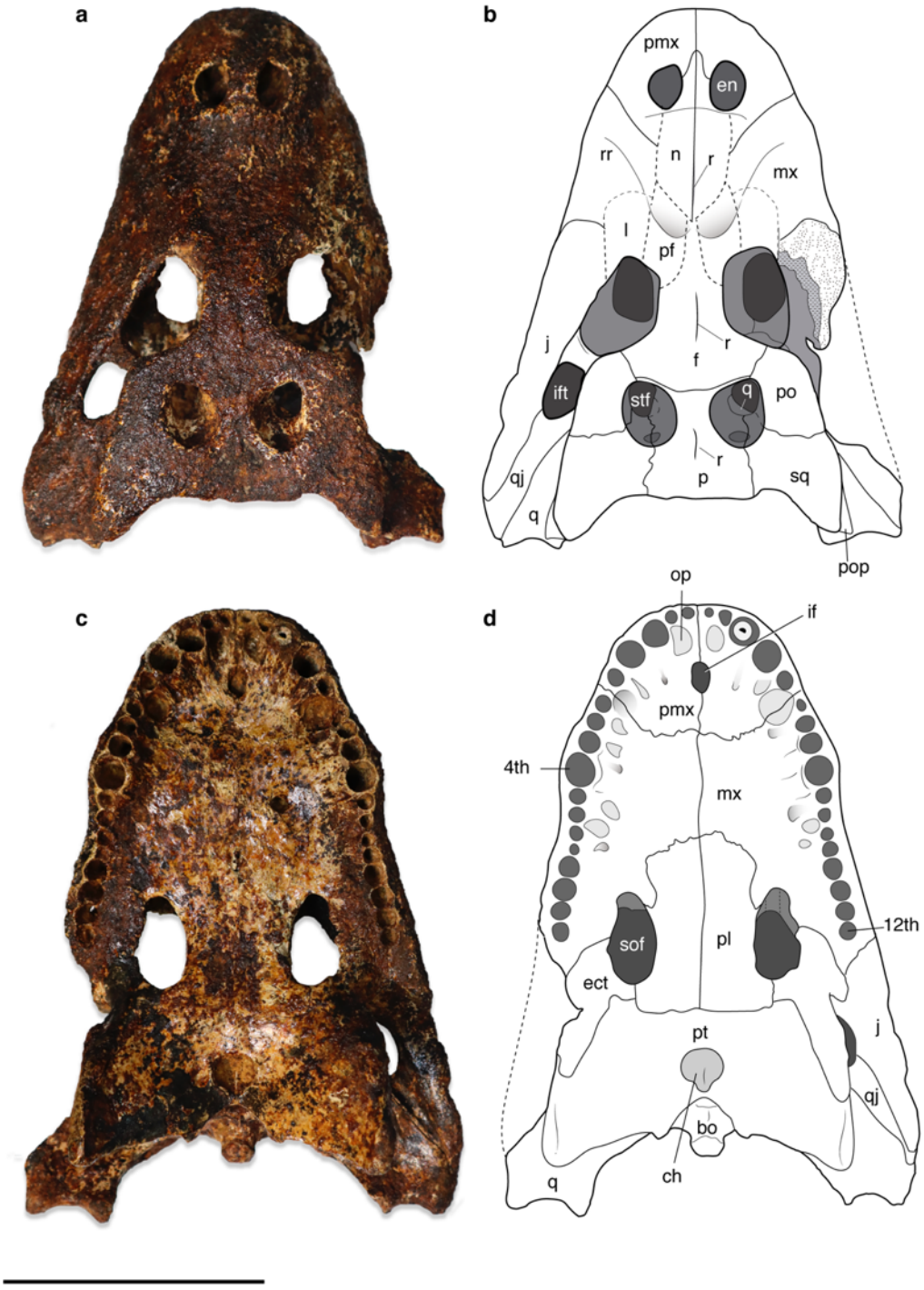

Figure 2. Skull of *Alligator munensis* sp. nov., holotype (DMR-BSL-2011-2). Photo and schematic drawing in (a,b) dorsal, and (c,d) ventral views, respectively. Abbreviations: bo, basioccipital; ch, choana; ect, ectopterygoid; en, external nares; f, frontal; if, incisive foramen; itf, infratemporal fenestra; j, jugal; l, lacrimal; mx, maxilla; n, nasal; p, parietal; pf, prefrontal; pl, palatine; pt, pterygoid; pmx, premaxilla; op, occlusal pit; po, postorbital; pop, paroccipital process; q, quadrate; qj, quadratojugal; r, ridge; rr, rostral ridge; sof, suborbital fenestra; sq,

squamosal; stf, supratemporal fenestra; 4th, fourth maxillary alveolus; 12th, twelfth maxillary alveolus. Scale bar: 10cm.

Comparative description. The following description will compare the cranial morphology of *Alligator munensis* to that of other extinct and extant species of *Alligator* (*A. mcgrewi* Schmidt, 1941; *A. luicus*; *A. mefferdi* Mook, 1946; *A. mississippiensis*; *A. olseni* White, 1942; *A. prenasalis* Loomis, 1904; and *A. sinensis*). The holotype skull (DMR-BSL-2011-2) of *Alligator munensis* presents exceptional three-dimensionality, almost complete except for missing the dentition, the right jugal, the quadratojugal, and fragments of the braincase. The skull is triangular shaped in dorsal view, markedly compressed anteroposteriorly and particularly deep at the level of the external nares (altirostral skull *sensu* Salisbury & Willis, 1996). The dorsal surface of the skull is ornamented, characterised by small rounded pits of varying size scattered along the cranial bones, gradually becoming less pronounced in the anterior portion of the snout. Dorsally, some of the sutures are difficult to trace owing to a thin iron-oxide layer covering large parts of the skull. However, we were able to reconstruct some of these using CT-scan imaging.

External naris. The external naris morphology of the *Alligator munensis* is unique compared to other *Alligator* species (as well as to most crocodyliforms) in its anterior margin being retracted to the level of the occlusal pit on the premaxilla-maxilla suture (Figs. 2a,b, 3a,e, 4). In other species of *Alligator*, the anterior margin of the external naris is in line with the level of the third premaxillary tooth. The external naris of *A. munensis* is subcircular instead of the commonly teardrop-shaped outline seen in *Alligator* spp. and the apertures are separated from one another by an unusually wide internarial bar formed mainly by the nasals with significant contributions from the premaxillae. In other species of *Alligator*, the internarial bar is thin and has a short

contribution from the premaxillae. The internarial bar of *A. munensis* forms a dorsoventrally high wall that is partially separating the narial cavity (Fig. 4c). Moreover, the posterior border of the external naris of *A. munensis* composed by the premaxillae and the nasals is raised, as in *A. sinensis*, and *A. mcgrewi*.

Orbit. The orbits are more rounded compared to most other *Alligator* species except *A. prenasalis.* Upturned orbital margins of the frontal are absent. (Fig. 2a,b)

Supratemporal fenestra. The supratemporal fenestra is oval shaped resembling those of other *Alligator* species, except for *A. sinensis* which presents a more constricted fenestra. However, the supratemporal fossa (i.e. the region composed of unornamented bone surfaces immediately ventral to the supratemporal fenestrae, *sensu* Holliday et al., 2020) of *A. munensis* and *A. sinensis* are similar in being broadly exposed except for the anterior portion bearing the parietal and postorbital (Figs. 2a,b, 3d). The interfenestral bar is flat and broad as in *A. mississippiensis*, *A. prenasalis*, *A. mcgrewi*, and *A. olseni*, as opposed to the constricted and laterally upturned condition of *A. sinensis* and *A. mefferdi*.

Suborbital fenestra. The suborbital fenestra is elliptical and relatively short, reaching anteriorly to the level of the tenth maxillary alveolus (Figs. 2c,d, 3c). The suborbital fenestra is composed of the maxilla, palatine and ectopterygoid, with the maxilla forming the anterolateral to anteromedial border, without a contribution from the palatine. This condition is present in *A. mefferdi*, whereas in the remaining *Alligator* species the anterior border of the suborbital fenestra receives a lateral process of the palatine. The ectopterygoid completes the remaining lateral margin and participates at least for half of the posterior border of the fenestra. Additionally, the lateral margin of the suborbital fenestra exhibits a medial projection consisting of the maxilla and the ectopterygoid, a condition only present in *A. mcgrewi* and *A. sinensis* among *Alligator*

species. The medial portion of the posterior border is formed by the palatine, excluding the pterygoid from the posterior border of the suborbital fenestra (Fig. 2c,d, 3c). In some specimens of *A. mississippiensis*, the anterior margin of the pterygoid has reduced participation in the fenestrae, in contrast to *A. sinensis*, where the pterygoid is involved.

Choana. The choana of *A. munensis* differs from the living *Alligator* species in two main aspects: it lacks the raised posterior margin and is semicircular in outline with a constricted posterior margin (Fig. 2c,d, 3f) instead of being elliptic. In *A. mcgrewi*, the constriction is present but less developed. The choanal septum is partially preserved in *A. munensis* and may be incomplete; whether the septum reaches ventrally the surface of the pterygoid cannot be assessed (Fig. 3f).

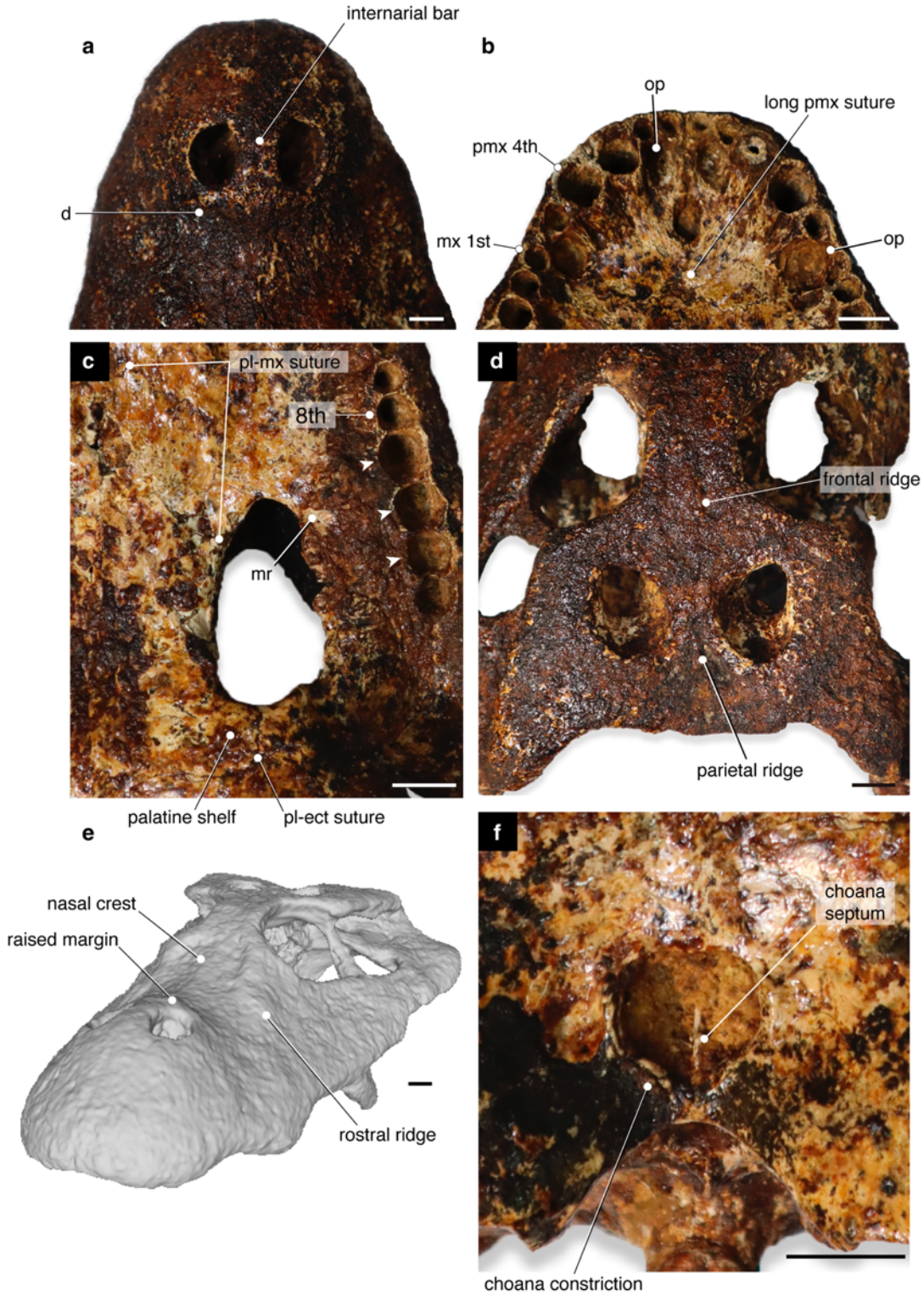

Figure 3. Details of the skull of *Alligator munensis* sp. nov. holotype (DMR-BSL-2011-2). (a) Anterior portion of the snout in dorsal view; (b) premaxillae in ventral view; (c) detail of the bone elements composing of the suborbital fenestra; (d) skull table in dorsal view; (e) digitally reconstructed skull of *Alligator munensis* sp. nov. in oblique view; (f) choana of *Alligator munensis* sp. nov. White arrows indicate enlarged maxillary alveoli. Abbreviations: d, depression;

ect, ectopterygoid; mr, maxillary rugosity; mx 1st, first alveolus of the maxilla; op, occlusal pit; pl, palatine; pmx, premaxilla; pmx 4th, fourth alveolus of the premaxilla; 8th, eighth maxillary alveolus. Scale bar: 1cm.

Premaxilla. The premaxilla is deep and prominent and is lacking a notch on the dorsal surface laterally to the external nares (Fig. 3a). In other *Alligator* species, the dorsal surface of the premaxilla bordering the lateral margin of the external naris presents a prominent notch (a groove), a character considered as an unambiguous synapomorphy for the genus (Brochu, 1999). The posterior premaxillary process extends approximately to the level of the third maxillary alveolus.

The external nares form only a third of the length of the premaxillae as opposed to other species of *Alligator* where they extend almost along the entire length of the elements (Fig. 2a,b, 3a). Ventrally, the premaxilla presents five alveoli, with the third and fourth being the largest, whereas the remaining ones are markedly smaller. The fourth alveolus is the largest of the premaxillary teeth but only slightly larger than the third. Four occlusal pits are present medially to the premaxilla alveolar margin. The pit for the insertion of the first and fourth dentary teeth are the deepest and the diameter of the fourth is comparable to the alveoli of the fourth maxillary tooth (Fig. 2c,d, 3b). The incisive foramen is small and oval and shifted posteriorly from the anterior alveolar margin. Its anterior margin reaches the posterior border of the occlusal pit for the reception of the first dentary tooth and the posterior margin reaches the level of the fifth premaxillary alveolus (Fig. 3b). Furthermore, the suture between the premaxillae posterior to the incisive foramen is longer than the foramen (Fig. 3b). Among *Alligator* species, a small incisive foramen and long premaxillary suture posterior to it is otherwise present in *A. sinensis* whereas in *A. mefferdi*, *A. mcgrewi*, *A. mississippiensis*,

and *A. prenasalis* the incisive foramen is reaching the level of the occlusal pit for the reception of the fourth dentary tooth. *A. olseni* has an intermediate condition.

Maxilla. The maxilla is dorsoventrally tall and presents a rostral ridge (*sensu* Rio & Mannion, 2021) laterally extending from the anterior portion of the lacrimals to the level of the fourth maxillary tooth (Figs. 3e), an autapomorphic condition for *A.munensis* among *Alligator* species. Alongside the medial margin of the maxillary tooth row, shallow occlusal pits are present up to between the eighth and ninth maxillary alveoli (Fig. 2c,d). A maxillary process is present posterior to the last maxillary alveolus contacting the ectopterygoid and the jugal, as in *A. mississippiensis*, *A*. *mcgrewi*, *A. olseni* and *A. prenasalis*. Posteriorly, the palatine-maxilla suture extends from the seventh to the 10th maxillary alveoli as in *A. sinensis* and in *A. mcgrewi*, differing from the suture of *A. mefferdi*, *A. mississippiensis*, *A. olseni*, and *A. prenasalis* where it extends from the ninth to the 12th maxillary alveoli. The posterior margin of the maxilla forms the entire anterior and anterolateral border of the suborbital fenestra and projects medially inside the fenestra by a rugose process that also contacts the ectopterygoid. The rugose process of the maxilla is also present in *A. sinensis* and *A. mcgrewi*. The toothrow is reduced compared to other *Alligator* species; there are only 12 alveoli in the maxilla. The largest maxillary alveolus is the fourth, followed by the ninth to 11th, which are markedly enlarged in comparison to the remaining ones.

Nasal. The nasals are short and broad elements with strongly upturned anterior portions and making the area immediately posterior to the naris considerably depressed (positioned ventrally to the level of the internarial bar). The proportions are comparable to that of *A. sinensis*, *A. mcgrewi*, and basal short-snouted alligatorines (see Fig. 13 in Brochu, 1999). The nasals are partially bisecting the premaxillae in the broad internarial (Fig. 4b,c). The nasal portions of the internarial bar form a deep vertical septum that

bisects the nasal cavity almost up to half of its dorsoventral extension (Fig. 4c). Immediately posterior to the naris, the nasals and premaxilla form a raised border (Fig. 2a,b). This condition is also present in *A. sinensis* and *A. mcgrewi*. Among *Alligator* spp., a unique condition of *A. munensis* is a shallow sagittal crest present along the midline contact of the nasals (Fig. 3e).

Jugal. The jugal is only preserved on the left side but the concavo-convex suture with the maxilla is visible on the right side (Fig. 5 a,b). In lateral view, the jugal forms a linear ventral margin of the orbit and the transition of the infraorbital to the infratemporal portions of the jugal is marked by a pronounced step, another autapomorphy of this taxon. The infratemporal bar is relatively thick presenting a straight ventral outline (Fig. 5 c,d). A straight ventral margin of the infratemporal bar is also observed in *A. prenasalis*. The infratemporal bar comprises most of the ventral border of the infratemporal fenestra, except for the posteroventral corner formed by the quadratojugal (Fig. 5c,d).

Lacrimal. Both lacrimals are preserved, however the dorsal outline and suture with the prefrontal and maxilla are difficult to precisely trace. As a consequence of a deep skull, the lacrimals are more laterally positioned in comparison to other *Alligator* species. CT scan images reveal a lacrimal-maxilla contact positioned anteriorly to the jugal (Fig. 4d,e), but resolution is not sufficient to track the exact articulation among lacrimal, prefrontal, and maxilla and therefore the reconstructed lacrimal in Figure 2b is speculative and merely follows the condition in most alligatorines (Brochu, 1999).

Prefrontal. The prefrontals are preserved on both sides, but similarly to the lacrimal, the sutures are difficult to be traced. The prefrontals bear a pair of smooth rostral ridges (*sensu* Rio & Mannion, 2021) that together form a low spectacle close to the level of the anterior orbital margin. A low spectacle (*sensu* Rio & Mannion, 2021) is

also present in all *Alligator* species except *A. mcgrewi*. The spectacle in *A. munensis* is positioned slightly more anteriorly compared to other *Alligator* species where it is positioned posterior to the anterior orbital margin. Owing to the subcircular orbits, the margins of the prefrontal and frontal are more arched than in other *Alligator* species (Fig. 5). On the right lateral side, a partially preserved prefrontal pillar is present, being posteriorly slightly convex at its dorsalmost portion.

Frontal. The frontal presents a uniquely broad and arched interorbital bar lacking upturned lateral margins. Upturned orbital margins are also absent in *A. prenasalis*. The dorsal surface of the frontal of *A. munensis* bears a thin midline crest posteriorly (Figs. 2a,b, 3d, 5), which is an autapomorphy of this species. The frontoparietal suture extends anterior to the supratemporal fenestra (Fig. 4a). The exact limits of the anterior process of the frontal cannot be fully assessed.

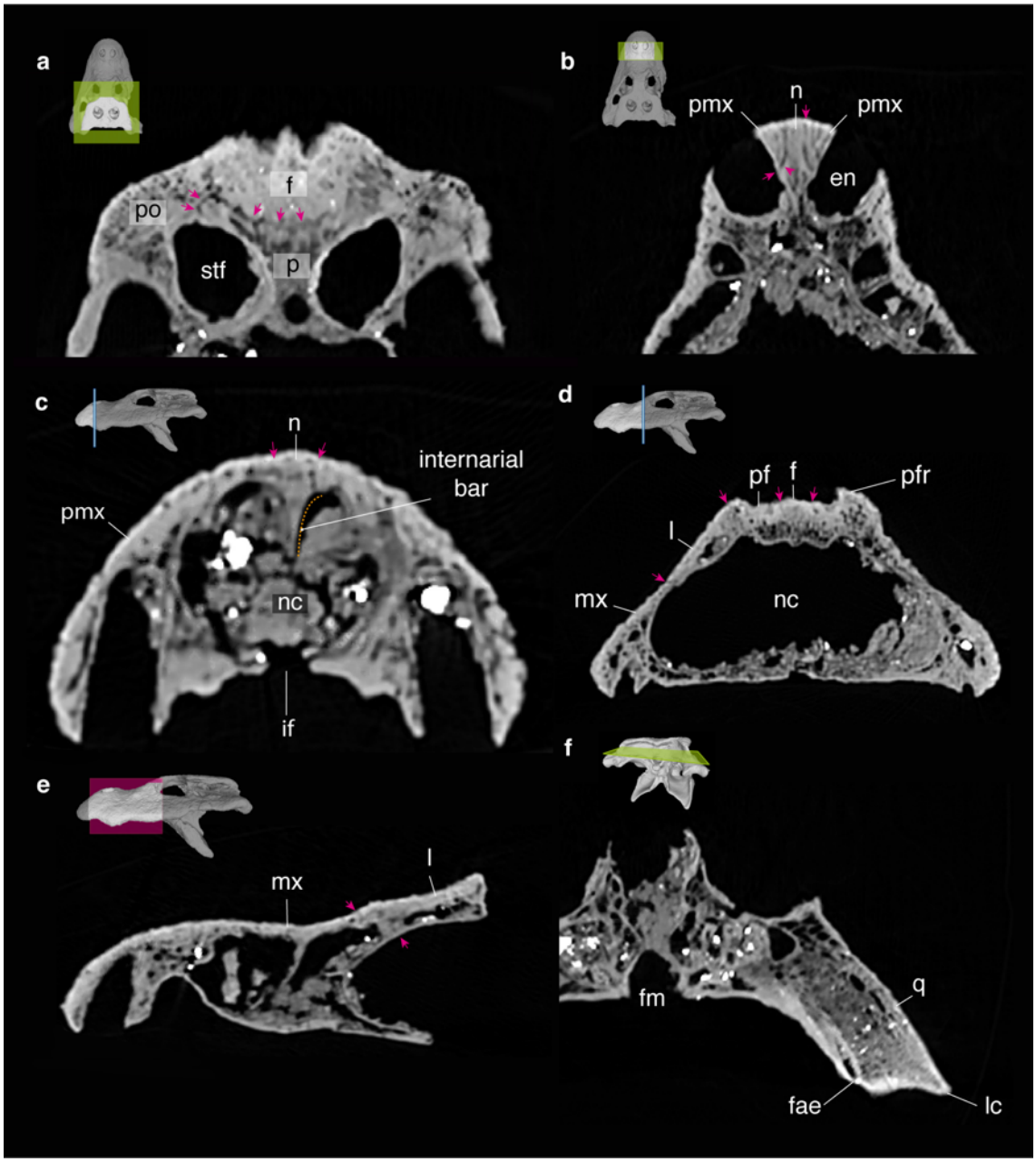

Figure 4. Selection of CT scan image stacks of *Alligator munensis* sp. nov. holotype (DMR-BSL-2011-2). Each figure component (a–f) is followed by the digitally reconstructed skull of *A. munensis* highlighting the area of interest. (a) axial cut of the skull table showing the fronto-parietal suture; (b) axial and (c) coronal cuts of the snout region showing the composition and morphology of the internarial bar; (d) coronal cut of the posterior portion of the nasal cavity; (e) sagittal cut of the antorbital region of the skull; (f) axial cut of the posterior position of the skull. Pink arrows indicate sutures between the bone elements. Dashed orange line indicates the contour of the internarial bar. Abbreviations: en, external nares. f, frontal; fae, foramen äerum; fm, foramen magnum; if, incisive foramen; l, lacrimal; lc, lateral quadrate hemicondyle; mx, maxila; n, nasal; nc, nasal cavity; p, parietal; pf, prefrontal; pfr, prefrontal ridge; pmx, premaxilla; po, postorbital; q, quadrate; stf, supratemporal fenestra.

Postorbital. The postorbital is wide and because of the iron oxide encrusting, it is unknown if a sulcus between the medial and lateral margins were present dorsally. (Fig. 2 a,b, 3d). In *A. sinensis*, the lateral margin develops a shallow crest whereas the medial margin is less pronounced but also upturned; together these delimit a sulcus. In *A. munensis*, a pronounced crest is absent but we cannot rule out the presence of a sulcus. The dermal part of the postorbital overhangs the supratemporal fenestra thereby obscuring the anterior margin of the supratemporal fossa. This is a condition shared with *A. sinensis*. The postorbital contacts the parietal medially along the anterior margin of the supratemporal fenestra, excluding the frontal from contacting the fenestra. The postorbital bar is inset from the dorsolateral margin of the jugal.

Squamosal. The squamosals are flat and prominent elements of the broad skull table unlike *A. sinensis*, where the lateral and posterior margins are decorated by a pair of shallow crests, the margins are smooth in *A. munensis* (Fig. 2a,b, 3d). The squamosal prongs at the dorsal contact with the quadrate are mostly covered by the lateral margin of the skull table (Fig. 2a,b) as in *A. mcgrewi*, differing from the dorsally exposed prongs of other *Alligator* species (Fig. 8a,d,g). Laterally, the squamosal composes the posterior border of the external auditory meatus.

Parietal. The dorsal surface of the parietal has a smooth midline crest (Fig. 3d), a condition also present in *A. sinensis* and *A. mcgrewi*. The posterior border of the parietal reaches the limit of the skull table excluding the dorsal exposure of the supraoccipital. The supratemporal fossa is broadly exposed along the medial margins of the parietal except at the parietal-postorbital suture, as also observed in *A. mcgrewi* and in some specimens of *A. sinensis* (IRScNB 13904; SNSB 178/1947; Fig. 8d). The parietal has a sagittal midline depression as in *A. mississippiensis* and *A. mefferdi*. An

opposite condition (i.e. flat dorsal outline of the parietal in occipital view) is seen in *A. sinensis*, and variable in *A. mcgrewi*. In the remaining fossil *Alligator* species, the parietal morphology is affected by poor preservation.

Quadratojugal. Only the left quadratojugal is preserved. It forms the posteroventral border and the posterior margin of the infratemporal fenestra (Fig. 5c,d) and is similar to other *Alligator* species in tapering dorsally.

***Quadrate*.** The quadrate is preserved on both sides and is characterised by a markedly concave intercondylar area with strong, ventrally directed hemicondyles, clearly visible in dorsal and ventral views (Fig. 2). In other species of *Alligator*, the area between the lateral and medial hemicondyles are less concave (Fig. 8d,e,g,h). The shape and size of the quadrate condyles are similar to other *Alligator* species, with the lateral condyle slightly larger than the medial, except for *A. sinensis*. The lateral condyle of *A. sinensis* has a unique morphology in having the lateral condyle dorsoventrally twice the size of the medial condyle. In occipital view, the portion of the quadrate bordering the braincase is not visible. This is like in all other species of *Alligator* except for *A. sinensis*. The foramen äerum is positioned on the dorsal surface of the quadrate ramus (Fig. 6b), as in all other alligatoroids (Brochu, 1999). The following crests for the insertion of jaw muscles (Iordansky, 1973) are preserved at the ventral surface of the quadrate: the crest A, positioned along the quadrate-quadratojugal suture, is well-developed and prominent as in *A. mcgrewi*, *A. prenasalis* and *A. sinensis*, differing from a smooth crest of *A. mississippiensis*, *A. mefferdi* and *A. olseni*. The crest B of *A. munensis* extends posteriorly on the quadrate ramus being continuous with the crest B' as in *A. mcgrewi* and *A. sinensis*, although in *A. sinensis* the crest B is well-developed and convex, a condition not present in *A. munensis* or in any other *Alligator* species. Finally, the quadrate ramus is exposed beneath the quadratojugal (Fig. 5c,d).

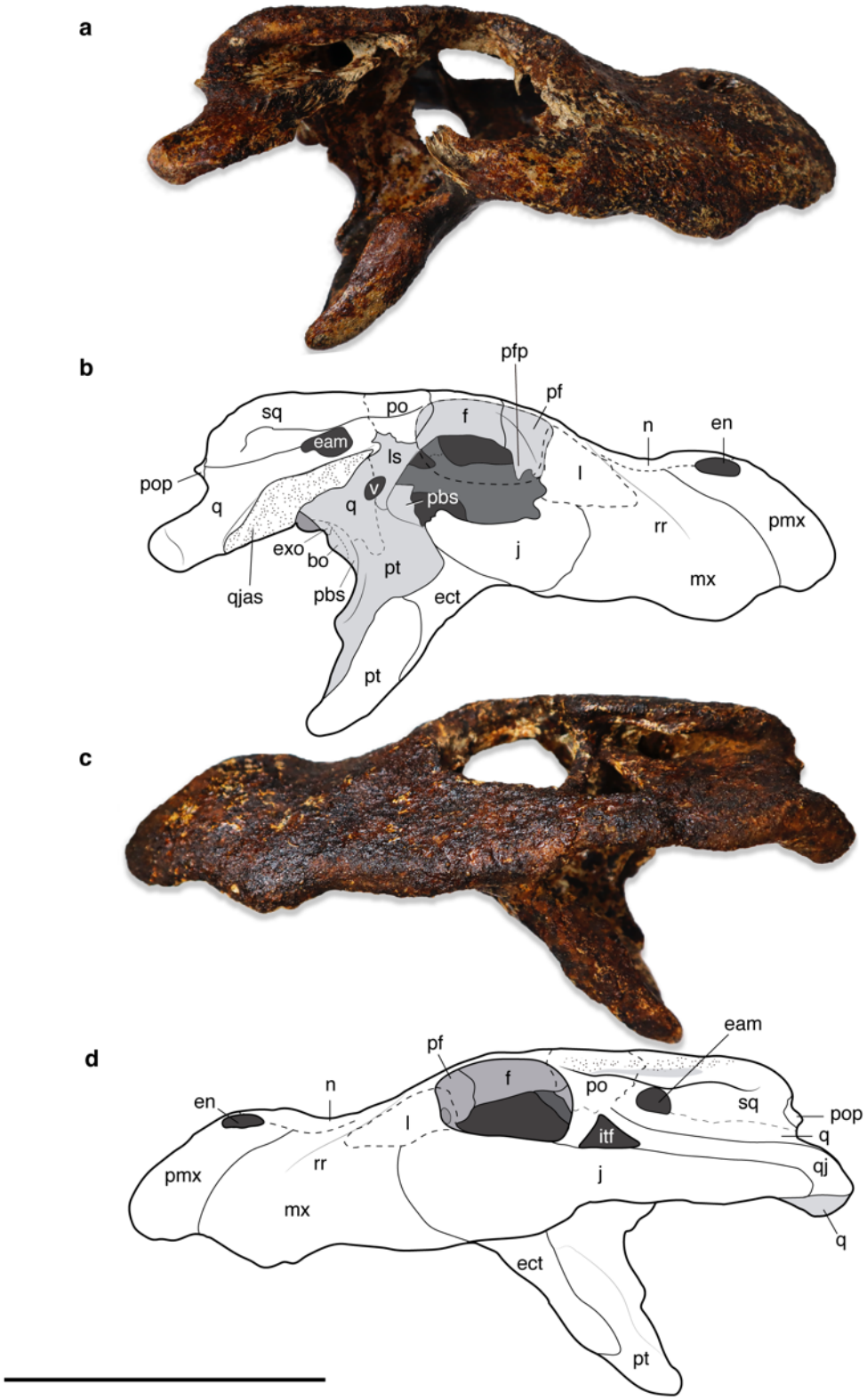

Figure 5. Skull of *Alligator munensis* sp. nov. holotype (DMR-BSL-2011-2) and schematic drawing in right (a,b) and left (c,d) lateral views, respectively. Abbreviations: bo, basioccipital; eam, external auditory meatus; ect, ectopterygoid; en, external nares; exo, exoccipital; f, frontal;

j, jugal; l, lacrimal; ls, laterosphenoid; mx, maxilla; n, nasal; pbs, parabasisphenoid; pf, prefrontal; pfp, prefrontal pillar; pmx, premaxilla; po, postorbital; pop, paroccipital process; pt, pterygoid; q, quadrate; qjas, quadratojugal articular surface; rr, rostral ridge; sq, squamosal; V, foramen for the trigeminal nerve. Scale bar: 10 cm.

Palatine. The palatines are wide and compose the medial and posteromedial margins of the suborbital fenestra. The anterior process of the palatine (i.e. palatine-maxilla suture) reaches the level of the seventh maxillary tooth (Fig. 2 c,d, 3c) as in *A. sinensis* and *A. mcgrewi*. The anterior process of the palatine is quadrangular in shape as seen in other *Alligator* species. The anterolateral process of the palatine is reduced compared to all other *Alligator* species and does not reach the anterior margin of the suborbital fenestra (Fig. 3c). Posteriorly, the palatine shelf strongly projects laterally forming almost an angle of 90 degrees with the sagittal plane of the palatine. A less pronounced lateral projection of the palatine shelf is also observed in *A. mcgrewi* (AMNH 7905). The palatine comprises the posteromedial border of the suborbital fenestra and contacts broadly the ectopterygoid, which completes the posterior border of the fenestra, excluding the pterygoid (Fig. 3c). The contact of the palatine and ectopterygoid hinders the participation of the pterygoid in the margin of the suborbital fenestra, another unique condition of *A. munensis*. In *A. mississippiensis* the palatine and ectopterygoid are broadly separated by the pterygoid (SZ 1057), but in one examined specimen (SNSB 4/1921) the ectopterygoid approaches the palatine, being briefly separated by the anterior margin of the pterygoid (Fig. 8h). Finally, the palatine-pterygoid suture is located far posterior to the suborbital fenestra (Fig. 3c), like in *A. mississippiensis* and *A. mcgrewi*.

Ectopterygoid. As in all alligatoroids, the ectopterygoid is not participating in the maxillary medial alveolar margin. It is partially composing the lateral and posterior margins of the suborbital fenestra (Figs. 2 c,d, 3c). The anterior portion of the

ectopterygoid extends to the level of the 11th alveolus. The ectopterygoid broadly contacts the palatine behind the suborbital fenestra, an autapomorphic condition for *A. munensis*. The posterior end of the ectopterygoid wing does not reach the posterior end of the pterygoid wing. Additionally, the ectopterygoid terminates at the base of the postorbital bar, as commonly observed in *Alligator*.

Pterygoid. The pterygoids are overall similar to other *Alligator* species except for being excluded from the posterior border of the suborbital fenestra (Fig. 2 c,d). The pterygoid contacts anteriorly the palatine and anterolaterally the ectopterygoid. The choana lacks a 'neck', presenting its posterior margin markedly constricted, and there is a pair of shallow depressions around the choanal aperture (Fig. 3f). A constricted posterior margin of the choana is also seen in *A. mcgrewi*, although not as marked as in *A. munensis*. In occipital view, the posterior process of the pterygoid is short and projects ventrally as in *A. sinensis* and *A. mcgrewi*. Dorsally to the process, the pterygoid articulates with the parabasisphenoid.

Parabasisphenoid. As in other species of *Alligator*, the parabasisphenoid is a thin, subtriangular element located between the basioccipital and the pterygoid and forming the anterior wall of the medial and lateral eustachian foramen. The parabasisphenoid is not exposed in the lateral braincase wall. Ventrally, it extends along the posterior surface of the pterygoid as exposed in occipital view (Fig. 6). The posterior portion of a partially preserved parabasisphenoid rostrum can be observed in right lateral view (Fig. 5a,b).

Basioccipital. The basioccipital is morphologically similar to other *Alligator* species, in which the basioccipital tubera is wide, presenting a pronounced midline crest almost reaching the ventral portion of the basioccipital condyle (Fig. 6). The occipital

condyle of *A. munensis* is relatively small and more spherical compared to other *Alligator* species.

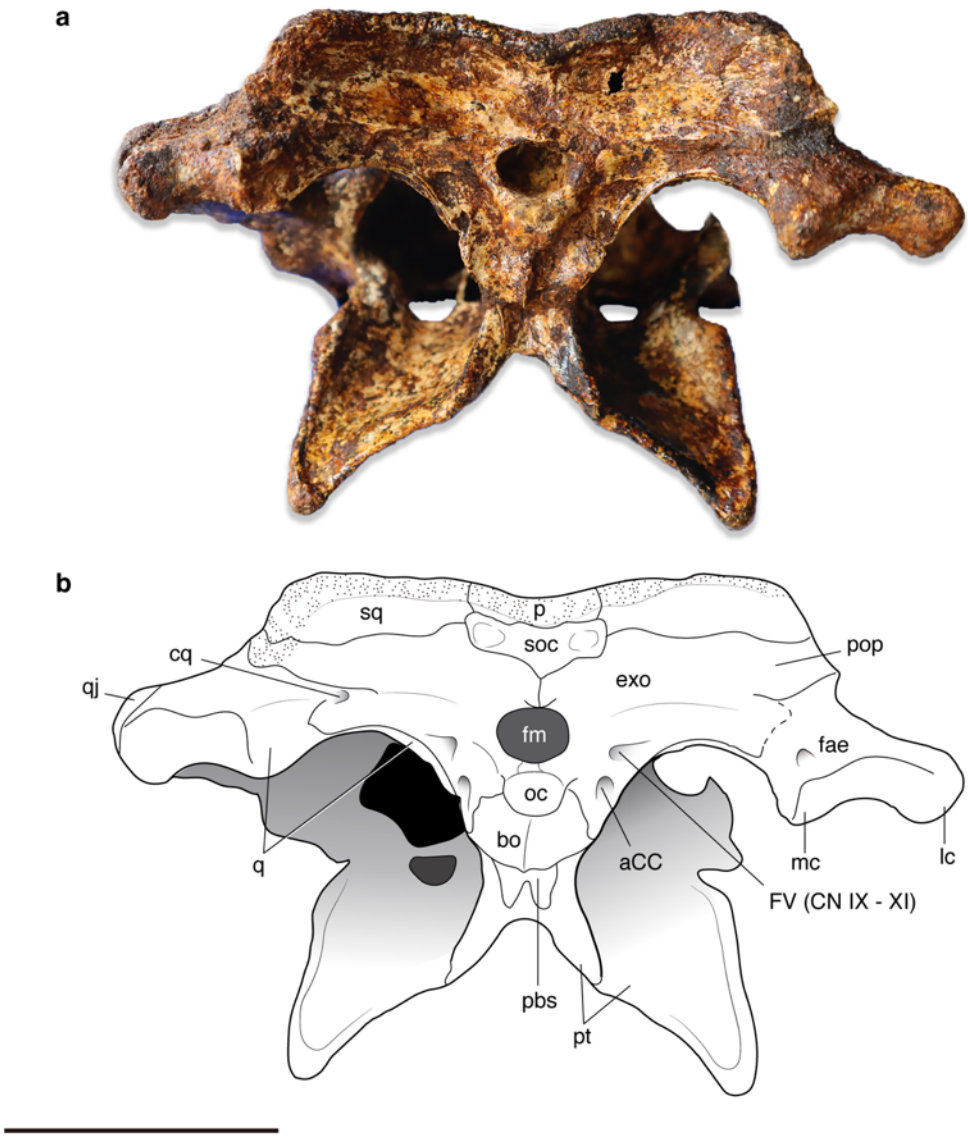

Figure 6. Skull of *Alligator munensis* sp. nov. holotype (DMR-BSL-2011-2) (a) photograph and (b) schematic drawing in occipital view. Abbreviations: aCC, foramen for cerebral carotid artery; bo, basioccipital; cq, cranioquadrate passage; exo, exoccipital; fae, foramen aerum; fm, foramen magnum; FV (CN IX–XI), foramen vagi for the passage of cranial nerves IX–XI; lc, lateral quadrate hemicondyle; mc, medial quadrate hemicondyle; oc, occipital condyle; p, parietal; pbs, parabasisphenoid; pop, paroccipital process; pt, pterygoid; q, quadrate; qj, quadratojugal; soc, supraoccipital; sq, squamosal. Scale bar: 5cm.

Supraoccipital. The supraoccipital is subtriangular shaped, excluded from the dorsal surface of the skull table, and covered dorsally by the parietal (Fig. 6). A pair of shallow depressions are present laterally on the occipital surface. The lateral portion of the supraoccipital is lacking any protuberances and the dorsal articulation with the parietal and squamosal forms a continuous surface, preventing the exposure of the postemporal fenestra (*sensu* Kuzmin et al., 2021), an autapomorphic condition for *A. munensis*. The midline of the occipital surface is slightly posteriorly pronounced, but not forming a marked midline crest, distinguishing *A. munensis* from other *Alligator* species.

Exoccipital/paroccipital process. The exoccipital composes the lateral and dorsal margins of the foramen magnum and extends slightly ventral to the basioccipital condyle, but not reaching ventrally the basioccipital tubera (Fig. 6), as commonly observed in *Alligator*. Two pairs of foramina, the one for the cerebral carotid artery lateral to the basioccipital condyle and one for the passage of cranial nerves IX–XI are positioned more dorsally at the level of the ventral margin of the foramen magnum (Iordansky, 1973; Kuzmin et al., 2021). The paroccipital process is laterally projected as in most *Alligator* species, differing from a marked dorsolaterally oriented process of *A. sinensis*. The dorsal margin of the foramen magnum at the contact of the exoccipitals is marked by a small protuberance, also commonly observed among *Alligator* species, except for *A. sinensis.*

Braincase. Some elements of the braincase are preserved but incomplete. The foramen ovale is present and is composed anteriorly by the laterosphenoid, ventrally by the pterygoid and posteriorly by the quadrate (Fig. 5a,b). The preservation around the foramen hampers the precise observation of the prootic exposure. Only the posterior

portion of the laterosphenoid (e.g. lateral bridge, *sensu* Holliday and Witmer, 2009) is preserved.

Phylogenetic analysis

A total of three most parsimonious trees (MPTs) with length of 92.8 steps were recovered (Fig. 7). A list of synapomorphies and node numbers can be found at supplementary material. The results are consistent to those of Rio & Mannion (2021) when using re-discretised characters dataset with an extended implying weighting using a *k*-value of 12 (analysis 2.3): The gharials *T. schlegelii* and *G. gangeticus* compose a clade (Gavialidae), reproducing the results of molecular topologies (i.e. Oaks, 2011; Pan et al., 2020; Rio & Mannion, 2021). Both gharial species are recovered within Gavialoidea that is furthermore composed by the non-gavialid gavialoids *Maroccosuchus zennaroi*, *Kentisuchus spenceri*, *Dollosuchoides densmorei*, and *Maomingosuchus petrolica*. Gavialoidea is sister group to Crocodyloidea and both clades compose Longirostres (*sensu* Harshman et al., 2003). Planocraniids are retrieved as sister taxa to Longirostres, as in the results of Rio & Mannion (2021).

The *Alligator* clade is monophyletic (node 197) and supported by: ratio of snout length to total skull length > 0.5 (C1: 0→1); presence of a notch posterolateral to naris (C44: 0→1); nasals completely bisecting nares (C47: 1→0); upturned dorsomedial margin of the orbit (C72: 0→1); posterolateral tuberosities in the supraoccipital visible in dorsal view (C79: 0→1); and sub-rectangular quadrate condyles (C119: 1→0); in which *A. prenasalis* is recovered as a first divergent lineage within the clade and the only *Alligator* species outside the crown group. The crown clade *Alligator* (node 196) is supported by: presence of spectacle between the orbits (C31: 0→1); dorsal orientation of the external nares (C41: 0→1); supraoccipital not exposed on dorsal skull table (C77:

0→1); stocky dentary and maxillary teeth posterior to alveoli 12/13 (C156: 1→0); anteromedially bowed posterolateral margin of suborbital fenestra (C171: 0→1); mandibular symphysis posteriorly extending at the level of 6 or less dentary alveoli (C221: 1→0); and nuchal osteoderms differentiated from dorsal shield (C322: 0→1). Two main clades are recovered within crown *Alligator*, the "*A. mississippinensis*-clade", composed by *A. mississippiensis* and *A. mefferdi* (node 199; synapomorphies: prefrontal pillar presenting pneumatic recess [C68 0→1]; presence of maxilla diastema between alveoli 6 and 8 [C154: 0→1]; large exposure of the prootic ventral to trigeminal foramen [C214: 0→1]; dentary height at the level of alveoli 1-4 at the same level or higher than the height at the level of alveoli 11-12 [C218: 1→0]; curved dentary dorsal profile between alveoli 4 – 10 in lateral view [C220: 2→1]; splenial does not participate on the mandibular symphysis [C222: 0→2];absence of surangular ascending process on lateral wall of glenoid fossa [C244:0→1]); and the "*A. sinensis*-clade clade" composed by *A. olseni*, *A. mcgrewi* and all the *Alligator* species from Asia, including the 'Penghu' *Alligator*, *A. sinensis*, *A. luicus*, and *A. munensis* (node 195; synapomorphies: lateral margin of suborbital fenestra projecting medially into fenestra) C169: 0→1). A clade composed by *Alligator* species from Asia in addition to *A. mcgrewi* (Miocene, North America) and to the exclusion of *A. olseni* (node 194, supplementary material 1) is supported by the presence of a midsagittal crest on the frontal (C70: 0→1); presence of a sagittal crest on the parietal (C83: 0→1); by the anterior process of the palatine anterior to the anterior of the suborbital fenestra and at the level of more than two full alveoli (C162: 1→0), and by a raised posterior border of the external nares (C332: 0→1). Furthermore, *A. luicus* shares with *A. munensis* and *A. mcgrewi* the ratio of snout length to total skull length < 0.5 (C1: 1→0) to the exclusion of *A. sinensis*. *A. mcgrewi* is recovered deeply nested as sister group to *A. munensis*

(node 191, supplementary material 1) by the presence of an angle between the dorsal profile of the paroccipital process and dorsal margin of the cranial table more than °50 (C109: 1→2).

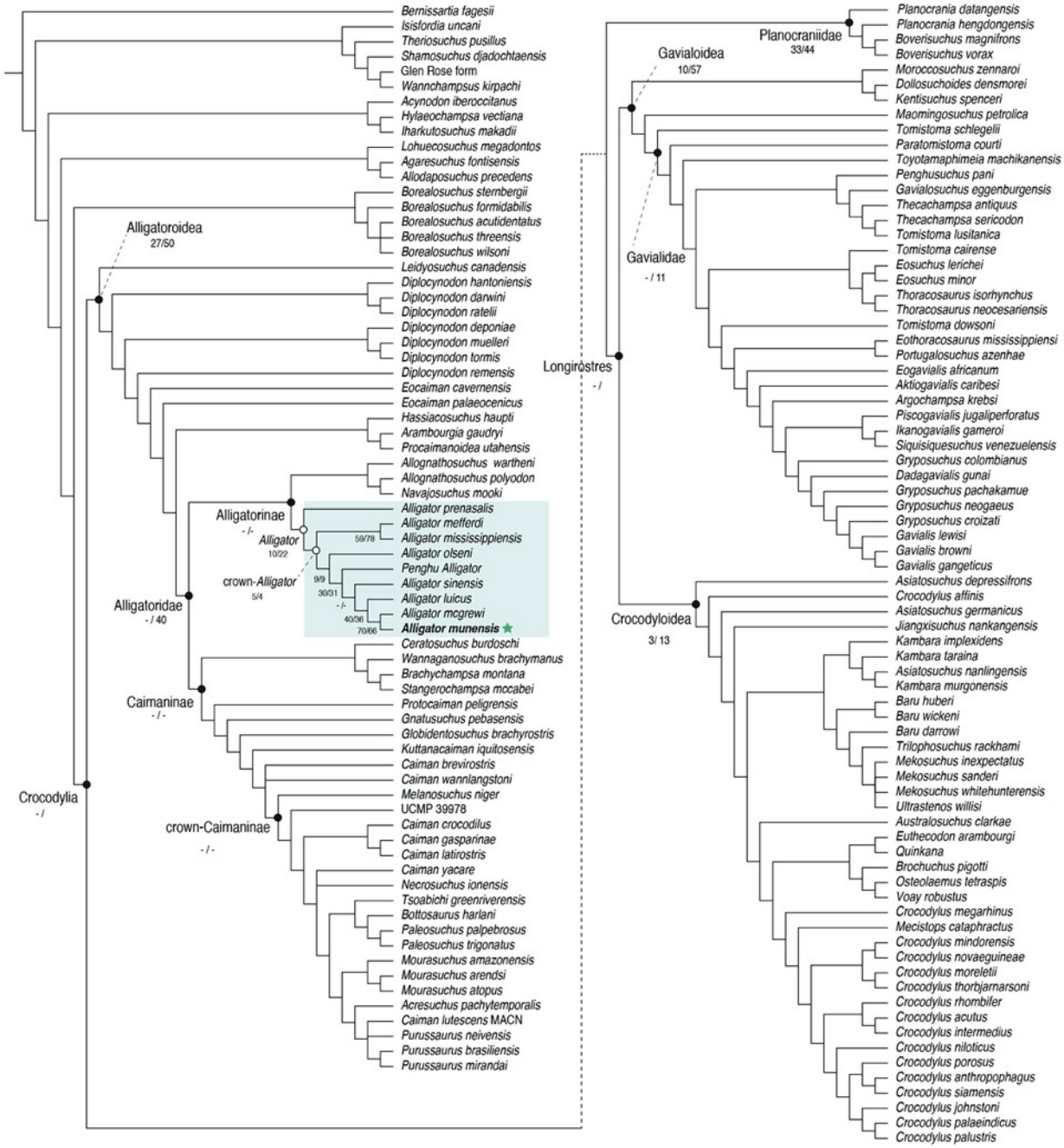

Figure 7. Strict consensus of the three most parsimonious trees recovered in the phylogenetic analysis. Green box indicates the *Alligator* clade. *Alligator munensis* is marked with a star. Support values (Bootstrap/ Jackknife) are indicated under the main nodes.

DISCUSSION

Taxonomy of *Alligator munensis*

A comprehensive time-scaled phylogenetic analysis of DMR-BSL-2011-2, the holotype of *Alligator munensis*, including an increased taxon sampling of *Alligator* spp., is in preparation and will be published elsewhere. The morphology of the skull nevertheless clearly implies an *Alligator* closely related to extant *A. sinensis*. Alligatoroid synapomorphies include a laterally shifted foramen äerum, a maxillary shelf separating the posterior toothrow from the ectopterygoid, whereas the full premaxillary-maxillary overbite, the largest 4th maxillary tooth, and a fronto-parietal suture entirely on the skull table diagnose the morphological features of Alligatoridae. Among alligatorids, only *Alligator* has bisected external nares (Brochu, 1999; Norell et al., 1994) as also present in *A. munensis*. *Alligator munensis* shares several apomorphic characters with *A. sinensis* to the exclusion of *A. mississippiensis*: (*i*) small incisive foramen occupying one third of the length of the premaxilla (Figs. 3b, 6a,b); (*ii*) ridge on the dorsal surface of the parietal (Fig. 3d); (*iii*) the presence of a raised posterior margin of the external nares (Fig. 3e); (*iv*) rugose ventral surface of lateral maxillary shelf projecting into the suborbital fenestra (Fig. 3c); (*v*) small, tubera-like posteroventrally projecting posterior pterygoid processes. These character states are furthermore shared with *A. mcgrewi* from the Miocene of North America (except for the small incisive foramen), in addition to the shelf of the palatine projecting laterally at the posterior border of the suborbital fenestra (Fig. 3c), a condition shared exclusively between *A. munensis* and *A. mcgrewi*. In *A. luicus* from the Miocene of China, characters (*ii*) and (*iii*) are present but the rest of the character states are not preserved in the only known specimen. Synapomorphies supporting the clade composed by *A. sinensis*, *A. luicus*, *A.munensis*, and *A. mcgrewi* include distance between posterior margin of quadrate condyle and the level of the

anterior margin of the occipital condyle less than the quadrate mediolateral width (C121: 1→0); and mandibular symphysis extending posteriorly to alveoli 6-8 (C221: 0→1).

DMR-BSL-2011-2 was preliminary reported by Claude et al. (2011) who tentatively referred it to *Alligator* cf. *sinensis* based on the presence of a straight posterior skull margin; long distance between the posterior margin of the skull table and the temporal fenestra; broad (wider than long) skull table; and a well-developed internarial bar. Subsequent preparation not possible at the time and detailed description in the present study reveal that a highly distinct morphology warrants a new species. *A. munensis* differs from *A. sinensis* in having a slightly convex dorsal surface of the frontal lacking upturned margins; reduced dentition with 12 instead of 14 maxillary alveoli; lacking a convex crest B of the quadrate; lacking a crest with a ventral protuberance on the ventral margin of the exoccipital dorsal to the cranioquadrate passage; lacking a pair of horns formed by the parietal and squamosal on the posterodorsal margin of the skull table (potentially correlated to the latter character); lacking a ridge above the dorsal rim of the lateral groove of the squamosal; and lacking a crest on the dorsal surface of the lateral margin of the palatine (Fig. 8). Additionally, *Alligator munensis* can be distinguished from all other fossil and extant *Alligator* species by the presence of the following autapomorphic characters: posteriorly retracted circular and reduced external nares; a wide internarial bar; a sagittal crest along the midline contact of the nasals; frontal slightly convex and lacking upturned margins; pterygoid excluded from the posterior margin of the suborbital fenestra by a broad ectopterygoid-palatine suture; and prominent quadrate condyles. These autapomorphies and phylogeny imply that *Alligator munensis* was not ancestral to *Alligator sinensis* and rather represent a divergent, possibly allopatric species.

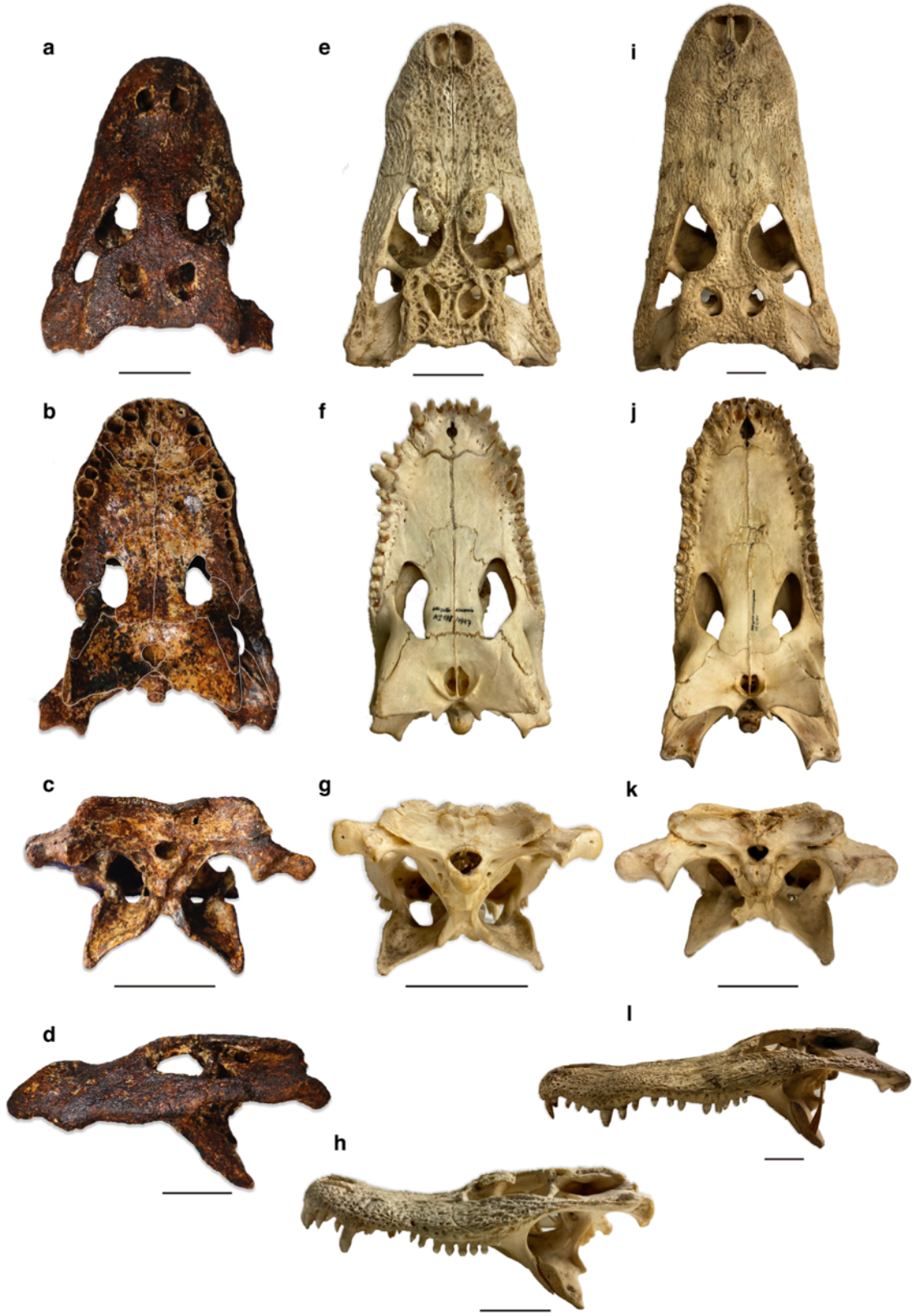

Figure 8. Comparison between the skulls of *Alligator munensis* sp. nov. holotype (DMR-BSL-2011-2) (a–d), *Alligator sinensis* (SNSB 178/1947) (e–h), and *Alligator mississippiensis* (SNSB

4/1921) (i–l) in dorsal, ventral, occipital and left lateral views from top to bottom, respectively. Scale bars: 5cm.

Biogeographical implications

The dispersal of *Alligator* from North America to Asia has been for long considered enigmatic in Crocodylia evolution: molecular studies estimate that the Chinese alligator (*A. sinensis*) shared a common ancestor with the American alligator (*A. mississippiensis*) at least 31 Mya (i.e. 31.3 Ma – 58.2 Ma, Pan et al., 2020 and Oaks, 2011, respectively), a conflicting estimate considering that unambiguous fossils assigned to *A. sinensis* are no older than the Pliocene (Brochu 1999, Thorbjarnarson & Wang, 2010; Iijima et al., 2016; Massonne et al., 2019). A potential dispersal route previously argued to explain *Alligator* dispersal to Asia during the Cenozoic is the Beringia Land Bridge (Brochu 1999; Massonne et al., 2019), as it is the most consistent considering the relative intolerance of *Alligator* to salt water (Taplin & Grigg, 1989; Grigg & Kirschner, 2015), in addition to fossil record and paleographical, climatic, and phylogenetic aspects (Brochu, 1999; Oaks, 2011; Massonne et al., 2019; Pan et al., 2020). Alternatively, a dispersal through Europe could have incurred, however support for phylogenetic relationships between European alligatorines and A*lligator* spp. is weak (Brochu, 1999; Rio & Mannion, 2021).

Results of the phylogenetic analysis of the present study showed for the first time a topology in which fossil *Alligator* species from Asia (*A. luicus*, *A. munensis*, and the 'Penghu' alligator) compose a clade with *A. sinensis* to the exclusion of *A. mississippiensis* (Fig. 7). Additionally, the North American Miocene taxa *A. olseni,* (Early Miocene), and *A. mcgrewi* (Lower Miocene) are recovered as a first divergent lineage, and in a deeply nested phylogenetic position as sister to *A. munensis*, respectively (Fig. 7), also representing a novelty in *Alligator* systematics. Both Miocene

taxa have been consistently recovered outside the crown-*Alligator* in previously published phylogenies (Brochu, 1999, 2010; Hastings et al., 2013; Bona et al., 2018; Massonne et al., 2019; Cossette & Brochu, 2021; Rio & Mannion, 2021). *A. olseni* at the base of the "*A. sinensis*-clade" suggests cladogenetic events taking place in North America in Early Miocene, preceding a dispersal to Asia, whereas the derived position of *A. mcgrewi* suggests a back dispersal of *Alligator* to North America still in early Stages of the Miocene, representing a complex biogeographic history for the lineage. The back dispersal suggested by the present phylogeny will be further tested under total-evidence tip dating analysis (in preparation), as the synapomorphy uniting *A. mcgrewi* and *A. munensis* (i.e. angle between the dorsal profile of the paroccipital process and dorsal margin of the cranial table more than °50; C109: 1→2) might be optimized differently considering that tip-dating is expected to identify it as a homoplasy instead (Lee & Yates, 2018; Darlim et al., 2022). Thus, an early divergent phylogenetic position of *A. mcgrewi* would be more likely to explain the relationships of this species within the "*A.sinensis*-clade".

Nevertheless, considering a dispersal through Beringia, climatic factors are still problematic given the crocodylian minimum limit of Mean Annual Temperature (MAT) of approximately 14.2°C (Markwick, 1998). Despite reports of *A. sinensis* occurring as far as 35°N, therefore able to tolerate slightly lower temperatures (Thorbjarnarson & Wang, 2010), longer exposition to low climatic condition is not compatible to the survival of alligators (Brisbin et al., 1982). Thus, periods younger than the Eocene would be too cold considering the glacial events and low Global temperatures (Zachos et al., 2001), and possible exceptions for the dispersal through the Beringia would have potentially take place during periods of warmer temperatures in higher latitudes: MAT temperatures were estimated to vary between 17 – 14.1°C in the Early Eocene artic

(Ellesmere Island, West et al., 2015); or during the Middle Miocene Climatic Optimum, as MAT in Alaska during this period was estimated to reach between 19.3 – 23.5°C (based on bivalve stable O isotopes, Oleinik et al., 2008). A dispersal via Beringia during the Miocene Climatic Optimum overlaps with the results of the present phylogenetic analysis, considering paleontological evidence of *Alligator* in Asia (*A. luicus*) during this time, in addition to phylogenetic affinities with early divergent North American representatives (*A. olseni,* and potentially *A.mcgrewi*).

Regarding the biogeography of *Alligator* within Asia, the unexpected presence of an alligatorid in northeastern Thailand requires explanation (Claude et al., 2011). The tentative referral of DMR-BSL-2011-2 to *A.* cf *sinensis* posed a biogeographic enigma because the geographically closest historical occurrences of *A. sinensis* come from the Yangtze and Xi river systems (Thorbjarnarson and Wang, 2010; Pan et al., 2019) that only approach the Mekong and Chao Phraya systems of Thailand along their upper sections at high elevations, unfavourable for alligators (Claude et al., 2011). Nevertheless, as we here demonstrate, the specimen DMR-BSL-2011-2 confidently represents a separate species albeit with close affinities particularly to *A. mcgrewi* and *A. luicus*, as these species occupy a more derived position in comparison to *A. sinensis* (Fig. 9). The highly distinct morphology of *A. munensis* is furthermore consistent with relatively deep divergence from *A. sinensis*. If that is the case, the presence of *Alligator* in Thailand may be explained by the presence of a common ancestor of *A. munensis, A. luicus, A. mcgrewi,* and *A. sinensis* distributed in the lowlands of both the proto Yangtze-Xi and Mekong-Chao Phraya river systems that was subsequently split into separate, vicariant species due to the accelerated Miocene uplift of the eastern Tibetan Plateau, fully hindering dispersal between these drainage basins. The Mun river, the locality of the *A. munensis* specimen described herein, feeds the Mekong today but was

connected to the proto-Chao Phraya river in the past (Hutchison, 1989; Brookfield, 1998; Breitfeld et al., 2022).

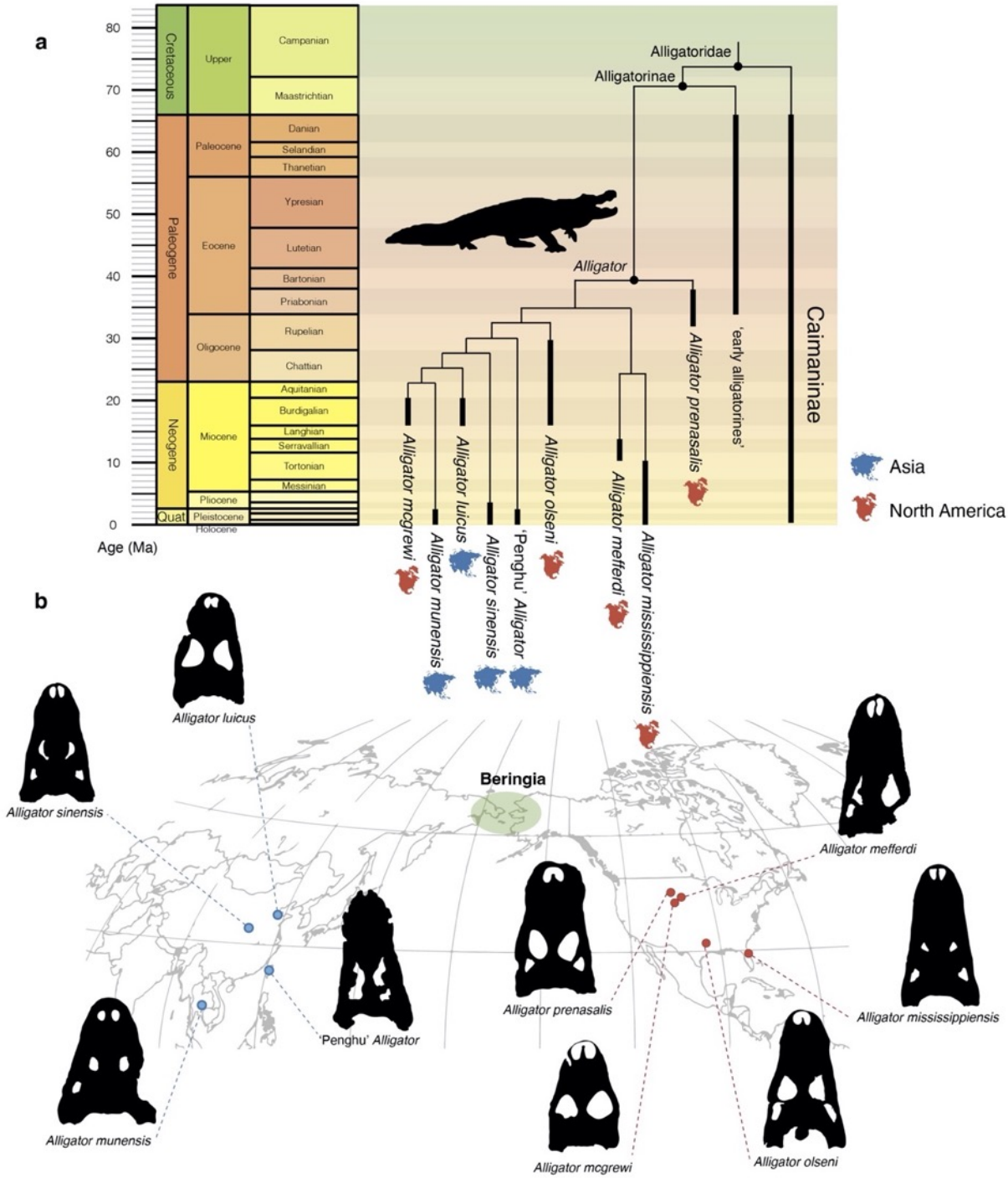

Figure 9. Simplified time-scaled topology resulted from the phylogenetic analysis focused on *Alligator* interrelationships (a); and distribution of *Alligator* species (b). Beringia strait is

indicated by the area highlighted in green. World map modified from Wikimedia commons (under the license CC-BY-SA-3.0; https://shorturl.at/gzEJU). Skull outlines not in scale.

However, some biogeographical aspects need to be further explored: (i) lack of *Alligator* fossil remains in the west coast of North America hampering a more precise time constraint; (ii) the deeply nested derived position of *A. mcgrewi* is inconsistent with its age and the age of *A. munensis* furthermore suggesting a complex biogeographical history for the "*A. sinensis*-clade"; (iii) the dispersal events within Asia remains unresolved, as the presence of *Alligator* to Thailand can only be better explored under time-scaled approaches considering the timing of the land uplift of the eastern Tibetan Plateau. The relation between time and climatic context is being further explored in an ongoing study regarding *Alligator* phylogenetic relationships analysed under total-evidence tip dating approach. The simultaneous analysis of morphology, molecular and stratigraphical data is expected to shed light on the relationship and divergence age of *Alligator* species, thus essential to evaluate the intercontinental dispersal of *Alligator*.

Although temporal inconsistency is present in the retrieved close relationship between *A. mcgrewi* and *A. munensis*, relevance of the results of the present phylogenetic analysis is acknowledged by the presence of Miocene taxa from both North America and Asia composing the "*A. sinensis*-clade", contributing on reducing the temporal gap otherwise inferred by the molecular estimates of the *A. mississippiensis–A. sinensis* split (Oaks, 2011; Pan et al., 2020). A tip-dating analysis (in preparation) will be critical to (i) revisit the phylogenetic position of *Alligator* spp. mainly concerning the deeply nested *A. mcgrewi*, as stratigraphical data might be adjusted for a more consistent topology (regarding age of species and detection of homoplasy; Lee & Yates, 2018; Darlim et al., 2022); and (ii) to constrain the divergence

age estimates within *Alligator* (total and crown groups) in order to compare it with the available warm periods compatible with the minimum MAT tolerance of crocodylians (i.e. 14.2°C), specifically targeting on the hypothesis of a dispersal during the Miocene Climatic Optimum, as it is most consistent with the *Alligator* fossil record (presence of *A. luicus* in the Middle Miocene of China), thus contributing to the understanding of *Alligator* paleobiogeography regarding both North America-Asia, and within-Asia dispersal events.

Remarks on the retracted external nares of *Alligator munensis*

Unlike other crocodylians, *A. munensis* bears unique small, rounded external nares that are posterodorsally retracted and are bisected by a wide internarial bar (Figs. 2a,b, 8). In Crocodylia, *Purussaurus* spp., possesses retracted external nares that are further characterised by the posterior expansion of the posterior margin (Aguilera et al., 2006), a condition absent in *A. munensis*. Retracted external nares are often associated with pelagic adaptation in cetaceans and marine reptiles such as ichthyosaurs, plesiosaurs, mesosaurs, and metriorhynchid crocodylomorphs (Massare, 1994; Young et al., 2020). However, it is highly unlikely that *A. munensis* was marine given the depositional environment and geographic origin of the fossil specimen. Moreover, *Alligator* species lack lingual salt-excreting glands (Taplin and Grigg, 1989; Grigg and Kirshner, 2015) and cannot survive indefinitely in hyperosmotic conditions (Lauren, 1985). Natural habitats of the Chinese alligators were low-elevation areas, alluvial floodplains with a variety of wetlands including marshes, ponds, and streams, although these have been significantly altered by human activities (Thorbjarnarson and Wang, 2010). How *A. munensis* would have taken advantage of its unique external narial morphology, if it

were living in similar habitats (consistent with depositional environments), remains unclear.

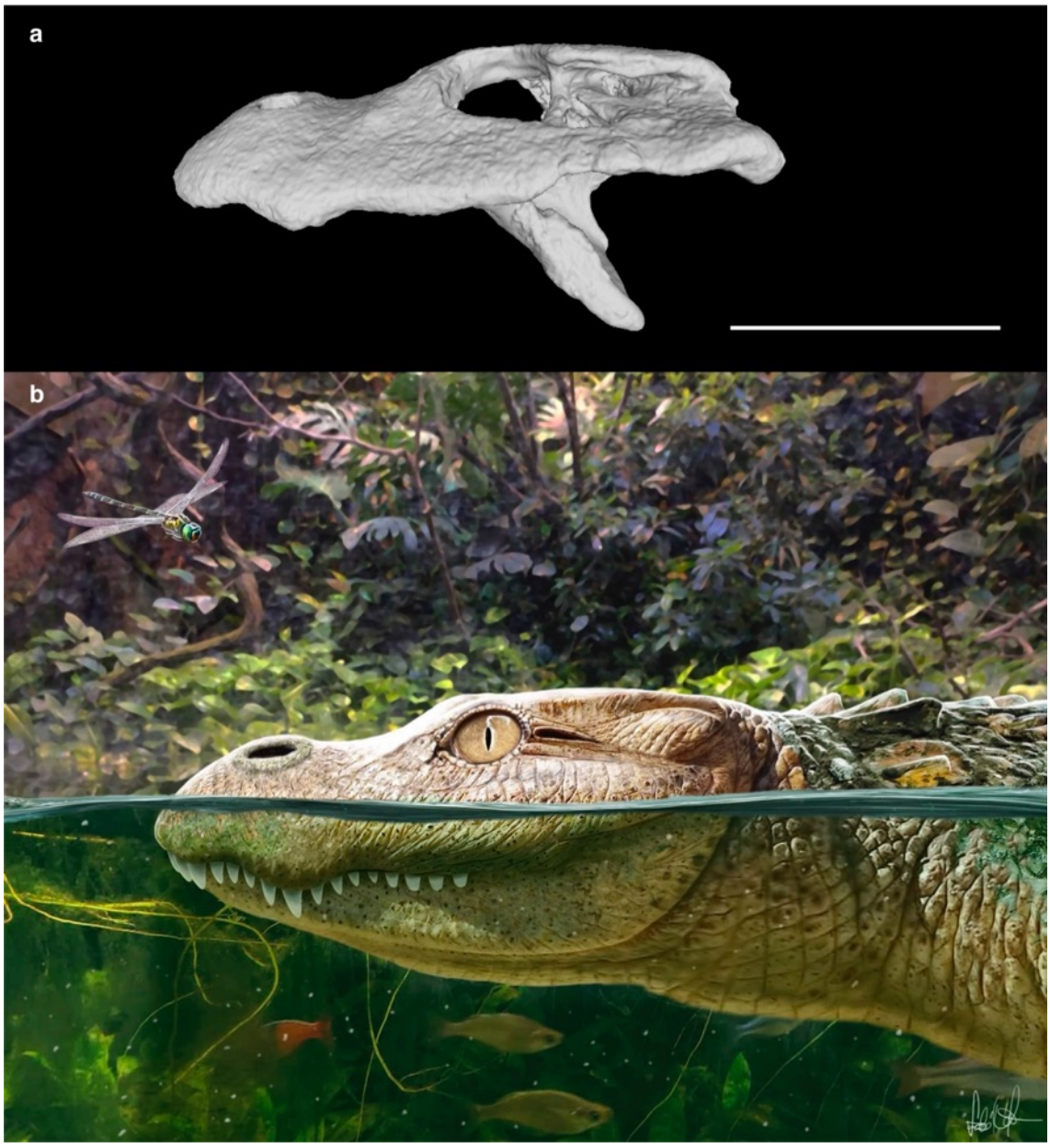

Figure 10. Virtual representation of *Alligator munensis* sp. nov. holotype (DMR-BSL-2011-2)**.** (a) Digital reconstruction and (b) artistic reconstruction, both in left lateral views. Art by Márton Szabó. Scale bar: 10cm.

Comments on the evolution of dietary specialisation in alligatorines

While the dentition of *Alligator munensis* is unknown, enlarged alveoli 9–11 and the deep, blunt snout may provide some clues to feeding ecology (Fig. 3c). In several short-snouted alligatoroids, the posterior maxillary/dentary alveoli are considerably enlarged and contain more globular teeth relative to more anterior alveoli posterior to the 4th maxillary/dentary alveolus (Brochu, 2004; Salas-Gismondi et al., 2015; Fig. 11), implying that *A. munensis* possessed hypertrophied globular or flattened crushing rear dentition (Supplementary Fig. 4). The presence of a robust, deep skull, enlarged suborbital fenestra, and extended pterygoid flanges further suggest well-developed jaw adductor muscles and strong bite force consistent with this type of dentition (Ősi, 2014). A crushing dentition is plesiomorphic for alligatorines (total-group of *Alligator*) and has been used to exemplify a case for “specialised” taxa giving rise to “generalist” taxa (*Alligator* spp.) and thus breaking the "Law of the Unspecialised" of Cope (1896) (Miller-Camp and Brochu, 2018). This concept proposes that "specialised" features would not revert to a generalised condition and generalists could not evolve from specialists. Translating morphology to ecology is usually not straightforward for fossils, however (as also noted by Brochu, 2004) a “specialisation” may simply represent deviation from the ancestral anatomy and may not be necessarily associated with a distinct (narrower) niche. Likewise, in case of alligatorines, crushing dentition does not automatically imply more specialised ecology - in the absence of evidence to the contrary, it might as well be interpreted as adaptation for a more opportunistic diet with potential seasonal preferences of hard-shelled preys (broader niche). The macrocephalic turtle, *Platysternon megacephalum* may serve as an example: this species potentially takes advantage of its large head when seasonally consuming molluscs but it otherwise an omnivorous species Sung et al. (2016). Moreover, crocodylians without enlarged (albeit stocky) posterior dentition occasionally prefer hard-shelled prey resulting in

advanced dental wear, as has been reported for *Caiman latirostris* (Ősi and Barrett, 2011). Information on the diet of *Alligator sinensis* is scarce; a single study reported snails as dominant prey (Chen et al., 1985). *A. sinensis* does not have enlarged posterior teeth or alveoli but the crowns are slightly rounded, more so than in e.g. *Alligator mississippiensis*. Although there is no evidence of molluscs in the type locality of *A. munensis*, gastropod shell remains were reported from the late Middle Pleistocene site of Khok Sung (Suraprasit et al., 2016), a site which might have been close to Ban Si Liam both geographically and chronologically (Duval et al., 2019) (Fig. 1).

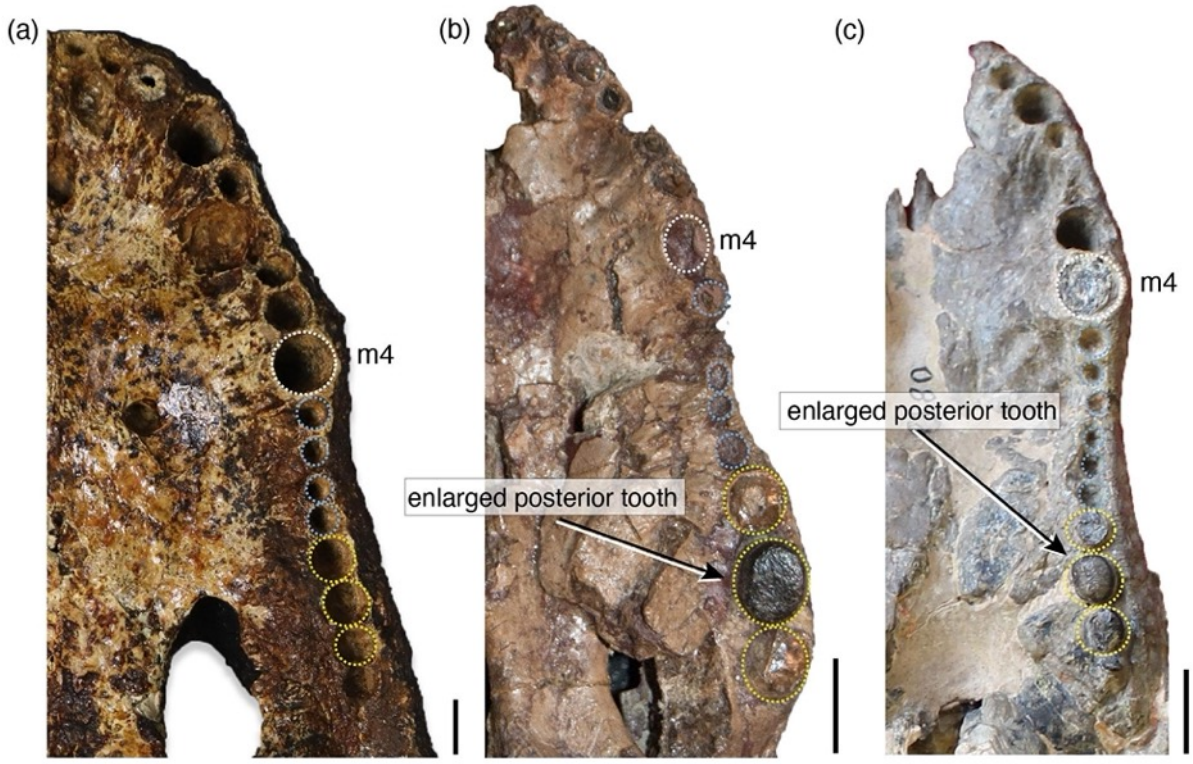

Figure 11. Ventral view of the palate showing maxillary alveolar pattern among the alligatoroids *Alligator munensis* sp. nov. holotype DMR-BSL-2011-2 (**a**), *Allognatosuchus wartheni* YPM-PU 16989 (**b**), and *Navajosuchus mooki* AMNH 6780 (**c**). White dotted circles indicate the fourth maxillary alveolus. Series of small maxillary alveoli posterior to the fourth alveolus are indicated with the blue dotted circles, whereas enlarged maxillary alveoli are indicated by yellow dotted circles. Note

that *Allognatosuchus wartheni* has extremely hypertrophied alveoli. Abbreviation: m4, fourth maxillary alveolus. Photo credits: Christopher Brochu (b-c). Scale bar: 1cm.

Regardless of ecological function, the pattern of morphological simplification of the dentition in crown-group *Alligator* and the apomorphic development of a longer snout in the *A. mississippiensis* lineage (Miller-Camp and Brochu, 2018) is apparent. *A. munensis*, on the other hand, may represent an outlier by reverting to the ancestral condition of enlarged posterior crushing dentition characterising early "specialized" alligatorines. Intriguingly, crocodylians with enlarged globular/flattened dentition were common in the past and evolved independently in multiple lineages (e.g. Brochu, 1999; Brochu, 2004; Ősi, 2014; Salas-Gismondi et al., 2015; Cossette, 2021) but this particular morphotype is absent in the living fauna. *A. munensis* may have been one of the last examples of the crushing-dentition morphotype.

REFERENCES

Aguilera, O. A., Riff, D. & Bocquentin-Villanueva, J. A new giant *Purussaurus* (Crocodyliformes, Alligatoridae) from the upper Miocene Urumaco formation, Venezuela. *J. Syst. Palaeontol.* **4,** 221–232 (2006).

Benton, M. J. & Clark, J. M. Archosaur phylogeny and the relationships of the Crocodylia in *The Phylogeny and Classification of the Tetrapods* (ed. Benton, M.J.) 295–338 (Oxford: Clarendon Press, 1988).

Bona, P., Ezcurra, M. D., Barrios, F., & Fernandez Blanco, M. V. A new Palaeocene crocodylian from southern Argentina sheds light on the early history of caimanines. *Proc. R. Soc. B*, **285,** 20180843. (2018).

Breitfeld, H. T. *et al*. Provenance of Oligocene–Miocene sedimentary rocks in the Cuu Long and Nam Con Son basins, Vietnam and early history of the Mekong River. *Int. J. Earth Sci.* **111,**1773–1804 (2022).

Brochu, C. A. Phylogenetics, taxonomy, and historical biogeography of Alligatoroidea. *J. Vertebr. Paleontol*. **19,** 9–100 (1999).

Brochu, C. A. Phylogenetic approaches toward crocodylian history. *Annu. Rev. Earth Planet. Sci*. **31,** 357–397 (2003).

Brochu, C. A. Alligatorine phylogeny and the status of *Allognathosuchus* Mook, 1921. *J. Vertebr. Paleontol*. **24,** 857–873 (2004).

Brochu CA. A new alligatoroid from the lower Eocene Green River Formation of Wyoming and the origin of caimans. J. Vertebr. Paleontol. **30,** 1109–1126 (2010).

Brochu, C. A. Phylogenetic relationships of Palaeogene ziphodont eusuchians and the status of *Pristichampsus* Gervais, 1853. *Earth and Environmental Science Transactions of the Royal Society of Edinburgh*, **103,** 521-550 (2012).

Brookfield, M. E. The evolution of the great river systems of southern Asia during the Cenozoic India-Asia collision: rivers draining southwards. *Geomorphology* **22,** 285–312 (1998).

Chaimanee, Y. *et al*. *Khoratpithecus piriyai,* a late Miocene hominoid of Thailand, *Amer. J. Phys. Anthrop*. (2006).

Chen, B. H., Hua, Z. H. & Li, B. H. *Alligator sinensis* Hefei (Anhui Technology, Hefei), 115–216 (1985).

Claude, J. *et al*. Neogene reptiles of northeastern Thailand and their paleogeographical significance. *Ann*. *Paleontol*. **97**, 113–131 (2011).

Cope, E. D. The primary factors of organic evolution, Open Court Publ. *Co., Chicago*. (1896).

Cossette, A. A new species of *Bottosaurus* (Alligatoroidea: Caimaninae) from the Black Peaks Formation (Paleocene) of Texas indicates early radiation of North American caimanines. *Zool. J. Linn. Soc.* **191,** 276–301 (2021).

Cuvier, F. G. Sur les alligatori espèces de Crocodiles vivans et Sur leurs alligatori distinctiss. *Ann*. *Mus*. *Hist*. *Nat. Paris* **10,** 8–66 (1807).

Daudin, F. M. Histoire naturelle, générale et particulière des reptiles: ouvrage faisant suite aux oeuvres de Leclerc de Buffon, et partie du cours complet d'histoire naturelle rédigée par CS Sonnini (F. Dufart) 397 (Paris, 1802).

Delfino, M., & Smith, T. Reappraisal of the morphology and phylogenetic relationships of the middle Eocene alligatoroid *Diplocynodon deponiae* (Frey, Laemmert, and Riess, 1987) based on a three-dimensional specimen. *J. Vertebr*. *Paleontol*. **32,** 1358-1369 (2012).

Duval, M. *et al*. Direct ESR dating of the Pleistocene vertebrate assemblage from Khok Sung locality, Nakhon Ratchasima province, northeastern Thailand. *Palaeontol. Electron.* **22,** 1–25 (2019).

Esposito, M., Chaimanee, Y., Jaeger, J. J. & Reyss, J. L. Datation des concrétions carbonatées de la Grotte du Serpent (Thaïlande) par la méthode Th/U. *Comptes rendus Acad. Sci. Ser. IIA.* **326,** 603–608 (1998).

Esposito, M., Reyss, J. L., Chaimanee, Y. & Jaeger, J. J. U-series Dating of Fossil Teeth and Carbonates from Snake Cave, Thailand. *J. Archaeol. Sci.* **29,** 341–349 (2002).

Fauvel A. A. Alligators in China. *J. North China Branch R Asiatic Soc*. **13,** 1–36 (1879).

Gmelin, J. Linnei systema naturae. Leipzig: GE Beer, 1057 (1789).

Gray, J. E. Catalogue of the tortoises, crocodiles, and amphisbaenians, in the collection of the British museum. *London: Br. Mus. Nat. Hist*. (1844).

Grigg, G. & Kirshner, D. Biology and Evolution of Crocodylians. (Cornell University Press, 2015).

Groh, S. S., Upchurch, P., Barrett, P. M., & Day, J. J. The phylogenetic relationships of neosuchian crocodiles and their implications for the convergent evolution of the longirostrine condition. *Zoo. J. Linn. Soc.* **188,** 473-506. (2020).

Godoy, P. L., Cidade, G. M., Montefeltro, F. C., Langer, M. C., & Norell, M. A. Redescription and phylogenetic affinities of the caimanine *Eocaiman cavernensis* (Crocodylia, Alligatoroidea) from the Eocene of Argentina. *P. Palaeontol.* **7,** 1205-1231. (2021).

Goloboff, P. A., & Catalano, S. A. TNT version 1.5, including a full implementation of phylogenetic morphometrics. *Cladistics*, ***32*,** 221-238 (2016).

Goloboff, P. A., & Morales, M. E. TNT version 1.6, with a graphical interface for MacOS and Linux, including new routines in parallel. *Cladistics*, ***39*,** 144-153 (2023).

Harshman, J., Huddleston, C. J., Bollback, J. P., Parsons, T. J., & Braun, M. J. True and false gharials: a nuclear gene phylogeny of Crocodylia. *Syst. Biol.* **52,** 386-402 (2003).

Hastings, A. K., Bloch, J. I., Jaramillo, C. A., Rincon, A. F., & Macfadden, B. J. Systematics and biogeography of crocodylians from the Miocene of Panama. *J. Vertebr. Paleontol.* **33,** 239-263 (2013).

Hastings, A. K., Schubert, B. W., Bourque, J. R. & Hulbert Jr, R. C. Oldest record of *Alligator* in southeastern North America. *Paleontol*. *Electron*. **26,** 1–19 (2023).

Holliday, C. M. & Witmer, L. M. The epipterygoid of crocodyliforms and its significance for the evolution of the orbitotemporal region of eusuchians. *J. Vertebr. Paleontol.* **29,** 715–733 (2009).

Holliday, C. M., Porter, W. R., Vliet, K. A. & Witmer, L. M. The frontoparietal fossa and dorsotemporal fenestra of archosaurs and their significance for interpretations of vascular and muscular anatomy in dinosaurs. *Anat. Rec.* **303,** 1060–1074 (2020).

Hutchison, C. S. Geological evolution of South-east Asia. Clarendon Press (1989).

Huxley, T. H. On *Stagonolepis robertsoni*, and on the evolution of the Crocodilia. *Quart*. *J. Geol*. *Soc*. **31,** 423–438 (1875).

Iijima, M., Takahashi, K. & Kobayashi, Y. The oldest record of *Alligator sinensis* from the Late Pliocene of Western Japan, and its biogeographic implication. *J. Asian Earth Sci.* **124,** 94–101(2016).

Iordansky, N. N. The skull of the Crocodilia. *Biol. Reptil*. **4,** 201–262 (1973).

Kälin, J. A. *Arambourgia* nov. gen. *gaudryi* de Stefano sp., ein kurzschnauziger Crocodilide aus den Phosphoriten des Quercy. *Eclogae Geol. Helv*. **32,** 185–186 (1940).

Kuzmin, I. T. *et al.* Braincase anatomy of extant Crocodylia, with new insights into the development and evolution of the neurocranium in crocodylomorphs. *J. Anat.*, **239,** 983–1038 (2021).

Lauren, D. J. The effect of chronic saline exposure on the electrolyte balance, nitrogen metabolism, and corticosterone titer in the American alligator, *Alligator mississipiensis*. *Comp. Biochem. Physiol.* **81,** 217–223 (1985).

Lee, M. S., & Yates, A. M. (2018). Tip-dating and homoplasy: reconciling the shallow molecular divergences of modern gharials with their long fossil record. *Proceedings of the Royal Society B*, *285*(1881), 20181071.

Li, J. & B. Wang. A new species of *Alligator* from Shanwang, Shandong. *Vert. PalAs.* **7,** 199–207 (1987).

Loomis, F. B. Two new river reptiles from the Titanothere Beds. *Am. J. Sci*. **18,** 1880–1910 (1904).

Markwick, P. J. (1998). Fossil crocodilians as indicators of Late Cretaceous and Cenozoic climates: implications for using palaeontological data in reconstructing palaeoclimate. *Palaeogeography, Palaeoclimatology, Palaeoecology*, *137*(3-4), 205-271.

Martin, J. E. A new species of *Diplocynodon* (Crocodylia, Alligatoroidea) from the Late Eocene of the Massif Central, France, and the evolution of the genus in the climatic context of the Late Palaeogene. *Geological Magazine*, **147,** 596-610 (2010).

Martin, J. E., & Lauprasert, K. A new primitive alligatorine from the Eocene of Thailand: relevance of Asiatic members to the radiation of the group. *Zool. J. Linn. Soc.* **158,** 608-628 (2010).

Martin, J. E., Smith, T., de Lapparent de Broin, F., Escuillié, F., & Delfino, M. Late Palaeocene eusuchian remains from Mont de Berru, France, and the origin of the alligatoroid *Diplocynodon*. *Zool. J Linn. Soc.* **172,** 867-891 (2014).

Massare, J. A. Swimming capabilities of Mesozoic marine reptiles in *The mechanics and physiology of animal swimming* (eds. Maddock, L., Bone, Q. & Rayner, J.M.V.) 133–147 (Cambridge University Press, 1994).

Massonne, T., Vasilyan, D., Rabi, M. & Böhme, M. A new alligatoroid from the Eocene of Vietnam highlights an extinct Asian clade independent from extant *Alligator sinensis*. *PeerJ*, **7,** e7562; https://doi.org/10.7717/peerj.7562 (2019).

Miller-Camp, J. *Patterns in alligatorine evolution*. The University of Iowa. PhD Thesis. (2016).

Miller-Camp, J. & C. Brochu. Crocodyliforms – Large-bodied carnivores in *Messel: An Ancient Greenhouse Ecosystem* (eds. Smith, K.T., Schaal, S.F.K. & Habersetzer, J.) 302–313 (Stuttgart: Schweizerbart, 2018).

Miller, K. G., Fairbanks, R. G., & Mountain, G. S. Tertiary oxygen isotope synthesis, sea level history, and continental margin erosion. *Paleoceanography*, ***2*****,** 1-19 (1987).
Mook, C. C. A new Pliocene alligator from Nebraska. *Am*. *Mus*. *Novit*. **1311,** 295–304 (1946).

Norell, M. A., Clark, J. M. & Hutchison, J. H. The Late Cretaceous alligators *Brachychampsa montana* (Crocodylia): new material and putative relationships. *Am*. *Mus*. *Novit*. **3116,** 1–26 (1994).

Oaks, J. R. A time-calibrated species tree of Crocodylia reveals a recent radiation of the true crocodiles. *Evolution: Int*. *J*. *Org*. *Evol*. **65,** 3285–3297. (2011).

Oleinik, A., Marincovich Jr, L., Barinov, K. B., & Swart, P. K. (2009). Magnitude of Middle Miocene warming in North Pacific high latitudes: stable isotope evidence from

Kaneharaia (Bivalvia, Dosiniinae). *Bulletin of the Geological Survey of Japan*, *59*(7-8), 339-353.

Opdyke, N. D. Magnetic stratigraphy of Cenozoic terrestrial sediments and mammalian dispersal. *J. Geol.*, **98,** 621-637 (1990).

Ősi, A. & Barrett, P. M. Dental wear and oral food processing in *Caiman latirostris*: analogue for fossil crocodylians with crushing teeth. *N. Jb. Geol. Paläeont. Abh*. **261,** 201–207 (2011).

Ősi, A. The evolution of jaw mechanism and dental function in heterodont crocodyliforms. *Hist. Biol.* **26,** 279–414 (2014).

Pan, T. *et al*. Historical population decline and habitat loss in a critically endangered species, the Chinese alligator (*Alligator sinensis*). *Glob. Ecol. Conserv.* **20,** e00692; https://doi.org/10.1016/j.gecco.2019.e00692 (2019).

Rio, J. P. & Mannion, P. D. Phylogenetic analysis of a new morphological dataset elucidates the evolutionary history of Crocodylia and resolves the long-standing gharial problem. *PeerJ*, 9, e12094; https://doi.org/10.7717/peerj.12094 (2021).

Salas-Gismondi, R. *et al*. O. A Miocene hyperdiverse crocodylian community reveals peculiar trophic dynamics in proto-Amazonian mega-wetlands. *Proc. Royal Soc. B* **282,** 20142490; https://doi.org/10.1098/rspb.2014.2490 (2015).

Salisbury, S. W. & Willis, P. M. A. A new crocodylian from the early Eocene of south-eastern Queensland and a preliminary investigation of the phylogenetic relationships of crocodyloids. *Alcheringa* **20,** 179–226 (1996).

Schmidt, K. P. A new fossil alligator from Nebraska. *Fieldiana: Geol.* **8,** 27–32 (1941).

Shan, H. Y., Cheng, Y. N. & Wu, X. C. The first fossil skull of *Alligator sinensis* from the Pleistocene, Taiwan, with a paleogeographic implication of the species. *J. Asian Earth Sci.* **69,** 17–25 (2013).

Snyder, D. Morphology and systematics of two Miocene alligators from Florida, with a discussion of *Alligator* biogeography. *J. Paleontol*. **81,** 917–928 (2007).

Stocker M.R., Brochu C.A., Kirk E.C. A new caimanine alligatorid from the Middle Eocene of Southwest Texas and implications for spatial and temporal shifts in Paleogene crocodyliform diversity. *PeerJ*. **9**:e10665 (2021).

Sung, Y. H., Hau, B. C. & Karraker, N. E. Diet of the endangered big-headed turtle *Platysternon megacephalum*. *PeerJ*, **4,** e2784; https://doi.org/10.7717/peerj.2784 (2016).

Suraprasit, K. *et al*. A complete skull of Crocuta crocuta ultima indicates a late Middle Pleistocene age for the Khok Sung (northeastern Thailand) vertebrate fauna. *Quat*. *Int*. **374,** 34–45 (2015).

Suraprasit, K. *et al.* The Middle Pleistocene Vertebrate Fauna from Khok Sung (Nakhon Ratchasima, Thailand): Biochronological and Paleobiogeographical Implications. *ZooKeys* **613,** 1–157 (2016).

Suraprasit, K., Jaeger, J. J., Chaimanee, Y. & Sucharit, C. Taxonomic reassessment of large mammals from the Pleistocene *Homo*-bearing site of Tham Wiman Nakin (Northeast Thailand): relevance for faunal patterns in mainland Southeast Asia. *Quat*. *Int*. **603,** 90–112 (2021).

Taplin, L. E. & Grigg, G. C. Historical zoogeography of the eusuchian crocodilians: a physiological perspective. *Am. Zool.* **29,** 885–901 (1989).

Thorbjarnarson, J. & Wang, X. The Chinese alligator: ecology, behavior, conservation, and culture. (JHU Press, 2010).

Wang Y., Sullivan, C. & Liu, J. Taxonomic revision of *Eoalligator* (Crocodylia, Brevirostres) and the paleogeographic origins of the Chinese alligatoroids. *PeerJ* **4,** e2356; https://doi.org/10.7717/peerj.2356 (2016).

West, C. K., Greenwood, D. R., & Basinger, J. F. (2015). Was the Arctic Eocene 'rainforest'monsoonal? Estimates of seasonal precipitation from early Eocene megafloras from Ellesmere Island, Nunavut. *Earth and Planetary Science Letters*, *427*, 18-30.

White, T. E. A new alligator from the Miocene of Florida. *Copeia*, **1942,** 3–7 (1942).

Young, M. T. *et al*. Convergent evolution and possible constraint in the posterodorsal retraction of the external nares in pelagic crocodylomorphs. *Zool. J. Linn. Soc.*, **189,** 494–520 (2020).

Zachos, J., Pagani, M., Sloan, L., Thomas, E., & Billups, K. Trends, rhythms, and aberrations in global climate 65 Ma to present. *science*, **292,** 686-693 (2001).

SUPPLEMENTARY INFORMATION

All data generated or analysed during this study are included in this published article (and its Supplementary Information files). Raw CT scan data (DICOM stack format) is available on the following link to MorphoSource Ark repository:

http://n2t.net/ark:/87602/m4/490374.

Supplementary Material 1. Complete geological settings, supplementary figures, and list of synapomorphies.

Supplementary Material 1

Institutional abbreviations. AMNH, American Museum of Natural History, New York, New York, USA; DMR–Department of Mineral Resources, Bangkok, Thailand; YPM-PU, Yale Peabody Museum-Princeton University collection, New Haven, Connecticut, USA.

Geological setting, faunal assemblage, and age

The fossil site is located at Ban Si Liam, Mai Subdistrict, Non Sung district, Nakhon Ratchasima Province in northeastern Thailand (Fig. 1a, b). In 2005, the square-shaped pond with an area of 8 m long x 8.4 m wide x 2 m deep was dug out by the villagers and yielded some vertebrate fossils (Supplementary Fig. 1). Regarding the stratigraphic profile of Ban Si Liam (Fig. 1c), the dark-colored topsoil is 30 cm in thickness and organic-rich in content, underlain by yellowish medium- to fine-grained sands with the thickness of 2 m. Some fragments of ancient pottery and ceramics were collected from the topsoil but vertebrate fossils (nine specimens) were entirely found from the yellowish sandy layer that overlies a thin layer of indurated iron oxide (10 cm thick), followed by the yellowish clay at the lowermost part of the pond. Three reptile fossils included a fragment of a turtle carapace (DMR-BSL2011-1) and a nearly complete cranium of an alligator (DMR-BSL2011-2), both of which have been previously reported by Claude et al. (2011), as well as a crocodylian vertebra represented by a well-preserved centrum and neural arch tentatively assigned as the fourteenth dorsal vertebra (DMR-BSL2011-3; Supplementary Fig. 2).

In addition to the alligator's skull described here in this study, fossils of two mammalian species collected from the same layer were identified as belonging to a wild

water buffalo (*Bubalus arnee*) and a sambar deer (*Rusa unicolor*) based on the comparisons of morphological features and dimensions with extant comparative specimens and fossils recovered nearby (i.e. the late Middle Pleistocene fauna from Khok Sung, Suraprasit et al., 2016). Six mammalian remains included two mandibular specimens (DMR-BSL2011-4 and DMR-BSL2011-8), a horn core fragment (DMR-BSL2011-5), and a cervical vertebra (DMR-BSL2011-9) of a wild water buffalo *Bubalus arnee* as well as a mandible (DMR-BSL2011-6) and a femur (DMR-BSL2011-7) of a sambar deer *Rusa unicolor* (Supplementary Fig. 3).

Although the right mandible DMR-BSL2011-4 (designated as *Bubalus arnee*) possesses a very worn p3 to m2, the p3 shows a shallower posterior valley than a medial one, which is a typical feature of *Bubalus* (Suraprasit et al., 2021) (Supplementary Fig. 3a, b). The horn core fragment DMR-BSL2011-5 is suboval in cross-section outline with a more flattened surface on the anterior side (Supplementary Fig. 3c). The left mandible DMR-BSL2011-6, assigned to *Rusa unicolor*, is characterized by well-developed conids and stylids on cheek teeth as well as basal pillars on molars, similar to extant sambar deer (Suraprasit et al., 2016, 2021) (Supplementary Fig. 3d, e) The sizes of cheek teeth embedded in these two jaws (DMR-BSL2011-4 and DMR-BSL2011-6) are comparable to those of extant wild water buffalo and sambar deer specimens, respectively (Table.1) (see Suraprasit et al. (2016; figs 22 and 27) and Suraprasit et al. (2021; tab. 5) for more detailed measurements and comparisons). The right femur DMR-BSL2011-7 is similar in morphology and size to extant *Rusa unicolor* (see Suraprasit et al., 2021; appendix 10) (Supplementary Fig. 3f). The fragmentary mandible DMR-BSL2011-8 preserves portions of a condyle, ascending ramus, and mandibular foramen and angle (Supplementary Fig. 3g). According to the size and shape, this mandibular fragment and the sixth cervical vertebra DMR-BSL2011-9 are assigned to *Bubalus arnee* (Supplementary Fig. 3h).

Supplementary figure 1. The fossil site of Ban Si Liam in Non Sung district (Nakhon Ratchasima), photo taken during the excavation.

Despite the ages of the possible Late Miocene to Pleistocene having previously been proposed by Claude et al. (2011), the two living mammal species contemporaneous with an alligator suggest a more limited range of faunal ages possibly spanning from the late Middle Pleistocene to Holocene because the presence of these taxa is congruent with fossils records from some late Middle Pleistocene localities in Thailand (Tham Wiman Nakin (dated to >169 ka, Esposito et al., 1998, 2002; Suraprasit et al., 2021)) and Khok Sung (dated to either 217 or 130 ka, Suraprasit et al., 2016; Duval et al., 2019). Moreover, the stratigraphic position of a fossiliferous layer at Ban Si Liam is quite shallow (around 2 m below the surface, Fig. 1c), compared to other Late Miocene sedimentary deposits along the Mun River systems (i.e. around 10 to 20 m deep in Tha Chang sandpits, Chaimanee et al. (2004)).

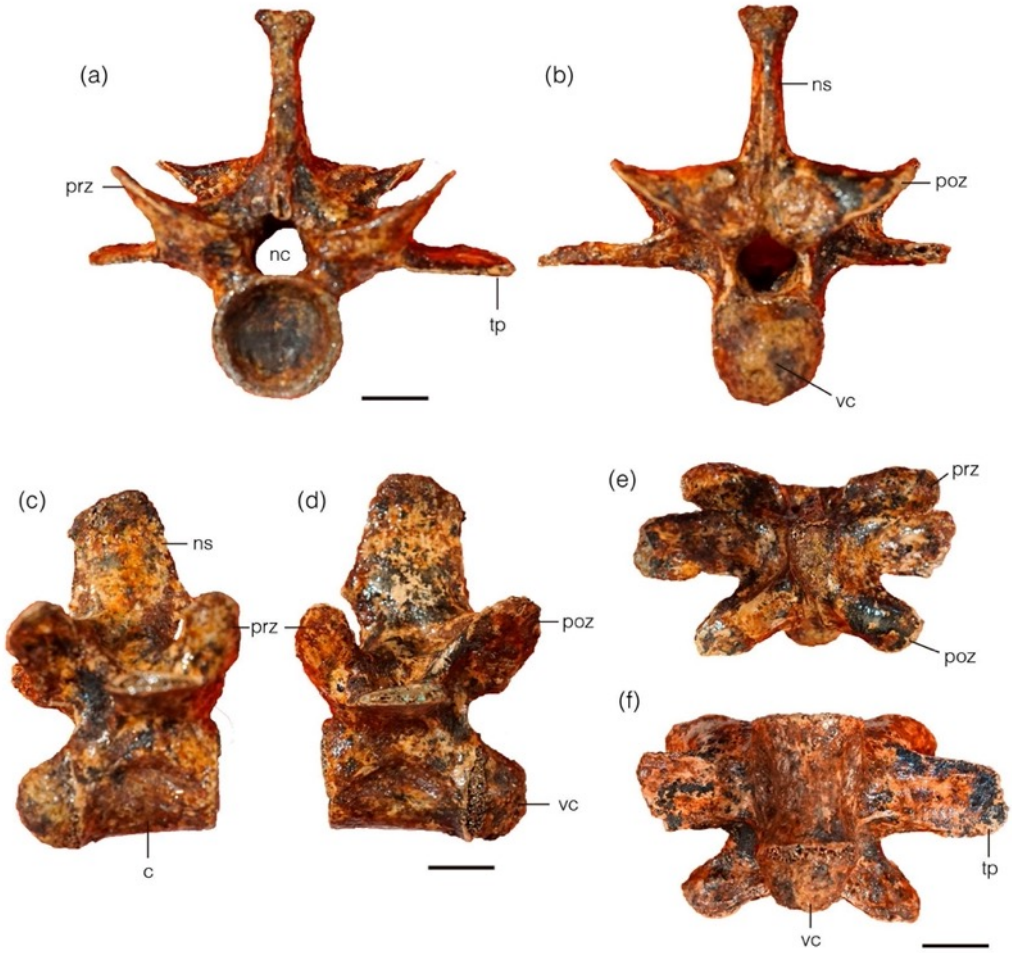

Supplementary figure 2. Crocodilian vertebra (DMR-BSL2011-3) tentatively assigned as the fourteenth dorsal vertebra in anterior (**a**), posterior (**b**), right lateral (**c**), left lateral (**d**), dorsal (**e**), and ventral (**f**) views. Abbreviations: c, centrum; nc, neural canal; ns, neural spine; poz, postzygapophysis; prz, prezygapophysis; tp, transverse process; vc, vertebral condyle. Scale bar: 1 cm. Figure generated using Adobe Illustrator CC.

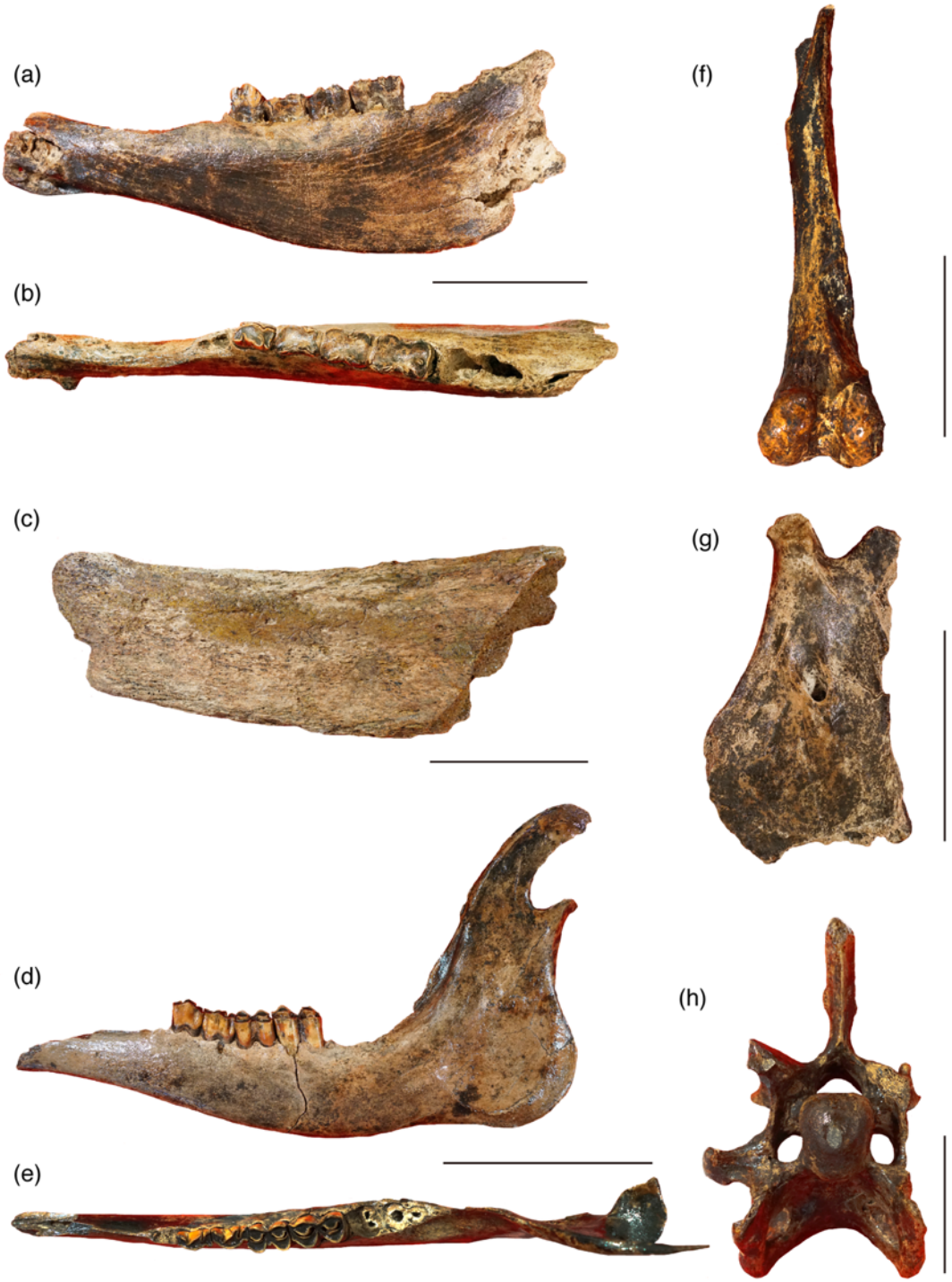

Supplementary figure 3. Mammalian remains from the fossil site of Ban Si Liam, same layer of *Alligator munensis* sp. nov., here assigned as *Bubalus arnee* (**a–c, g, h**), and *Rusa unicolor* (**d–f**). Right mandible (DMR-BSL2011-4) in medial (**a**) and occlusal (**b**) views; horn core fragment (DMR-BSL2011-5) in dorsal view (**c**); left mandible (DMR-BSL2011-6) in lateral

(**d**) and occlusal (**e**) views; femur (DMR-BSL2011-7) in posterior view (**f**); fragmentary mandible (DMR-BSL2011-8) in medial view (**g**); and cervical vertebra (DMR-BSL2011-9) in anterior view (**h**). Scale bar: 10 cm (a–g); 5 cm (h). Figure generated using Adobe Illustrator CC.

Table 1. Dental measurements of cheek teeth of ruminants from Ban Si Liam.

Specimen no.	**Teeth**	**L**	**W**
		(mm)	**(mm)**
Bubalus arnee			
DMR-BSL2011-4	p3 (right)	21.36	14.50
	p4 (right)	25.41	16.42
	m1 (right)	26.21	18.82
	m2 (right)	31.33	21.36
Rusa unicolor			
DMR-BSL2011-6	p3 (left)	14.80	8.62
	p4 (left)	15.22	9.66
	m1 (left)	18.80	12.55
	m2 (left)	22.92	14.43

Phylogenetic analysis

New added taxa

Alligator munensis Darlim et al. (2023) (holotype, DMR-BSL2011-2);
Alligator luicus Li and Wang, 1987 (holotype, LPM 850001);
'Penghu' *Alligator* Shan et al. 2013 (NMNS006394-F051722).

Scoring modifications and new character proposals

Based on extensive review of the morphology of *Alligator* species, some characters states were modified accordingly and three new characters were proposed as follows:

Character 4. External nares, anterior margin thickness, ratio of distance between anterior margin of nares and anterior margin of rostrum to maximum anteroposterior length of external nares in dorsal view: <0.5 (0); 0.5 (1) (Rio and Mannion, 2021 after Hastings et al., 2010; Groh et al., 2020).

Alligator olseni ? → 0
Alligator prenasalis ? → 0

Character 9. Cranial table shape, minimum angle subtended by the posterolateral cranial table margin and sagittal axis of skull: < 10 (0); 10 (1) (Rio and Mannion, 2021 new character, after Brochu and Storrs, 2012).

Alligator mississippiensis 1 → 0
Alligator sinensis 1 → 0
Alligator prenasalis 0 → 1

Character 12. Incisive foramen size, ratio of maximum mediolateral width to the mediolateral width of the rostrum at the premaxilla-maxilla suture: < 0.3 (0); 0.3 (1) (Rio and Mannion, 202 after Brochu, 1997; Jouve et al., 2008; Groh et al., 2020).

Alligator mississippiensis 0 → 1

Character 31. Rostral ornamentation, transverse ridge between the orbits (i.e. spectacle): absent (0); present (1) (Rio and Mannion, 2021 after Barrios, 2011; Cidade et al., 2017; Lee and Yates, 2018)

Alligator mcgrewi 0 → 1

Character 32. Rostral ornamentation, morphology of the transverse orbital ridge (i.e. spectacle): low, lacking a posterior fossa (0); tall, with deep posterior fossa (1) (new character of Rio and Mannion, 2021).

Alligator mcgrewi ? → 0

Character 33. Rostral ornamentation: anterior extent of transverse bridge between orbits (i.e. spectacle): posterior to anterior orbital margin (0); level with or anterior to anterior orbitalmargin (1) (new character by Rio and Mannion, 2021 after Cossette and Brochu, 2018).

Alligator mcgrewi ? → 0

Character 41. External nares, orientation: projects anterodorsally (0); dorsally (1) (Rio and Mannion, 2021 after Brochu, 1997).

Alligator mcgrewi 0 → 1

Character 70. Frontal, ornamentation, midsagittal crest on fused frontals: absent (0); or present (1) (Rio and Mannion, 2021 after Brochu and Storrs, 2012 [188]).

Alligator mcgrewi 0 → 1
Alligator sinensis 0 → 0/1 (sample shows polymorphism)

Character 79. Supraoccipital, posterolateral tuberosities in dorsal view: not visible (0); visible (1) (Rio and Mannion, 2021 after Jouve, 2004; in Jouve, 2016)

Alligator mcgrewi 0/1 → 1

Character 83. Parietal, sagittal crest between supratemporal fenestrae: absent (0); present (1) (Rio and Mannion, 2021 after Clark, 1994; Pol et al., 2009).

Alligator sinensis 0 → 1

Alligator mcgrewi 0 → 1

Character. 121. Quadrate, posterior ramus length: distance between posterior margin of quadrate condyle and the level of the anterior margin of the occipital condyle, less than quadrate condyle mediolateral width (0); equal to or greater than quadrate condyle mediolateral width (1) (Rio and Mannion, 2021 after Buscalioni et al., 2011).

Alligator sinensis 1 → 0

Character 138. Incisive foramen, anterior margin intersection with premaxillary tooth row: absent (anterior margin around 2nd or 3rd alveolus) (0); present (projects between or abuts first premaxillary teeth) (1) (Rio and Mannion 2021 after Brochu, 1997).

Alligator sinensis 1 → 0

Character 169. Suborbital fenestra, lateral margin shape: straight (0); projecting medially into fenestra (1) (Rio and Mannion, 2021 rephrased from Brochu, 1997).

Alligator sinensis 0 → 1

Alligator mefferdi ? → 0

Alligator olseni 1 → 0

Alligator prenasalis 0 → 1

Caiman latirostris 0 → 1

Melanosuchus niger 0 → 1

Wannaganosuchus brachymanus 0 →1

Character 170. Suborbital fenestra, contribution of maxilla to medial projection: (0) absent, projection entirely formed by ectopterygoid; (1) present.

Alligator sinensis ? → 1

Caiman latirostris ? → 1

Melanosuchus niger ? → 1
Wannaganosuchus brachymanus ? →1

In all species in which the maxilla projects medially into the suborbital fenestra, the maxillary surface at the projection is rugose. Although, the poor preservation of *Globidentosuchus brachyrostris* (Scheyer et al., 2013) hampers a precise evaluation of the presence or absence of a rugosity in the area.

Character 171. Suborbital fenestra, posterolateral margin shape at ectopterygoid-pterygoid suture intersection: straight (0); bowed anteromedially (1) (Rio and Mannion, 2021 after Brochu, 1997; Brochu, 2010).

Alligator mcgrewi 0 → 1

Character 196. Choanae, morphology of posterior wall: not notched, or with broadly rounded notch (0); acutely notched (1) (Rio and Mannion 2021 after Brochu, 1997).

Alligator mefferdi 1 → ?

Character 218. Dentary, dorsoventral height at the level of alveoli 1–4 relative to alveoli 11–12: at the same level or higher (0); lower (1) (Rio and Mannion 2021 adapted from Bona, 2007; Pinheiro et al., 2013; Cidade et al., 2017).

Alligator sinensis 0 → 1

*Probably related to ontogeny based on limited sample. Smaller younger specimens have condition 0

Character 219. Dentary, numerical position of largest alveolus posterior to 4th dentary alveolus: 13 and/or 14 (0); 13 and/or 14 and a posterior series (1); 10, 11 and/or 12 (2); no differentiation posterior to 4th alveolus (3); posterior to 14 (4) (Rio and Mannion, 2021 after Brochu, 2004; Brochu, 2010; Brochu, 2011).

Alligator mcgrewi 1 → 0
Alligator olseni 1 → 0

Character 299. Scapula, deltoid crest shape: thin, with sharp margin (0); wide, with broadmargin (1) (Rio and Mannion, 2021 after Brochu, 1997).

Alligator olseni 0 → 1

New character proposals

[new] Character 331. Palatine, shape of palatine shelf: rounded (0); forming a pointed tip (1)

The palatine shelf in *Alligator* species varies in morphology: in *A. mefferdi*, *A. mississippiensis*, *A. olseni* and *A. sinensis* a broad palatine shelf is present, whereas in *A. mcgrewi* and *A. munensis*, the lateral shelf is more acute and laterally projected. The palatines are not observed *A. luicus* and in the 'Penghu' *Alligator*.

Alligator luicus → ?

Alligator mcgrewi → 1

Alligator mefferdi → 0

Alligator mississippiensis → 0

Alligator munensis → 1

Alligator olseni → 0

Alligator prenasalis → 0

Alligator sinensis → 0

Penghu *Alligator* → ?

[new] Character 332. External nares, posterior border: flat (0); raised (1)

The external nares of *Alligator* are bisected by the internarial bar formed by the nasals. The posterior border of the external nares, at the base of the internarial bar, is raised in *A. luicus*, *A. mcgrewi*, *A. munensis*, *A. sinensis*, and in the 'Penghu' *Alligator*. Such elevation of the posterior border of the external nares hence emphasizes a depression immediately posterior to it. A flat surface of the posterior border of the external nares is present in *A. mefferdi*, *A. mississippiensis*, *A. olseni*, and *A. prenasalis* instead.

Alligator luicus → 1

Alligator mcgrewi → 1

Alligator mefferdi → 0

Alligator mississippiensis → 0

Alligator munensis → 1

Alligator olseni → 0

Alligator prenasalis → 0

Alligator sinensis → 1

Penghu *Alligator* →1

[new] Character 333. Pterygoid, shape of tall pterygoid process: dorsoventrally expanded (0); tubera-like (1).

In *Alligator* species, a tall pterygoid process is present, although a variation in the shape of this process is observed: A posteriorly or postero-ventrally pointed process (tubera-like) is present in *A. mcgrewi*, *A. munensis*, and *A. sinensis*, whereas a tall and flat process is present in *A. mississippiensis*, *A. olseni*, and *A. prenasalis*. The pterygoid process of the 'Penghu' *Alligator* and of *A. luicus* is not preserved.

Alligator luicus → ?

Alligator mcgrewi → 1

Alligator mefferdi → 0

Alligator mississippiensis → 0

Alligator munensis → 1

Alligator olseni → 0

Alligator prenasalis → 0

Alligator sinensis → 1

Penghu *Alligator* → ?

Comparison between the scorings of Penghu *Alligator* x *Alligator sinensis*

Character 221. Mandibular symphysis, posterior extent, adjacent to number of full dentary alveoli: <6 (0); 6–8 (1); 9–12 (2): 13–20 (3); >20 (4) (Rio and Mannion, 2021 after Jouve, 2004; Brochu, 2004; Salas-Gismondi et al., 2016) (ORDERED).

Alligator sinensis → 1
Penghu *Alligator* → 0

List of synapomorphies from consensus tree of the phylogenetic analysis.

Node 149 :
Char. 36: 1 --> 2
Char. 110: 0 --> 1
Char. 145: 3 --> 0
Char. 253: 1 --> 0
Node 150 :
Char. 48: 0 --> 1
Char. 52: 0 --> 1
Char. 129: 0 --> 1
Char. 180: 1 --> 0
Char. 189: 1 --> 2
Node 151 :
Char. 56: 0 --> 1
Char. 144: 1 --> 0
Char. 272: 1 --> 0
Char. 273: 1 --> 0
Char. 308: 0 --> 1
Node 152 :
Char. 31: 1 --> 0
Char. 307: 0 --> 1
Node 153 :
Char. 27: 1 --> 0
Char. 138: 0 --> 1
Char. 153: 0 --> 1
Node 154 :
Char. 2: 0 --> 1
Char. 48: 1 --> 0
Char. 93: 1 --> 2
Char. 161: 0 --> 1
Node 155 :
Char. 56: 1 --> 0
Char. 155: 1 --> 0
Char. 220: 1 --> 0
Node 156 :
Char. 27: 0 --> 1
Char. 32: 0 --> 1
Char. 71: 0 --> 1
Char. 184: 0 --> 1
Node 157 :
Char. 221: 0 --> 2
Node 158 :
Char. 255: 0 --> 1
Node 159 :
Char. 9: 1 --> 0
Char. 77: 01 --> 2
Char. 117: 1 --> 2
Node 160 :
Char. 80: 0 --> 1
Node 161 :
Char. 2: 1 --> 0
Char. 61: 0 --> 1
Char. 84: 0 --> 1
Char. 161: 1 --> 0
Char. 217: 1 --> 0
Char. 256: 0 --> 1
Char. 322: 1 --> 2
Node 162 :
Char. 54: 0 --> 1
Char. 66: 0 --> 1
Char. 99: 0 --> 1
Char. 145: 0 --> 3
Char. 180: 0 --> 12
Char. 229: 0 --> 1
Node 163 :
Char. 219: 1 --> 2
Char. 221: 2 --> 0
Node 164 :
Char. 218: 2 --> 0
Node 165 :
Char. 75: 1 --> 0
Char. 141: 0 --> 1
Char. 146: 3 --> 2
Char. 150: 1 --> 0
Char. 162: 1 --> 0
Char. 167: 0 --> 1
Char. 194: 2 --> 1
Char. 216: 0 --> 1
Char. 217: 0 --> 1
Node 166 :
Char. 31: 0 --> 1
Char. 74: 0 --> 1
Char. 86: 1 --> 2
Node 167 :
Char. 24: 0 --> 1
Char. 71: 1 --> 0
Char. 222: 0 --> 1
Char. 328: 0 --> 1
Node 168 :
Char. 86: 0 --> 1
Char. 93: 0 --> 1
Char. 102: 0 --> 1
Char. 151: 0 --> 1
Char. 179: 0 --> 1
Char. 221: 0 --> 2
Char. 228: 0 --> 1
Char. 327: 1 --> 2
Node 169 :
Char. 30: 0 --> 1
Char. 103: 0 --> 1
Char. 104: 1 --> 0
Char. 141: 1 --> 0
Char. 192: 1 --> 0
Char. 194: 0 --> 2
Char. 240: 0 --> 1
Char. 244: 0 --> 1
Char. 247: 0 --> 1
Char. 250: 1 --> 0
Node 170 :
Char. 57: 1 --> 0
Char. 89: 0 --> 1
Char. 241: 1 --> 0
Char. 278: 1 --> 0
Char. 300: 0 --> 1
Char. 304: 0 --> 1
Char. 305: 0 --> 1
Char. 323: 1 --> 2
Char. 326: 0 --> 1
Node 171 :
Char. 83: 0 --> 1
Char. 117: 0 --> 1
Char. 153: 0 --> 1
Char. 233: 0 --> 1
Node 172 :
Char. 120: 0 --> 1
Char. 130: 0 --> 1
Char. 249: 0 --> 1
Char. 250: 0 --> 1
Node 173 :
Char. 116: 0 --> 1
Char. 186: 0 --> 1
Char. 187: 1 --> 2
Char. 192: 0 --> 1
Char. 244: 1 --> 0
Node 174 :
No synapomorphies
Node 175 :
Char. 48: 0 --> 1
Char. 52: 0 --> 1
Char. 102: 0 --> 1
Char. 141: 12 --> 3
Char. 146: 3 --> 6
Char. 151: 0 --> 1
Char. 155: 0 --> 2
Char. 165: 0 --> 1
Char. 173: 0 --> 1
Node 176 :
Char. 53: 0 --> 1
Char. 87: 1 --> 0
Char. 92: 0 --> 1
Char. 108: 1 --> 0
Char. 123: 0 --> 1
Node 177 :
Char. 30: 0 --> 1
Char. 146: 3 --> 2
Char. 174: 0 --> 12
Char. 221: 0 --> 2
Char. 228: 0 --> 1
Char. 246: 0 --> 1
Node 178 :
Char. 109: 1 --> 2
Char. 118: 2 --> 0
Char. 132: 0 --> 1
Char. 178: 0 --> 1
Node 179 :
Char. 79: 0 --> 1
Char. 125: 0 --> 1
Char. 213: 1 --> 0
Char. 244: 0 --> 1
Node 180 :

Char. 2: 0 --> 1
Char. 16: 0 --> 1
Node 181 :
Char. 62: 0 --> 1
Char. 107: 0 --> 1
Char. 157: 0 --> 1
Char. 200: 0 --> 1
Node 182 :
Char. 89: 1 --> 0
Char. 104: 1 --> 0
Char. 146: 15 --> 7
Char. 180: 2 --> 0
Char. 303: 1 --> 0
Node 183 :
Char. 138: 1 --> 0
Char. 148: 0 --> 1
Char. 182: 1 --> 0
Char. 252: 0 --> 1
Char. 301: 1 --> 0
Node 184 :
Char. 88: 1 --> 0
Char. 246: 1 --> 0
Node 185 :
Char. 106: 0 --> 1
Char. 205: 1 --> 0
Node 186 :
Char. 46: 1 --> 2
Char. 78: 0 --> 1
Char. 172: 1 --> 0
Char. 279: 0 --> 1
Char. 327: 1 --> 0
Node 187 :
Char. 45: 0 --> 1
Char. 97: 0 --> 1
Char. 138: 0 --> 1
Char. 174: 1 --> 0
Char. 219: 1 --> 0
Char. 223: 1 --> 2
Node 188 :
Char. 18: 1 --> 0
Char. 74: 1 --> 2
Char. 135: 0 --> 1
Char. 143: 0 --> 1
Char. 150: 1 --> 2
Char. 153: 1 --> 0
Char. 182: 0 --> 1
Char. 190: 1 --> 0
Char. 220: 1 --> 2
Char. 236: 1 --> 2
Node 189 :
Char. 40: 0 --> 1
Char. 117: 1 --> 0
Char. 146: 3 --> 1
Char. 239: 1 --> 0
Char. 246: 0 --> 1
Char. 274: 0 --> 1
Node 190 :
Char. 116: 1 --> 0
Char. 174: 0 --> 1
Char. 307: 0 --> 1

Node 191 (*A. mcgrewi* + *A. munensis*):
Char. 108: 1 --> 2
Node 192 :
Char. 0: 1 --> 0
Node 193 :
Char. 120: 1 --> 0
Char. 220: 0 --> 1

Node 194 (*A. mcgrewi* + Asian *Alligator* species):
Char. 69: 0 --> 1
Char. 82: 0 --> 1
Char. 161: 1 --> 0
Char. 331: 0 --> 1

Node 195 ("*A. sinensis*-clade"):
Char. 168: 0 --> 1

Node 196 (crown *Alligator*):
Char. 30: 0 --> 1
Char. 40: 0 --> 1
Char. 76: 0 --> 1
Char. 155: 1 --> 0
Char. 170: 0 --> 1
Char. 220: 1 --> 0
Char. 321: 0 --> 1

Node 197 (*Alligator*):
Char. 0: 0 --> 1
Char. 43: 0 --> 1
Char. 46: 1 --> 0
Char. 71: 0 --> 1
Char. 78: 0 --> 1
Char. 118: 1 --> 0
Node 198 :
Char. 31: 1 --> 0
Char. 252: 0 --> 1
Char. 261: 0 --> 1

Node 199 (*A. mississippiensis*-clade):
Char. 67: 0 --> 1
Char. 153: 0 --> 1
Char. 213: 0 --> 1
Char. 217: 1 --> 0
Char. 219: 2 --> 1
Char. 221: 0 --> 2
Char. 243: 0 --> 1
Node 200 :
Char. 48: 1 --> 0
Char. 226: 0 --> 1
Node 201 :
Char. 136: 0 --> 1
Char. 235: 0 --> 1
Char. 241: 1 --> 0
Node 202 :
Char. 52: 0 --> 1
Char. 154: 0 --> 1
Node 203 :
Char. 26: 0 --> 1
Node 204 :
Char. 96: 0 --> 1
Node 205 :
Char. 71: 1 --> 0
Char. 158: 0 --> 1
Char. 161: 1 --> 2
Char. 221: 0 --> 1
Char. 228: 0 --> 1
Node 206 :
Char. 40: 1 --> 0
Char. 75: 0 --> 1
Char. 306: 0 --> 1
Node 207 :
Char. 9: 1 --> 0
Char. 104: 1 --> 0
Char. 213: 1 --> 0
Char. 325: 0 --> 1
Node 208 :
Char. 220: 0 --> 1
Node 209 :
Char. 245: 0 --> 1
Node 210 :
Char. 35: 0 --> 1
Char. 40: 0 --> 1
Char. 49: 0 --> 1
Char. 150: 1 --> 2
Char. 194: 0 --> 2
Char. 225: 1 --> 0
Char. 246: 1 --> 0
Node 211 :
Char. 117: 0 --> 1
Char. 176: 0 --> 1
Char. 197: 0 --> 1
Node 212 :
Char. 144: 0 --> 1
Char. 161: 2 --> 1
Char. 196: 0 --> 1
Node 213 :
Char. 98: 0 --> 1
Char. 220: 1 --> 0
Char. 221: 1 --> 2
Node 214 :
Char. 158: 1 --> 0
Node 215 :
Char. 45: 0 --> 1
Char. 57: 1 --> 2
Node 216 :
Char. 57: 0 --> 1
Char. 62: 0 --> 1
Char. 141: 1 --> 0
Char. 167: 0 --> 1
Node 217 :
Char. 29: 0 --> 1
Node 218 :
Char. 74: 0 --> 1
Char. 114: 1 --> 0
Char. 234: 1 --> 0
Char. 235: 0 --> 1
Node 219 :
Char. 150: 1 --> 2
Char. 192: 1 --> 0
Node 220 :

Char. 14: 0 --> 1
Char. 16: 0 --> 1
Char. 71: 1 --> 0
Char. 324: 1 --> 0
Char. 327: 1 --> 2
Node 221 :
Char. 154: 0 --> 1
Node 222 :
Char. 57: 2 --> 1
Char. 61: 1 --> 0
Char. 75: 0 --> 1
Char. 77: 2 --> 1
Char. 140: 0 --> 1
Node 223 :
Char. 29: 0 --> 1
Char. 148: 0 --> 1
Char. 156: 0 --> 1
Node 224 :
Char. 150: 1 --> 0
Node 225 :
Char. 26: 0 --> 1
Char. 114: 1 --> 0
Char. 154: 0 --> 2
Node 226 :
Char. 69: 0 --> 1
Node 227 :
Char. 61: 1 --> 0
Char. 136: 0 --> 2
Char. 219: 2 --> 1
Node 228 :
Char. 44: 0 --> 1
Char. 52: 0 --> 1
Node 229 :
Char. 165: 0 --> 1
Node 230 :
Char. 93: 0 --> 1
Node 231 :
Char. 29: 0 --> 1
Char. 112: 0 --> 1
Char. 145: 3 --> 2
Node 232 :
Char. 150: 1 --> 2
Char. 182: 0 --> 1
Node 233 :
Char. 61: 1 --> 0
Char. 264: 0 --> 1
Node 234 :
Char. 81: 0 --> 1
Char. 208: 0 --> 1
Node 235 :
Char. 2: 1 --> 0
Char. 32: 1 --> 0
Char. 114: 1 --> 0
Node 236 :
Char. 19: 0 --> 1
Char. 72: 0 --> 1
Char. 73: 1 --> 0
Char. 258: 0 --> 1
Char. 274: 1 --> 0
Node 237 :
Char. 28: 0 --> 1
Char. 164: 0 --> 1
Node 238 :
Char. 101: 1 --> 2
Node 239 :
Char. 50: 0 --> 1
Char. 77: 1 --> 0
Char. 174: 1 --> 2
Char. 320: 0 --> 1
Node 240 :
Char. 3: 0 --> 1
Char. 133: 0 --> 1
Char. 175: 0 --> 1
Char. 196: 1 --> 0
Char. 243: 0 --> 1
Node 241 :
Char. 40: 0 --> 1
Char. 75: 1 --> 0
Char. 135: 0 --> 1
Char. 173: 0 --> 1
Node 242 :
Char. 37: 0 --> 1
Char. 98: 1 --> 0
Node 243 :
Char. 95: 0 --> 1
Char. 274: 1 --> 0
Char. 315: 1 --> 0
Node 244 :
Char. 272: 1 --> 0
Node 245 :
Char. 208: 1 --> 2
Char. 209: 0 --> 1
Char. 236: 1 --> 2
Node 246 :
Char. 25: 1 --> 0
Node 247 :
Char. 29: 0 --> 1
Char. 73: 1 --> 0
Char. 166: 0 --> 1
Char. 204: 0 --> 1
Node 248 :
Char. 8: 0 --> 1
Char. 141: 1 --> 2
Char. 242: 0 --> 1
Node 249 :
Char. 5: 0 --> 1
Char. 196: 0 --> 1
Node 250 :
Char. 22: 0 --> 1
Char. 48: 0 --> 1
Char. 138: 1 --> 0
Char. 173: 1 --> 0
Char. 196: 0 --> 1
Char. 236: 2 --> 1
Node 251 :
Char. 109: 2 --> 1
Node 252 :
Char. 71: 1 --> 2
Char. 87: 1 --> 2
Char. 140: 1 --> 2
Char. 142: 0 --> 1
Node 253 :
Char. 10: 0 --> 1
Char. 60: 0 --> 1
Char. 78: 0 --> 1
Char. 127: 0 --> 1
Char. 166: 0 --> 1
Node 254 :
Char. 40: 0 --> 1
Char. 75: 1 --> 0
Char. 114: 1 --> 0
Char. 170: 0 --> 1
Char. 250: 0 --> 1
Node 255 :
Char. 72: 0 --> 1
Char. 183: 0 --> 1
Char. 189: 0 --> 1
Char. 193: 0 --> 1
Char. 263: 1 --> 0
Char. 326: 1 --> 0
Node 256 :
Char. 2: 1 --> 0
Char. 42: 0 --> 1
Node 257 :
Char. 43: 0 --> 1
Char. 62: 0 --> 1
Node 258 :
Char. 78: 0 --> 1
Char. 159: 0 --> 1
Node 259 :
Char. 10: 0 --> 1
Char. 53: 0 --> 1
Char. 81: 0 --> 1
Char. 89: 1 --> 0
Char. 106: 0 --> 1
Node 260 :
Char. 71: 1 --> 0
Char. 115: 0 --> 1
Char. 140: 1 --> 0
Char. 143: 1 --> 0
Char. 159: 1 --> 0
Char. 160: 0 --> 1
Char. 161: 0 --> 1
Node 261 :
Char. 63: 0 --> 1
Char. 74: 2 --> 01
Char. 135: 1 --> 0
Node 262 :
Char. 94: 0 --> 1
Node 263 :
Char. 71: 1 --> 0
Char. 74: 12 --> 0
Char. 135: 1 --> 0
Char. 234: 1 --> 0
Node 264 :
Char. 3: 0 --> 1
Char. 49: 0 --> 1
Char. 172: 1 --> 0
Node 265 :
Char. 165: 0 --> 1

Node 266 :
Char. 91: 1 --> 0
Char. 232: 0 --> 1
Node 267 :
Char. 140: 2 --> 1
Node 268 :
Char. 47: 0 --> 1
Char. 251: 1 --> 0
Node 269 :
Char. 198: 0 --> 1
Char. 242: 01 --> 2
Node 270 :
Char. 56: 1 --> 0
Char. 60: 0 --> 1
Char. 93: 0 --> 1
Node 271 :
Char. 8: 0 --> 1
Char. 189: 0 --> 3
Char. 234: 1 --> 2
Node 272 :
Char. 14: 0 --> 1
Char. 152: 0 --> 1
Node 273 :
Char. 52: 0 --> 1
Char. 146: 3 --> 0
Char. 192: 0 --> 1
Char. 200: 0 --> 1
Char. 244: 1 --> 0
Node 274 :
Char. 36: 1 --> 0
Char. 46: 1 --> 0
Char. 102: 0 --> 1
Char. 120: 0 --> 1
Char. 141: 12 --> 0
Char. 304: 0 --> 1
Char. 305: 0 --> 1
Node 275 :
Char. 57: 1 --> 0
Char. 82: 0 --> 1
Char. 187: 1 --> 0
Char. 288: 1 --> 0
Node 276 :
Char. 57: 1 --> 2
Char. 59: 0 --> 1
Char. 109: 1 --> 0
Char. 124: 0 --> 1
Char. 174: 0 --> 2
Char. 177: 0 --> 1
Char. 199: 0 --> 1
Node 277 :
Char. 223: 2 --> 3
Node 278 :
Char. 8: 0 --> 1
Char. 118: 0 --> 3
Char. 141: 2 --> 5
Char. 220: 3 --> 4
Node 279 :
Char. 64: 1 --> 2
Char. 75: 1 --> 0
Char. 108: 1 --> 2
Node 280 :
Char. 59: 0 --> 1
Char. 64: 0 --> 1
Char. 69: 0 --> 1
Node 281 :
Char. 1: 0 --> 1
Char. 34: 0 --> 1
Char. 38: 1 --> 0
Char. 45: 0 --> 1
Char. 49: 0 --> 1
Char. 71: 1 --> 2
Char. 82: 0 --> 1
Char. 93: 2 --> 3
Char. 117: 2 --> 0
Char. 118: 1 --> 0
Char. 128: 0 --> 1
Char. 161: 1 --> 0
Char. 184: 1 --> 0
Char. 218: 2 --> 3
Node 282 :
Char. 31: 0 --> 1
Node 283 :
Char. 2: 0 --> 1
Char. 75: 1 --> 0
Char. 80: 0 --> 1
Char. 144: 1 --> 0
Char. 238: 0 --> 1
Node 284 :
Char. 80: 1 --> 2
Char. 109: 1 --> 0
Char. 238: 0 --> 1
Char. 253: 1 --> 0
Node 285 :
Char. 27: 0 --> 1
Char. 30: 1 --> 0
Char. 33: 0 --> 1
Char. 47: 0 --> 1
Char. 141: 1 --> 2
Char. 145: 0 --> 2
Node 286 :
Char. 62: 0 --> 1
Char. 76: 0 --> 1
Char. 96: 0 --> 1
Node 287 :
Char. 10: 1 --> 0
Node 288 :
Char. 75: 0 --> 1
Char. 87: 1 --> 0

References

Chaimanee, Y., Suteethorn, V., Jintasakul, P., Vidthayanon, C., Marandat, B., and Jaeger, J. J. (2004) A new orangutan relative from the Late Miocene of Thailand. *Nature* 427, 439–441.

Claude, J., Naksri, W., Boonchai, N., Buffetaut, E., Duangkrayom, J., Laojumpon, C., Jintasakul, P., Lauprasert, K., Martin, J., Suteethorn, V., and Tong, H. (2011). Neogene reptiles of northeastern Thailand and their paleogeographical significance. *Ann. de Paléontol.* 97, 113–131.

Department of Mineral Resources (2007). Geological map of Nakhon Ratchasima Province. Geological map by Province.

Duval, M., Fang, F., Suraprasit, K., Jaeger, J-J., Benammi, M., Chaimanee, Y., Cibanal, J.I., and Grun, R. (2019). Direct ESR dating of the Pleistocene vertebrate assemblage from Khok Sung locality, Nakhon Ratchasima province, northeastern Thailand. *Palaeontol. Electron*. 22, 1–25.

Esposito, M., Chaimanee, Y., Jaeger, J.J., and Reyss, J.L. (1998). Datation des concrétions carbonatées de la Grotte du Serpent (Thaïlande) par la méthode Th/U. C. R. *Acad. Sci. Ser. IIA* 326, 603–608.

Esposito, M., Reyss, J.L., Chaimanee, Y., and Jaeger, J.J. (2002). U-series Dating of Fossil Teeth and Carbonates from Snake Cave, Thailand. *J. Archaeol. Sci*. 29, 341–349.

Suraprasit, K., Jaeger, J.-J., Chaimanee, Y., Benammi, M., Chavasseau, O., Yamee, C., Tian, P., Panha, S. (2015). A complete skull of Crocuta crocuta ultima indicates a late Middle Pleistocene age for the Khok Sung (northeastern Thailand) vertebrate fauna. *Quat. Int*. 374, 34–45.

Suraprasit K, Jaeger JJ, Chaimanee Y, Chavasseau O, Yamee C, Tian P, Panha S. (2016). The Middle Pleistocene Vertebrate Fauna from Khok Sung (Nakhon Ratchasima, Thailand): Biochronological and Paleobiogeographical Implications. *ZooKeys* 613, 1–157.

Suraprasit, K., Jaeger, J.-J., Chaimanee, Y., Sucharit, C. (2021). Taxonomic reassessment of large mammals from the Pleistocene Homo-bearing site of Tham Wiman Nakin (Northeast Thailand): relevance for faunal patterns in mainland Southeast Asia. *Quat. int.* 603, 90–112.